

ISSN 1881-7815 Online ISSN 1881-7823

BST

BioScience Trends

Volume 12, Number 1
February, 2018



www.biosciencetrends.com

BST

BioScience Trends



ISSN: 1881-7815

Online ISSN: 1881-7823

CODEN: BTIRCZ

Issues/Year: 6

Language: English

Publisher: IACMHR Co., Ltd.

BioScience Trends is one of a series of peer-reviewed journals of the International Research and Cooperation Association for Bio & Socio-Sciences Advancement (IRCA-BSSA) Group and is published bimonthly by the International Advancement Center for Medicine & Health Research Co., Ltd. (IACMHR Co., Ltd.) and supported by the IRCA-BSSA and Shandong University China-Japan Cooperation Center for Drug Discovery & Screening (SDU-DDSC).

BioScience Trends devotes to publishing the latest and most exciting advances in scientific research. Articles cover fields of life science such as biochemistry, molecular biology, clinical research, public health, medical care system, and social science in order to encourage cooperation and exchange among scientists and clinical researchers.

BioScience Trends publishes Original Articles, Brief Reports, Reviews, Policy Forum articles, Case Reports, News, and Letters on all aspects of the field of life science. All contributions should seek to promote international collaboration.

Editorial Board

Editor-in-Chief:

Norihiro KOKUDO
National Center for Global Health and Medicine, Tokyo, Japan

Co-Editors-in-Chief:

Xue-Tao CAO
Nankai University, Tianjin, China
Rajendra PRASAD
University of Delhi, Delhi, India
Arthur D. RIGGS
Beckman Research Institute of the City of Hope, Duarte, CA, USA

Chief Director & Executive Editor:

Wei TANG
The University of Tokyo, Tokyo, Japan

Senior Editors:

Xunjia CHENG
Fudan University, Shanghai, China
Yoko FUJITA-YAMAGUCHI
Beckman Research Institute of the City of Hope, Duarte, CA, USA
Na HE
Fudan University, Shanghai, China
Kiyoshi KITAMURA
The University of Tokyo, Tokyo, Japan
Misao MATSUSHITA
Tokai University, Hiratsuka, Japan
Munehiro NAKATA
Tokai University, Hiratsuka, Japan
Takashi SEKINE

Toho University, Tokyo, Japan
Ri SHO
Yamagata University, Yamagata, Japan
Yasuhiko SUGAWARA
Kumamoto University, Kumamoto, Japan
Ling WANG
Fudan University, Shanghai, China

Managing Editor:

Jianjun GAO
Qingdao University, Qingdao, China

Web Editor:

Yu CHEN
The University of Tokyo, Tokyo, Japan

Proofreaders:

Curtis BENTLEY
Roswell, GA, USA
Christopher HOLMES
The University of Tokyo, Tokyo, Japan
Thomas R. LEBON
Los Angeles Trade Technical College, Los Angeles, CA, USA

Editorial Office

Pearl City Koishikawa 603,
2-4-5 Kasuga, Bunkyo-ku, Tokyo 112-0003, Japan
Tel: +81-3-5840-8764 Fax: +81-3-5840-8765
E-mail: office@biosciencetrends.com

BioScience Trends

Editorial and Head Office

Pearl City Koishikawa 603, 2-4-5 Kasuga, Bunkyo-ku,
Tokyo 112-0003, Japan

Tel: +81-3-5840-8764, Fax: +81-3-5840-8765
E-mail: office@biosciencetrends.com
URL: www.biosciencetrends.com

Editorial Board Members

Girdhar G. AGARWAL <i>(Lucknow, India)</i>	Takahiro HIGASHI <i>(Tokyo, Japan)</i>	Masatoshi MAKUUCHI <i>(Tokyo, Japan)</i>	Tadatoshi TAKAYAMA <i>(Tokyo, Japan)</i>
Hirotugu AIGA <i>(Geneva, Switzerland)</i>	De-Fei HONG <i>(Hangzhou, China)</i>	Francesco MAROTTA <i>(Milano, Italy)</i>	Shin'ichi TAKEDA <i>(Tokyo, Japan)</i>
Hidechika AKASHI <i>(Tokyo, Japan)</i>	De-Xing HOU <i>(Kagoshima, Japan)</i>	Yutaka MATSUYAMA <i>(Tokyo, Japan)</i>	Sumihito TAMURA <i>(Tokyo, Japan)</i>
Moazzam ALI <i>(Geneva, Switzerland)</i>	Sheng-Tao HOU <i>(Ottawa, Canada)</i>	Qingyue MENG <i>(Beijing, China)</i>	Puay Hoon TAN <i>(Singapore, Singapore)</i>
Ping AO <i>(Shanghai, China)</i>	Yong HUANG <i>(Ji'ning, China)</i>	Mark MEUTH <i>(Sheffi eld, UK)</i>	Koji TANAKA <i>(Tsu, Japan)</i>
Hisao ASAMURA <i>(Tokyo, Japan)</i>	Hirofumi INAGAKI <i>(Tokyo, Japan)</i>	Satoko NAGATA <i>(Tokyo, Japan)</i>	John TERMINI <i>(Duarte, CA, USA)</i>
Michael E. BARISH <i>(Duarte, CA, USA)</i>	Masamine JIMBA <i>(Tokyo, Japan)</i>	Miho OBA <i>(Odawara, Japan)</i>	Usa C. THISYAKORN <i>(Bangkok, Thailand)</i>
Boon-Huat BAY <i>(Singapore, Singapore)</i>	Chunlin JIN <i>(Shanghai, China)</i>	Fanghua QI <i>(Ji'nan, Shandong)</i>	Toshifumi TSUKAHARA <i>(Nomi, Japan)</i>
Yasumasa BESSHO <i>(Nara, Japan)</i>	Kimitaka KAGA <i>(Tokyo, Japan)</i>	Xianjun QU <i>(Beijing, China)</i>	Kohjiro UEKI <i>(Tokyo, Japan)</i>
Generoso BEVILACQUA <i>(Pisa, Italy)</i>	Ichiro KAI <i>(Tokyo, Japan)</i>	John J. ROSSI <i>(Duarte, CA, USA)</i>	Masahiro UMEZAKI <i>(Tokyo, Japan)</i>
Shiuan CHEN <i>(Duarte, CA, USA)</i>	Kazuhiro KAKIMOTO <i>(Osaka, Japan)</i>	Carlos SAINZ-FERNANDEZ <i>(Santander, Spain)</i>	Junming WANG <i>(Jackson, MS, USA)</i>
Yuan CHEN <i>(Duarte, CA, USA)</i>	Kiyoko KAMIBEPPU <i>(Tokyo, Japan)</i>	Yoshihiro SAKAMOTO <i>(Tokyo, Japan)</i>	Xiang-Dong Wang <i>(Boston, MA, USA)</i>
Naoshi DOHMAE <i>(Wako, Japan)</i>	Haidong KAN <i>(Shanghai, China)</i>	Erin SATO <i>(Shizuoka, Japan)</i>	Hisashi WATANABE <i>(Tokyo, Japan)</i>
Zhen FAN <i>(Houston, TX, USA)</i>	Bok-Luel LEE <i>(Busan, Korea)</i>	Takehito SATO <i>(Isehara, Japan)</i>	Lingzhong XU <i>(Ji'nan, China)</i>
Ding-Zhi FANG <i>(Chengdu, China)</i>	Mingjie LI <i>(St. Louis, MO, USA)</i>	Akihito SHIMAZU <i>(Tokyo, Japan)</i>	Masatake YAMAUCHI <i>(Chiba, Japan)</i>
Xiaobin FENG <i>(Beijing, China)</i>	Shixue LI <i>(Ji'nan, China)</i>	Zhifeng SHAO <i>(Shanghai, China)</i>	Aitian YIN <i>(Ji'nan, China)</i>
Yoshiharu FUKUDA <i>(Ube, Japan)</i>	Ren-Jang LIN <i>(Duarte, CA, USA)</i>	Judith SINGER-SAM <i>(Duarte, CA, USA)</i>	George W-C. YIP <i>(Singapore, Singapore)</i>
Rajiv GARG <i>(Lucknow, India)</i>	Lianxin LIU <i>(Harbin, China)</i>	Raj K. SINGH <i>(Dehradun, India)</i>	Xue-Jie YU <i>(Galveston, TX, USA)</i>
Ravindra K. GARG <i>(Lucknow, India)</i>	Xinqi LIU <i>(Tianjin, China)</i>	Peipei SONG <i>(Tokyo, Japan)</i>	Benny C-Y ZEE <i>(Hong Kong, China)</i>
Makoto GOTO <i>(Tokyo, Japan)</i>	Daru LU <i>(Shanghai, China)</i>	Junko SUGAMA <i>(Kanazawa, Japan)</i>	Yong ZENG <i>(Chengdu, China)</i>
Demin HAN <i>(Beijing, China)</i>	Hongzhou LU <i>(Shanghai, China)</i>	Hiroshi TACHIBANA <i>(Isehara, Japan)</i>	Xiaomei ZHU <i>(Seattle, WA, USA)</i>
David M. HELFMAN <i>(Daejeon, Korea)</i>	Duan MA <i>(Shanghai, China)</i>	Tomoko TAKAMURA <i>(Tokyo, Japan)</i>	<i>(as of February 26, 2018)</i>

Policy Forum

- 1 - 6 **Core factors promoting a continuum of care for maternal, newborn, and child health in Japan.**
Hidechika Akashi, Miwa Ishioka, Akiko Hagiwara, Rumiko Akashi, Yasuyo Osanai
- 7 - 11 **Japan's healthcare policy for the elderly through the concepts of self-help (Ji-jo), mutual aid (Go-jo), social solidarity care (Kyo-jo), and governmental care (Ko-jo).**
Kyoko Sudo, Jun Kobayashi, Shinichiro Noda, Yoshiharu Fukuda, Kenzo Takahashi

Review

- 12 - 23 **Optical coherence tomography for precision brain imaging, neurosurgical guidance and minimally invasive theranostics.**
Yingwei Fan, Yan Xia, Xinran Zhang, Yu Sun, Jie Tang, Liwei Zhang, Hongen Liao

Original Article

- 24 - 31 **Association of biobehavioral factors with non-coding RNAs in cervical cancer.**
Qiyu Liu, Chong Lu, Wanjun Dai, Ke Li, Jing Xu, Yunke Huang, Guiling Li, Yu Kang, Anil K. Sood, Congjian Xu
- 32 - 39 **Chromosomal karyotype in chorionic villi of recurrent spontaneous abortion patients.**
Yan Du, Lanting Chen, Jing Lin, Jun Zhu, Na Zhang, Xuemin Qiu, Dajin Li, Ling Wang
- 40 - 46 **FL118, a novel camptothecin analogue, suppressed migration and invasion of human breast cancer cells by inhibiting epithelial-mesenchymal transition via the Wnt/ β -catenin signaling pathway.**
Zhihong Yang, Lixia Ji, Guohui Jiang, Ranran Liu, Zhantao Liu, Yuecheng Yang, Qingxia Ma, Hongqin Zhao
- 47 - 53 **Pain perception after colorectal surgery: A propensity score matched prospective cohort study.**
Fabian Grass, Matthieu Cachemaille, David Martin, Nicolas Fournier, Dieter Hahnloser, Catherine Blanc, Nicolas Demartines, Martin Hübner
- 54 - 59 **Outcome of elderly patients after acute biliary pancreatitis.**
Didier Roulin, Raphaël Girardet, Rafael Duran, Steven Hajdu, Alban Denys, Nermin Halkic, Nicolas Demartines, Emmanuel Melloul
- 60 - 67 **Safety and feasibility of a novel non-thermal device for tissue dissection: A preliminary study of the DD1 differential dissector.**
Nao Yoshida, Shintaro Yamazaki, Masahiko Sugitani, Tadatoshi Takayama
- 68 - 72 **Neither ischemic parenchymal volume nor severe grade complication correlate transient high transaminase elevation after liver resection.**
Tokio Higaki, Shintaro Yamazaki, Yusuke Mitsuka, Masaru Aoki, Nao Yoshida, Yutaka Midorikawa, Hisashi Nakayama, Tadatoshi Takayama

CONTENTS

(Continued)

- 73 - 78 **Arterial infusion of cisplatin plus S-1 against unresectable intrahepatic cholangiocarcinoma.**
Tokio Higaki, Osamu Aramaki, Masamichi Moriguchi, Hisashi Nakayama, Yutaka Midorikawa, Tadatoshi Takayama

Brief Report

- 79 - 86 **Tracking hospital costs in the last year of life — The Shanghai experience.**
Bifan Zhu, Fen Li, Changying Wang, Linan Wang, Zhimin He, Xiaoxi Zhang, Peipei Song, Lingling Ding, Chunlin Jin
- 87 - 93 **Exploring the determinants that influence end-of-life hospital costs of the elderly in Shanghai, China.**
Fen Li, Bifan Zhu, Zhimin He, Xiaoxi Zhang, Changying Wang, Linan Wang, Peipei Song, Lingling Ding, Chunlin Jin
- 94 - 101 **The response of common marmoset immunity against cedar pollen extract.**
Yoshie Kametani, Yuko Yamada, Shuji Takabayashi, Hideki Kato, Kenji Ishiwata, Naohiro Watanabe, Erika Sasaki, Sonoko Habu

Guide for Authors

Copyright

Core factors promoting a continuum of care for maternal, newborn, and child health in Japan

Hidechika Akashi^{1,*}, Miwa Ishioka¹, Akiko Hagiwara², Rumiko Akashi³, Yasuyo Osanai⁴

¹Bureau of International Health Cooperation, National Center for Global Health and Medicine (NCGM), Tokyo, Japan;

²Human Development Department, Japan International Cooperation Agency (JICA), Tokyo, Japan;

³Faculty of Sociology and Social Work, Meiji Gakuin University, Tokyo, Japan;

⁴Nursing Department, National Center for Global Health and Medicine, Tokyo, Japan.

Summary

Providing a continuum of care (CoC) is important strategy for improving maternal, newborn, and child health (MNCH). Japan's current very low maternal and infant mortality rates suggest that its CoC for MNCH is good. In this paper, we attempt to clarify how CoC and low mortality rates are being maintained in Japan, by examining the entire MNCH service provision system. First, we examine two important tools for integrated service provision, the Maternal and Child Health (MCH) Handbook and registration of pregnant women with local governments, both introduced in 1942. Second, we explore the incentives provided by the MNCH system that prompt actors to participate in it. The three actors identified are service users (e.g., mothers and babies), medical professionals, and local governments. Through system design, all three actors benefit in ways that incentivize them to use MNCH services, which consequently connects service users with resources: all service users regardless of financial status, nationality, and location can receive free MNCH services such as antenatal care, assistance with childbirth, postnatal care, and immunizations; using the handbook, service users obtain health information, and medical professionals obtain the health records of pregnant women and their children as well as access examination fees from the local government by submitting vouchers in the handbook; local governments can then identify pregnant women for follow-up and provide health information and administrative services. As a result, the coverage rate of the MCH Handbook has reached 100% and MNCH services coverage could potentially reach the same level.

Keywords: Maternal and Child Health Handbook, maternal, newborn, and child health, continuum of care, registration of pregnant women, universal health coverage

1. Introduction

Providing a continuum of care (CoC) for maternal, newborn, and child health (MNCH) helps to improve the health status of mothers and children (1). However, the strategies suggested to achieve this, such as obstetric care, caring for sick children, antenatal care (ANC), postnatal care (PNC), and children's healthcare

services, can often be fragmented. Japan's CoC for MNCH seems to be good, as evidenced by very low current maternal and infant mortality rates (2,3), and integrated services are provided nationwide. At the core of the current system are the Maternal and Child Health (MCH) Handbook and the registration of pregnant women with local governments. In addition, we have highly skilled childbirth attendants, high delivery rates at healthcare facilities, and a high literacy rate (4,5). It is unclear, however, exactly how the MNCH service provision system is working to keep the maternal and infant mortality rates so low.

Previous research has tended to focus on use of the MCH Handbook and its influence on service users and medical service providers. In this article, we attempt to clarify how CoC and low mortality rates are being

Released online in J-STAGE as advance publication February 26, 2018.

*Address correspondence to:

Dr. Hidechika Akashi, Bureau of International Health Cooperation, National Center for Global Health and Medicine (NCGM), 1-21-1 Toyama, Shinjuku-ku, Tokyo, Japan.
E-mail: hakashi@it.ncgm.go.jp

maintained in Japan, by examining the role of several factors in the entire MNCH system: the core use of the MCH Handbook, registration of pregnant women, and the incentives provided by the integrated system that prompt all actors to participate in it. We start by summarizing how the current system developed and then examine the role of each factor in Japan's CoC, compare some aspects of the system with those of other countries, and highlight aspects that might be beneficial for other countries to consider in their efforts to improve CoC for MNCH.

2. History of Japan's current MNCH system

The Maternal and Child Health (MCH) Handbook is considered an important tool in Japan's MNCH service provision today (4,6), helping to keep infant mortality low (4). Its prototype was the Maternal Health (MH) Handbook for expectant and nursing mothers that was introduced in 1942 with the goal of producing healthy soldiers to fight in World War II (7-9). For the government to identify pregnant women and provide them additional resources to keep them healthy, each pregnant woman received an MH Handbook and by law had to register with the government. The handbook containing vouchers for commodities, such as rice, clothes, and sugar, incentivizing mothers to use the handbook (7-10). The coverage rate of this handbook (number of registered pregnant women compared with number of live births) was about 70% (9). After the war, the handbook was expanded to include more child healthcare records and information, and led to the issuance of the Maternal and Child (MC) Handbook in 1948 (7,11). With one MC Handbook provided for each baby (rather than for each mother) and mandatory registration of pregnant women (11,12), coverage grew to exceed 100% (11). In 1965, this handbook was renamed the Maternal and Child Health (MCH) Handbook; one handbook was still provided for each baby, but registration became "recommended" rather than mandatory (11,13,14). This handbook and the recommended registration procedure remain at the core of today's MNCH system.

The main contents of the MCH Handbook are standardized and updated by the Ministry of Health, Labour and Welfare, and municipalities can add contents they deem necessary. The handbook contents are described in detail elsewhere (6) but include parents' name and address, a birth certificate form, previous health condition, records of ANC, child birth, PNC, motherhood classes, child health and development check-ups (birth to 6 years), and immunization and a child growth curve (15). This standardization helps avoid *i*) confusion between healthcare providers and mothers, *ii*) fragmentation of records into different MNCH stages (*e.g.*, handbooks for mothers and handbooks for children), and *iii*) duplication of data

from using different unstandardized MCH home-based records, such as occurs in Vietnam (16).

3. How core factors in the MNCH system trigger CoC in Japan

The CoC for MNCH is triggered by pregnant women registering their pregnancy with the local government (municipal level) (13,15), after which they begin receiving all MNCH services (Figure 1). Municipalities must provide the handbook to every woman who registers (13,14,17). This registration connects to civil registration, which can be used to appropriately follow up with pregnant women within the municipality and avoid duplicating services. This process of registration and handbook provision is guaranteed for all women in Japan regardless of income level, religion, location, or nationality (14,17). Pregnant women can use both public and private medical facilities, which contributes to universal health coverage.

They bring the handbook to their maternity clinic of choice for ANC and doctors record the ANC results for them and their fetus in the handbook. The handbook also provides health information to pregnant woman and their family. All relevant doctors and midwives are required by law to provide entries (14), even when a woman changes clinic during her pregnancy.

Local governments encourage pregnant women to attend ANC, and provide health advice, motherhood classes, and other services through their public health centers. They also send public health nurses to follow up with registered mid-to-high risk women, as well as with pregnant women who registered but do not appear to be taking advantage of ANC (13,18).

After giving birth, all data regarding childbirth is recorded in the handbook and mothers receive birth certificates from their doctors or midwives that they take to the local government to register the birth. Local governments then provide all registered women with health information, health advice, vouchers for child health check-ups (with follow-ups for mothers), and immunizations for children so that they and their babies can receive these services in clinics in a timely, standardized manner.

4. How the MNCH system works: The three actors and the benefits they receive

The combined "Maternal" and "Child" Health Handbook is a useful tool for linking maternal health and child health services and for connecting service users with medical professionals to increase ANC, immunizations, and health-seeking behavior (19-25). It is also useful for service users to increase their knowledge and awareness of the value of routine health check-ups (21) and to change their attitudes about MNCH (19-21,26-28).

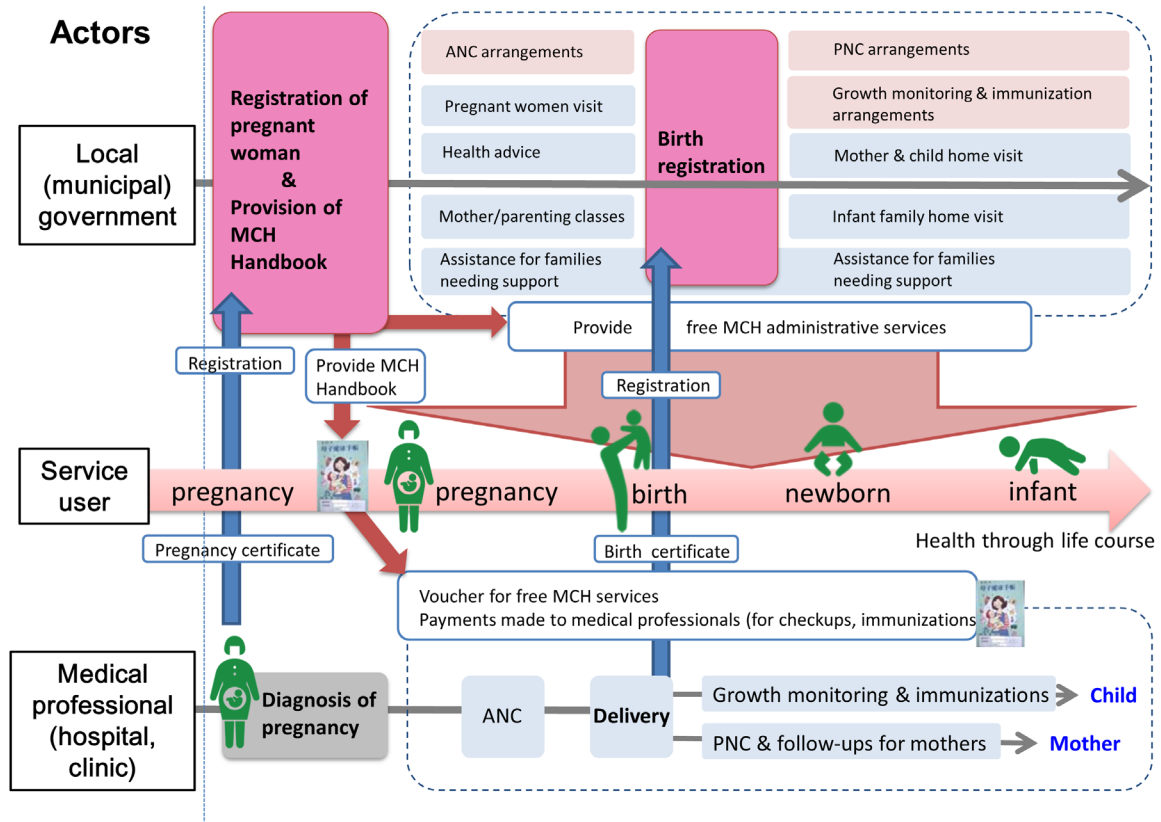


Figure1. The continuum of care for maternal, newborn, and child health in Japan. The X-axis indicates time, and the Y-axis indicates the three actors in the MNCH service provision system. The registration of pregnant women with the local government (municipality level) triggers the continuum of care in Japan. When pregnant women register, the local government provides them with the MCH Handbook and all services start and follow a standard schedule. Birth registration also plays an important role in the MNCH system. (ANC, antenatal care; PNC, postnatal care; MCH, maternal and child health; MNCH, maternal, newborn, and child health.)

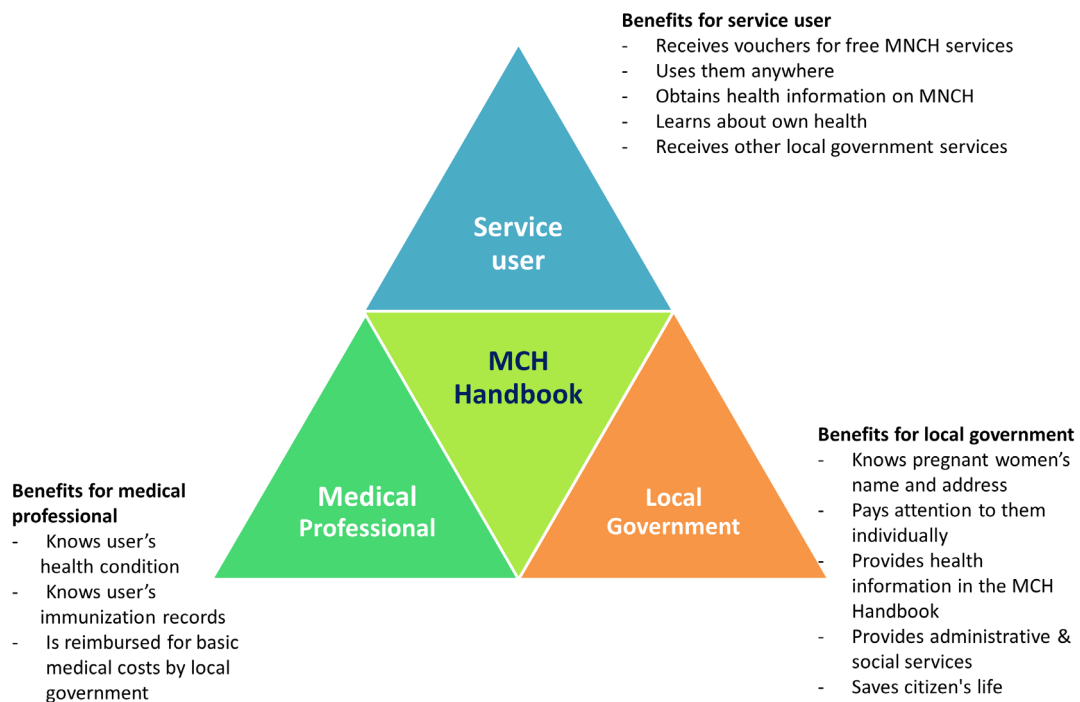


Figure 2. Benefits for the three actors. The MCH Handbook and the registration of pregnant women connect the three actors in the system: service users, medical professionals, and local governments. These three actors obtain benefits by participating in the system, through use of the MCH Handbook. (MCH Handbook, Maternal and Child Health Handbook; MNCH, maternal, newborn, and child health.)

However, challenges can still occur for these two actors – service users and service providers – in the system. Because registration is not mandatory, not all pregnant women register with their local government and so do not receive any ANC; they visit a healthcare facility just to give birth, without providing medical information about the pregnancy or immunizations. In some cases, this may lead to health problems for the child or child abuse after birth (18). Also, medical professionals do not always fill out the handbook correctly, and this can lead to relatively low utilization of the handbook, as reported in Thailand (29). Furthermore, some mothers and children can have difficulty accessing healthcare services and connecting with healthcare resources (30). The handbook and registration of pregnant women are tools to mitigate these difficulties in Japan, and they seem to be made more effective by requiring the involvement of a third actor – local governments – in the system. Local governments work to fairly and equally provide administrative resources such as financial or social support to expectant families (18), and they are in an important position to combine social and medical approaches for MNCH (31) and provide social support for early child development (32).

To promote functioning of the current system, the system provides benefits to all three actors to incentivize their participation. Users benefit from access to free vouchers for MNCH services at any healthcare facility, information on MNCH, knowledge about their personal health, and access to other related government services. Healthcare professionals benefit from using the handbook by gaining easy access to their clients' complete pregnancy records, which helps them provide appropriate services and advice. They can also receive payment from the local government for their services, by submitting vouchers collected from the handbook after performing examinations. Local governments benefit by obtaining information on pregnant women at the time of registration, which makes it possible to provide suitable administrative and social services (13,33). These incentives promote the actors' participation in the MNCH service provision system (Figure 2).

As Misawa stated, "The MCH Handbook is a tool to ensure continuous MNCH services by different professionals, at different occasions, and at different times" (34). These services are ensured by local governments. Thus, combined use of the handbook and registration has made it possible to connect between and provide some necessary CoC components, as suggested by Kerber (1).

5. Effectiveness of Japan's MNCH system

After the first handbook was introduced in 1942, the maternal mortality rate (MMR) fell from 160 in 1948 to < 50 in the late 1960s (35) and the infant mortality

rate (IMR) also fell from around 75 to < 20 (36,37). The handbook has therefore been suggested as one of the causes of IMR reduction in Japan (4,5). However, the picture is not so clear cut. For example, on the one hand, these declining trends in MMR and IMR actually began in the early 1900s (35,36); on the other hand, the handbook does seem to have contributed to reducing diphtheria cases in this period – the number of cases had plateaued or even slightly increased from the 1900s to the 1940s but gradually fell after routine immunizations were introduced in 1948 under the Preventive Vaccination Act (38,39). The introduction of other national laws and interventions around WWII are also potential influencing factors, including the Public Health Center Law of 1937 that designated public health centers as the main providers for public health interventions including MCH services (10,40), and the national health insurance (NHI) system that was implemented nationally in 1961 (41).

It is therefore difficult to conclude that use of the MCH Handbook and registration of pregnant women solely and directly initiated the changes in these health indicators. Nonetheless, the handbook does forge connections between the different interventions, making for a more integrated rather than fragmented system; for example, the handbook refers mothers and children to immunization services; pregnant women register and receive the handbook at public health centers; and childbirth costs are usually supported by NHI. MNCH service users in Japan have also reported the handbook's utility and helpfulness (42).

6. Possible limitations of the current system

One of the arguments against Japan's current system is whether combining the handbook with registration is actually necessary. Reports from other countries show that it is possible and useful to introduce a handbook alone (19,22,23,28). However, in Japan's case, the combination seems to be effective for MNCH by connecting service users with local government resources.

Another argument concerns whether registering a pregnancy with the local government is appropriate, because pregnancy is a personal matter and possibly not a topic for sharing with the government. This question arose between Japanese officials and American medical officers during the United States' occupation after WWII (8). Thus, registration might be a cultural issue.

As already mentioned, some pregnant women decide not to register with the local government, and this can result in some of the aforementioned problems (18). Focusing on the benefits offered is important to encourage women to register and participate.

Lastly, information about women and babies obtained at registration is transferable across local government administrations when users relocate, but only when women inform the local government. Therefore, local

governments might not be able to follow up some high-risk cases. Additionally, the handbook records are handwritten and medical professionals can access them only at health examinations, so records can be lost in times of disasters. A possible solution is to store registration, handbook records, and identification numbers electronically (6).

7. Conclusion

Combining the MCH Handbook with registration of pregnant women appears to be an efficient way to incentivize users, providers, and local governments to participate, promoting CoC for MNCH in Japan. Benefits for the three actors should be publicized to encourage more use of the system.

Acknowledgements

This work was supported by a grant from the National Center for Global Health and Medicine (No. 29-3). We also appreciate the support and advice from Professor Anthony Zwi at the University of South Wales, Australia.

References

1. Kerber K, de Graft-Johnson JE, Bhutta ZA, Okong P, Starrs A, Lawn JE. Continuum of care for maternal, newborn, and child health: From slogan to service delivery. *Lancet*. 2007; 370:1358-69.
2. Ministry of Health, Labour and Welfare of Japan. Statistics on the infant mortality rate in Japan: Vital statistics in Japan. Tokyo (Japan): Ministry of Health, Labour and Welfare; 2017. pp. 24-25. (in Japanese)
3. National Institute of Population and Social Security Research. Latest demographic statistics. Population research series, no. 334. Tokyo (Japan): National Institute of Population and Social Security Research; 2016. p. 94. (in Japanese)
4. Nakamura Y. Maternal and Child Health – Work together and learn together for maternal and child health handbook. *Japan Med Assoc J*. 2014; 57:19-23.
5. Leppert PC. An analysis of the reasons for Japan's low infant mortality rate. *J Nurse Midwifery*. 1993; 38:353-357.
6. Takeuchi J, Sakagami Y, Perez RC. The Mother and Child Health Handbook in Japan as a health promotion tool: An overview of its history, contents, use, benefits, and global influence. *Glob Pediatr Health*. 2016; 3:1-9.
7. Committee for Japanese History on Maternal and Child Health. Maternal and child health in Japan and Dr. Yutaka Moriyama. Tokyo (Japan): Japan Family Planning Association; 1988. pp. 46-8. (in Japanese)
8. Kouno G, Fukushima M. (Kodomonoshiro Health Section, Tokyo, Japan). Historical review of the Maternal and Child Health Handbook. Research report. Tokyo (Japan): Ministry of Health, Labour and Welfare; 1999. pp.1-10 and appendix. (in Japanese)
9. Morita S. Maternal and Child Health Handbook: Past and present. *Kenko Bunka (Health and Culture)*. 2000; 26:1-4. (in Japanese)
10. Kawahara Y. History of maternal and newborn health guidance. Final report. Tokyo (Japan): Ministry of Health, Labour and Welfare; 2013. pp. 1-13. (in Japanese)
11. Nakajima M. Changes in the handbook system supporting maternal and child health and its significance to public health administration. *Jpn J Public Health Nurs*. 2011; 58:515-25. (in Japanese)
12. Child Welfare Act. 1947 [revised 2011]. <http://www.mhlw.go.jp/bunya/kodomo/pdf/tuuchi-01.pdf> (in Japanese) (accessed November 11, 2017).
13. Yokoyama T, Kato N, Takimoto H, Fukushima F. Guidelines for the issuance and practical use of the Maternal and Child Health Handbook. Tokyo (Japan): National Institute of Public Health; 2012. <https://www.niph.go.jp/soshiki/07shougai/hatsuiku/index.files/koufu.pdf> (accessed November 11, 2017). (in Japanese)
14. Maternal and child health act. 1965 [revised 2016]. <http://law.e-gov.go.jp/htldata/S40/S40HO141.html> (accessed November 11, 2017). (in Japanese)
15. Ministry of Health, Labour and Welfare. The Ministry's standard forms for the MCH Handbook (revised January 15, 2002). Tokyo (Japan): Ministry of Health, Labour and Welfare; 2002. <https://www.mhlw.go.jp/shingi/2002/01/s0115-2a.html> (accessed December 14, 2017). (in Japanese)
16. Aiga H, Nguyen VD, Nguyen CD, Nguyen TT, Nguyen LT. Fragmented implementation of maternal and child health home-based records in Vietnam: Need for integration. *Glob Health Action*. 2016; 9:29924.
17. House of Councilors, The National Diet of Japan. Written reply (no. 26) for medical and welfare services for foreign residents in Japan. Tokyo (Japan): House of Councilors, The National Diet of Japan; 2000. <http://www.sangiin.go.jp/japanese/johol/kousei/syuisyo/147/touh/t147026.htm> (accessed November 11, 2017). (in Japanese)
18. Committee on the Maternal and Child Health Handbook. Report on the Maternal and Child Health Handbook. Tokyo (Japan): Committee on the Maternal and Child Health Handbook; 2011. (in Japanese)
19. Hagiwara A, Ueyama M, Ramlawi A, Sawada Y. Is the Maternal and Child Health handbook effective in improving health-related behavior? Evidence from Palestine. *J Public Health Policy*. 2013; 34:31-45.
20. Kawakatsu Y, Sugishita T, Oruenjo K, Wakhule S, Kibosia K, Were E, Honda S. Effectiveness of and factors related to possession of a mother and child health handbook: An analysis using propensity score matching. *Health Educ Res*. 2015; 30:935-946.
21. Aiga H, Nguyen VD, Nguyen CD, Nguyen TT, Nguyen LT. Knowledge, attitude and practices: Assessing maternal and child health care handbook intervention in Vietnam. *BMC Public Health*. 2016; 16:129.
22. Mori R, Yonemoto N, Noma H, Ochirbat T, Barber E, Soyolgerel G, Nakamura Y, Lkhagvasuren O. The Maternal and Child Health (MCH) Handbook in Mongolia: A cluster-randomized, controlled trial. *PLoS One*. 2015; 10:e0119772.
23. Osaki K, Hattori T, Kosen S. The role of home-based records in the establishment of a continuum of care for mothers, newborns, and children in Indonesia. *Glob Health Action*. 2013; 6:1-12.
24. Yanagisawa S, Soyano A, Igarashi H, Ura M, Nakamura

- Y. Effect of a maternal and child health handbook on maternal knowledge and behavior: A community-based controlled trial in rural Cambodia. *Health Policy Plan.* 2015; 30:1184-1192.
25. Kusumayati A, Nakamura Y. Increased utilization of maternal health services by mothers using the maternal and child health handbook in Indonesia. *J Int Health.* 2007; 22:143-151.
 26. Matsuyama E. Japan shows how to save the children. *JOICFP Rev.* 1987; 14:24-29.
 27. Kaneko K, Niyonkuru J, Juma N, Mbonabuca T, Osaki K, Aoyama A. Effectiveness of the Maternal and Child Health handbook in Burundi for increasing notification of birth at health facilities and postnatal care uptake. *Glob Health Action.* 2017; 10:1297604.
 28. Nashi C. Effectiveness of introducing "Maternal and Child Healthcare Notebook System" in Indonesia: Changes in mother for child care. *Bunkyo Univ Inst Educ J.* 2005; 14:79-85. (in Japanese)
 29. Isaranurug S. Maternal and Child Health (MCH) Handbook in the world – Maternal and Child Health Handbook in Thailand. *J Int Health.* 2009; 24:61-66.
 30. Zupan J. Perinatal mortality and morbidity in developing countries. A global view. *Med Trop (Mars).* 2003; 63:366-368.
 31. Wagner M. Pursuing the birth machine: The search for appropriate birth technology. Camperdown (Australia): ACE Graphics; 1994. pp 242-243. (Japanese translation)
 32. Richter LM, Doelmans B, Lombardi J, Heymann J, Boo FL, Behrman JR, Lu C, Lucas JE, Perez-Escamilla R, Dua T, Bhutta ZA, Stenberg K, Gertler P, Darmstadt GL; Paper 3 Working Group and the Lancet Early Childhood Development Series Steering Committee. Investing in the foundation of sustainable development: Pathways to scale up for early childhood development. *Lancet.* 2017; 389:103-118.
 33. Takayanagi K, Iwasaki S, Yoshinaka Y. The role of the Maternal and Child Health Handbook system in reducing perinatal mortality in Japan. *Clin Perform Qual Health Care.* 1993; 1:29-33.
 34. Misawa A. Current status and problems of maternal and child health. *Kyoto Pref Univ Med J.* 2013; 122:687-695. (in Japanese)
 35. Ministry of Health, Labour and Welfare. Present status of maternal and child health. Tokyo (Japan): Ministry of Health, Labour and Welfare; 2010. <http://www.mhlw.go.jp/stf/shingi/2r9852000001oujo-att/2r9852000001oumv.pdf> (accessed November 11, 2017). (in Japanese)
 36. Ministry of Health, Labour and Welfare. Annual changes of vital statistic data and the general view of vital statistics in 2011. Tokyo (Japan): Ministry of Health, Labour and Welfare; 2011. <http://www.mhlw.go.jp/toukei/saikin/hw/jinkou/geppo/nengai11/toukei02.html> (accessed November 11, 2017). (in Japanese)
 37. Nakanishi Y. Development of public health centers in Tokyo. Tokyo (Japan): Japanese Association of Public Health Care Directors; 2004. pp. 1-7. http://www.phcd.jp/01/enkaku/pdf/2008_ayumi.pdf (accessed November 11, 2017) (in Japanese)
 38. Kimura M, Sakai H. Guidance for immunization. 14th ed. Tokyo (Japan): Kindai Press Co.; 2014. pp. 7-8. (in Japanese)
 39. Infectious Disease Surveillance Center (IDSC). Infectious diseases of children. Tokyo (Japan): National Institute of Infectious Diseases; 2004. <http://idsc.nih.go.jp/disease/children.html> (accessed November 11, 2017) (in Japanese)
 40. Committee for Community Medicine Research. Obsolete regulations for public health centers. Tokyo (Japan): Science Council of Japan, 7th Chapter; 1997. pp. 105-6. (in Japanese)
 41. Reich MR, Ikegami N, Shibuya K, Takemi K. 50 years of pursuing a healthy society in Japan. *Lancet.* 2011; 378:1051-1053.
 42. Fujimoto S, Nakamura Y, Ikeda M, Takeda Y, Higurashi M. Utilization of the Maternal and Child Health Handbook in Japan. *Nihon Koshu Eisei Zasshi.* 2001; 48:486-494. (in Japanese)

(Received December 1, 2017; Revised January 18, 2018; Accepted January 25, 2018)

Japan's healthcare policy for the elderly through the concepts of self-help (Ji-jo), mutual aid (Go-jo), social solidarity care (Kyo-jo), and governmental care (Ko-jo)

Kyoko Sudo¹, Jun Kobayashi², Shinichiro Noda³, Yoshiharu Fukuda⁴, Kenzo Takahashi^{4,*}

¹ National College of Nursing, Japan, Tokyo, Japan;

² Department of Global Health, School of Health Sciences, Faculty of Medicine, University of the Ryukyus, Okinawa, Japan;

³ Bureau of International Health Cooperation, National Center for Global Health and Medicine, Tokyo, Japan;

⁴ Graduate School of Public Health, Teikyo University, Tokyo, Japan.

Summary

Elderly care is an emerging global issue threatening both developed and developing countries. The elderly in Japan increased to 26.7% of the population in 2015, and Japan is classified as a super-aged society. In this article, we introduce the financial aspects of the medical care and welfare services policy for the elderly in Japan. Japan's universal health insurance coverage system has been in place since 1961. Long-term care includes welfare services, which were separated from the medical care insurance scheme in 2000 when Japan was already recognized as an aging society. Since then, the percentage of the population over 65 has increased dramatically, with the productive-age population on the decrease. The Japanese government, therefore, is seeking to implement "The Community-based Integrated Care System" with the aim of building comprehensive up-to-the-end-of-life support services in each community. The system has four proposed elements: self-help (Ji-jo), mutual aid (Go-jo), social solidarity care (Kyo-jo), and government care (Ko-jo). From the financial perspective, as the government struggles against the financial burdens of an aging population, they are considering self-help and mutual aid. Based on Japan's present situation, both elements could lead to positive results. The Japanese government must also entrust the responsibility for implementing preventive support to municipalities through strongly required regional autonomy. As Japan has resolved this new challenge through several discussions over a long period of time, other aging countries could learn from the Japanese experience of solving barriers to healthcare policy for the elderly.

Keywords: The Community-based Integrated Care System, universal health insurance, long-term care, policy reform

1. Introduction

Elderly care is an emerging global issue threatening both developed and developing countries. Worldwide, the number of people over the age of 80 is estimated to double by 2050, with one quarter to one half of them

requiring everyday assistance due to their reduced functional and cognitive capabilities. The cost of this long-term care (LTC) is estimated to be a minimum of 1.6% of the worldwide GDP by the Organisation for Economic Co-operation and Development (OECD) and to at least double by 2050 (1).

In 2015, 26.7% of the population in Japan was over 65 years of age. Japan's population is aging more rapidly than in other developed countries and has taken only 24 years to move from an aged to an aging society, with the proportion of the population aged 65 years and over doubling from 7% to 14% from 1970 to 1994, compared to more than 100 years in France and almost 50 years in the United Kingdom (UK) and

Released online in J-STAGE as advance publication February 26, 2018.

*Address correspondence to:

Dr. Kenzo Takahashi, Graduate School of Public Health, Teikyo University, 2-11-1 Kaga, Itabashi City, Tokyo 173-8605, Japan.

E-mail: kenzo.takahashi.chgh@med.teikyo-u.ac.jp

Germany (2). The main cause for this rapid rise in the aging population is attributed to the low death rate due to improved living standards and medical care (3). Likewise, increasing proportions of aging populations are expected to accelerate rapidly across Asia, even in low- and middle-income countries such as Thailand and Vietnam. The aging challenges that most countries are facing include the delivery of appropriate medical and welfare care to the elderly, the human resources required for long-term caregiving, and the funding for such care. In this article, we introduce Japan's medical care and welfare services policy for the elderly. In particular, the lessons learned from Japan's incorporation of self-help and mutual aid into the elderly care policy are elucidated to inform others about possible choices for dealing with their aging populations in the future.

2. Transitions in Japanese health policies for the super-aged society (Tables 1, 2)

2.1. Universal Health Insurance

Japan's universal health insurance coverage system was initiated in 1961 and was characterized by compulsory affiliation, free access, low copayments, and coverage by insurance premiums and public subsidies (4). Initially, the copayment rate for all was the same when the proportion of elderly requiring many more medical care services was only 5.7% (5). Subsequently, medical costs for the elderly became free due to social pressure based on an increasingly aging population combined with rapid economic growth from 1973 onward. However, economic stagnancy led to the implementation of a 10-year limit on free medical care for the elderly. All people over 70 years are now required to pay 20% of the copayment rate, and those over 75 must pay 10% (4). Even though Japan has the highest life expectancy in the world, national medical expenses have been constantly increasing as the birth rate declines and the aging population grows. As a result, the Japanese government is now struggling to find the necessary funding to ensure an effective elderly healthcare policy.

2.2. Long-term Care

In 1997, LTC was introduced that included welfare services but not medical care services. From the 1980s to the 1990s, many beds in Japanese hospitals were occupied for long periods by disabled elderly because of the absence of post-discharge caregivers and/or a lack of adequate care facilities. This was called "social hospitalization", and the hospitalization fee was paid from medical care insurance. It was evident that elderly care services were not sufficient from the data on the proportion of Japanese receiving formal home care aimed at providing nursing care and welfare assistance

for daily living to the elderly, which was lower than that of other industrialized countries in 1995 (6). This could be due to the traditional Japanese cultural belief that caregiving for the elderly is the younger generation's obligation (7). However, because of the growing nuclear family structure, elderly care provided by the younger generation had already started to collapse even before the World Assembly on Aging in 1982, which defined the primary role of the family in supporting the elderly (8). In 2000, LTC insurance was implemented following a nationwide discussion on the national needs of aged care.

LTC services in Japan are now available 24 hours a day, if necessary, and are provided by trained, licensed, and skilled care workers. The number of beneficiaries of LTC services has increased by 2.1 times since its introduction; however, since then, the aging profile in Japan has changed again, and the productive-age population has almost halved compared to that of 2000 (9). LTC insurance is funded 50% by taxes and 50% by premiums. Every taxpayer aged 40 or over is obligated to pay LTC insurance premiums based on their public medical care insurance premium rating. Thus, the decrease in the productive-age population is evoking concern over a shortage of financial resources. As this brief history shows, the Japanese LTC system has gone through a paradigm shift and is in need of further review and refinement.

2.3. The Community-based Integrated Care System

To this end, the Japanese government is seeking to establish a new care structure called "The Community-based Integrated Care System" (CbICS). This concept originated in the comprehensive social security and tax reforms launched in 2012 through an argument for amending LTC insurance. CbICS comprehensively ensures the provision of five factors: health care, nursing care, prevention, housing, and livelihood support. The primary aim of CbICS is to build comprehensive support and services within intimate communities up to the end of life while preserving the dignity of the elderly and supporting independent living (10).

Essentially, CbICS has two dimensions: community-based care based on and driven by community health care needs (11) and integrated care that is conceptualized as methods or types that often aim to reduce fragmentation of health care delivery by enhancing coordination and collaboration between health care professionals (12). CbICS focuses on community power and the coordination and integration of clinical care and welfare services.

CbICS comprises four main elements: self-help (Ji-jo) provided by the individual or their family, mutual aid (Go-jo) provided through an informal network involving local health volunteers, social solidarity care (Kyo-jo) provided by organized social security

Table 1. Critical events in the history of Japanese national policy regarding the elderly

Year	Event pertaining to Japanese national policy	Proportion of population aged 65+ at the time of the event (%)
1961	Achievement of nationwide full coverage of National Health Insurance – Government's commitment to health for all	5.7
1973	Free healthcare policy for people aged 70+ by public funds	7.1
1982	Conclusion of Health and Medical Services Act for the Aged – Health care for people aged 70+ and bedridden aged 65+ was financed by public funds (30%) and health insurance (70%) with a small co-payment	9.1
2000	Introduction of Long-Term Care Insurance System – Provide institutional-based care, home health care services, and community-based services for those 65+ and those between 40 and 64 years with aging-related disabilities	17.4
2012	Establishment of The Community-based Integrated Care System – Community-based care and integrated clinical care and welfare services	23.0

Table 2. Changes in the copayment rate for medical insurance in Japan

Items	1960s	1970s	1980s	1990s	2000s to present
National Health Insurance Insured	30%	→	→	→	30%
Employee insurance Insured	Fixed rate	Fixed rate	(1984~) 10%	(1997~) 20%	(2003~) 30%
Dependents	50%	30%	(1981~) Outpatient: 30% Hospitalization: 20%	→	(2003~) 30%
Aged 70+ (including bedridden aged 65+)	Same as for the insured	0%	(1983~) Outpatient: 400 yen/day Hospitalization: 300 yen/day	(1997~) Outpatient: 500 yen/day (max 4 visits) Hospitalization: 1000 yen/day	(2001~) 10% (2008~) Age 75+: 10% Age 70-74: 20%

programs such as LTC insurance, and government care (Ko-jo) provided by public medical and welfare services or by public assistance funded by tax revenues (10). Of these four elements, we focus on self-help and mutual aid as we believe that these elements are key to the promotion of CbICS.

We believe that CbICS can be major strategy to achieve healthy aging in Japan due to its exact strategy for maintaining a healthy aging society while reaffirming the elderly's and community's own capital. However, this new policy approach was launched just five years ago, and the first evaluation is yet to be completed. Thus, it is unclear whether this approach will become fully established.

3. New challenges for the elderly health policy

To promote CbICS, Japan should address three challenges, each of which is intricately interlinked: *i*) Accountability for financial benefits, *ii*) Interaction between the four elements of CbICS, and *iii*)

Applicability of CbICS to communities.

3.1. Accountability for financial benefits

The first challenge to CbICS is accountability for the financial benefits government gains by promoting self-help and mutual aid.

Generally speaking, government spending on healthcare delivery is based on some amount of public assistance usually financed through taxation and social insurance. For example, in the UK, comprehensive health services are provided virtually entirely through the National Health Service (NHS), which is funded through general taxation (13); in the Swedish model, both health and welfare service spending is completely covered by taxes (14); and in Germany, spending on health care is covered completely by social insurance (15). The situation is completely different in the United States as all out-of-pocket expenses including LTC services are provided by private voluntary insurance funds (16). Japan currently funds healthcare through a mixture of

taxation and social security. While governments have various options to generate the resources required to fund health care, all are facing a financial sustainability challenge, especially for LTC. In Japan, medical and LTC costs are much higher for those over 65 than for other age groups (17). However, the proportion of people over 65 is estimated to be more than 30% in 2025, whereas the productive-age and juvenile populations are expected to continue to decrease (18). Medical and LTC costs from 2012 to 2025 are estimated to increase by 1.5 and 2.3 times, respectively, despite a GDP increase of only 1.2 times (19). Therefore, it will be hard to maintain the current trend of economic growth as aging in Japan becomes a silent but severe financial burden.

In contrast, self-help and mutual aid are crucial healthcare resources for community-dwelling elderly people (20). Active social participation and easy access to assistance from others are associated with good self-help practices (21), and paid work also encourages elderly people to maintain their health later in life (22). From this viewpoint, healthcare policies targeted specifically toward the elderly should actively include self-help or mutual aid. Therefore, as Japan's first challenge, it is important to balance formal and informal assistance in the healthcare financial framework and show evidence that self-help and mutual aid can bring financial benefits such as a reduction in premiums (23,24).

3.2. Interaction between the four elements of CbICS

The second challenge for promoting CbICS is the interaction between the four elements of self-help, mutual aid, social solidarity care, and government care. We especially focus on self-help and mutual aid highlighted in the CbICS.

Previous research in some aging countries has shown evidence that well-designed health promotion programs (25) and self-management (26) can reduce healthcare utilization and related expenditures. Ideally, the government could reduce its financial burden from aged healthcare by not providing funding for the government care element and promoting self-help and mutual aid instead, although these two labels are somewhat controversial as they are abstract concepts (27). As well, the actual financial benefits of self-help and mutual-aid in Japan should be identified.

Interaction between the four elements is important in promoting CbICS not only because of its reliance on the financial perspective but also in considering such regional context as cultural background. This system can be flexibly adjusted due to regional contexts such as demographic changes, disease structure, and health levels.

3.3. Applicability of CbICS to communities

The third challenge is the applicability of CbICS to

elderly care in each community.

The Japanese government is urging all municipalities to establish CbICS by 2025 with strong encouragement of municipal autonomy and independence because situations are quite different and there is no one-size-fits-all approach to establishing CbICS. In Japan, actually, support for preventive care that encourages informal power such as that of individuals themselves or friends and neighborhood networks, that is, self-help and mutual aid, has been spotlighted and strengthened by municipalities authorized by public support. In the UK, for example, self-care is a lifelong component of the LTC model under NHS policy (28), and self-help has already led to positive results there. Thus, Japan's national policy is required to interpret the existential value of both self-help and mutual aid.

Japan's proposed CbICS, which is the new challenge in healthcare policy for the elderly, has finally reached common understanding through several dialogues. Japan seeks to reduce excessive health care expenditures by encouraging regional and community involvement through the four elements of self-help (Ji-jo), mutual aid (Go-jo), social solidarity care (Kyo-jo), and government care (Ko-jo). As one solution to the barriers to healthcare policy for the elderly, this model could be applied in other communities and countries in which aging is an emerging issue. As implementation of the policy should be undertaken by each municipality based on its unique social, cultural, economic, and political conditions, it would be our further challenge to clarify the factors that promote the establishment of CbICS in a variety of communities.

Acknowledgements

This study was supported by The Grant for National Center for Global Health and Medicine (28-7).

References

1. OECD. A Good Life in Old Age? Monitoring and Improving Quality in Long-term Care. OECD Health Policy Studies. <http://www.oecd.org/els/health-systems/a-good-life-in-old-age-9789264194564-en.htm> (accessed December 23, 2018).
2. OECD. OECD Data, Elderly population. <https://data.oecd.org/pop/elderly-population.htm> (accessed October 3, 2017).
3. Okamoto Y. Health care for the elderly in Japan: Medicine and welfare in an aging society facing a crisis in long term care. *BMJ*. 1992; 305:403-405.
4. Ministry of Health, Labour, and Welfare, Japan. Overview of Medical Service Regime in Japan. http://www.mhlw.go.jp/bunya/iryouhoken/iryouhoken01/dl/01_eng.pdf (accessed October 3, 2017).
5. Statistics Bureau, Japanese Ministry of Internal affairs and Communications. 1960 Population census. Portal Site of Official Statistics of Japan website. <http://www.e-stat.go.jp/> (accessed October 3, 2017). (in Japanese)

6. Anderson GF, Hussey PS. Population aging: A comparison among industrialized countries. *Health Aff (Millwood)*. 2000; 19:191-203.
7. Campbell JC, Ikegami N. Long term care insurance comes to Japan. *Health Aff (Millwood)*. 2000; 19:26-39.
8. United Nations. Vienna International Plan of Action on Aging. 1982.
9. Statistics Bureau, Japanese Ministry of Internal affairs and Communications. Japan in numbers. Portal Site of Official Statistics of Japan website. <http://www.e-stat.go.jp/> (accessed October 3, 2017). (in Japanese)
10. Mitsubishi UFJ Research and Consulting Co., Ltd. Project Report; Study on the ideal institutions and services to build the Community-based Integrated Care System. http://www.murc.jp/sp/1509/houkatsu/houkatsu_01/h28_01.pdf (accessed December 23, 2018). (in Japanese)
11. Plochg T, Klazinga NS. Community-based integrated care: Myth or must? *Int J Qual Health Care*. 2002; 14:91-101.
12. Plochg T, Ilinca S, Noordegraaf M. Beyond integrated care. *J Health Serv Res Policy*. 2017; 22:195-197.
13. Thorlby R, Arora S. The English Health Care System, 2015. 2015 International Profiles of Health Care Systems. pp. 49-58. http://www.commonwealthfund.org/~media/files/publications/fund-report/2016/jan/1857_mossialos_intl_profiles_2015_v7.pdf (accessed October 3, 2017).
14. Glenngård AH. The Swedish Health Care System, 2015. 2015 International Profiles of Health Care Systems. pp. 153-160. http://www.commonwealthfund.org/~media/files/publications/fund-report/2016/jan/1857_mossialos_intl_profiles_2015_v7.pdf (accessed October 3, 2017).
15. Blümel M, Busse R. The German Health Care System, 2015. 2015 International Profiles of Health Care Systems. pp. 69-76. http://www.commonwealthfund.org/~media/files/publications/fund-report/2016/jan/1857_mossialos_intl_profiles_2015_v7.pdf (accessed October 3, 2017).
16. The Commonwealth Fund. The U.S. Health Care System, 2015. 2015 International Profiles of Health Care Systems. pp. 171-179. http://www.commonwealthfund.org/~media/files/publications/fund-report/2016/jan/1857_mossialos_intl_profiles_2015_v7.pdf (accessed October 3, 2017).
17. Ministry of Health, Labour, and Welfare, Japan. Data of medical insurance. http://www.mhlw.go.jp/file/06-Seisakujouhou-12400000-Hokenkyoku/kiso26_4.pdf (accessed December 23, 2017). (in Japanese)
18. National Institute of Population and Social Security Research. Population Projections for Japan (2017): 2016 to 2065. http://www.ipss.go.jp/pp-zenkoku/e/zenkoku_e2017/pp29_summary.pdf (accessed December 23, 2017).
19. Ministry of Health, Labour, and Welfare, Japan. Revision of estimated expenses related to social security. <http://www.mhlw.go.jp/seisakunitsuite/bunya/hokabunya/shakaihoshou/dl/shouraisuiki.pdf> (accessed December 23, 2017). (in Japanese)
20. Rechel B, Grundy E, Robine JM, Cylus J, Mackenbach JP, Knai C, McKee M. Ageing in the European Union. *Lancet*. 2013; 381:1312-1322.
21. Nummela O, Sulander T, Karisto A, Uutela A. Self-rated health and social capital among aging people across the urban-rural dimension. *Int J Behav Med*. 2009; 16:189-194.
22. Di Gessa G, Grundy E. The relationship between active ageing and health using longitudinal data from Denmark, France, Italy and England. *J Epidemiol Community Health*. 2014; 68:261-267.
23. Costa-Font J, Courbage C, Zweifel P. Policy Dilemmas in Financing Long-term Care in Europe. *Global Policy*. 2017; 8:38-45.
24. Brown JR, Finkelstein A. Why is the market for long-term care insurance so small? *J Public Econ*. 2007; 91:1967-1991.
25. Goetzl RZ, Shechter D, Ozminkowski RJ, Stapleton DC, Lapin PJ, McGinnis JM, Gordon CR, Breslow L. Can health promotion programs save Medicare money? *Clin Interv Aging*. 2007; 2:117-122.
26. Panagioti M, Richardson G, Small N, Murray E, Rogers A, Kennedy A, Newman S, Bower P. Self-management support interventions to reduce health care utilisation without compromising outcomes: A systematic review and meta-analysis. *BMC Health Serv Res*. 2014; 14:356.
27. Matsushige T. Agenda for the promotion of self care and mutual aid in the construction of community-based integrated care system. *J Natl Inst Public Health*. 2012; 61:113-118.
28. Department of Health. Self Care - A Real Choice: Self Care Support - A Practical Option. 2005. <https://www.gov.uk/government/organisations/department-of-health> (accessed October 3, 2017).

(Received October 24, 2017; Revised January 10, 2018; Accepted January 23, 2018)

Optical coherence tomography for precision brain imaging, neurosurgical guidance and minimally invasive theranostics

Yingwei Fan¹, Yan Xia¹, Xinran Zhang¹, Yu Sun², Jie Tang², Liwei Zhang², Hongen Liao^{1,*}

¹Department of Biomedical Engineering, School of Medicine, Tsinghua University, Beijing, China;

²Department of Neurosurgery, Beijing Tiantan Hospital, Capital Medical University, Beijing, China.

Summary

This review focuses on optical coherence tomography (OCT)-based neurosurgical application for imaging and treatment of brain tumors. OCT has emerged as one of the most innovative and successful translational biomedical-diagnostic techniques. It is a useful imaging tool for noninvasive, *in vivo*, *in situ* and real-time imaging in soft biological tissues, such as brain tumor imaging. OCT can detect the structure of biological tissue in a micrometer scale, and functional OCT has some clinical researches and applications, such as nerve fiber tracts and neurovascular imaging. OCT is able to identify tumor margins, and it gives intraoperative precision identification and resection guidance. OCT-based theranostics is introduced into preclinical neurosurgical resection, such as the integration of OCT and laser ablation. We discuss the challenges and opportunities of OCT-based system in the field of combination of intraoperative structural and functional imaging, neurosurgical guidance and minimally invasive theranostics. We point out that OCT and laser ablation-based theranostics can give more precision and intelligence for intraoperative diagnosis and therapeutics in clinical applications. The theranostics can precisely locate, or specifically target cancerous tissues, and then as much as possibly eliminate them.

Keywords: Optical coherence tomography, brain imaging, neurosurgical guidance, brain tumor, minimally invasive theranostics

1. Introduction

Minimally invasive theranostics is one of the most recent clinical hot topics. Theranostics will give huge simplification for clinical application in the future (1). Optical coherence tomography (OCT) is one of the most promising, innovative and rapidly emerging biomedical imaging modalities. It gradually serves for minimally invasive surgical guidance. It can acquire real-time tomographic images with micrometer resolution by using visible or infrared light (2,3). OCT imaging has been diffusely implemented across various disciplines due to its high-resolution, high-speed, low-cost, radiative-free, invasive-free, and convenience performance (4).

Typical types of OCT scanning include galvanometer scanning, microscope, fiber-optic catheter, handheld probe, endoscope, *etc.* Therefore, OCT is widely used in intraoperative imaging, pre-operative diagnostic and postoperative evaluation (2,5-9), especially, in ophthalmic lesion detection and diagnosis (10-12). OCT is treated as a minimally invasive, real-time diagnostic approach for minimally invasive integration of diagnostics and therapeutics.

Intraoperative neurosurgical imaging with real-time identification are special and significant research for neurosurgical guidance and resection, which can save patients' lives and improve postoperative quality of lives. Furthermore, many advanced technologies are widely used in intraoperative brain tumor detection and neurosurgical guidance, including computer tomography (CT) (13), diffusion-weighted magnetic resonance imaging (MRI) (14), fluorescence (15,16) and fluorescence spectral analysis (17), Raman spectroscopy (18,19), ultrasound (20), photoacoustic imaging (21), biomarkers (22), and evaporative ionization mass spectrometry (23) *etc.* OCT can visualize sub-surface

Released online in J-STAGE as advance publication January 15, 2018.

*Address correspondence to:

Dr. Hongen Liao, Department of Biomedical Engineering, School of Medicine, Tsinghua University, Beijing 100084, China.

E-mail: liao@tsinghua.edu.cn

tissue structure non-invasively, the micro-meter depth microstructure of tissue also has an intuitive demonstration for neurosurgeons, and the research of neurosurgical OCT are launching gradually in neurosurgical diagnostics and guidance.

In clinical applications, the precision of minimally invasive theranostics, which integrates multimodal diagnosis and therapeutic methods, plays an important role in the treatment of lesions (1). A 5-aminolevulinic acid (5-ALA) guided laser ablation system has been proposed, and it has been applied in clinical research by Liao *et al.* (17,24,25). A fluorescence-guided laser ablation system to resect residual cancer for soft tissue sarcoma has been investigated in a mouse model by Lazarides *et al.* (26). Integration of diagnostics and therapeutics has been used in the treatment of tumorous tissue, such as the integration of ultrasound and robotic technology (27-29). OCT has been widely used in imaging to improve diagnostic accuracy and precision, and it can guide therapies *via* providing intraoperative *in situ* abundant information of tumorous tissue (30-32).

In this paper, we review brain imaging, neurosurgical guidance and theranostics using OCT-based system. In brain imaging, "optical biopsy", brain cerebral vascular detection, and fiber nerve tracts are the preclinical and clinical targets. In neurosurgery, the neurosurgical guidance-based OCT system can realize the identification of tumorous tissue and non-tumorous tissue, as well as intraoperative guidance. As future research and clinical applications, we introduce the key technologies and clinical research of theranostics, which is the integration of OCT and other therapies in neurosurgery. Furthermore, we discuss the development and future application of integrated OCT and laser ablation for minimally invasive theranostics in a prospective intelligent medical system.

2. Brain tissue imaging with OCT system

Optical imaging and detection are a non-invasive

or minimally invasive method to diagnose lesions, so that the optical imaging system can widely be devoted to biomedical imaging. Due to the feature of high resolution, OCT can present a more precise microstructure of brain tissue. Moreover, functional imaging based on the polarization property and Doppler effect has been applied in detecting brain function for nerve fiber tracking and cerebral metabolism. The functional imaging also includes angiography imaging to detect blood flow information.

Time domain (TD) and Fourier domain (FD) OCT system are usually devoted in biomedical imaging. A coupler divides a beam of low-coherence light into two paths. The two light beams, which reflect or scatter from the sample and reference arm, form an interference field in a coupler. The ability to discriminate two scattering objects in-depth is up to coherence length of the low coherence light source (2,33). The fundamental principal schematic of time domain OCT is as shown in Figure 1A. By contrast, in FD-OCT, the reference mirror keeps motionless. The basic principal of FD-OCT is that optical coherence frequency of the coherence pattern within the envelope of the light source spectrum increases with the distance of the scattering event from a reference mirror increase (33). Applying a Fourier transform provides the reflectivity profile as a function of depth along the A-scan within the sample or biological tissue (Figure 1B). The depth information of sample is an afforded signal transform without A-scan.

In brain imaging, OCT is a useful tool for detecting brain tissue and lesions. It can provide micrometer level information and the function of optical biopsy. Functional information such as cerebral vascular and fiber bundle, gives an important indicator for avoiding this position to save brain function.

2.1. Brain imaging and 'biopsy' with OCT system

OCT is high-resolution imaging for brain imaging and optical biopsy (34). OCT demonstrates that micrometer-

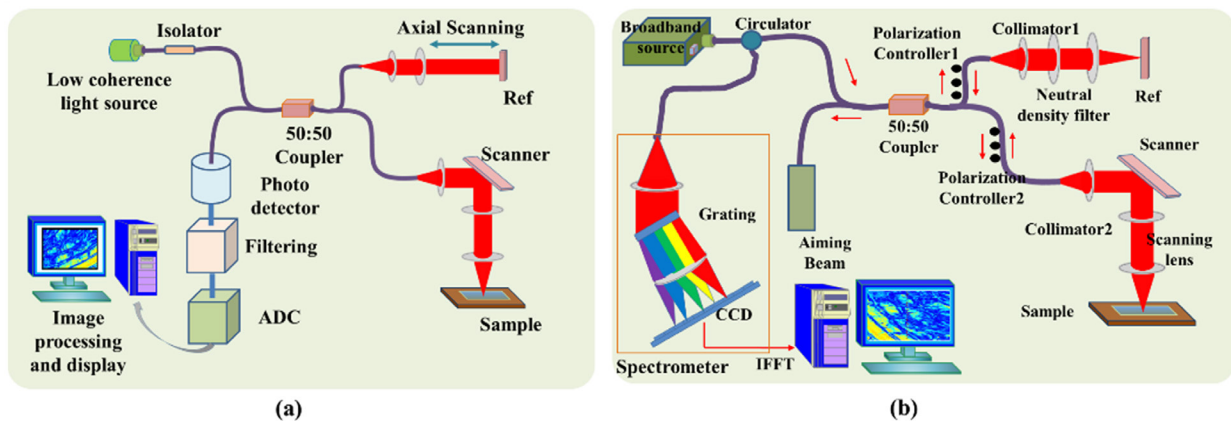


Figure 1. Basic schematic representation. (a) Time domain optical coherence tomography. (b) Spectral domain optical coherence tomography.

scaled, cross-sectional imaging could provide micro-morphological information to diagnose and analyze. Therefore, OCT has the potential to serve as a type of optical biopsy where morphology is assessed with *in situ*, real-time imaging, unlike histological section, which needs removal of specimens and long-time processing for microscopic examination (35). It is possible that OCT will replace histological section in some degree.

Ultrahigh resolution (UHR) OCT, of which the resolution can reach one micrometer or sub-micrometer level, is investigated to image high scattering tissue. Ultrahigh resolution has remarkable characteristics for detecting microstructure in OCT imaging. OCT has been widely used in brain imaging (36-38). Bizheva *et al.* reported that UHR OCT was investigated for imaging of brain tissue morphology using a number of animal models *ex vivo* and *in vitro* (39). The scale of UHR OCT imaging is from neuron cells to an intact animal brain. Moreover, UHR OCT is a successfully translational diagnosis tool, since it is capable of discriminating healthy brain tissue and various neuro-pathologies. For imaging deep brain tissue *in vivo*, a forward scanning single mode fiber ($\phi 125 \mu\text{m}$) is used as detecting probe (40,41). Some advanced technologies have been integrated into the OCT system for improving light penetration to enhance imaging depth in highly scattering brain tissue. Imaging depth of OCM is improved through intrinsic scattering contrast (41). This method does not require the addition of dyes or contrast agents. Vertical cavity surface emitting laser (VCSEL) sweep source OCT offers an extended imaging depth range of more than 2 mm in highly scattering turbid biological tissue (42). With technical improvement, imaging depth of OCT will increase in research and clinical application. Whole brain imaging in an animal model is a big challenge in the current optical field, especially in a freely moving animal. It is meaningful for future research in brain imaging. Whole brain imaging has been developed through techniques for reconstruction and segmentation of sliced brains (43), and quantitative analysis make brain imaging a more practical clinical value (44). However, whole brain imaging is unnecessary with OCT-based system in intraoperative brain imaging, while a large-field view can provide a great amount of information for a specialist to guide and identify brain tissue feature.

2.2. Cerebral vascular and angiography imaging with OCT-based system

Brain is a complicated and comprehensive component in the central nervous system. A brain tumor will affect nervous function and quality of patients' lives. OCT is gradually applied into cerebral functional imaging during brain activity or disease progression. Recently, to investigate blood flow and cerebral hemodynamics in neuroscience, many researchers have been investigating

the angiography and Doppler effect-based OCT imaging system. Furthermore, a novel technique combining optogenetic stimulation and OCT technology can monitor blood flow and cerebral hemodynamics.

During seizures' progression, optical characteristics will change with cerebral function. Yaseen *et al.* reported that OCT detects the changes of optical properties of cortical tissue in mice during the induction of global and focal seizures *in vivo* (45). Yashin *et al.* investigated a contrast-enhanced optical Doppler tomography system (ODT) with intralipid to provide monitoring of cerebral blood flow velocity (46). Furthermore, imaging of the hippocampal area and white matter are presented by OCT system *in vivo* in an animal model (47). Optogenetic stimulation combined with OCT system is proposed for monitoring cerebral hemodynamics (48). Srinivasan *et al.* proposed an optical microscopic method with a multi-parametric OCT platform for measuring blood flow and recovery of ischemic stroke in brain (49). Recent development of OCT-based angiography has started to shed some new light on cerebral hemodynamics in neuroscience. Baran *et al.* demonstrated the effectiveness of proposed automatic image segmentation and enhancement methods for OCT-based micro-angiography (OMAG) and tissue injury mapping (TIM) in a mouse cerebral cortex (50,51).

Multimodal optical imaging system can acquire the information of multiple intrinsic visualization view and facets of cerebral blood flow, and metabolism in healthy tissue and tumorous tissue (52,53). Moreover, a summary of OCT angiography studies is provided for stroke, traumatic brain injury, and subarachnoid hemorrhage cases on rodents (54). This review gave an overview of the recent developments of angiography-based OCT imaging techniques for neuroscience applications in an animal model. Figure 2 shows that dual-wavelength laser speckle contrast imaging (DWLS) (Figure 2A) enabled rapid prediction of the intact infarct area and hemoglobin oxygenation throughout the intact brain in a mouse model. The OMAG system (Figure 2B) provides detailed information of blood perfusion dynamics down to the microvascular or capillary level in a region of interest (ROI) in regard to ischemia.

2.3. Brain nerve fiber bundle imaging based on functional OCT/OCM

Fiber bundle imaging and orientation tracts are outstanding doubts and troubles. The method of nerve fiber tracts imaging is usually based on MRI-diffusion tensor imaging (MRI-DTI) tractography (55) with a high intensity MRI imaging system. However, this diagnosis method is not enough accurate due to the low resolution of MRI imaging compared to other modal imaging systems. Thus, the nerve fiber tracts will give more intuitive and more precise viewing with micrometer-level resolution imaging. Recently, Wang *et al.* reported

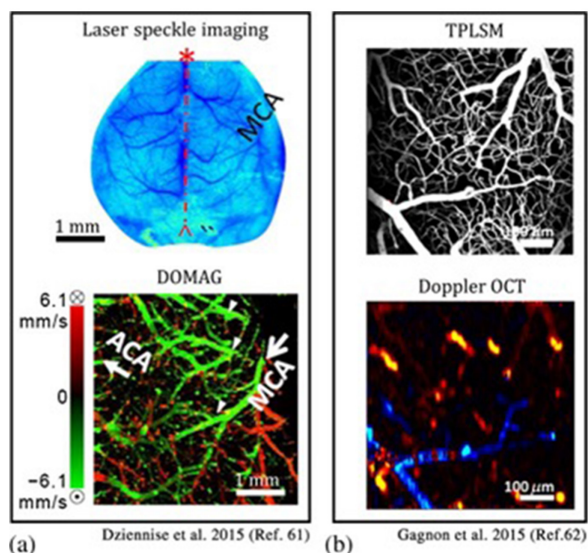


Figure 2. (a) A system combined DWLS with OCT used to monitor microvasculature and microstructure in mouse cortex through whole skull. (b) Combination of TPLSM angiography with Doppler OCT imaging for blood flow in the mouse cortex. From Ref. (54) (Reprinted with permission).

that a multi-contrast OCT (MC-OCT) shows nerve fiber tracts and comprehensive brain anatomy *ex vivo* in animal brain. The MC-OCT has a novel high resolution and improvement of scanning structure with a serial optical coherence scanner (SOCS). Neighboring fiber tracts with different orientations can be distinguished in tomographic optical slices, two-dimensional *en face* images and three-dimensional volumetric images (56,57). Furthermore, a combination of diffusion tensor imaging (DTI) and SOCS imaging can describe the orientation of nerve fiber tracts on postmortem human medulla (58,59). Figure 3 shows the *en face* optic axis orientation maps in fiber orientations of the coronal plane. Different colors represent the different fiber directions as shown on the color wheel; the brightness of colors is determined by the *en face* retardant values (58).

The nerve fiber tracts are equally important for neuroimaging and neurosurgical guidance. Deep-OCM allows, after minor surgery, *in situ* imaging of single myelinated fibers over a large fraction of the sciatic nerve (60). To detect nerve fiber bundles based on measurement of birefringence, polarization sensitive OCT (PS-OCT) demonstrated good quality for detection (61-63). However, these studies are still based on animal experiments, and usually implement the detection of brain function the brain *in vivo* living mouse. These studies are meaningful and significant to recognize brain function of nerve fiber tracts.

3. Neurosurgical monitoring and neurosurgical guidance based on OCT technology

OCT-based clinical application in neurosurgical procedures is a main direction in biological tissue. It is

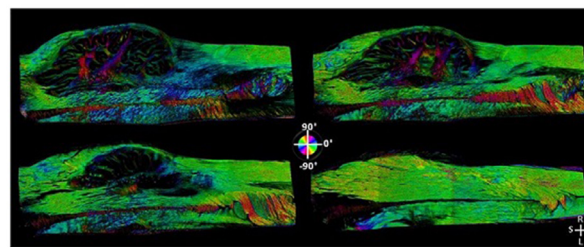


Figure 3. *En-face* optic axis orientation maps produced by SOCS quantitatively depict in-plane fiber orientations in the medulla. Each map is composed of eight (2×4) serial scans. The color wheel shows the orientation values ranging between -90° and 90° . The brightness of colors in the images is determined by the *en-face* retardance values. From Ref. (58) (Reprinted with permission).

more important for intraoperative imaging with high spatial resolution and identification of tumor margins for neurosurgical guidance.

In neurosurgery, OCT-related system will give real-time information for guiding neurosurgical resection. The information can include morphology of tumorous tissue and non-tumorous tissue. In order to acquire more information and a larger imaging field of view, integration of OCT and other imaging modalities can provide appropriate neurosurgical guidance and treatment. Furthermore, integration of OCT and laser ablation system can give precision treatment for brain tumors.

3.1. Identification of tumorous and non-tumorous tissue with OCT system

High-resolution cerebral tumor imaging is very useful for resetting of brain tumors, where the tumor or abnormal lesion can be discriminated from normal brain tissue by OCT system. Many scientists and surgeons are turning *in vivo* OCT tumor imaging research and clinical translational practice into reality. OCT imaging plays a significant role in the resection of brain tumors. Deep brain tumor imaging also has profound significance for identification of tumorous tissue.

During neurosurgical tumor resection, real-time identification of tumors gives ample evidence for operation. Boppart *et al.* reported that an intraoperative OCT system could identify tumor regions and localize tumor margins based on the optical attenuation in backscatter intensity. OCT images of the cortex were acquired in two and three dimensions in the cadaveric human cortex with metastatic melanoma (64). Bizheva *et al.* reported the first studies on *ex vivo* human tissues (65). Böhringer *et al.* reported imaging of human brain tumor specimens using TD-OCT and SD-OCT system to identify tumor and normal tissue using optical characteristics (66-68). Due to the intrinsic optical property of brain tissue, near-infrared OCT has a deeper viewing field/range than visible light used in the OCT system (42,67-69). For the discrimination of tumor, the

longitudinal tomographic OCT image is the basis through measuring the optical attenuation of signal in three-dimensional topology. Furthermore, brain tumor has a more complex microstructure and micromorphology. However, it is difficult to identify tumor margins from the longitudinal/axial map, because the algorithm based on the optical attenuation coefficient of A-scan will get the map of an alignment in the B- or C-scan. Such an algorithm adds the longitudinal analysis to identify the boundary of tumorous tissue.

Multimodal optical imaging can image the microstructure, cerebral oxygen delivery and energy metabolism of brain tumors. Yaseen *et al.* investigated the combination of two-photon microscopy (TPM) and confocal lifetime microscopy, laser speckle imaging, OCT imaging, and optical intrinsic signal imaging to monitor cerebral oxygen delivery and energy metabolism (51). It will be used into intraoperative imaging and neurosurgical guidance for detecting metabolism and identification of tumorous tissue. Two-imaging modalities, including cross-polarization OCT and microangiographic OCT, are integrated into multimodal (MM) OCT system for differential diagnostics of normal and diseased brain tissue with glioblastoma (52). Microangiographic OCT allowed the visualization of blood vessels in brain tissues, revealing changes in the form and sizes typical of the tumor vessels.

For identifying different kinds of brain tumors, full-field OCT (FF-OCT) system, which can detect the microstructure of tumor, has been proposed. Assayag *et al.* applied a FF-OCT imaging system to structural imaging of brain tumor specimens (70). However, the diagnostics of brain tumors are only implemented in brain specimens *ex vivo*. FF-OCT in *LLTech Corporation* (71) uses infrared light to take optical biopsies beneath the surface of tissue under analysis instead of histological section. Intraoperative precision diagnostics has some space for improvement. Figure 4 demonstrates that FF-OCT detects cerebral tissue architecture modification. Infiltrating tumorous glial cells are not detectable in this system, but low-grade gliomas are mistaken for normal brain tissue on FF-OCT images. However, in high-grade gliomas (Figure 4 G-K), the infiltration zone of brain tumors has occurred to such an extent that normal parenchyma structure is lost (70).

3.2. Neurosurgical guidance with intraoperative OCT imaging and integrated multi-modality imaging

Intraoperative neurosurgical imaging and guidance are crucial for non-invasive identification of brain tumor and non-tumor tissue on a facial map together with longitudinal tumor margin in real time. However, the image quality and the imaging depth limits the identification of longitudinal tumor margin. During neurosurgery, intraoperative diagnosis plays an important role in surgical guidance. The speed of OCT

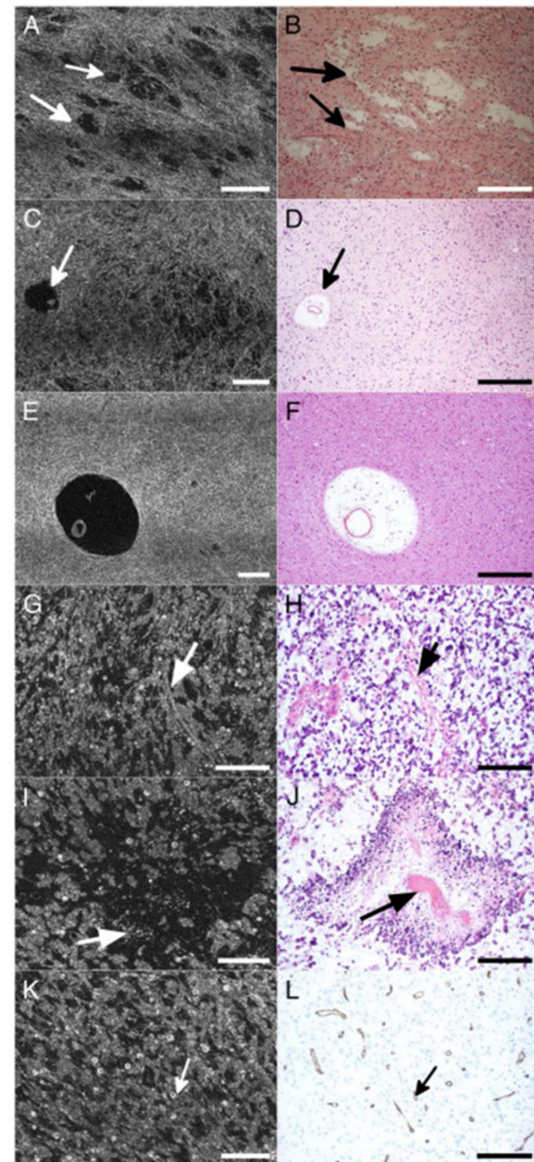


Figure 4. Glioma. Assayag *et al.* reported three different cases shown in (A-B; C-F; G-L). (A-B) Microcysts (arrows) in an oligo-astrocytoma grade 2; (C-D) microcystic areas and Virchow-Robin space (arrows) in an astrocytoma grade 2; (E-F) enlarged Virchow-Robin spaces in an astrocytoma grade 2; (G-H) microvessels (arrow) and tumorous glial cells in an oligoastrocytoma grade 3; and (I-J) pseudo-palisading necrosis in an oligo-astrocytoma grade 3. (K-L) Vasculature (arrows) in an oligo-astrocytoma grade 3. (B, D, F, H and J) Hemalun and phloxin stainings and CD34 immunostaining (L). Scale bars show 250 μm (A, B), 100 μm (C-F), 20 μm (G, H), and 10 μm (I-L). From Ref. (70) (Reprinted with permission).

imaging will strongly influence intraoperative diagnosis and visualization. The improvement of imaging speed promotes the efficient of identification and diagnosis.

For giving an intuitive view of brain tissue, some researchers have designed and manufactured a neurosurgical probe of OCT, including endoscopic, needle-type, hand-held probe, and other kinds of neurosurgical OCT robotic arms (68,72-79). Böhringer *et al.* used a modified rigid endoscopic probe to mount OCT device for detecting tumor during resection of

intrinsic brain tumors (68). In microsurgery, Kang *et al.* proposed a common-path OCT system with an applicable fiber-optic endoscopic probe (74,76). Furthermore, a hand-held forward-viewing probe is useful for neurosurgical imaging and residual tumor detection due to the irregular and limited resection cavity. Liang *et al.* and Sun *et al.* developed a needle-type forward-imaging OCT probe, which was fit for minimally invasive tools (77-79).

Another issue is the intraoperative detection of residual tumor in neurosurgery. Giese *et al.* reported that tumorous tissues of human brain and areas of the resection cavity were analyzed during the resection of gliomas within OCT guidance (80). Recently, excellent research reported by Kut *et al.* investigated a self-regulating OCT system on *ex vivo* human tissue specimens of 32 patients (81), and the method to discriminate between normal and tumorous tissues is based on the optical attenuation coefficient measured by developing nanoparticle-based OCT imaging contrast agents during operation (82,83). The substantial contribution of this research is the performance of diagnostic analysis to derive an attenuation threshold to distinguish tissues with high sensitivity and specificity. For the identification of tumor margins, some algorithms assist the diagnosis of tumorous tissue, such as pixel classification-based method (84), and attenuation coefficient-based method (85). Machine learning method has been used in the classification of skin tumors with OCT images (86), it has potential application on brain tumor imaging. Furthermore, on the aspect of imaging speed, the technology of graphic processing unit (GPU)-based acceleration provides a huge potential application. Zhang *et al.* use the

dual GPU to accelerate the speed of FD-OCT system so that the system can be used in the intraoperative microscopic guidance. This research provides an access to fast image processing for microscopic surgery. It has potential to translate into a typical clinical application in the future (87). The intraoperative real-time identification of cancerous tissue and non-cancerous tissue provides a similar function for real-time histological section to guide neurosurgery. OCT system is a promising intraoperative imaging tool for neurosurgical guidance (88). However, there is still lack of brain functional information in the cerebral cortex and deep brain tissue. Figure 5 shows that OCT attenuation maps aided the neurosurgeon in identifying regions of tumorous tissue versus non-tumorous tissue (white matter) before and after surgery.

Multimodal imaging system is more convenient for neurosurgical guidance for tumor resection. Sun *et al.* reported that a hand-held probe has been proposed in the cadaveric *in situ* testing for providing updated image information; however, the probe has a forwarding viewing for neurosurgical OCT attached with tracking markers (89). Liang *et al.* investigated a combination of OCT with an MRI-compatible needle-type probe for tumor resection in neurosurgical guidance. The probe has capability of providing microscale architecture in conjunction with macroscale MRI tissue morphology for human patients in real-time for *in situ* imaging and neurosurgical guidance (90). An integrated system of photoacoustic OCT and surgical microscope has been proposed, and it can guide surgeons through providing the intraoperative real-time tumor margins, tissue structure and a magnified view of region of interest (91). Multimodal imaging system will acquire multi-

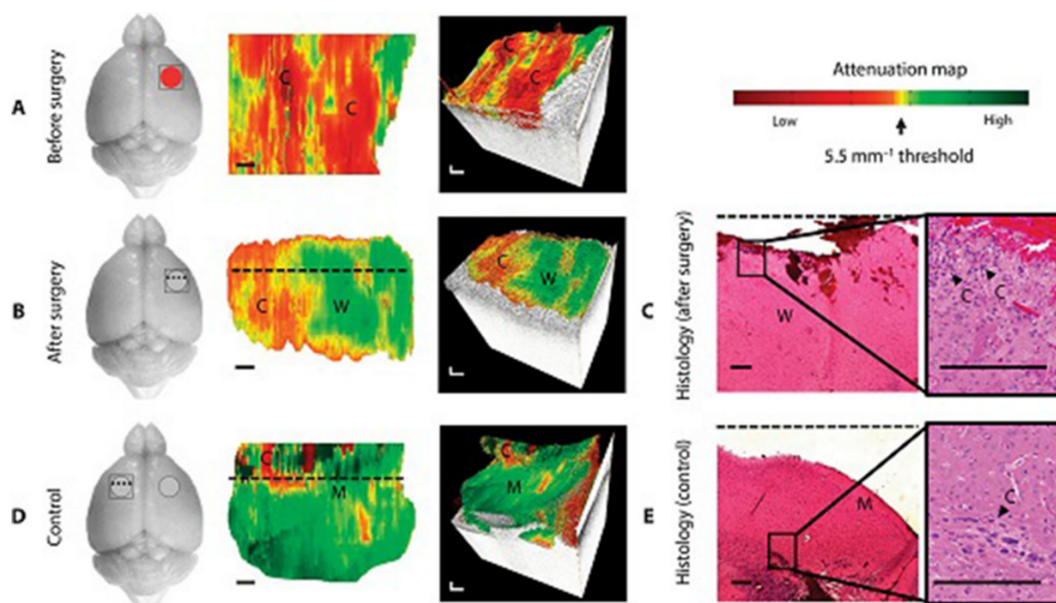


Figure 5. *In vivo* OCT imaging brain cancer in a mouse with patient-derived high-grade brain cancer (GBM272). From Ref. (81). (Reprinted with permission).

dimension information of intraoperative biological tissue for helping real-time surgical diagnosis and analysis. It can decrease the difficulty of intraoperative identification of tumor margins for neurosurgical guidance.

The main challenges of large-scale/wide-field scanning of the resection zone are the creating a map of the cavity, scanning of the perpendicular surface and merging an intraoperative visualization of the three-dimensional data. Some novel techniques may assist surgeons to achieve micrometer precision incisions, reducing the risks of damage to the surrounding tissue, and minimizing intraoperative complications (92). Overlaying microscopy images with depth information from OCT could lead to improved detection of residual tumor cells (58,93). Combining OCT imaging with an operating microscope (94,95) can offer intuitionistic viewing of the surgical area. Robotized operating microscope integrated OCT imaging could scan larger scale tissue surface area through automated movement of the microscope. Hence, the microscope assisted OCT-based neurosurgical guidance can provide more high-resolution and wide-field intuitive viewing to perform precision surgical resection.

3.3. Integrated OCT and laser ablation system for real-time treatment of diseased tissue

Minimally invasive theranostics for treatment of the diseased soft biological tissue is a developmental and potential clinical application. Integration of *in vivo/in situ* imaging and therapy will provide some more possibilities for intraoperative diagnosis and therapeutic (17,24-29,96). With respect to tumor resection in soft biological tissue, OCT-guided laser ablation is a novel theranostics method, especially in brain tumor resection. Some research demonstrated that the integration of OCT and laser ablation provide a novel treatment approach for the tissue's lesion. For malignant tumor treatment, the challenge is visualization of the treatment response dynamics in microscale spatiotemporal resolution during the surgical operation. Minimally invasive integration of diagnosis and therapy will decrease the radiative dose and increase the efficiency of tumor treatment.

In surgical procedures, OCT can monitor and capture the dynamic changes during the laser ablation or laser surgery for the diseased tissue. OCT-guided laser surgery has been developed for use in ophthalmic surgery (97,98). Boppart *et al.* reported that it is a new approach, where the integration of real-time high-resolution OCT and laser ablation can realize the treatment of brain tumors *in vivo* and *in situ*; the system could image the dynamic changes before, during, and after intraoperative laser ablation scenarios (30). Meng-Tsan Tsai *et al.* proposed an OCT guided laser-assisted drug delivery system, which can monitor drug diffusion through an induced microthermal ablation zones array

(99). The integration of OCT and laser ablation will provide an intuitive view for real-time treatment of diseased tissue.

With respect to soft tissue *in situ* treatment, the *in situ* monitoring of laser ablation results provides intuitive observation for evaluating the laser ablation during the operation. Ohmi and Haruna *et al.* demonstrated an effective method for *in situ* observation of laser ablation of soft-biological tissue based on OCT imaging (100,101). For the improvement of imaging speed, the swept source OCT has been investigated in the system with 25 Frames/s imaging speed for *in situ* observation (102-104). In Ohmi's research, OCT system is only used in monitoring the process of laser ablation and post-operation imaging. It is still a dilemma how to use integration of OCT and laser ablation treatment. OCT guided laser resection in surgery has also been developed by Nitesh Katta *et al.* The smart laser knife system is used for surgical guidance (105,106). These research methods take the utility of OCT imaging and monitoring the laser ablation into consideration. Enhanced tissue ablation efficiency with a mid-infrared nonlinear frequency conversion laser system has been proposed, and the results can be monitored using OCT imaging (107). However, a large-scale OCT scanning and laser ablation model during OCT-guided laser ablation treatment are still problematic, as well as real-time monitoring laser ablation. The integration of OCT and laser ablation has met same dilemmas. Therefore, we proposed a novel SD-OCT guided laser ablation system for resection of brain tumors (109). We have proposed and designed the prototype of integration of diagnosis and therapeutic systems, which is an optical theranostics system, and includes OCT imaging, analytical outcome of laser ablation, and automatic scanning platform. It has a promising application for neurosurgical treatment. Figure 6 shows the *ex vivo* porcine brainstem validation experiment for evaluating OCT imaging of pre- and post-ablated craters. In the future, integration of OCT and laser ablation will provide more precise diagnosis and therapy through precisely controlled radiation power and duration times.

In the imaging and treatment of brain tumors, OCT-related system can give an optional approach for precision identification and therapy. OCT-based diagnosis has the function of intraoperative histological sections for real-time identification of tumorous tissue, non-tumorous tissue, and infiltrated zone. In the future, a combination of morphological and functional information for imaging brain tumors will further prompt the clinical application of OCT in neurosurgery. Some novel optical attenuation coefficient- and artifact intelligence-based approaches of OCT image processing will play a greater advantage in diagnostics for real-time identification, classification and segmentation of tumorous tissue. Minimally invasive theranostics is the developmental trend for future clinical practice. Integration of OCT and laser ablation system

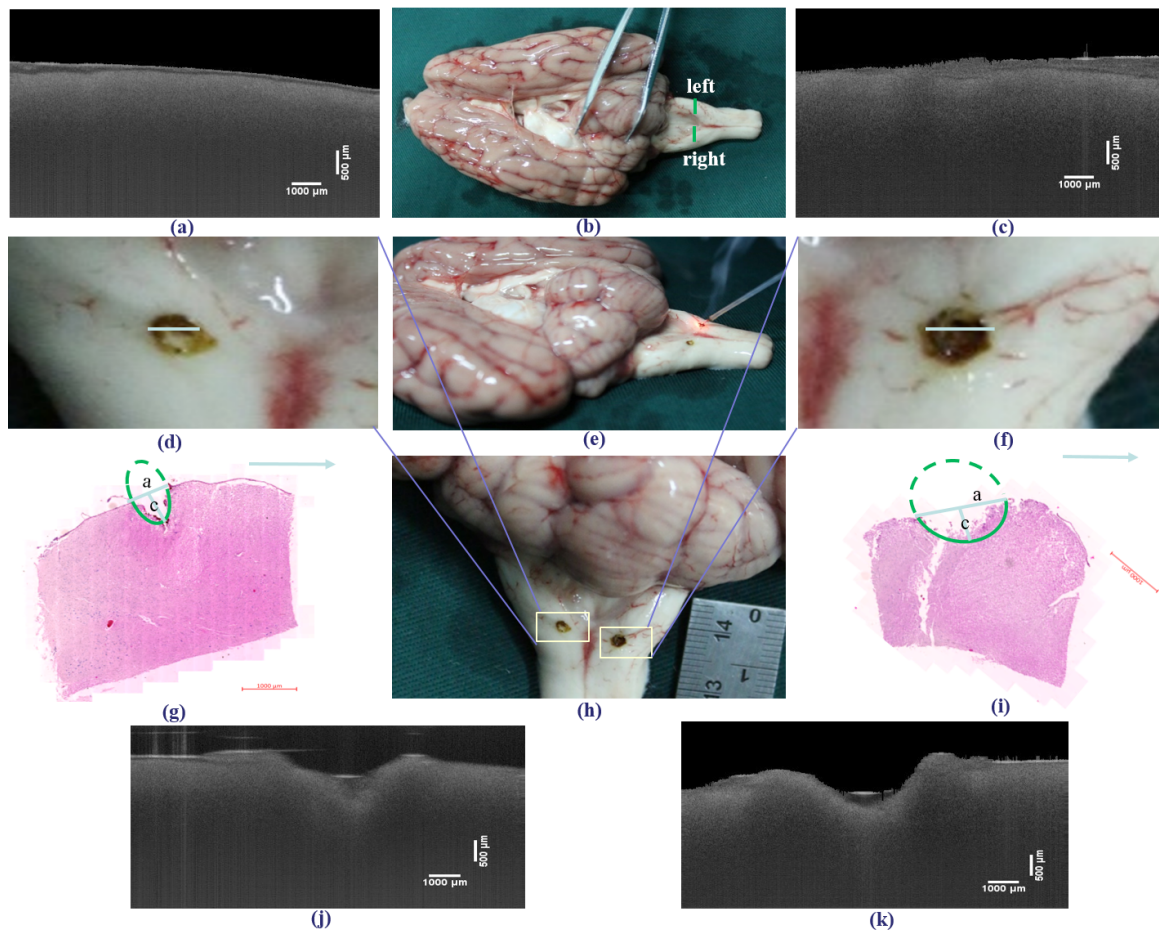


Figure 6. The validation experiment of imaging the pre- and post-ablated craters on the *ex vivo* porcine brainstem (a) and (c). The OCT images of the pre-ablated craters corresponding to the left and right locations in *ex vivo* porcine brainstem. (b) The *ex vivo* porcine brainstem, with the green line showing the scanning location. (d, f) The ablated craters corresponding to a radiation power of 5 W and radiation durations of 5 and 10 s, respectively. (e) The performance of laser ablation on the porcine brainstem. (g, i) Histological sections corresponding to (d) and (f), respectively (scale bar = 1,000 μm). (h) Laser-ablation results. (j, k) OCT images of post-ablated craters at a radiation power of 5 W for radiation durations of 5 and 10 s, respectively. From Ref. (108). (Reprinted with permission).

can carry out treatment of brain tumors. Endoscopic or robotic-assisted integration of OCT and laser ablation system will make minimally invasive theranostics a reality. This will be one of the clinical trends due to the characteristics of precision and real time in integration of diagnosis and therapeutics.

4. Conclusion

In summary, OCT has performed some advantages and has great potential in ultra-high resolution brain imaging, neurosurgical guidance, and minimally invasive theranostics integrated with laser ablation. Local intraoperative brain imaging can provide extensible sufficient structural and functional information including nerve fiber tracts and neurovascular structure. Improvement of OCT imaging depth is the trend for precision imaging and identification of brain tumorous and non-tumorous tissue. Functional imaging will provide more precise information for neurosurgical guidance. Optical

Doppler tomography or Doppler OCT has also been used to acquire tomographic images of animals' brain hemodynamics in the cerebral cortex. Brain functional imaging, which includes nerve fiber tracts and cerebral vascular hemodynamics, can be incorporated into intraoperative neurosurgical imaging and guidance procedures to avoid damage of cranial nerve's function during resection treatment.

In OCT-guided neurosurgical theranostics, the system needs higher technical advancements for faster automatic diagnosis and therapy as well as fusion of multimodal information. The intelligence of theranostics system can be improved by adding visual feedback to make treatment safer, less invasive and more effective. Hence, minimally invasive theranostics, which combines OCT and laser ablation to reach high precision, automation and intelligence on intraoperative neurosurgical operation and treatment, is a novel method for diagnosis and therapy of brain tumor. It could be a promising technology in translational medicine.

Acknowledgements

The authors acknowledge support from Beijing Municipal Science & Technology Commission (Z151100003915079), Beijing Municipal Natural Science Foundation (7172122), National Key Research and Development Program of China (2017YFC0108000), and National Natural Science Foundation of China (Grant No. 81427803, 81771940).

References

- Liao H. Integrated diagnostic and therapeutic techniques: Toward an intelligent medical system. *Comput Med Imaging Graph.* 2014; 38:421-422.
- Huang D, Swanson EA, Lin CP, Schuman JS, Stinson WG, Chang W, Hee MR, Flotte T, Gregory K, Puliafito CA, Fujimoto JG. Optical coherence tomography. *Science.* 1991; 254:1178-1181.
- Fujimoto GJ, Pitris C, Boppart AS, Brezinski EM. Optical coherence tomography: An emerging technology for biomedical imaging and optical biopsy. *Neoplasia.* 2000; 2:9-25.
- <http://www.octnews.org/> (accessed October 8, 2017).
- Zysk AM, Nguyen FT, Oldenburg AL, Marks DL, Boppart SA. Optical coherence tomography: A review of clinical development from bench to bedside. *J Biomed Opt.* 2007; 12:05140.
- Banc A, Stan C, and Florian IS. Optical coherence tomography impacts the evaluation of visual pathway tumors. *Neurosurgical Review.* 2016; DOI 10.1007/s10143-016-0772-1.
- Fercher AF. Optical coherence tomography-development, principles, applications. *Zeitschrift für Medizinische Physik.* 2010; 20:251-276.
- Drexler W, Liu M, Kumar A, Kamali T, Unterhuber A, Leitgeb RA. Optical coherence tomography today: Speed, contrast, and multimodality. *J Biomed Opt.* 2014; 19:071412.
- Falkner-Radler CI, Glittenberg C, Gabriel M, Binder S. Intraoperative microscope-integrated spectral domain optical coherence tomography assisted membrane peeling. *Retina.* 2015; 35: 2100-2106.
- Fujimoto JG, Swanson E. The development, commercialization, and impact of optical coherence tomography. *Invest Ophthalmol Vis Sci.* 2016; 57:OCT1-OCT13.
- Rebolleda G, Diez-Alvarez L, Casado A, Sánchez-Sánchez C, de Dompablo E, González-López JJ, Muñoz-Negrete FJ. OCT: New perspectives in neuro-ophthalmology. *Saudi J Ophthalmol.* 2015; 29:9-25.
- Hitzenberger CK, Drexler W, Leitgeb RA, Findl O, Fercher AF. Key developments for partial coherence biometry and optical coherence tomography in the human eye made in Vienna. *Invest Ophthalmol Vis Sci.* 2016; 57:OCT460-OCT474.
- Zausinger S, Schichor C, Uhl E, Reiser MF, Tonn JC. Intraoperative CT in Neurosurgery (ed): Intraoperative Imaging and Image-Guided Therapy. Springer Science Business Media New York, USA, 2014; pp 529-536.
- Bisdas S, Roder C, Ernemann U, Tatagiba MS. Intraoperative MR imaging in neurosurgery. *Clin Neuroradiol.* 2015; 25 Suppl 2:237-244.
- Su X, Huang QF, Chen HL, Chen J. Fluorescence-guided resection of high-grade gliomas: A systematic review and meta-analysis. *Photodiagnosis Photodyn Ther.* 2014; 11:451-458.
- Valdés PA, Roberts DW, Lu FK, and Golby A. Optical technologies for intraoperative neurosurgical guidance. *Neurosurg Focus.* 2016; 40:E8.
- Liao H, Noguchi M, Maruyama T, Muragaki Y, Kobayashi E, Iseki H, Sakuma I. An integrated diagnosis and therapeutic system using intraoperative 5-Aminolevulinic-Acid-Induced fluorescence guided robotic laser ablation for precision neurosurgery. *Med Image Anal.* 2012; 16:754-766.
- Ji M, Orringer DA, Freudiger CW, *et al.* Rapid, label-free detection of brain tumors with stimulated Raman scattering microscopy. *Sci Transl Med.* 2013; 5:921-925.
- Jermyn M, Mok K, Mercier J, Desroches J, Pichette J, Saint-Arnaud K, Bernstein L, Guiot MC, Petrecca K, Leblond F. Intraoperative brain cancer detection with Raman spectroscopy in humans. *Sci Transl Med.* 2015; 7:274ra19.
- Moiyadi, Aliasgar V, Shetty P. Direct navigated 3D ultrasound for resection of brain tumors: A useful tool for intraoperative image guidance. *Neurosurg Focus.* 2016; 40:E5.
- Yao JJ, Xia J, Maslov KI, Nasirivanaki M, Tsytsarev V, Demchenko AV, Wang LV. Noninvasive photoacoustic computed tomography of mouse brain metabolism *in vivo*. *NeuroImage.* 2013; 64:257-266.
- Lu C, Xia J, Bin W, Wu, Y, Liu X, Zhang Y. Advances in diagnosis, treatments, and molecular mechanistic studies of traumatic brain injury. *Biosci Trends.* 2015; 9:138-148.
- Balog J, Sasi-Szabó L, Kinross J, Lewis MR, Muirhead LJ, Veselkov K, Mirnezami R, Dezső B, Damjanovich L, Darzi A, Nicholson JK, Takáts Z. Intraoperative tissue identification using rapid evaporative ionization mass spectrometry. *Sci Transl Med.* 2013; 5:153-154.
- Liao H, Shimaya K, Wang K, Maruyama T, Noguchi M, Muragaki Y, Kobayashi E, Iseki H, Sakuma I. Combination of intraoperative 5-aminolevulinic acid induced fluorescence and 3-D MR imaging for guidance of robotic laser ablation precision neurosurgery. *Med Image Comput Assist Interv.* 2008; 5242:373-380.
- Liao H, Fujiwara K, Ando T, Maruyama T, Kobayashi E, Muragaki Y, Iseki H, Sakuma I. Automatic laser scanning ablation system for high-precision treatment of brain tumors. *Lasers Med Sci.* 2013; 28:891-900
- Lazarides AL, Whitley MJ, Strasfeld DB, Cardona DM, Ferrer JM, Mueller JL, Fu HL, Bartholf DeWitt S, Brigman BE, Ramanujam N, Kirsch DG, Eward WC. A fluorescence-guided laser ablation system for removal of residual cancer in a mouse model of soft tissue sarcoma. *Theranostics.* 2016; 6:155-166.
- An CY, Syu JH, Tseng CS, Chang C-J. An ultrasound imaging-guided robotic HIFU ablation experimental system and accuracy evaluations. *Appl Bionics Biomech.* 2017; 2017:5868695.
- Norihiro K, Joonho S, Deukhee L, Akira N, Kiyoshi Y, Naohiko S, Matsumoto Y, Homma Y, Mitsushishi M. Integration of diagnostics and Therapy by ultrasound and robot technology. *International Symposium on Micro-Nanomechatronics and Human Science IEEE.* 2010; 53-58.
- Norihiro K, Kohei O, Akira N, Hiroyuki T, Kiyoshi Y,

- Takashi A, Sugita N, Homma Y, Matsumoto Y, Mitsuishi M. A mechanical system identification method for non-invasive ultrasound theragnostic system. *Procedia CIRP*. 2013; 5:315-320.
30. Boppart SA, Herrmann J, Pitris C, Stamper DL, Brezinski ME, Fujimoto JG. High-resolution optical coherence tomography-guided laser ablation of surgical tissue. *J Surg Res*. 1999; 82:275-284.
 31. Li Z, Shen JH, Kozub JA, Prasad R, Lu P, Joos KM. Miniature forward-imaging B-scan optical coherence tomography probe to guide real-time laser ablation. *Laser Surg Med*. 2014; 46:193-202.
 32. Wong R, Jivraj J, Vuong B, Ramjist J, Dinn NA, Sun C, Huang Y, Smith JA, Yang VX. Development of an integrated optical coherence tomography-gas nozzle system for surgical laser ablation applications: Preliminary findings of *in situ* spinal cord deformation due to gas flow effects. *Biomed Opt Express*. 2015; 6:43-53.
 33. De Boer JF, Leitgeb R, Wojtkowski M. Twenty-five years of optical coherence tomography: the paradigm shift in sensitivity and speed provided by Fourier domain OCT [Invited]. *Biomed Opt Express*. 2017; 8:3248-3280.
 34. Fujimoto JG, Brezinski ME, Tearney GJ, Boppart SA, Bouma B, Hee MR, Southern JF, Swanson EA. Optical biopsy and imaging using optical coherence tomography. *Nat Med*. 1995; 1:970-972.
 35. Fujimoto JG, Pitris C, Boppart SA, Brezinski ME. Optical coherence tomography: An emerging technology for biomedical imaging and optical biopsy. *Neoplasia* 2000; 2:9-25.
 36. Liu G, and Chen Z. Optical coherence tomography for brain imaging. *Optical methods and Instrumentation in Brain Imaging and Therapy*. Springer New York, USA, 2013; pp. 285-290.
 37. Lopez WOC, Angelos JS, Martinez RCR, Takimura CK, Teixeira MJ, Lemos PA, Fonoff ET. Optical coherence tomography imaging of the basal ganglia: Feasibility and brief review. *Braz J Med Biol Res*. 2015; 48:1156-1159.
 38. Men J, Huang Y, Solanki J, Zeng X, Alex A, Jerwick J, Zhou C. Optical coherence tomography for brain imaging and developmental biology. *IEEE J Sel Top Quantum Electron*. 2016; 22: pii: 6803213.
 39. Bizheva K, Unterhuber A, Hermann B, Povazay B, Sattmann H, Drexler W, Stingl A, Le T, Mei M, Holzwarth R, Reitsamer HA, Morgan JE, Cowey A. Imaging *ex vivo* and *in vitro* brain morphology in animal models with ultrahigh resolution optical coherence tomography. *J Biomed Opt*. 2004; 9:719-724.
 40. Xie Y, Bonin T, Loeffler S, Huettmann G, Tronnier V, Hofmann UG. Fiber spectral domain optical coherence tomography for *in vivo* rat brain imaging. *Proc. SPIE*. 2010; 7715:77152F.
 41. Srinivasan VJ, Radhakrishnan H, Jiang JY, Barry S, Cable AE. Optical coherence microscopy for deep tissue imaging of the cerebral cortex with intrinsic contrast. *Opt Express*. 2012; 20:2220-2239.
 42. Choi WJ, Wang RK. Swept-source optical coherence tomography powered by a 1.3- μm vertical cavity surface emitting laser enables 2.3-mm-deep brain imaging in mice *in vivo*. *J Biomed Opt*. 2015; 20:106004.
 43. Lefebvre J, Castonguay A, Pouliot P, Descoteaux M, Lesage F. Whole mouse brain imaging using optical coherence tomography: Reconstruction, normalization, segmentation, and comparison with diffusion MRI. *Neurophotonics* 2017; 4:041501.
 44. Xie Y, Harsan LA, Bienert T, Kirch RD, Elverfeldt DV, Hofmann UG. Qualitative and quantitative evaluation of *in vivo* SD-OCT measurement of rat brain. *Biomed Opt Express*. 2017; 8:593-607.
 45. Eberle MM, Hsu MS, Rodriguez CL, Szu JI, Oliveira MC, Binder DK, Park BH. Localization of cortical tissue optical changes during seizure activity *in vivo* with optical coherence tomography. *Biomed Opt Express*. 2015; 6:1812-1827.
 46. Pan Y, You J, Volkow ND, Park K, Du C. Ultrasensitive detection of 3D cerebral microvascular network dynamics *in vivo*. *NeuroImage*. 2014; 103:492-501.
 47. Chong SP, Merkle CW, Cooke DF, Zhang T, Radhakrishnan H, Krubitzer L, Srinivasan VJ. Noninvasive, *in vivo* imaging of subcortical mouse brain regions with 1.7 μm optical coherence tomography. *Opt Lett*. 2015; 40:4911-4914.
 48. Atry F, Frye S, Richner TJ, Brodnick SK. Monitoring cerebral hemodynamics following optogenetic stimulation *via* optical coherence tomography. *IEEE Trans Biomed Eng*. 2015; 62:766-773.
 49. Srinivasan VJ, Mandeville ET, Can A, Blasi F, Climov M, Daneshmand A, Lee JH, Yu E, Radhakrishnan H, Lo EH, Sakadžić S, Eikermann-Haerter K, Ayata C. Multiparametric, longitudinal optical coherence tomography imaging reveals acute injury and chronic recovery in experimental ischemic stroke. *Plos One*. 2013; 8:e71478-e71478.
 50. Baran U, Zhu W, Choi WJ, Omori M, Zhang W, Alkayed NJ, Wang RK. Automated segmentation and enhancement of optical coherence tomography- acquired images of rodent brain. *J Neurosci Methods*. 2016; 270:132-137.
 51. Jia Y, Wang RK. Optical micro-angiography images structural and functional cerebral blood perfusion in mice with cranium left intact. *J Biophotonics*. 2011; 4:57-63.
 52. Yaseen MA, Srinivasan VJ, Gorczynska I, Fujimoto JG, Boas DA, Sakadžić S. Multimodal optical imaging system for *in vivo* investigation of cerebral oxygen delivery and energy metabolism. *Biomed Opt Express*. 2015; 6:4994-5007.
 53. Yashin KS, Karabut MM, Fedoseeva VV, Khalansky AS, Matveev LA, Elagin VV, Kuznetsov SS, Kiseleva EB, Kravets LYa, Medyanik IA, Gladkova ND. Multimodal optical coherence tomography in visualization of brain tissue structure at glioblastoma (experimental study). *Sovremennye Tehnologii V Medicine*. 2016; 8:73-81.
 54. Baran U, Wang RK. Review of optical coherence tomography based angiography in neuroscience. *Neurophoton*. 2016; 3:010902.
 55. Wenz H, Al-Zghloul M, Hart E, Kurth S, Groden C, Förster A. Track-density imaging of the human brainstem for anatomic localization of fiber tracts and nerve nuclei *in vivo*: Initial experience with 3-T magnetic resonance imaging. *World Neurosurg*. 2016; 93:286-292.
 56. Wang H, Zhu J, Akkin T. Serial optical coherence scanner for large-scale brain imaging at microscopic resolution. *Neuroimage*. 2014; 84:1007-1017.
 57. Wang H, Black AJ, Zhu J, Stigen TW, Al-Qaisi MK, Netoff TI, Abosch A, Akkin T. Reconstructing micrometer-scale fiber pathways in the brain: Multi-contrast optical coherence tomography based tractography. *Neuroimage*. 2011; 58:984-992.
 58. Wang H, Zhu J, Reuter M, Vinke LN, Yendiki A, Boas DA, Fischl B, Akkin T. Cross-validation of serial optical coherence scanning and diffusion tensor imaging: A

- study on neural fiber maps in human medulla oblongata. *Neuroimage*. 2014; 100:395-404.
59. Wang H. Multi-contrast optical coherence tomography for brain imaging and mapping. <https://search.proquest.com/docview/1627154053?pq-origsite=gscholar> (accessed October 8, 2017).
 60. Arous JB, Binding J, Léger JF, Casado M, Topilko P, Gigan S, Boccara AC, Bourdieu L. Single myelin fiber imaging in living rodents without labeling by deep optical coherence microscopy. *J Biomed Opt*. 2011; 16:116012.
 61. Nakaji H, Kouyama N, Muragaki Y, Kawakami Y, Iseki H. Localization of nerve fiber bundles by polarization-sensitive optical coherence tomography. *J Neurosci Methods*. 2008; 174:82-90.
 62. Wang H, Akkin T, Magnain C, Wang R, Dubb J, Kostis WJ, Yaseen MA, Cramer A, Sakadžić S, Boas D. Polarization sensitive optical coherence microscopy for brain imaging. *Opt Lett*. 2016; 41:2213-2216.
 63. Henry FP, Wang Y, Rodriguez CL, Randolph MA, Rust EA, Winograd JM, de Boer JF, Park BH. *In vivo* optical microscopy of peripheral nerve myelination with polarization sensitive-optical coherence tomography. *J Biomed Opt*. 2015; 20:1-7.
 64. Boppart SA, Brezinski ME, Pitris CM, Fujimoto JG. Optical coherence tomography for neurosurgical imaging of human intracortical melanoma. *Neurosurgery*. 1998; 43:834-841.
 65. Bizheva K, Unterhuber A, Hermann B, Povazay B, Sattmann H, Fercher AF, Drexler W, Preusser M, Budka H, Stingl A, Le T. Imaging *ex vivo* healthy and pathological human brain tissue with ultra-high-resolution optical coherence tomography. *J Biomed Opt*. 2005; 10:011006.
 66. Böhringer HJ, Boller D, Leppert J, Knopp U, Lankenau E, Reusche E, Hüttmann G, Giese A. Time-domain and spectral-domain optical coherence tomography in the analysis of brain tumor tissue. *Laser Surg Med*. 2006; 38:588-597.
 67. Böhringer HJ, Lankenau E, Stellmacher F, Reusche E, Hüttmann G, Giese A. Imaging of human brain tumor tissue by near-infrared laser coherence tomography. *Acta Neurochir (Wien)*. 2009; 151:507-517.
 68. Böhringer HJ, Lankenau E, Rohde V, Hüttmann G, Giese A. Optical coherence tomography for experimental neuroendoscopy. *Minim Invasive Neurosurg*. 2006; 49:269-275.
 69. Vuong B, Skowron P, Kiehl TR, Kyan M, Garzia L, Sun C, Taylor MD, Yang VX. Measuring the optical characteristics of medulloblastoma with optical coherence tomography. *Biomed Opt Express*. 2015; 6:1487-1501.
 70. Assayag O, Grieve K, Devaux B, Harms F, Pallud J, Chretien F, Boccara C, Varlet P. Imaging of non-tumorous and tumorous human brain tissues with full-field optical coherence tomography. *Neuroimage Clin*. 2013; 2:549-557. <http://www.lltechimaging.com/> (accessed October 8, 2017).
 71. Mathews MS, Su J, Heidari E, Levy EI, Linskey ME, Chen Z. Neuroendovascular optical coherence tomography imaging and histological analysis. *Neurosurgery*. 2011; 69:430-439.
 72. Finke M, Kantelhardt S, Schlaefer A, Bruder R, Lankenau E, Giese A, Schweikard A. Automatic scanning of large tissue areas in neurosurgery using optical coherence tomography. *Int J Med Robot*. 2012; 8:327-336.
 73. Kang JU, Han JH, Liu X, Zhang K, Song CG, Gehlbach P. Endoscopic functional fourier domain common-path optical coherence tomography for microsurgery. *IEEE J Sel Top Quantum Electron*. 2010; 16:781-792.
 74. Gora M, Suter M, Tearney G, and Li X. Endoscopic optical coherence tomography: Technologies and clinical applications (Invited). *Biomed Opt Express*. 2017; 8:2405-2444.
 75. Song C, Gehlbach PL, Kang JU. Active tremor cancellation by a "Smart" handheld vitreoretinal microsurgical tool using swept source optical coherence tomography. *Opt Express*. 2012; 20:23414-23421.
 76. Liang CP, Wierwille J, Moreira T, Schwartzbauer G, Jafri MS, Tang CM, Chen Y. A forward-imaging needle-type OCT probe for image guided stereotactic procedures. *Opt Express*. 2011; 19:26283-26294.
 77. Liang CP. Optical coherence tomography for neurosurgery and cancer research. 2014. https://drum.lib.umd.edu/bitstream/handle/1903/15325/Liang_umd_0117E_15136.pdf?sequence=1&isAllowed=y (accessed October 8, 2017).
 78. Sun C, Lee KKC, Vuong B, Cusimano M, Brukson A, Mariampillai A, Standish BA, Yang VX. Neurosurgical hand-held optical coherence tomography (OCT) forward-viewing probe. *Proc. SPIE 8207, Photonic Therapeutics and Diagnostics VIII*. 2012; 82074V. <http://dx.doi.org/10.1117/12.909116>
 79. Giese A, Böhringer HJ, Leppert J, Kantelhardt SR, Lankenau E, Koch P, et al. Non-invasive intraoperative optical coherence tomography of the resection cavity during surgery of intrinsic brain tumors-art. *Proceedings of SPIE-The International Society for Optical Engineering*. 2006; 6078:60782Z- 60782Z-8. <http://dx.doi.org/10.1117/12.674436>.
 80. Kut C, Chaichana KL, Xi J, Raza SM, Ye X, McVeigh ER, Rodriguez FJ, Quiñones-Hinojosa A, Li X. Detection of human brain cancer infiltration *ex vivo* and *in vivo* using quantitative optical coherence tomography. *Sci Transl Med*. 2015; 7:292ra100.
 81. Yuan W, Kut C, Liang W, and Li X. Robust and fast characterization of OCT-based optical attenuation using a novel frequency-domain algorithm for brain cancer detection. *Sci Rep*. 2017; 7:4490.
 82. Xi J, Chen Y, Li X. Characterizing optical properties of nano contrast agents by using cross-referencing OCT imaging. *Biomed Opt Express*. 2013; 4:842-851.
 83. Moiseev A, Snopova L, Kuznetsov S, Buyanova N, Elagin V, Sirotkina M, Kiseleva E, Matveev L, Zaytsev V, Feldchtein F, Zagaynova E, Gelikonov V, Gladkova N, Vitkin A, Gelikonov G. Pixel classification method in optical coherence tomography for tumor segmentation and its complementary usage with OCT microangiography. *J Biophotonics*. 2017; doi: 10.1002/jbio.201700072.
 84. Yücel D, Themstrup L, Manfredi M and Jemec, GBE. Optical coherence tomography of basal cell carcinoma: Density and signal attenuation. *Skin Res Technol*. 2016; 22:497-504.
 85. Marvdashti T, Duan L, Aasi SZ, Tang JY, and Bowden AKE. Classification of basal cell carcinoma in human skin using machine learning and quantitative features captured by polarization sensitive optical coherence tomography. *Biomed Opt Express*. 2016; 7, 3721-3735.
 86. Zhang K and Kang JU. Real-time intraoperative 4D full-range FD-OCT based on the dual graphics processing units architecture for microsurgery guidance. *Biomed Opt Express*. 2011; 2, 764-770.
 87. Garzon-Muvdi T, Kut C, Li X, and Chaichana KL.

- Intraoperative imaging techniques for glioma surgery. *Future Oncol.* 2017; 13:1731-1745.
89. Sun C, Khan OH, Siegler P, Jivraj J, Wong R, Yang VXD. Cadaveric in-situ testing of optical coherence tomography system-based skull base surgery guidance. *Proc. SPIE 9305, Optical Techniques in Neurosurgery, Neurophotonics, and Optogenetics II.* 2015; 930507. doi: 10.1117/12.2080614.
 90. Liang CP, Yang B, Kim IK, Makris G, Desai JP, Gullapalli RP, Chen Y. Concurrent multiscale imaging with magnetic resonance imaging and optical coherence tomography. *J Biomed Opt.* 2013; 18:046015.
 91. Lee D, Lee C, Kim S, Zhou Q, Kim J, Kim C. *In vivo* near infrared virtual intraoperative surgical photoacoustic optical coherence tomography. *Sci Rep.* 2016; 6:35176.
 92. Farooq H, Genis H, Alarcon J, Vuong B, Jivraj J, Yang VX, Cohen-Adad J, Fehlings MG, Cadotte DW. High-resolution imaging of the central nervous system: How novel imaging methods combined with navigation strategies will advance patient care. *Prog Brain Res.* 2015; 218:55-78.
 93. Finke M, Kantelhardt S, Schlaefer A, Bruder R, Lankenau E, Giese A, Schweikard A. Automatic scanning of large tissue areas in neurosurgery using optical coherence tomography. *Int J Med Robot.* 2012; 8:327-336.
 94. Lankenau E, Klinger D, Winter C, Malik A, Müller HH, Oelckers S, et al. Combining optical coherence tomography (OCT) with an operating microscope. *Adv Med Eng.* 2007; 343-348.
 95. Kantelhardt SR, Finke M, Schweikard A, Giese A. Evaluation of a completely robotized neurosurgical operating microscope. *Neurosurgery.* 2013; 72 Suppl 1:19-26.
 96. Wang L, Zhao H, Cui K, Yao L, Ren M, Hao A, Hao A, Smollen P, Nie F, Jin G, Liu Q, Wong ST. Identification of novel small-molecule inhibitors of glioblastoma cell growth and invasion by high-throughput screening. *Biosci Trends.* 2012; 6:192-200.
 97. Palanker DV, Blumenkranz MS, Andersen D, Wiltberger M, Marcellino G, Gooding P, Angeley D, Schuele G, Woodley B, Simoneau M, Friedman NJ, Seibel B, Batlle J, Feliz R, Talamo J, Culbertson W. Femtosecond laser-assisted cataract surgery with integrated optical coherence tomography. *Sci Transl Med.* 2010; 2:3879-3890.
 98. Matthias B, Zabic M, Brockmann D, Krüger A, Ripken T. Adaptive optics assisted and optical coherence tomography guided fs-laser system for ophthalmic surgery in the posterior eye. *J Biomed Opt.* 2016; 21:121512.
 99. Tsai MT, Tsai TY, Shen SC, Ng CY, Lee YJ, Lee JD and Yang CH. Evaluation of laser-assisted trans-nail drug delivery with optical coherence tomography. *Sensors* (Basel). 2016; 16: pii: E2111.
 100. Haruna M, Konoshita R, Ohmi M, Kunizawa N, and Miyachi M. *In-situ* tomographic observation of tissue surface during laser ablation. *Proc. SPIE 4257, Laser-Tissue Interaction XII: Photochemical, Photothermal, and Photomechanical.* 2001; 329. <http://dx.doi.org/10.1117/12.434717>.
 101. Ohmi M, Tanizawa M, Fukunaga A, Haruna M. *In-situ* observation of tissue laser ablation using optical coherence tomography. *Optical and Quantum Electronics.* 2005; 37:1175-1183.
 102. Ohmi M, Ohnishi M, Takada D and Haruna M. Dynamic analysis of laser ablation of biological tissue using real-time optical coherence tomography. *Meas Sci Technol.* 2010; 21:094030 (7pp). doi:10.1088/0957-0233/21/9/094030.
 103. Ohmi M, Ohnishi M, Takada D and Haruna M. Real-time OCT imaging of laser ablation of biological tissue. *Proc. SPIE 7562, Optical Interactions with Tissues and Cells XXI.* 2010; 756210. <file:///C:/Users/TU-TKW/Desktop/756210.pdf> (accessed October 8, 2017).
 104. Ohmi M, and Haruna M. Dynamic analysis of laser ablation of biological tissue by optical coherence tomography. *Lasers-Applications in Science and Industry. InTech,* 2011, pp 215-228. http://cdn.intechopen.com/pdfs/24746/InTech-Dynamic_analysis_of_laser_ablation_of_biological_tissue_by_optical_coherence_tomography.pdf (accessed October 8, 2017).
 105. Katta N, McElroy AB, Estrada AD and Milner TE. Optical coherence tomography image-guided smart laser knife for surgery. *Lasers Surg Med.* 2017; doi: 10.1002/lsm.22705.
 106. Katta N, Rector JA, Gardner MR, McElroy AB, Choy KC, Crosby C, Zoldan J, Milner TE. Image-guided smart laser system for precision implantation of cells in cartilage. *Proc. SPIE 10135, Medical Imaging 2017: Image-Guided Procedures, Robotic Interventions, and Modeling.* 2017; 101350V. <http://dx.doi.org/10.1117/12.2253812>.
 107. Kim B, Kim DY. Enhanced tissue ablation efficiency with a mid-infrared nonlinear frequency conversion laser system and tissue interaction monitoring using optical coherence tomography. *Sensors* (Basel). 2016;16: pii: E598.
 108. Fan Y, Zhang B, Chang W, Zhang X, Liao H. A novel integration of spectral-domain optical-coherence-tomography and laser-ablation system for precision treatment. *Int J Comput Assist Radiol Surg.* 2017; doi: 10.1007/s11548-017-1664-8.

(Received October 10, 2017 Revised December 12, 2017; Accepted December 14, 2017)

Association of biobehavioral factors with non-coding RNAs in cervical cancer

Qiyu Liu^{1,§}, Chong Lu^{1,§}, Wanjun Dai^{1,§}, Ke Li¹, Jing Xu¹, Yunke Huang¹, Guiling Li^{1,2,3}, Yu Kang^{1,2,3,*}, Anil K. Sood^{4,*}, Congjian Xu^{1,2,3,*}

¹Department of Obstetrics and Gynecology of Shanghai Medical School, Fudan University, Shanghai, China;

²Department of Integrated Traditional Chinese and Western Medicine, Obstetrics and Gynecology Hospital, Fudan University, Shanghai, China;

³Shanghai Key Laboratory of Female Reproductive Endocrine Related Diseases, Shanghai, China;

⁴Departments of Gynecologic Oncology, Cancer Biology, and Center for RNA Interference and Noncoding RNA, University of Texas, M.D. Anderson Cancer Center, TX, United States.

Summary

In order to elucidate the mechanisms underlying the biobehavioral factors responsible for cervical cancer from the perspective of lncRNAs. Tumor samples were obtained from patients with stage Ib-IIb squamous cervical cancer, which were divided into high- and low-risk groups according to biobehavioral risk factors. A lncRNA + mRNA microarray was performed, and the results were validated using qRT-PCR. Gene ontology (GO), pathway, and lncRNA-mRNA co-expression analysis were performed to predict the potential functions of the differentially expressed transcripts. 1,621 lncRNAs and 1,345 mRNAs were found to be differentially expressed between the high-risk and low-risk groups. The results of the qRT-PCR validation were in 100% agreement with the microarray analysis results. GO analysis revealed that the transcripts showing significantly different expression were mainly associated with various aspects of immune response. Pathway analysis indicated that systemic lupus erythematosus signaling was the most significantly down-regulated pathway in the high-risk group. Co-expression analysis indicated NONHSAT002712, NONHSAT095060, and TCONS_00026535 had significant correlations with ZNF683 and BTLA, which were found to be associated with the GO term "adaptive immune response". The levels of genome-wide lncRNAs are significantly altered in cervical tumors from patients with higher biobehavioral risk factors.

Keywords: Cervical cancer, biobehavioral factor, psychoimmunology, adaptive immune response

1. Introduction

Cervical cancer is the second most commonly diagnosed cancer and the third leading cause of cancer

death among females in developing countries. Among the females diagnosed with cervical cancer, many are diagnosed at the advanced stages of the disease where they have limited treatment options and show poor prognosis (1). There were an estimated 98,900 new cervical cancer cases and 30,500 related deaths in China in 2015 (2).

Cervical cancer patients experience significantly more depression and anxiety than the general population (3). Women who receive results of an abnormal Pap smear or a positive HPV DNA test may often experience unwarranted fear, distress, and anxiety about cervical cancer (4). A recent analysis indicates that 25.7% of early stage cervical cancer (ECC) cases and 22.2% of locally advanced cervical cancer (LACC) cases have elevated anxiety levels (5).

[§]These authors contributed equally to this work.

*Address correspondence to:

Drs. Yu Kang and Congjian Xu, Department of Obstetrics and Gynecology of Shanghai Medical School, Fudan University, 413 Zhaozhou Road, Shanghai 200011, China.
E-mail: yukang@fudan.edu.cn (Kang Y), xucongjian@fudan.edu.cn (Xu CJ)

Dr. Sood AK, Departments of Gynecologic Oncology, Cancer Biology, and Center for RNA Interference and Noncoding RNA, University of Texas, M.D. Anderson Cancer Center, 1515 Holcombe Blvd, Houston, TX 77030, United States.
E-mail: asood@mdanderson.org

In addition, cervical cancer survivors are more likely to have a lower quality of life (QOL) and higher levels of depression and anxiety (26% and 28%, respectively) compared to other cancer survivors (6).

Biobehavioral factors such as depression, anxiety, and stressful life events have long been suspected to underlie cancer progression (7). Animal studies have also revealed that behavioral stress can promote the progression of ovarian cancer, breast cancer, pancreatic cancer, and several other types of malignant tumors (8,9). The mechanisms underlying the effects of biobehavioral stress on cancer progression have been studied through psychoneuroimmunology (7,10), and these studies have shown that biobehavioral factors influence the neuroendocrine regulation of hormones (*i.e.*, catecholamine neurotransmitters, dopamine, adrenaline, and noradrenaline), which may impair the immune response and contribute to cancer onset and development.

Long noncoding RNAs (lncRNAs) are transcripts longer than 200 nucleotides with no apparent protein-coding role. lncRNAs are involved in numerous important biological processes such as chromatin modification, genomic imprinting, and enzymatic activity regulation (11). The overexpression, deficiency, or mutation of lncRNAs has been implicated in various malignant tumors and other human diseases (12). However, few studies have evaluated the changes and potential functions of lncRNAs in cervical cancer patients experiencing higher psychological stress.

In the current study, we performed a high-throughput analysis to compare the lncRNA and mRNA expression profiles between high- and low-psychological stress cervical cancer groups. Our aim was to discover the mechanisms underlying the potential psychoimmunological effects of behavioral stress on cervical cancer from the perspective of lncRNAs. Our findings provide new insights into the psychological epidemiology of cervical cancer.

2. Materials and Methods

2.1. Patients

Women older than 18 years of age with an abnormal Pap test result suspected for cervical carcinoma were determined to be potentially eligible for this study. The study inclusion was confirmed after the histologic diagnosis of squamous cell carcinoma of the uterine cervix. Patients with a previous cancer diagnosis, regular use of a systemic steroidal medication in the last 4 months, comorbidities known to alter the immune response (such as autoimmune diseases), or the inability to accurately answer questions were excluded. This study was approved by the Ethics Committee of the Obstetrics and Gynecology Hospital affiliated to Fudan University.

2.2. Psychological measures

2.2.1. Depression

Depressive symptoms were assessed using the Center for Epidemiologic Studies Depression Scale (CESD) and the Zung's Self-rating Depression Scale (SDS). The CESD is a validated 20-item scale that assesses depressive symptoms occurring in the prior week. Scores of 16 or higher indicate a high biobehavioral risk (13). Four subscales of CESD have been confirmed by factor analysis: depressed affect, vegetative depression, positive affect, and interpersonal relationships. On the other hand, the SDS is a 20-item self-reported scale that assesses psychological and somatic symptoms of depression. Cut-off scores for the SDS were as follows: < 50 = normal, 50 to 59 = mild depression, 60 to 69 = moderate depression, and > 69 = severe depression (14).

2.2.2. Social support

Social support was assessed by the Chinese version of the Social Support Rating Scale (SSRS), which demonstrates good validity and reliability among Chinese populations (15). The SSRS consists of ten items that measure three dimensions of social support: objective support, subjective support, and support utilization.

2.2.3. Anxiety

The Zung's Self-rating Anxiety Scale (SAS) was used to quantify the level of anxiety (16). The self-reported questionnaire contained 20 items. Cut-off scores were as follows: < 45 = normal, 45 to 59 = mild to moderate anxiety, 60 to 74 = marked to severe anxiety, and > 75 = extreme anxiety.

2.2.4. Sleep quality

The Pittsburgh Sleep Quality Index (PSQI) is a 19-item self-reported questionnaire used to assess the type and frequency of sleep disturbances occurring in the prior month (17). A global score greater than 5 indicated poor sleep.

2.3. Tissue collection and RNA extraction

Six cervical carcinoma samples were harvested during the laparoscopic surgery from each study participant. All the samples were rapidly frozen in liquid nitrogen, followed by storage at -80°C. Total RNA was extracted from the frozen tumor tissues using the mirVana RNA Isolation Kit (Ambion). RNA concentration and purity were then determined using the NanoDrop ND-2000 Spectrophotometer (Thermo Fisher Scientific). RNA integrity was determined by standard denaturing

agarose gel electrophoresis.

2.4. Microarray analysis

Total RNA was labeled using the Quick-Amp Labeling Kit, One-Color (Agilent Technologies) and hybridized onto the Agilent Human lncRNA Array (4*180K). The chip detected 46506 human lncRNAs and 30656 human mRNAs. Hybridization signals were detected using the Microarray Scanner (Agilent p/n G2505C). Agilent Feature Extraction Software was utilized to extract the raw data. Quantile normalization and subsequent processing of the data were carried out using GeneSpring Software version 12.0 (Agilent Technologies). Differentially expressed genes were defined as those with an absolute value of fold change (FC) > 2 and a *p*-value < 0.05 (Student's *t*-test). Microarray profiling was performed by OE Biotech, Shanghai, China.

2.5. Quantitative real-time PCR assay

Total RNA was reverse transcribed into cDNA using the PrimerScript RT Kit with gDNA Eraser (Takara, Shiga, Japan) according to the manufacturer's standard protocols. Quantitative real-time PCR (qRT-PCR) was performed on an Applied Biosystems Vii™ A7 System (Life Technologies, Tokyo, Japan). Each 20- μ L reaction contained 10 μ L of SYBR Premix Ex Taq II (2 \times) (Takara), 2 μ L of cDNA, 0.8 μ L of the forward primer, 0.8 μ L of the reverse primer, and 6 μ L of dH₂O. The PCR cycling conditions were as follows: incubation at 95°C for 10 min, followed by 40 cycles at 95°C for 10 s and 60°C for 30 s. Each sample was run in triplicate for analysis. Melting curve analysis was performed to validate the specificity of each PCR product. The expression levels of the mRNAs and lncRNAs were normalized to the GAPDH level and calculated using the 2^{- $\Delta\Delta$ Ct} method.

2.6. Gene ontology and pathway analysis

Gene Ontology (GO) analysis and Kyoto Encyclopedia of Genes and Genomes (KEGG) pathway analysis were used to determine the potential roles of the differentially expressed mRNAs. GO analysis (<http://geneontology.org/>) provides three-structured networks of defined terms that describe genes and their properties, which includes information on their biological processes, cellular components, and molecular functions. We also adopted the KEGG pathway (<http://www.genome.jp/kegg/>) to predict the biological functions of the target genes.

2.7. Construction of the lncRNA–mRNA co-expression network

The lncRNA-mRNA co-expression network was constructed to explore the relationship between the

lncRNAs and mRNAs. For each pair of genes, the Pearson correlation coefficient (PCC) was calculated, and the pairs with significant correlations (PCC > 0.90) were chosen to construct the network. Cytoscape Software version 3.4.0 (U.S. National Institute of General Medical Sciences) was used to illustrate the co-expression network.

3. Results

3.1. Patient characteristics

Six squamous cervical carcinoma patients who had undergone primary surgical resection between November 2014 and September 2015 were enrolled in this study. The clinical characteristics of the patients are shown in Supplementary Table S1 (<http://www.biosciencetrends.com/action/getSupplementalData.php?ID=18>). All the tumor samples were confirmed to be stage Ib1-IIb squamous cervical carcinomas.

Psychological factors were measured during the pre-surgical clinic visits 1 to 7 days prior to tumor resection. Based on the established threshold of CESD \geq 16, three participants were determined to show high levels of psychological risk factors. The only measured property that differed significantly between the two groups was the level of depressive scores (CESD, *p* = 0.0327; SDS, *p* = 0.0399).

3.2. LncRNA and mRNA expression profiles

Using a 2 or 0.5-fold change as the cut-off, a total of 1,621 lncRNAs were found to be differentially expressed between the high-risk and low-risk groups; of these, 510 were up-regulated and 1,111 were down-regulated in the high-risk group (Supplementary Table S2, <http://www.biosciencetrends.com/action/getSupplementalData.php?ID=19>). Table 1 shows the top ten up-regulated and down-regulated lncRNAs. Using the same criteria, we found 1,345 mRNAs showing differential expression between the high-risk and low-risk groups; of these, 325 were up-regulated and 1,020 were down-regulated in the high-risk group (Supplementary Table S3, <http://www.biosciencetrends.com/action/getSupplementalData.php?ID=20>). The top ten up-regulated and down-regulated mRNAs are listed in Table 2. The volcano plot of the differentially expressed lncRNAs and mRNAs is shown in Supplementary Figure S1 (<http://www.biosciencetrends.com/action/getSupplementalData.php?ID=21>). Hierarchical clustering analysis was performed to categorize the lncRNAs and mRNAs based on their expression levels in the microarray (Figure 1).

3.3. Quantitative real-time PCR validation

To validate the microarray results by real-time PCR

Table 1. Top ten up-regulated and down-regulated lncRNAs in the high-risk group

lncRNAs	Source database	Fold change (up-regulated)	Fold change (down-regulated)	P-value
NONHSAT026375	NONCODE v4	83.38818		0.004714203
NONHSAG051449	NONCODE v4	56.622337		0.007290442
NONHSAT006501	NONCODE v4	54.330788		0.028635195
NR_040072.1	RefSeq	29.504402		0.00305648
NR_045603.1	RefSeq	21.908543		0.034243103
NONHSAT029137	NONCODE v4	16.355997		0.001712117
NONHSAT142855	NONCODE v4	15.255895		0.00395211
NONHSAT006296	NONCODE v4	13.86696		0.044070113
NONHSAT026373	NONCODE v4	13.66836		0.049752276
NONHSAT029135	NONCODE v4	12.5354595		0.00199061
NONHSAT097055	NONCODE v4		21.751446	0.008822498
NONHSAT059677	NONCODE v4		20.691536	0.025407365
NONHSAT130141	NONCODE v4		20.616901	0.00182173
TCONS_12_00010069	broadlincRNA		19.297148	0.001462107
TCONS_12_00010131	broadlincRNA		18.281479	0.038280915
NONHSAT145020	NONCODE v4		15.2914095	0.004498216
NONHSAT029287	NONCODE v4		15.215009	0.014417922
NONHSAT040550	NONCODE v4		14.950378	0.014418174
NONHSAT026886	NONCODE v4		14.94323	0.002577477
NONHSAG023913	NONCODE v4		14.099488	0.005995478

Table 2. Top ten up-regulated and down-regulated mRNAs in the high-risk group

lncRNAs	Fold change (up-regulated)	Fold change (down-regulated)	P-value
SPRR1A	68.54885		0.037800513
A2ML1	47.889496		0.01010738
VTCN1	47.843727		0.012803975
PSCA	38.76277		0.001021038
SH3BGRL2	25.990252		0.01292145
MLPH	20.98717		1.38E-04
POF1B	18.330408		0.03179252
RHCG	17.668486		0.025924051
DNAH14	15.095662		0.011291295
FAM189A2	12.6118145		0.041048728
SLC44A5		63.488415	9.77E-04
CXCL13		22.780071	0.004740034
GLDC		22.185339	0.002045446
CXCL11		18.150942	0.019471126
ELAVL2		14.732332	0.020086708
IFNG		13.957739	0.007875251
KLRC3		12.96415	0.001003543
MMP7		12.581658	0.027674025
UBD		12.484317	0.04345015
IL12RB2		12.357619	0.010752848

quantification, we selected three mRNAs and two lncRNAs from the six cervical cancer samples that were subjected to the microarray analysis. The qRT-PCR results showed that the expression of lncRNA NONHSAT097055 and the CCL5, CXCL9, and HIST1H2AM mRNAs was significantly decreased (p -values for all < 0.05) in the high-risk samples compared to that in the low-risk samples. By contrast, the expression of lncRNA NONHSAT029137 was significantly increased in the high-risk group ($p < 0.05$) (Figure 2). The qRT-PCR results were consistent with those obtained from the microarray analysis, thus confirming the microarray results.

3.4. Gene enrichment and pathway analysis

GO analysis was performed for all the differentially expressed mRNAs to identify the potential functions of their coding transcripts. We found that the mRNAs showing significant differential expression between the high-risk and low-risk groups were mainly associated with the immune response (GO:0006955), adaptive immune response (GO:0002250), regulation of immune response (GO:0050776), protein heterodimerization activity (GO:0046982), and transmembrane signaling receptor activity (GO:0004888), which are all involved in various biological processes and molecular functions.

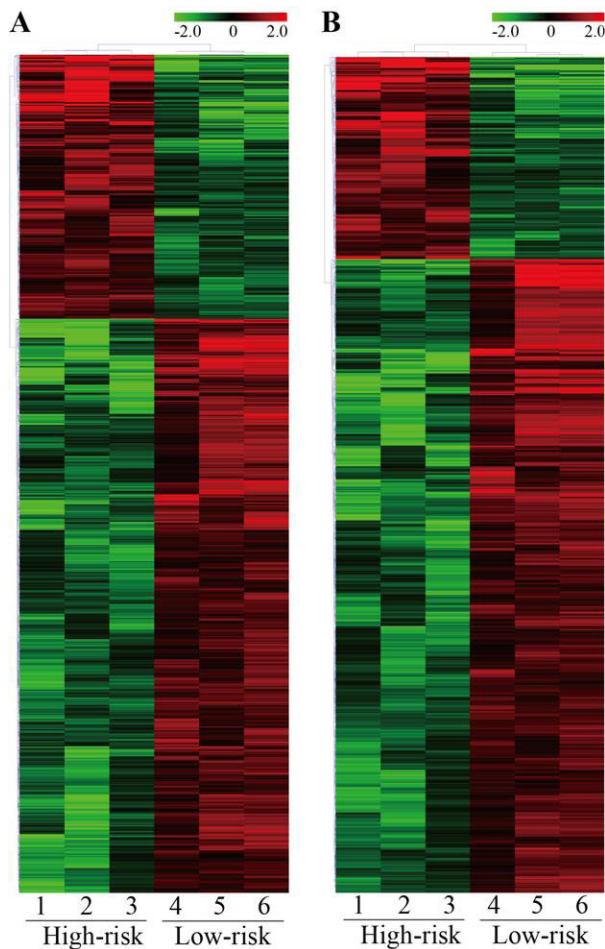


Figure 1. Heat map and hierarchical clustering of the differentially expressed lncRNAs (A) and mRNAs (B) in the high-risk and low-risk groups. The red and green bars indicate the expression levels above and below the relative expression across all the samples.

The detailed results are presented in Figures 3 A-C.

KEGG pathway analysis indicated that the most significantly enriched pathways consisted of those that regulate systemic lupus erythematosus (hsa05322), antigen processing and presentation (hsa04612), and natural killer (NK) cell mediated cytotoxicity (hsa04650). The top 20 enriched pathways of the differentially expressed mRNAs are shown in Figure 3 D.

3.5. Construction of the lncRNA-mRNA co-expression network

In order to investigate the correlation between the differentially expressed lncRNAs and mRNAs, the lncRNA-mRNA co-expression network was constructed. In total, 509 lncRNAs and 230 mRNAs were included in the co-expression network (Supplementary Table S4, <http://www.biosciencetrends.com/action/getSupplementalData.php?ID=22>). To draw the co-expression network, we selected several mRNAs that were found to be involved in the dysregulated functions and pathways in the GO and

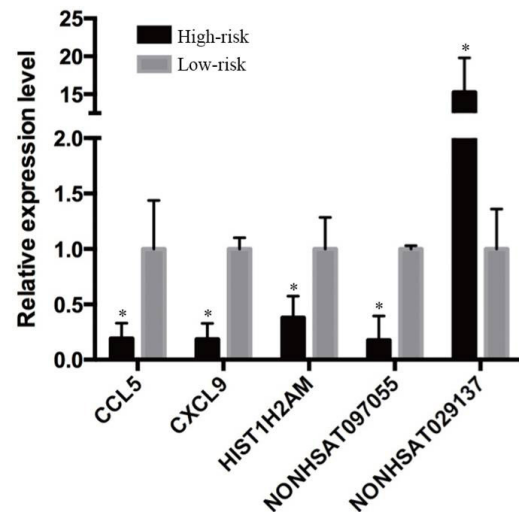


Figure 2. Validation of microarray data using quantitative real-time PCR. Three mRNAs (CCL5, CXCL9, and HIST1H2AM) and two lncRNAs (NONHSAT097055 and NONHSAT029137) were selected and analyzed by qRT-PCR to validate their expression levels. The relative expression level of the target mRNA/lncRNA was normalized, and data displayed in the histograms are expressed as means \pm standard deviation (SD), * $p < 0.05$ upon comparison between the high-risk and low-risk groups.

KEGG pathway analysis. As shown in Figure 4, 52 lncRNAs were found to interact with two mRNAs (CBL and PRKCQ) in the KEGG term of "T cell receptor signaling pathway" (A), 51 lncRNAs were found to interact with two mRNAs (CXCR5 and IL12B) in the KEGG term of "cytokine-cytokine receptor pathway" (B), and 39 lncRNAs were found to interact with two mRNAs (BTLA and ZNF683) in the GO term of "adaptive immune response" (C).

4. Discussion

In this study, we profiled the expression of lncRNAs and mRNAs in cervical cancer samples from patients with different psychological risk levels by microarray analysis. We found that 1,621 lncRNAs and 1,345 mRNAs were differentially expressed between the two groups. GO and KEGG pathway analysis was performed to predict the potential functions of the differentially expressed mRNAs. Moreover, we predicted the target genes of the differentially expressed lncRNAs by constructing lncRNA-mRNA co-expression networks. Based on our results, we predicted that some of the differentially expressed genes play important roles in the psychological stress-induced psychoimmunological effects on cervical cancer.

There are a substantial number of studies on the effects of the chronic activation of the stress response on the immune response associating with cancer initiation and progression (10). Psychological stress has been shown to suppress the non-specific and specific components of the immune response, such as antigen presentation, NK cell activity, T cell

proliferation, cytotoxic T cell activity, and production of inflammatory cytokines via mechanisms that involve adrenergic and glucocorticoid-mediated pathways (7).

Cancers caused by DNA tumor viruses might be more affected by psychological and immunological factors than those induced by chemical carcinogens (10). Researchers have identified persistent infection with a high-risk human papillomavirus (HPV) as the cause of over 99% of cervical cancers (18). Fang *et al.* also reported that higher levels of perceived stress are associated with impaired HPV-specific immune response in women with cervical dysplasia (19). Moreover, a recent clinical study showed that bereavement is associated with an increased risk of HPV infection and cervical cancer in Sweden (20). Stressful life events might also be associated with impaired immune surveillance and possibly poor control over HPV infection and thus increase the risk of cervical cancer.

The ZNF683 (Zinc finger protein 683) and BTLA (B and T Lymphocyte Associated) mRNAs were found to be associated with the GO term "adaptive immune response". ZNF683, also known as Hobit (Homolog of Blimp-1 in T cells), is a transcription factor that mediates a transcriptional program in tissue-resident memory T (Trm) and natural killer T (NKT) cells (21,22). Hobit mediates the development and retention of Trm cells and NKT cells in non-lymphoid organs and other nonbarrier tissues and may provide immediate immunological protection against re-infections. BTLA is an immunoglobulin-like molecule belonging to the B7 family, which relays inhibitory signals that suppress the immune response (23). Moreover, the interaction between BTLA and its ligand has been reported to be actively involved in the adaptive immune response (24). In our study, we constructed a lncRNA-mRNA co-expression network to predict the potential functions of the differentially expressed lncRNAs. Our results showed that several lncRNAs, such as NONHSAT002712, NONHSAT095060, and TCONS_00026535, had significant correlations with ZNF683 and BTLA, suggesting that these lncRNAs had roles in the regulation of the adaptive immune response.

The major limitation of this study is that the data were obtained from a small sample size. In the future, larger studies will be required to establish the generality of these findings. Nevertheless, this study is novel in that it identified genome-wide lncRNAs correlating with psychological stress specifically in cervical cancer tissues and thus provides new insights into the psychological epidemiology of cervical cancer.

Acknowledgements

This work was supported by the National Key Research and Development Program of China (2016YFC1303100, 2016YFC1303102), the National Natural Science Foundation of China (81472423),

Shanghai Municipal Health and Family Planning Commission (ZYKC201701020), and the Natural Science Foundation of Shanghai (14430723000).

References

1. Torre LA, Bray F, Siegel RL, Ferlay J, Lortet-Tieulent J, Jemal A. Lortet-Tieulent J, Jemal A. Global cancer statistics, 2012. *CA Cancer J Clin.* 2015; 65:87-108.
2. Chen W, Zheng R, Baade PD, Zhang S, Zeng H, Bray F, Jemal A, Yu XQ, He J. Cancer statistics in China, 2015. *CA Cancer J Clin.* 2016; 66:115-132.
3. Bradley S, Rose S, Lutgendorf S, Costanzo E, Anderson B. Quality of life and mental health in cervical and endometrial cancer survivors. *Gynecol Oncol.* 2006; 100:479-486.
4. Herzog TJ, Wright JD. The impact of cervical cancer on quality of life--the components and means for management. *Gynecol Oncol.* 2007; 107:572-577.
5. Mantegna G, Petrillo M, Fuoco G, Venditti L, Terzano S, Anchora LP, Scambia G, Ferrandina G. Long-term prospective longitudinal evaluation of emotional distress and quality of life in cervical cancer patients who remained disease-free 2-years from diagnosis. *BMC Cancer.* 2013;13:127.
6. Osann K, Hsieh S, Nelson EL, Monk BJ, Chase D, Cella D, Wenzel L. Factors associated with poor quality of life among cervical cancer survivors: implications for clinical care and clinical trials. *Gynecol Oncol.* 2014;135: 266-272.
7. Antoni MH, Lutgendorf SK, Cole SW, Dhabhar FS, Sephton SE, McDonald PG, Stefanek M, Sood AK. The influence of bio-behavioural factors on tumour biology: Pathways and mechanisms. *Nat Rev Cancer.* 2006; 6:240-248.
8. Thaker PH, Han LY, Kamat AA, *et al.* Chronic stress promotes tumor growth and angiogenesis in a mouse model of ovarian carcinoma. *Nat Med.* 2006; 12:939-944.
9. Cole SW, Nagaraja AS, Lutgendorf SK, Green PA, Sood AK. Sympathetic nervous system regulation of the tumour microenvironment. *Nat Rev Cancer.* 2015; 15:563-572.
10. Reiche EM, Nunes SO, Morimoto HK. Stress, depression, the immune system, and cancer. *Lancet Oncol.* 2004; 5:617-625.
11. Quinn JJ, Chang HY. Unique features of long non-coding RNA biogenesis and function. *Nat Rev Genet.* 2016; 17:47-62.
12. Esteller M. Non-coding RNAs in human disease. *Nat Rev Genet.* 2011; 12:861-874.
13. Ensel W. Measuring Depression: The CES-D Scale. In: Lin N, Dean A, Ensel W (eds): *Social Support, Life Events, and Depression.* New York:Academic Press, 1986; 51-70.
14. Zung WW, Magruder-Habib K, Velez R, Alling W. The comorbidity of anxiety and depression in general medical patients: a longitudinal study. *J Clin Psychiatry.* 1990; 51(Suppl):77-80; discussion 81.
15. Dai W, Chen L, Tan H, Wang J, Lai Z, Kaminga AC, Li Y, Liu A. Association between social support and recovery from post-traumatic stress disorder after flood: A 13-14 year follow-up study in unan, China. *BMC Public Health.* 2016; 16:194.
16. Zung WW. A rating instrument for anxiety disorders.

- Psychosomatics. 1971; 12:371-379.
17. Buysse DJ, Reynolds CF, Monk TH, Berman SR, Kupfer DJ. The pittsburgh sleep quality index: A new instrument for psychiatric practice and research. *Psychiatry Res.* 1989; 28:193-213.
 18. Moody CA, Laimins LA. Human papillomavirus oncoproteins: Pathways to transformation. *Nat Rev Cancer.* 2010;10:550-560.
 19. Fang CY, Miller SM, Bovbjerg DH, Bergman C, Edelson MI, Rosenblum NG, Bove BA, Godwin AK, Campbell DE, Douglas SD. Perceived stress is associated with impaired T-cell response to HPV16 in women with cervical dysplasia. *Ann Behav Med.* 2008; 35:87-96.
 20. Lu D, Sundström K, Sparén P, Fall K, Sjölander A, Dillner J, Helm NY, Adami HO, Valdimarsdóttir U, Fang F. Bereavement is associated with an increased risk of HPV infection and cervical cancer: An epidemiological study in Sweden. *Cancer Res.* 2016; 76:643-651.
 21. Mackay LK, Minnich M, Kragten NA, *et al.* Hobit and Blimp1 instruct a universal transcriptional program of tissue residency in lymphocytes. *Science.* 2016; 352: 459-463.
 22. Van Gisbergen KP, Kragten NA, Hertoghs KM, Wensveen FM, Jonjic S, Hamann J, Nolte MA, Van Lier RA. Mouse Hobit is a homolog of the transcriptional repressor Blimp-1 that regulates NKT cell effector differentiation. *Nat Immunol.* 2012; 13:864-871.
 23. Yang C, Chen Y, Guo G, Li H, Cao D, Xu H, Guo S, Fei L, Yan W, Ning Q, Zheng L, Wu Y. Expression of B and T lymphocyte attenuator (BTLA) in macrophages contributes to the fulminant hepatitis caused by murine hepatitis virus strain-3. *Gut.* 2013; 62:1204-1213.
 24. Derré L, Rivals JP, Jandus C, Pastor S, Rimoldi D, Romero P, Michielin O, Olive D, Speiser DE. BTLA mediates inhibition of human tumor-specific CD8⁺ T cells that can be partially reversed by vaccination. *J Clin Invest.* 2010; 120:157-167.

(Received December 29, 2017; Revised February 11, 2018; Accepted February 12, 2018)

Chromosomal karyotype in chorionic villi of recurrent spontaneous abortion patients

Yan Du^{1,2}, Lanting Chen^{2,3,4}, Jing Lin^{2,3,4}, Jun Zhu⁵, Na Zhang^{2,3,4}, Xuemin Qiu^{2,3,4}, Dajin Li^{2,3,4}, Ling Wang^{2,3,4,*}

¹Office of Clinical Epidemiology, Obstetrics and Gynecology Hospital of Fudan University, Shanghai, China;

²Laboratory for Reproductive Immunology, Hospital & Institute of Obstetrics and Gynecology, Fudan University Shanghai Medical College, Shanghai, China;

³The Academy of Integrative Medicine of Fudan University, Shanghai, China;

⁴Shanghai Key Laboratory of Female Reproductive Endocrine-related Diseases, Shanghai, China;

⁵Department of Obstetrics and Gynecology, Wenling People's Hospital, Wenzhou Medical University, Wenling, China.

Summary

Recurrent spontaneous abortion (RSA) is a multifactorial disease of which the exact causes are still unknown. In the current study, we aimed to analyze the distribution of abnormal embryonic karyotypes in RSA. 781 RSA patients of 17 hospitals in Shanghai from January 2014 to September 2016 were enrolled. Fetal villus tissues were collected during uterine curettage and then cultured in situ for karyotyping. All of the 781 cases were successfully cultured. There were 393 cases of abnormal karyotypes, accounting for 50.3% of the total cases. Women with abnormal embryonic karyotype were significantly older compared to those with normal karyotype ($P < 0.001$). The majority of patients with abnormal karyotype fell among age groups of 25-29 and 30-34. There were 247 cases of aneuploidy, accounting for 62.8% of the total abnormal karyotype cases. Autosomal trisomy was the primary form of aneuploidy (189/247, 76.5%), and the most common types were trisomy-16 ($n = 69$), trisomy-22 ($n = 28$), trisomy-21 ($n = 21$), trisomy-15 ($n = 15$), and trisomy-13 ($n = 10$). Abnormal karyotype is a major factor related to RSA. Further studies are needed to elucidate the etiology of RSA in order to achieve more effective prevention and treatment.

Keywords: Recurrent spontaneous abortion (RSA), fetal chorionic villi, karyotype, chromosomal abnormality

1. Introduction

Recurrent spontaneous abortion (RSA), also known as recurrent miscarriage, habitual abortion or recurrent pregnancy loss (RPL), is usually defined as at least two consecutive pregnancy losses prior to the 20th gestational week of pregnancy (1). The probability of couples of childbearing age affected by RSA has been estimated to approach 2-5%, and it varies according to different definitions and criteria (2). Most of these abortions occur prior to the 10th gestational week of pregnancy (3). The etiology of RSA has not been well elucidated

and may be multifactorial, as previous research has demonstrated that several factors may play roles in RSA, including uterine anomalies, chromosomal abnormalities in either partner, antiphospholipid syndrome (APS), thrombophilic disorders, endocrine factors, microbial infections, maternal diseases, and male factors such as sperm deformation and DNA fragmentation (1,2,4).

The majority (50-60%) of early pregnancy losses are caused by chromosomal abnormalities, which are either of parental origins or *de novo* abnormalities from parents with normal karyotypes (5,6). Embryonic aneuploidy, which increases significantly with advanced maternal age, accounts for a large portion of spontaneously abortus (5).

Previous studies have suggested that abnormal embryonic karyotype may contribute to RSA (7-11). *De novo* numerical abnormalities, particularly autosomal trisomies, may explain a proportion of RSA (10). There

*Address correspondence to:

Dr. Ling Wang, Hospital and Institute of Obstetrics and Gynecology, Fudan University, 413 Zhaozhou Road, Shanghai 200011, China.

E-mail: Dr.wangling@fudan.edu.cn

is also a notion that most chromosomal abnormalities occur *de novo*, probably led by random errors during gametogenesis (12). The current study aimed to analyze the distribution of abnormal embryonic karyotypes in RSA using the next generation sequencing techniques (NGS). The method of NGS enables detailed analysis of the entire genomic makeup of the fetus based on either a biopsy sample from the fetus directly or a blood sample from the pregnant women. Due to its high resolution, this method can provide information down to the smallest detail. Also, the broad coverage of this method enables obstetricians and gynecologists to identify even the very rare diseases associated with certain karyotypes. With the help of different databases (such as DECIPHER and ISCA), it is now possible to make more accurate diagnoses as well as predict prognoses for patients. Compared with the traditional chromosomal karyotyping method, NGS has obvious advantages in accuracy and coverage, therefore providing more detailed information about the sample, including etiology, risk stratification, molecular diagnosis and prognosis.

2. Materials and Methods

2.1. Study population

Patients who sought treatment for RSA between January 2014 and September 2016 at the following 17 hospitals in Shanghai were enrolled: Obstetrics and Gynecology Hospital of Fudan University, Shanghai First Maternity and Infant Hospital, Zhongshan Hospital, Renji Hospital of Shanghai Jiaotong University School of Medicine, Shuguang Hospital, Yueyang Hospital, Shanghai General Hospital, Shanghai Sixth People's Hospital, Shanghai Eighth People's Hospital, Shanghai Ninth People's Hospital, Shanghai Pudong Hospital, Central Hospital of Minhang District, Changning Maternity and Infant Health Hospital, Putuo Maternity and Infant Health Hospital, Jiading Maternity and Infant Health Hospital, Maternity and Infant Health Hospital of Pudong New District, Shanghai Institute of Planned Parenthood Research Hospital. A total of 781 patients were recruited for the current study.

The study protocol conformed to the ethical guidelines of the 2000 Declaration of Helsinki and was approved by the institutional review board at Obstetrics and Gynecology Hospital of Fudan University. All participants provided written informed consent.

2.2. DNA preparation and sequencing

Villus samples were collected from the aborted tissue. DNA from these samples was extracted using the QIAamp DSP DNA Mini Kit (Qiagen) according to the manufacturer's protocol. The extracted DNA was then digested using NEBNext dsDNA Fragments (NEB).

Library construction, quality control, and pooling were performed according to instructions of JingXin Fetal Chromosome Aneuploidy (T21, T18, T13) Testing Kits (CapitalBio Corporation, China). For DNA sequencing, 15~20 libraries were pooled and sequenced with ~200 bp reads using JingXin BioelectronSeq 4000 System semiconductor sequencer (CapitalBio Corporation).

2.3. Data extraction

Reads were aligned to the human genomic reference sequences (hg19) using the BWA (30). Reads, which were unmapped or had multiple primary alignment records were filtered by FLAG field in the alignment file, using an in-house Perl script. Duplicate reads were identified by Picard (<http://picard.sourceforge.net/>) and removed by an in-house Perl script. The remaining reads were considered unique reads for further analysis. To eliminate the effect of GC bias, we applied an integrated method for GC correction using a three-step process (LOESS regression, intrarun normalization, and linear model regression) according to Liao's paper (13). Combining the Z scores of adjacent 1Mb blocks would increase the precision to detect subchromosome aberrations using Stouffer's Z-score method (14). When Stouffer's Z score is larger than 5, we classify it as microduplication, whereas when it is less than -5, we classify it as microdeletion.

2.4. Statistical analysis

Age was compared using Student's *t* test as a continuous variable and Chi-square test as a categorical variable. All above analyses were two-sided and performed using EXCEL2007 and SPSS 16.0 (SPSS, Inc., Chicago, IL). A *P* value of < 0.05 was considered statistically significant.

3. Results

3.1. The demographics of patients

Of the 781 enrolled subjects, 388 (49.7%) abortuses had normal karyotype and 393 (50.3%) had abnormal karyotypes. Patients were from almost all parts of China, while most of them resided in metropolitan Shanghai, Zhejiang province, and Jiangsu province (Supplementary Table 1).

The age distribution of the subjects is shown in Table 1, and women with abnormal karyotypes were significantly older compared to women with normal karyotype ($P < 0.001$). Figure 1 shows the distribution of abnormal karyotypes among different age categories. The prevalence of abnormal embryonic karyotypes increased with age after age 25, although there was no significant difference detected across all age categories ($P = 0.136$).

Table 1. Age distribution of two groups

Age	Normal karyotype (n = 382)	Abnormal karyotype (n = 364)	P
Age (year), mean \pm SD	30.67 \pm 4.03	32.23 \pm 5.02	< 0.001
Age (year), median (range)	30 (21, 45)	32 (20, 45)	
Age category, n (%)			< 0.001
20-24	13 (3.4%)	11 (3.0%)	
25-29	156 (40.8%)	118 (32.4%)	
30-34	147 (38.5%)	122 (33.5%)	
35-39	54 (14.1%)	76 (20.9%)	
\geq 40	12 (3.1%)	37 (10.2%)	

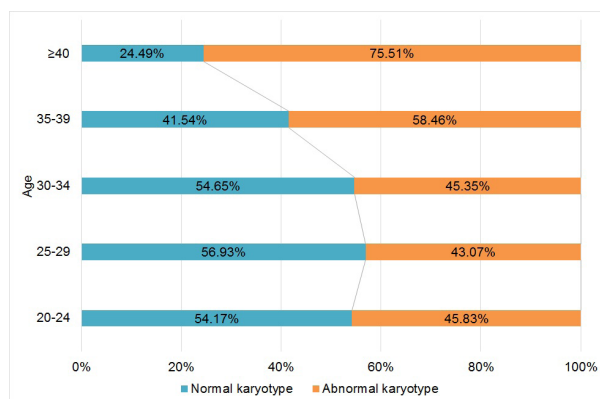


Figure 1. Distribution of embryonic karyotypes among different age categories. Among 24 women aged 20-24, the proportion of abnormal embryonic karyotype was 45.83%, and the normal embryonic karyotype proportion was 54.17%. Among 274 women aged 25-29, the percentages of abnormal karyotypes and normal karyotypes were 43.07% and 56.93%, respectively. Among 269 women aged 30-34, the abnormal karyotype proportion was 45.35%, and the normal karyotype was 54.65%. Among 130 women aged 35-39, the abnormal karyotype versus normal karyotype proportion was 58.46% versus 41.54%. Among 49 women aged over 40, the proportion of abnormal karyotype was 75.51%, and the normal karyotype proportion was 24.49%.

3.2. The details of embryonic abnormalities

Details of embryonic abnormalities are presented in Table 2. The most frequent type of chromosomal abnormalities was aneuploidy (247/393, 62.8%), followed by structural abnormalities (83/393, 21.1%), unbalanced structural abnormalities (45/393, 11.5%), mosaicism not involving sex chromosomes (12/393, 3.1%), and sex chromosome mosaicism (6/393, 1.5%).

Most patients with abnormal karyotypes fell among age groups 25-29 and 30-34 (Table 3). The average age for women with aneuploidy, structural abnormalities, and mosaicism (involving both sex chromosomes and autosomes) was 32.59 ± 4.86 , 30.68 ± 4.53 , and 32.11 ± 6.37 , respectively. The distribution profile of abnormal karyotypes varied slightly among different age categories (Figure 2). Aneuploidy was still the most common form of abnormal karyotype among all age categories. The highest aneuploidy rate was among women between 20 and 24 years of age (72.7%), and the lowest rate occurred in those aged 25-29 (55.1%). Structural abnormalities were the second most common form of abnormal

karyotype among age groups 25-29, 30-34, and 35-39, while other karyotype abnormalities sharply increased in those aged over 40. The frequency of mosaicism stayed stable across different age groups (Figure 2).

Most of the fetuses with aneuploidy presented autosomal trisomy (189/247, 76.5%). Other types of aneuploidy included autosomal monosomy (6/247, 2.4%), autosomal double trisomy (13/247, 5.3%), Turner syndrome (45, XO) (30/247, 12.1%), Triple X syndrome (2/247, 0.8%), Jacob's syndrome (2/247, 0.8%), and Triploidy 69XXY (5/247, 2.0%). The most common types of autosomal trisomies in our group of fetuses were trisomy-16 (69/189, 36.5%), trisomy-22 (28/189, 14.8%), trisomy-21 (21/189, 11.1%), trisomy-15 (15/189, 7.9%), and trisomy-13 (10/189, 5.3%) (Table 2). Trisomy-16 was the most common type of autosomal trisomy among women between 25 and 39 years of age, and trisomy-22 was commonly found in age group 30-34 (Figure 3).

We also presented selected karyotypes (Table 4) with known clinical indications such as microduplication syndromes and microdeletions.

4. Discussion

Miscarriage is clinically recognized in 10-20% of pregnancies. Recurrent spontaneous abortion (RSA) is defined as two or more pregnancy losses, which is diagnosed clinically by ultrasonography or histopathologic examination (1). There is about 5% of women going through two consecutive spontaneous abortions, and the proportion is even higher in those over 35 years old. Less than 1% of women are affected by three consecutive spontaneous abortions (3). Despite the long debate about the exact definition among different international societies, RSA is an important health issue (15-17). With the implementation of second child policy in China, many couples are now having difficulty getting pregnant or facing the problem of pregnancy loss when expecting a second baby, thus the issue of RSA will continuously affect an increasing number of couples. Therefore, it is essential to investigate the etiology of RSA for complete evaluation and targeted treatment provided to couples with a history of RSA during a subsequent pregnancy.

The causes of RSA are complicated, involving genetics, uterine anomalies, hormonal or metabolic

Table 2. Karyotypes of 781 RSA patients

Karyotype	<i>n</i>	% of total patients	% of patients with abnormal karyotype
Normal karyotype	388	49.7%	
Abnormal karyotype	393	50.3%	
Aneuploidy			
Autosomal monosomy	6	0.8%	1.5%
Autosomal trisomy			
47, XN,+2	6	0.8%	1.5%
47, XN,+3	3	0.4%	0.8%
47, XN,+4	6	0.8%	1.5%
47, XN,+5	2	0.3%	0.5%
47, XN,+6	4	0.5%	1.0%
47, XN,+7	6	0.8%	1.5%
47, XN,+8	3	0.4%	0.8%
47, XN,+9	2	0.3%	0.5%
47, XN,+10	1	0.1%	0.3%
47, XN,+11	1	0.1%	0.3%
47, XN,+12	2	0.3%	0.5%
47, XN,+13	10	1.3%	2.5%
47, XN,+14	3	0.4%	0.8%
47, XN,+15	15	1.9%	3.8%
47, XN,+16	69	8.8%	17.6%
47, XN,+17	1	0.1%	0.3%
47, XN,+18	5	0.6%	1.3%
47, XN,+20	1	0.1%	0.3%
47, XN,+21	21	2.7%	5.3%
47, XN,+22	28	3.6%	7.1%
Autosomal double trisomy	13	1.7%	3.3%
Turner syndrome (45,XO)	30	3.8%	7.6%
Triple X syndrome (XXX)	2	0.3%	0.5%
Jacob's syndrome (47,XYY)	2	0.3%	0.5%
Triploidy 69XXY	5	0.6%	1.3%
Structural abnormalities			
Deletion	16	2.0%	4.1%
Duplication	54	6.9%	13.7%
Unbalanced translocation	13	1.7%	3.3%
Mosaicism not involving sex chromosomes	12	1.5%	3.1%
Sex chromosome mosaicism	6	0.8%	1.5%
Unbalanced structural abnormalities	45	5.8%	11.5%

Table 3. Major karyotype abnormalities by age categories

Age category (year)	Aneuploidy (<i>n</i> , %)	Structural abnormalities (<i>n</i> , %)	Mosaicism* (<i>n</i> , %)	Other (<i>n</i> , %)	Total (<i>n</i>)
20-24	8 (72.7%)	1 (9.1%)	1 (9.1%)	1 (9.1%)	11
25-29	65 (55.1%)	35 (29.7%)	5 (4.2%)	13 (11.0%)	118
30-34	82 (67.2%)	23 (18.9%)	7 (5.7%)	10 (8.2%)	122
35-39	53 (69.7%)	13 (17.1%)	3 (4.0%)	7 (9.2%)	76
40+	24 (64.9%)	2 (5.4%)	2 (5.4%)	9 (24.3%)	37
Missing	15 (51.7%)	9 (31.0%)	0 (0%)	5 (17.2%)	29

*Mosaicism: involving both sex chromosomes and autosomes.

disorders, infection, reproductive immunity, and thrombophilias. Genetic factors include abnormal karyotypes, mutations, genetic polymorphisms, and so on. Previous studies have suggested that abnormal embryonic karyotype is one of the most common causes of RSA. Abnormal karyotypes contribute to the majority of miscarriages, accounting for about 51% in patients with RSA and up to 76.3% in women with sporadic abortion (18). Consistent with other studies (10,19), we observed that about half of our RSA abortus had abnormal karyotypes (393/781, 50.3%). In addition,

previously diagnosed abnormal embryonic karyotypes can be a predictor of subsequent miscarriages. It was reported that for patients who had been diagnosed with abnormal embryonic karyotype in the first determination, 76.2% of them had a subsequent abnormal embryonic karyotype (5).

The common types of chromosomal abnormalities include aneuploidy, structural abnormalities, unbalanced structural abnormalities, and mosaicism. It is reported that in older women (over 35 years old) with RSA, the majority of miscarriages are caused by fetal

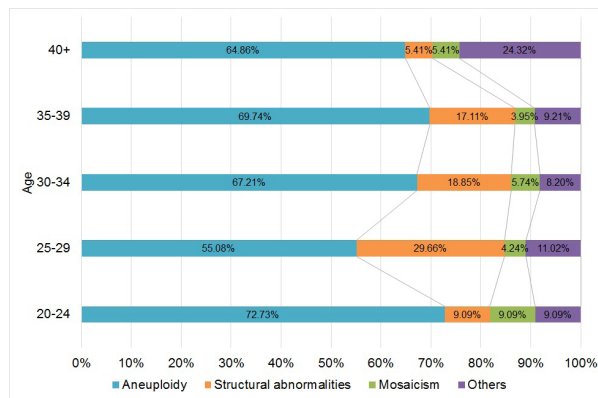


Figure 2. Distribution profile of abnormal karyotypes among different age categories. Comparison of the distribution profile of abnormal karyotypes among different age categories. *Mosaicism: involving both sex chromosomes and autosomes.

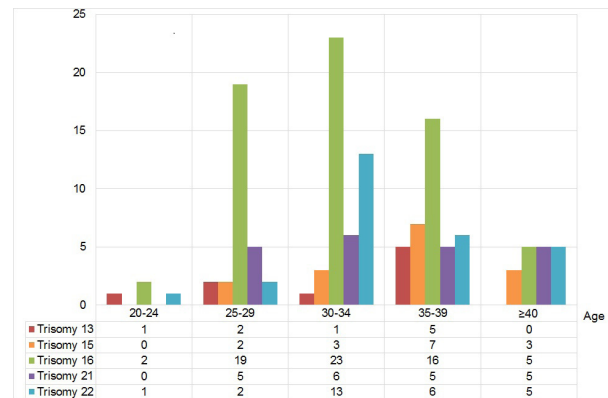


Figure 3. Distribution profile of autosomal trisomies among different age categories. Comparison of the distribution profile of autosomal trisomies among different age categories.

Table 4. Selected karyotypes with known clinical indications

No.	Karyotype	Indications
1	46,XY,del(7)(q11.23)	Chromosome 7q11.23 deletion syndrome
2	46,XY,del(8)(p23.3p21.2)	Chromosome 8p23.1 deletion syndrome. Deleted fragments contain many genes such as <i>ZNF596</i> and <i>FBXO25</i> .
3	46,XY,del(8)(p23.3p11.23)	Chromosome 8p deletion syndrome
4	46,XY,del(5)(p15.33p14.3)	Cri du Chat Syndrome -5p deletion. Deleted fragments contain many genes such as <i>PLEKHG4B</i> and <i>LRRC14B</i> .
5	46,XX,del(22)(q11.23q12.1)	Chromosome 22q11.2 distal deletion syndrome
6	46,XX,del(7)(q36.3)	Acheiropody and preaxial polydactyly, Currarino syndrome, and Holoprosencephaly 3
7	46,XY,del(7)(q11.23)	Chromosome 7q11.23 deletion syndrome
8	46,XN,del(11)(q24.1-q25)	Jacobsen syndrome
9	46,XN,del(Xp22.31).[GRCH37/hg19](6.48Mb-8.14Mb)×1	Steroid sulphatase deficiency (STS)
10	46,XN,dup(5)(q31.1q35.3)	The duplicated fragment includes the <i>NKX2-5</i> gene, which is associated with Tetralogy of Fallot and autism.
11	46,XN,dup(X)(q28)	The duplicated fragment includes genes such as <i>IDS</i> and <i>MAGEA8</i> . Reported cases with this duplication show retarded language development, mental retardation, head and facial deformity, and toe deformity.
12	46,XN,dup(1)(p32.3)	The duplicated fragment includes genes such as <i>DHCR24</i> , which is associated with physical and mental retardation.
13	46,XN,dup(14)(q11.2)	The duplicated fragment includes genes such as <i>OR11H2</i> and <i>ORAQ3</i> , and <i>ORAQ3</i> is associated with congenital ectodermal dysplasia syndrome.
14	46,XN,dup(17)(q21.31)	The duplicated fragment includes genes such as <i>SOST</i> and <i>DUSP3</i> , and <i>SOST</i> is associated with craniodiaphyseal dysplasia; Chromosome 17q21.31 duplication syndrome
15	47,XY,+15,del(16)(p11.2)	Chromosome 16p11.2 deletion syndrome
16	47,XX,+2,del(16)(p13.11)	16p13.11 recurrent microdeletion
17	46,XX/47,XX,+19,dup(16)(p13.3)	Chromosome 16p13.3 duplication syndrome
18	47,XN,+9,dup(16)(p11.2)	The duplicated fragment includes genes such as <i>CD19</i> and <i>ATXN2L</i> . Cases with duplication in this area show mental retardation.

chromosomal abnormalities (20), which is consistent with our study. It is proved that aneuploidy of embryonic chromosome increases dramatically with increasing maternal age. Hassold *et al.* have reported that the incidence of trisomy is about 2% when mothers are in their 20s, while about 35% of women in their 40s

are carrying babies with trisomies (21). Meanwhile, a study by Kroon *et al.* showed that the rate of embryonic aneuploidy from women aged over 35 was significantly higher than that in the group of ≤ 35 years old (45.7% vs 34.8%) (22). Our study also showed a sharp increase of trisomies when the maternal age exceeded 35 years

old. The existing evidence leads to the conclusion that advancing maternal age is associated with the increasing possibility of miscarriage. Over 90% of embryonic trisomies are caused by errors in paternal and maternal gametogenesis, and most of these errors occur in oocyte meiosis, while some others occur during the first few mitotic divisions of the fertilized ovum (23,24). A review by Chiang stated that the majority of abortus trisomies were maternal rather than paternal (25-30), and it was the aging oocyte rather than the uterus to blame (31,32).

In our study, among all the trisomies found in the abortuses, trisomy-16 is the most common type, which is in accordance with the study by Jia *et al.* (33). Further investigation into all these types of trisomies leads to an observation that trisomy-16 has hardly been found in live births, while fetuses with other types of trisomies may live with certain types of malfunctions (34-37). The exact mechanism of trisomy-16 being lethal is still unclear.

We employed NGS for karyotype analysis in this study. Compared with the traditional chromosome karyotyping method, NGS has its advantages in methodology, specifically in resolution and coverage. Our results have proved that NGS is both efficient and reliable; however, there are drawbacks to its use. The final result of NGS is formed by assembling various lengths of fragmented reads together with stringent algorithms applied to ensure the accuracy of the process. Therefore, one concern is false positive results, which are inevitable due to the large volume of acquired data. So NGS results should be interpreted in combination with other evidence. Another concern is that only part of the NGS result is of clinical significance.

Although abnormal karyotypes are confirmed in nearly half of the abortuses, the proportion of abnormal karyotypes in the parents is notably slight, at a percentage ranging from 2.78% to 4.32% in several retrospective studies (38-40). Miscarriages caused by abnormal karyotypes can occur in couples with normal chromosome karyotypes. The detective rate of abnormal karyotypes between villus of abortus and parental peripheral blood is significantly different, as is the abnormal karyotype profile. Studies have shown that abnormal chromosomal karyotypes in peripheral blood samples of RSA couples mainly involve balanced translocation, Robertsonian translocation, inversions, and X chromosome inactivation (41). Structural abnormalities with balanced translocations are the most common type of karyotype abnormalities detected in RSA couples, accounting for 3%-6% of the total abnormalities depending on the population studied (42,43). Incidence of reciprocal translocations is one in 500 live births, and the carriers may present normal physical and intellectual development. However, they are at risk for having genetically abnormal offspring because of the occurrence of unbalanced translocations in germ cells. Even if those germ cells with unbalanced translocations

are fertilized and developed into embryos, most of them end up with pregnancy loss. Preimplantation genetic diagnosis is now utilized to help couples with detected abnormal chromosomal karyotypes to analyze and select genetically healthy embryos before implantation, which greatly improves pregnancy outcomes. Robertsonian translocation occurs in about 1/1,000 of the general population (44). The RSA rate in couples with Robertsonian translocation is significantly higher (45,46). A study by Kolgeci revealed that Robertsonian translocation between 15q;15q resulted in intrauterine death and spontaneous failures of all pregnancies (45).

There are a few limitations in the current study. We only collected information of fetal chromosomal aberrations and maternal age; the recommended chromosome analysis of both parents in RSA cases has not been performed. In addition, the distributions of recognized RSA risk factors such as antiphospholipid syndrome (APS) and major uterine anomaly of the patients should be further studied. It is estimated that the percentage of truly unexplained causes of RSA is around 25% (47).

In summary, our study suggests that abnormal embryonic karyotype is a main factor in RSA. A well-structured prenatal diagnosis, both clinically and genetically, and preimplantation genetic diagnosis for couples with detected abnormal chromosomal karyotypes, along with healthy life styles may be beneficial to improve reproductive outcomes for RSA couples.

Acknowledgements

This work was supported by the National Natural Science Foundation of China No. 31571196 (to Ling Wang), the Science and Technology Commission of Shanghai Municipality 2015 YIXUEYINGDAO project No. 15401932200 (to Ling Wang), the FY2008 JSPS Postdoctoral Fellowship for Foreign Researchers P08471 (to Ling Wang), the National Natural Science Foundation of China No. 30801502 (to Ling Wang), the Shanghai Pujiang Program No. 11PJ1401900 (to Ling Wang), Development Project of Shanghai Peak Disciplines-Integrative Medicine No.20150407

References

1. Practice Committee of American Society for Reproductive M. Definitions of infertility and recurrent pregnancy loss: a committee opinion. *Fertil Steril*. 2013; 99:63.
2. El Hachem H, Crepau V, May-Panloup P, Descamps P, Legendre G, and Bouet PE. Recurrent pregnancy loss: current perspectives. *Int J Womens Health*. 2017; 9:331-345.
3. Branch DW, Gibson M, and Silver RM. Clinical practice. Recurrent miscarriage. *N Engl J Med*. 2010; 363:1740-1747.
4. Pandey MK, Rani R, and Agrawal S. An update in

- recurrent spontaneous abortion. *Arch Gynecol Obstet.* 2005; 272:95-108.
5. Sugiura-Ogasawara M, Ozaki Y, Katano K, Suzumori N, Kitaori T, and Mizutani E. Abnormal embryonic karyotype is the most frequent cause of recurrent miscarriage. *Hum Reprod.* 2012; 27:2297-2303.
 6. Werner M, Reh A, Grifo J, and Perle MA. Characteristics of chromosomal abnormalities diagnosed after spontaneous abortions in an infertile population. *J Assist Reprod Genet.* 2012; 29:817-820.
 7. Sugiura-Ogasawara M, Ozaki Y, Sato T, Suzumori N, and Suzumori K. Poor prognosis of recurrent aborters with either maternal or paternal reciprocal translocations. *Fertil Steril.* 2004; 81:367-373.
 8. Stern JJ, Dorfmann AD, Gutierrez-Najar AJ, Cerrillo M, and Coulam CB. Frequency of abnormal karyotypes among abortuses from women with and without a history of recurrent spontaneous abortion. *Fertil Steril.* 1996; 65:250-253.
 9. Carp H, Toder V, Aviram A, Daniely M, Mashiach S, and Barkai G. Karyotype of the abortus in recurrent miscarriage. *Fertil Steril.* 2001; 75:678-682.
 10. Stephenson MD, Awartani KA, and Robinson WP. Cytogenetic analysis of miscarriages from couples with recurrent miscarriage: A case-control study. *Hum Reprod.* 2002; 17:446-451.
 11. Sullivan AE, Silver RM, LaCoursiere DY, Porter TF, and Branch DW. Recurrent fetal aneuploidy and recurrent miscarriage. *Obstet Gynecol.* 2004; 104:784-788.
 12. Carvalho B, Doria S, Ramalho C, Brandao O, Sousa M, Matias A, Barros A, and Carvalho F. Aneuploidies detection in miscarriages and fetal deaths using multiplex ligation-dependent probe amplification: an alternative for speeding up results? *Eur J Obstet Gynecol Reprod Biol.* 2010; 153:151-155.
 13. Liao C, Yin AH, Peng CF, *et al.* Noninvasive prenatal diagnosis of common aneuploidies by semiconductor sequencing. *Proc Natl Acad Sci U S A.* 2014; 111:7415-7420.
 14. Straver R, Sistermans EA, Holstege H, Visser A, Oudejans CB, and Reinders MJ. WISECONDOR: Detection of fetal aberrations from shallow sequencing maternal plasma based on a within-sample comparison scheme. *Nucleic Acids Res.* 2014; 42:e31.
 15. Kolte AM, Bernardi LA, Christiansen OB, Quenby S, Farquharson RG, Goddijn M, Stephenson MD, and Eshre Special Interest Group EP. Terminology for pregnancy loss prior to viability: A consensus statement from the ESHRE early pregnancy special interest group. *Hum Reprod.* 2015; 30:495-498.
 16. Jauniaux E, Farquharson RG, Christiansen OB, and Exalto N. Evidence-based guidelines for the investigation and medical treatment of recurrent miscarriage. *Hum Reprod.* 2006; 21:2216-2222.
 17. Practice Committee of the American Society for Reproductive M. Evaluation and treatment of recurrent pregnancy loss: a committee opinion. *Fertil Steril.* 2012; 98:1103-1111.
 18. Ogasawara M, Aoki K, Okada S, and Suzumori K. Embryonic karyotype of abortuses in relation to the number of previous miscarriages. *Fertil Steril* 2000; 73: 300-304.
 19. Zhang S, Gao L, Liu Y, Tan J, Wang Y, Zhang R, Liu Y, Chen H, and Zhang J. Reproductive outcome and fetal karyotype of couples with recurrent miscarriages. *Clin Exp Obstet Gynecol.* 2014; 41:249-253.
 20. Marquard K, Westphal LM, Milki AA, and Lathi RB. Etiology of recurrent pregnancy loss in women over the age of 35 years. *Fertil Steril.* 2010; 94:1473-1477.
 21. Hassold T, and Hunt P. To err (meiotically) is human: the genesis of human aneuploidy. *Nat Rev Genet.* 2001; 2:280-291.
 22. Kroon B, Harrison K, Martin N, Wong B, and Yazdani A. Miscarriage karyotype and its relationship with maternal body mass index, age, and mode of conception. *Fertil Steril.* 2011; 95:1827-1829.
 23. Hu XD, Yin B, Zhu YC, Li HY, Lu YL, Zeng Y, and Wu TH. Relationship between Maternal Age and Numerical Abnormalities of Fetal Chromosomes in Spontaneous Abortion during the First Trimester. *Reprod Contracep.* 2014; 34:735-741.
 24. Waltman LA, Eckel-Passow JE, Sharma RG, and Van Dyke DL. Advanced maternal age in polyploidy with concurrent aneuploidy. *Am J Med Genet A.* 2013; 161A:1200-1202.
 25. Chiang T, Schultz RM, and Lampson MA. Meiotic origins of maternal age-related aneuploidy. *Biol Reprod.* 2012; 86:1-7.
 26. May KM, Jacobs PA, Lee M, Ratcliffe S, Robinson A, Nielsen J, and Hassold TJ. The parental origin of the extra X chromosome in 47,XXX females. *Am J Hum Genet.* 1990; 46:754-761.
 27. Hassold T, Jacobs PA, Leppert M, and Sheldon M. Cytogenetic and molecular studies of trisomy 13. *J Med Genet.* 1987; 24:725-732.
 28. Hassold TJ, Pettay D, Freeman SB, Grantham M, and Takaesu N. Molecular studies of non-disjunction in trisomy 16. *J Med Genet.* 1991; 28:159-162.
 29. Takaesu N, Jacobs PA, Cockwell A, Blackston RD, Freeman S, Nuccio J, Kurnit DM, Uchida I, Freeman V, and Hassold T. Nondisjunction of chromosome 21. *Am J Med Genet Suppl.* 1990; 7:175-181.
 30. Li H, and Durbin R. Fast and accurate short read alignment with Burrows-Wheeler Transform. *Bioinformatics.* 2009; 25:1754-1760.
 31. Sauer MV. The impact of age on reproductive potential: lessons learned from oocyte donation. *Maturitas.* 1998; 30:221-225.
 32. Stolwijk AM, Zielhuis GA, Sauer MV, Hamilton CJ, and Paulson RJ. The impact of the woman's age on the success of standard and donor in vitro fertilization. *Fertil Steril.* 1997; 67:702-710.
 33. Jia CW, Wang L, Lan YL, Song R, Zhou LY, Yu L, Yang Y, Liang Y, Li Y, Ma YM, and Wang SY. Aneuploidy in Early Miscarriage and its Related Factors. *Chin Med J (Engl).* 2015; 128:2772-2776.
 34. Emer CS, Duque JA, Muller AL, Gus R, Sanseverino MT, da Silva AA, and Magalhaes JA. Prevalence of congenital abnormalities identified in fetuses with 13, 18 and 21 chromosomal trisomy. *Rev Bras Ginecol Obstet.* 2015; 37:333-338. (in Portuguese)
 35. Baumgartner BJ, Shurafa M, Terebello H, Tapazoglou E, and Van Dyke DL. Trisomy 15, sex chromosome loss, and hematological malignancy. *Cancer Genet Cytogenet.* 2000; 117:132-135.
 36. Roy A, Cowan G, Vyas P, and Roberts I. The impact of trisomy 21 on early human hematopoiesis. *Cell Cycle.* 2013; 12:533-534.
 37. Kontomanolis EN, Pandya P, and Limperis V. Trisomy 22: the heart aspect. *J Obstet Gynaecol.* 2010; 30:627-

- 628.
38. Gaboon NE, Mohamed AR, Elsayed SM, Zaki OK, and Elsayed MA. Structural chromosomal abnormalities in couples with recurrent abortion in Egypt. *Turk J Med Sci.* 2015; 45:208-213.
39. Zhang Z, Gao H, Li S, Hong M, and Liu R. Chromosomal abnormalities in patients with recurrent spontaneous abortions in northeast China. *J Reprod Med.* 2011; 56:321-324.
40. Gada Saxena S, Desai K, Shewale L, Ranjan P, and Saranath D. Chromosomal aberrations in 2000 couples of Indian ethnicity with reproductive failure. *Reprod Biomed Online.* 2012; 25:209-218.
41. Taulavičiūtė G, Česaitytė K, Jokšas A, Serapinienė A, and Serapinas D. Genetic causes of recurrent miscarriages. *Sveikatos Mokslai.* 2016; 26:61-64.
42. Sierra S, and Stephenson M. Genetics of recurrent pregnancy loss. *Semin Reprod Med.* 2006; 24:17-24.
43. Meza-Espinoza JP, Anguiano LO, and Rivera H. Chromosomal abnormalities in couples with reproductive disorders. *Gynecol Obstet Invest.* 2008; 66:237-240.
44. Nielsen J, and Wohler M. Chromosome abnormalities found among 34,910 newborn children: results from a 13-year incidence study in Arhus, Denmark. *Hum Genet.* 1991; 87:81-83.
45. Kolgeci S, Kolgeci J, Azemi M, Shala R, Dakas A, and Sopjani M. Reproductive risk of the silent carrier of Robertsonian translocation. *Med Arch.* 2013; 67:56-59.
46. Keymolon K, Van Berkel K, Vorrsselmans A, Staessen C, and Liebaers I. Pregnancy outcome in carriers of Robertsonian translocations. *Am J Med Genet. A* 2011; 155A:2381-2385.
47. Sugiura-Ogasawara M, Ozaki Y, and Suzumori N. Management of recurrent miscarriage. *J Obstet Gynaecol Res.* 2014; 40:1174-1179.
- (Received November 23, 2017; Revised February 20, 2018; Accepted February 21, 2018)

Supplemental Data

Supplementary Table 1. Geographic distribution of the patients

Region	Normal karyotype (n = 388)		Abnormal karyotype (n = 393)	
	n	%	n	%
Metropolitan Shanghai	135	34.8%	265	67.4%
Zhejiang Province	23	6.0%	37	9.4%
Jiangsu Province	22	5.7%	37	9.4%
Fujian Province	4	1.0%	6	1.5%
Anhui Province	9	2.3%	6	1.5%
Hubei Province	3	0.8%	4	1.0%
Jiangxi Province	6	1.5%	3	0.8%
Henan Province	1	0.3%	3	0.8%
Shandong Province	2	0.5%	3	0.8%
Sichuan Province	1	0.3%	2	0.5%
Xinjiang Uygur Autonomous Region	0	0.0%	2	0.5%
Hebei Province	1	0.3%	1	0.3%
Gansu Province	0	0.0%	1	0.3%
Yunnan Province	0	0.0%	1	0.3%
Heilongjiang Province	1	0.3%	0	0.0%
Missing data	180	46.4%	22	5.6%

FL118, a novel camptothecin analogue, suppressed migration and invasion of human breast cancer cells by inhibiting epithelial-mesenchymal transition *via* the Wnt/ β -catenin signaling pathway

Zhihong Yang, Lixia Ji, Guohui Jiang*, Ranran Liu, Zhantao Liu, Yuecheng Yang, Qingxia Ma, Hongqin Zhao

Department of Pharmacology, School of Pharmacy, Qingdao University, Qingdao, Shandong, China.

Summary

The aim of the current study was to investigate the effects of FL118, a novel camptothecin analogue, on migration and invasion of human breast cancer cells and the underlying mechanisms of those effects. A 3-(4,5-dimethylthiazol-2-yl)-2,5-diphenyl-2H-tetrazolium bromide (MTT) assay and a plate clone formation assay were used to examine inhibition of the proliferation of MDA-MB-231 cells by FL118. Cell cycle distribution was detected using flow cytometry. A wound healing assay and a transwell assay were performed to detect the effects of FL118 on migration and invasion of MDA-MB-231 cells, respectively. qRT-PCR, Western blotting, and immunocytochemistry were used to study the effects of FL118 on expression of epithelial-mesenchymal transition (EMT)-related molecules and Wnt/ β -catenin signaling components in MDA-MB-231 cells. The current results indicated that FL118 inhibited the proliferation, migration and invasion of MDA-MB-231 cells in a dose- and time-dependent manner. FL118 caused MDA-MB-231 cells to accumulate in the S phase. FL118 significantly suppressed the expression of vimentin while enhancing the expression of E-cadherin. Moreover, decreased expression of β -catenin and its targets survivin and cyclin D1 was detected in the nucleus of MDA-MB-231 cells. Taken together, the current results suggest that FL118 inhibited Wnt/ β -catenin signaling, leading to suppressed EMT and decreased migration and invasion of breast cancer cells.

Keywords: FL118, invasion, metastasis, EMT, Wnt/ β -catenin, breast cancer

1. Introduction

Breast cancer is currently the leading cause of cancer-related deaths in women (1). Worldwide, more than 1.7 million women were diagnosed with breast cancer and 521,900 women died from breast cancer in 2012 (1). According to data from the National Central Cancer Registry of China, breast cancer alone is expected to account for 15% of all new cancers in women in 2015 (2). Invasion and metastasis, which are estimated to be responsible for approximately 90% of all cancer deaths, are the primary factors that result in the failure of breast

cancer treatment (3,4). Medications that can suppress invasion and metastasis of breast cancer are greatly needed in clinical settings (5,6).

Studies revealed that epithelial-mesenchymal transition (EMT) is one of the major molecular mechanisms promoting cancer invasion and metastasis (7-9). EMT is a biological process that allows a polarized epithelial cell, which normally interacts with the basement membrane *via* its basal surface, to undergo multiple biochemical changes that enable it to assume a mesenchymal cell phenotype, which includes enhanced migratory and invasive capacities (10). Studies have reported that Wnt/ β -catenin is among the main pathways that regulate EMT, which may be the key mechanism that mediates breast cancer progression (11,12). Agents that target Wnt/ β -catenin and downstream molecules such as survivin and cyclin D1 have a potent inhibitory effect on cell proliferation, invasion, and metastasis in

*Address correspondence to:

Dr. Guohui Jiang, Department of Pharmacology, School of Pharmacy, Qingdao University, 38 Deng Zhou Road, Qingdao, Shandong, China.

E-mail: 13370830026@163.com

breast cancer (13-15).

FL118, a novel camptothecin analogue, was first discovered in high-throughput screening for survivin inhibitors in a previous study by the current authors (16). FL118 was found to display potent anticancer activity against several different types of cancer both *in vitro* and *in vivo* (17-20). Moreover, its antitumor activity was superior to that of several camptothecin analogues, such as irinotecan and topotecan, that have been approved by the FDA for cancer treatment (21,22). FL118 is rapidly cleared from circulation and it effectively accumulates in tumors with a long half-life of elimination, suggesting its potential for use in cancer therapy (18,20). However, the effects of FL118 on breast cancer invasion and metastasis have not been reported.

The current study used an aggressive breast cancer cell line, MDA-MB-231, to examine the effects of FL118 on migration and invasion of human breast cancer and the mechanisms for those effects. The aim of this study was to determine whether FL118 would suppress cell migration and invasion and to identify the molecular mechanisms for that anticancer activity.

2. Materials and Methods

2.1. Reagents and antibodies

FL118, 11-methylenedioxy-camptothecin (Figure 1), was obtained from a cooperating lab, the American Roswell Park Cancer Institute (RPCI), and was dissolved with dimethyl sulphoxide (DMSO). Antibodies against survivin, E-cadherin, vimentin, and β -actin were purchased from Santa Cruz Biotechnology, Inc. (Santa Cruz, CA, USA). Antibodies against β -catenin, lamin B1, and cyclin D1 were purchased from Abcam, Inc. (Cambridge, MA, USA).

2.2. Cell line and cell culture

MDA-MB-231 cells were donated by Prof. Luo Bing (Department of Microbiology, Qingdao University, Qingdao, Shandong, China). Cells were cultured in RPMI 1640 medium supplemented with 10% fetal bovine serum (FBS) and 1% antibiotic-antimycotic (Hyclone Laboratories, Inc., Logan UT) at 37°C in a 5% CO₂ atmosphere.

2.3. 3-(4,5-dimethylthiazol-2-yl)-2,5-diphenyl-2H-tetrazolium bromide (MTT) assay

Cell proliferation was assessed with an MTT assay. Cells were incubated in 96-well plates (5×10^3 cells/well) 24 h prior to treatment. The cells were then treated with FL118 (0, 1, 10, 100, and 200 nM) for 24, 48, 72, and 96 h and incubated with MTT (5 mg/mL) for 4 h. The culture medium was then replaced with 100 μ L DMSO. The optical density (OD) value for each well at 490 nm was

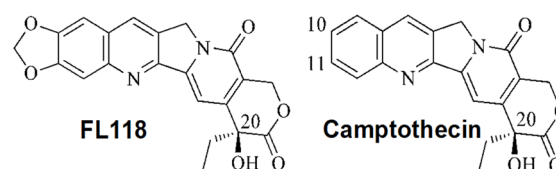


Figure 1. Chemical structures of FL118 and camptothecin.

measured with a Microplate Reader (BioTek, Winooski, VT, USA) to assess the degree of cell proliferation (23).

2.4. Plate clone formation assay

Cells (100/well) were seeded in 6-well plates and treated after 24 h. After 12 days, the cells were stained with methylrosanilinium chloride. The number of colonies containing 50 cells was counted under a microscope. Plate clone formation efficiency was calculated using the formula: plate clone formation efficiency = (number of colonies/number of cells inoculated) \times 100%.

2.5. Cell cycle analysis

Cells were incubated in 6-well plates (3×10^4 cells/well) overnight and then treated with FL118 (100 nM) for 12, 24, 36, and 48 h. The cells were harvested and gently resuspended in a single cell suspension in fluorescence-activated cell sorting (FACS) buffer (PBS containing 2% FBS), followed by drop-wise fixation with 70% ethanol at 4°C overnight. Fixed cells were washed with cold PBS and incubated with RNaseA (10 mg/mL) and propidium iodide (PI, 1 mg/mL) at 37°C in the dark for 30 min, and then analyzed with FACS flow cytometer (Backman Coulter) (24). Each assay was repeated in three independent experiments.

2.6. Transwell assay

Cell invasions were analyzed in 24-well transwell chambers (8- μ m pore size, Corning). About 10 μ g/mL Matrigel Matrix (Corning Incorporated, New York, USA) was used to cover the upper side of the chamber. Cells at a concentration of 1×10^5 /mL were suspended in 200 μ L of serum-free medium and then seeded into the upper chamber, and 650 μ L of medium with 15% fetal bovine serum was added to the lower chamber. After incubation for 48 h, cells that had not invaded were removed from the upper surface using cotton swabs. The cells that had invaded were fixed in methanol for 20 min, stained with 0.1% crystal violet, and counted under a phase contrast microscope (five different fields per chamber were examined).

2.7. Wound healing assay

Cells were seeded in 6-well plates at a density of 10^6

cells/well and allowed to reach 100% confluence. After treatment with mitomycin C (10 µg/mL, 12 h), a scratch wound was created on the cell surface using a 200-µL pipette tip. The detached cells were washed away with PBS. The medium was changed to serum-free RPMI-1640 with FL118 (10 or 100 nM), and the cells were continuously cultured for 48 h. The wound area was photographed with an inverted phase contrast microscope (Olympus; magnification, 40×) at 0, 12, 24, and 48 h. The migration distance was calculated using Image-Pro Plus.

2.8. Western blot analysis

The cells were washed twice with ice-cold PBS before being lysed in 200 µL of RIPA buffer containing protease and phosphatase inhibitors. A BCA Protein Kit (Beyotime biotechnology, Shanghai, China) was used to quantify protein concentrations. Equal amounts of protein were separated using 10% SDS-PAGE and transferred to PVDF membranes (Millipore, Billerica, MA, USA). Membranes were blocked with 5% skim milk in TBST for 2 h and incubated with a primary antibody overnight. The primary antibodies used in this study were as follows: anti-β-actin antibody 1:2,000; anti-survivin antibody 1:500; anti-E-cadherin antibody 1:1,000; anti-vimentin antibody 1:1,000; anti-lamin B1 antibody 1:2,000; anti-β-catenin antibody 1:5,000; and anti-cyclin D1 antibody 1:10,000. The membranes were then incubated with the appropriate HRP-conjugated secondary antibodies. Protein bands were detected with an eECL Western blot kit (CW BIO, China) and visualized using autoradiography on x-ray films (CW BIO, China).

2.9. Quantitative real-time PCR

Total RNA from treated cells was isolated using TRIzol reagent (CW BIO, China) in accordance with the manufacturer's instructions. The quality and quantity of total RNA were determined with a Nano-Drop 1000 Spectrophotometer (Thermo Fisher Scientific, Waltham, MA, USA). Total RNA was reverse transcribed into cDNA using the FAST Quant RT kit (TIANscript, Beijing, China). Quantitative real-time PCR reactions were carried out on a CFX96 Touch™ Deep Well Real-time PCR Detection System (BIO- RAD, California, USA). The primers used in this study were: Survivin: sense 5'-ATACCAGCACTTTGGGAGG-3' and antisense 5'-AGAAAGGAAAGCGCAACC-3'; Vimentin: sense 5'-GGAAGAGAACTTTGCCGTTG-3' and antisense 5'-TGGTATT CACGAAGGTGACG-3'; E-Cadherin: sense 5'-CTGAGAACGAGGCTAACG-3' and antisense 5'-GTCCACCATCATCATTCAATAT-3'; β-catenin: sense 5'-TGGTGA CAGGGAAGACATCA-3' and antisense 5'-CCATAGTGAAGGCCGAAGTGC-3';

cyclin D1: sense 5'-GCGAGGAACAGAAGTGCG-3' and antisense 5'-GGAGTTGT CGGTGTAGATGC-3'; and β-actin: sense 5'-ACTCTTCCAGCCTTCCTTC-3' and anti-sense 5'-ATCTCCTTCTGCATCCTGTGC-3'. Following normalization to β-actin, levels of target gene expression were calculated using the $2^{-\Delta\Delta CT}$ method.

2.10. Immunocytochemistry

Cells (10^5 /well) were cultured with or without 10 nM FL118 on chamber slides for 48 h and then rinsed three times with PBS. The cells were subsequently fixed with 4% paraformaldehyde for 30 min, permeabilized with 0.3% Triton X-100 for 10 min, and then incubated with primary antibodies against survivin, E-cadherin, vimentin (Santa Cruz, CA, USA), β-catenin, and cyclin D1 (ABCAM, Cambridge, MA, USA) overnight at 4°C. The cells were rewashed and incubated with the appropriate secondary antibodies (ABGENT, San Diego, USA) for 1 h in room temperature. Finally, the cells were washed and restained with DAB for 3-5 min, followed by nuclear staining with hematoxylin. The cover slips were observed under a microscope (Eclipse E-800, Nikon, Japan).

2.11. Statistical analysis

Assay results were the average of at least 3 replicates from three independent experiments. The data were analyzed with the Student's *t* test and are presented as mean ± SD. A *p*-value of less than 0.05 was considered statistically significant.

3. Results

3.1. FL118 inhibited the proliferation of MDA-MB-231 cells

The effect of FL118 on proliferation of MDA-MB-231 cells was examined first. An MTT assay was used to detect the survival rate of MDA-MB-231 cells after treatment with FL118. Results indicated that FL118 inhibited the growth of MDA-MB-231 cells in a dose- and time-dependent manner (Figure 2A). In MDA-MB-231 cells, the IC₅₀ of FL118 was 414.3 nM at 48, 102.5 nM at 72 h, and 41.1 nM at 96 h. In a plate clone formation assay, FL118 suppressed colony formation by MDA-MB-231 cells in a dose-dependent manner (Figure 2B). The number of clones that formed decreased significantly after FL118 treatment compared to that in the control. To further investigate the mechanism of FL118-mediated inhibition of the proliferation of MDA-MB-231 cells, cell cycle distribution was analyzed using flow cytometry at 12, 24, 36, and 48 h. Results indicated that FL118 treatment resulted in a reduction in the percentage of cells in the G₀/G₁ and G₂/M phase, while the percentage of S

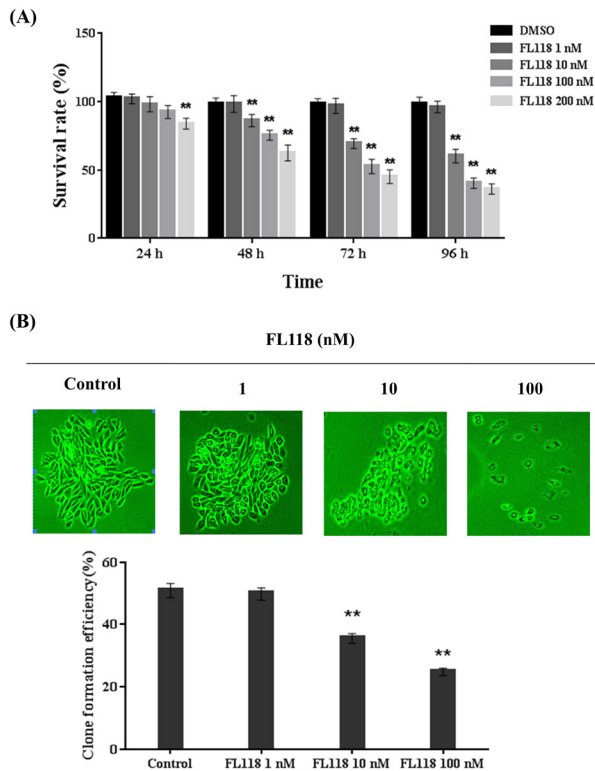


Figure 2. FL118 inhibited the proliferation of MDA-MB-231 cells. (A) The cells were exposed to various concentrations of FL118 for 24, 48, 72, and 96 hours and then subjected to an MTT assay. (B) The cells were exposed to various concentrations of FL118 for 12 days and their colony formation activity was evaluated using a plate clone formation assay. **p < 0.01 vs. control.

phase increased significantly (Figure 3). These results suggested that FL118 suppressed the proliferation of breast cancer cells by halting the cell cycle in the S phase.

3.2. FL118 suppressed the invasive and migratory capabilities of MDA-MB-231 cells

Tumor cell invasion and migration are critical steps in the metastatic process (25). To assess the ability of breast cancer cells to invade Matrigel, a transwell insert system was used to monitor the process of invasion. In this assay, a low concentration of FL118 that had little effect on cell proliferation was used. After treatment with 10 nM of FL118 for 48 h, the number of invading MDA-MB-231 cells decreased markedly in comparison to the control group, as shown in Figure 4A. The effect of FL118 on cancer cell migration was examined using a wound healing assay. Results indicated that cells treated with FL118 at 10 nM or 100 nM had a markedly reduced migratory capacity compared to that of the control group 24 and 48 h after wound creation (Figure 4B). Taken together, these results suggest that FL118 inhibits the invasion and migration of MDA-MB-231 cells at low concentrations.

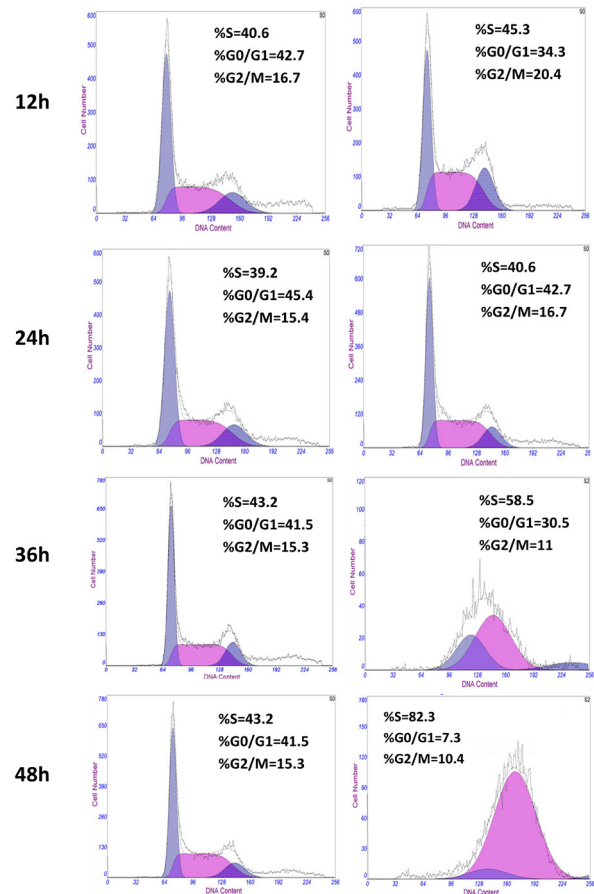


Figure 3. Cell cycle distribution of MDA-MB-231 cells after FL118 treatment. The cells were exposed to 100 nM of FL118 for 12, 24, 36, and 48 h. Cell cycle distribution in the control group (left) and the treatment group (right) was examined using flow cytometry.

3.3. FL118 increased E-cadherin and decreased vimentin expression in MDA-MB-231 cells

The effect of FL118 on the expression of EMT markers, including E-cadherin and vimentin, was examined in MDA-MB-231 cells using Western blotting, qRT-PCR, and an immunocytochemistry assay. As shown in Figure 5A, the results of Western blotting indicated that 10 or 100 nM of FL118 significantly decreased vimentin expression while markedly increasing E-cadherin expression. Expression of vimentin and E-cadherin mRNA in MDA-MB-231 cells was examined using qRT-PCR. Results indicated that FL118 reduced the level of vimentin mRNA while increasing the level of E-cadherin, which is consistent with the results of Western blotting (Figure 5B). After treatment with FL118, the expression profiles of EMT-related markers were verified using an immunocytochemistry assay. Consistent with the above results, the immunocytochemistry assay indicated that the expression of vimentin decreased significantly while expression of E-cadherin increased when MDA-MB-231 cells were treated with 10 or 100 nM FL118 for 48 h (Figure 5C). All of these results suggest that

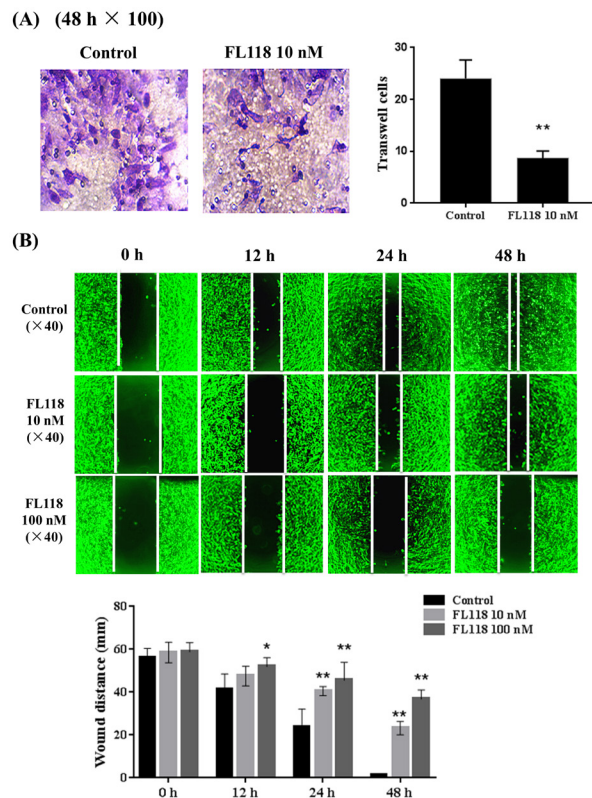


Figure 4. FL118 suppressed invasion and migration of MDA-MB-231 cells. (A) Effect of FL118 on cell invasion was examined using a transwell assay. The cells were exposed to 10 nM of FL118 for 48 h, and images (100×) from a Matrigel-coated Boyden chamber were used to count invading cells. $^{**}p < 0.01$ vs. control. (B) The effect of FL118 on cell migration was determined using a wound healing assay. The cells were exposed to 10 or 100 nM of FL118 for 12, 24, and 48 h, respectively, and the wound width was measured at each time point. $^{*}p < 0.05$ and $^{**}p < 0.01$ vs. control.

low concentrations of FL118 that had little effect on cell proliferation markedly suppressed the EMT of MDA-MB-231 cells.

3.5. FL118 decreased the levels of β -catenin, survivin, and cyclin D1 in MDA-MB-231 cells

To investigate whether FL118 suppressed EMT via the Wnt/ β -catenin pathway, Western blotting and qRT-PCR were used to examine changes in protein and mRNA levels of β -catenin and its downstream targets survivin and cyclin D1. After treatment with 10 or 100 nM of FL118 for 48 h, the levels of β -catenin, survivin, and cyclin D1 protein and mRNA were down-regulated in MDA-MB-231 cells (Figure 6A and 6B). Expression of β -catenin, survivin, and cyclin D1 was verified using an immunocytochemistry assay. Results indicated that β -catenin, survivin, and cyclin D1 expression decreased significantly after treatment with FL118 (10 nM) for 48 h. These results suggest that FL118 downregulated the Wnt/ β -catenin pathway, which may have contributed to the inhibition of cell migration and invasion by FL118.

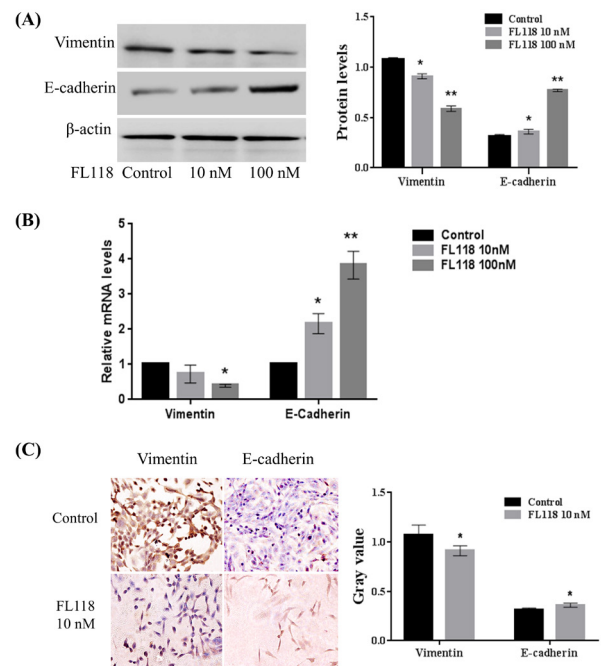


Figure 5. FL118 increased E-cadherin while decreasing vimentin expression in MDA-MB-231 cells. The cells were exposed to 10 or 100 nM of FL118 for 48 h, and E-cadherin and vimentin expression was examined using Western blotting (A), qRT-PCR (B), and an immunocytochemistry assay (C), respectively. $^{*}p < 0.05$ and $^{**}p < 0.01$ vs. control.

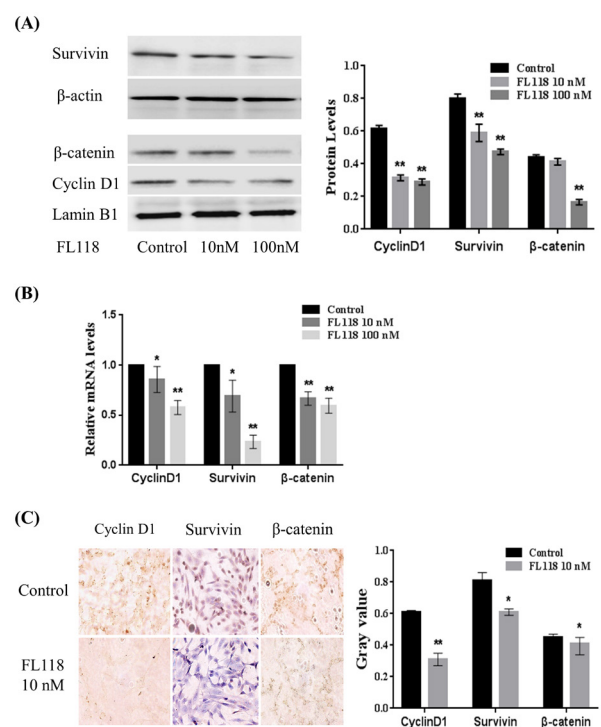


Figure 6. FL118 decreased the levels of β -catenin, survivin, and cyclin D1 in MDA-MB-231 cells. The cells were exposed to 10 or 100 nM of FL118 for 48 h, and β -catenin, survivin, and cyclin D1 expression was examined using Western blotting (A), qRT-PCR (B), and an immunocytochemistry assay (C), respectively. $^{*}p < 0.05$ and $^{**}p < 0.01$ vs. control.

4. Discussion

Invasion and metastasis remains a challenge in the treatment of breast cancer (26). The MDA-MB-231 cell line is a well-established cell line used to examine cancer metastasis (27), which is why the current study examined the effects of FL118 on that cell line. FL118 at low concentrations that had little effect on cell proliferation significantly suppressed migration and invasion by MDA-MB-231 cells. FL118 decreased the level of vimentin expression while increasing the level of E-cadherin, suggesting that it reversed the process of EMT. Furthermore, FL118 reduced the level of expression of β -catenin and its downstream targets cyclin D1 and survivin, implying that the Wnt/ β -catenin signaling pathway might play a role in the antitumor activity of FL118.

EMT plays a key role in tumor metastasis and progression. In this significant biological process, epithelial cells lose their polarity and cell-cell adhesion, and those cells acquire migratory and invasive properties to become mesenchymal stem cells (28). Loss of the epithelial marker E-cadherin and acquisition of the mesenchymal marker vimentin are considered to be important characteristics of EMT (28). E-cadherin is an adhesion molecule expressed in the epithelioid cell phenotype and it plays a key role in the process of cancer invasion. Low expression of E-cadherin might significantly enhance the invasion and metastasis of breast cancer (29). Vimentin is also an important marker of mesenchymal cells. The up-regulation of vimentin is closely related to invasion by and metastasis and EMT of breast cancer cells (30). The current results indicated that FL118 effectively increased the expression of E-cadherin and it decreased the expression of vimentin in MDA-MB-231 cells, supporting the contention that FL118 suppresses cell migration and invasion by inhibiting EMT.

The Wnt/ β -catenin pathway is one of the key signaling pathways triggering EMT, and survivin and cyclin D1 are known downstream targets of Wnt/ β -catenin signaling (31). The current study thus explored whether Wnt/ β -catenin signaling was involved in the anti-invasive activity of FL118. Results indicated that levels of β -catenin expression and its downstream targets cyclin D1 and survivin were significantly suppressed by FL118. FL118 may accelerate the degradation of β -catenin in the cytoplasm, thereby suppressing the translocation of β -catenin into the nucleus and thus suppressing the expression of downstream targets. A study has indicated that survivin is an evolutionarily conserved activator of cell migration, invasion, and metastatic dissemination (32). Cyclin D1 can activate the downstream gene Snail and mediate the occurrence of EMT (33,34). Thus, blocking of the Wnt/ β -catenin signaling pathway by FL118 presumably contributed to its suppression of migration

and invasion of breast cancer cells.

In conclusion, this study found that FL118 suppressed migration and invasion of breast cancer cells by inhibiting EMT *via* the Wnt/ β -catenin signaling pathway. These findings revealed new molecular mechanisms for the anticancer activity of FL118 and provide an experimental basis for the further development of FL118.

Acknowledgements

This work was supported by grants from the Project to Bring in Talented Personnel of Qingdao University's College of Medicine (80402010104/063-06301104) and the Innovative Teacher Training Program of Qingdao University's College of Medicine (2015). The authors wish to thank Dr. Fengzhi Li and his team (Roswell Park Cancer Institute RPCI, Buffalo, New York) for providing FL118.

References

1. Torre LA, Bray F, Siegel RL, Ferlay J, Lortet-Tieulent J, Jemal A. Global cancer statistics, 2012. *CA Cancer J Clin.* 2015; 65:87-108.
2. Chen W, Zheng R, Baade PD, Zhang S, Zeng H, Bray F, Jemal A, Yu XQ, He J. Cancer statistics in China, 2015. *CA Cancer J Clin.* 2016; 66:115-132.
3. Siegel R, DeSantis C, Virgo K, *et al.* Cancer treatment and survivorship statistics, 2012. *CA Cancer J Clin.* 2012; 62:220-241.
4. Perret GY. Pharmacological strategies and micrometastasis: What is known? What must be done? *Minerva Med.* 2010; 101:163-178.
5. Nakata M, Kawaguchi S, Oikawa A, Inamura A, Nomoto S, Miyai H, Nonaka T, Ichimi S, Fujita-Yamaguchi Y, Luo C, Gao B, Tang W. An aqueous extract from toad skin prevents gelatinase activities derived from fetal serum albumin and serum-free culture medium of human breast carcinoma MDA-MB-231 cells. *Drug Discov Ther.* 2015; 9:417-421.
6. Nakata M, Mori S, Kamoshida Y, Kawaguchi S, Fujita-Yamaguchi Y, Gao B, Tang W. Toad skin extract cinobufatini inhibits migration of human breast carcinoma MDA-MB-231 cells into a model stromal tissue. *Biosci Trends.* 2015; 9:266-269.
7. Polyak K, Weinberg RA. Transitions between epithelial and mesenchymal states: Acquisition of malignant and stem cell traits. *Nat Rev Cancer.* 2009; 9:265-273.
8. Shilpa P, Kaveri K, Salimath BP. Anti-metastatic action of anacardic acid targets VEGF-induced signalling pathways in epithelial to mesenchymal transition. *Drug Discov Ther.* 2015; 9:53-65.
9. Ding Y, Li X, Hong D, Jiang L, He Y, Fang H. Silence of MACC1 decreases cell migration and invasion in human malignant melanoma through inhibiting the EMT. *Biosci Trends.* 2016; 10:258-264.
10. Zhang LM, Wang P, Liu XM, Zhang YJ. LncRNA SUMO1P3 drives colon cancer growth, metastasis and angiogenesis. *Am J Transl Res.* 2017; 9:5461-5472.
11. Ma X, Yan W, Dai Z, Gao X, Ma Y, Xu Q, Jiang J, Zhang S. Baicalein suppresses metastasis of breast cancer cells by inhibiting EMT *via* downregulation of SATB1 and

- Wnt/beta-catenin pathway. *Drug Des Devel Ther.* 2016; 10:1419-1441.
12. Lv ZD, Yang ZC, Liu XP, Jin LY, Dong Q, Qu HL, Li FN, Kong B, Sun J, Zhao JJ, Wang HB. Silencing of *Prrx1b* suppresses cellular proliferation, migration, invasion and epithelial-mesenchymal transition in triple-negative breast cancer. *J Cell Mol Med.* 2016; 20:1640-1650.
 13. Fatima I, El-Ayachi I, Taotao L, Lillo MA, Krutilina R, Seagroves TN, Radaszkiewicz TW, Hutnan M, Bryja V, Krum SA, Rivas F, Miranda-Carboni GA. The natural compound Jatrophone interferes with Wnt/beta-catenin signaling and inhibits proliferation and EMT in human triple-negative breast cancer. *PloS One.* 2017; 12:e0189864.
 14. Li X, Meng Y, Xie C, Zhu J, Wang X, Li Y, Geng S, Wu J, Zhong C, Li M. Diallyl Trisulfide inhibits breast cancer stem cells *via* suppression of Wnt/beta-catenin pathway. *J Cell Biochem.* 2017. doi: 10.1002/jcb.26613
 15. Krishnamurthy N, Kurzrock R. Targeting the Wnt/beta-catenin pathway in cancer: Update on effectors and inhibitors. *Cancer Treat Rev.* 2018; 62:50-60.
 16. Li F. Discovery of survivin inhibitors and beyond: FL118 as a proof of concept. *Int Rev Cell Mol Biol.* 2013; 305:217-252.
 17. Wang J, Liu Z, Zhang D, Liu R, Lin Q, Liu J, Yang Z, Ma Q, Sun D, Zhou X, Jiang G. FL118, a novel survivin inhibitor, wins the battle against drug-resistant and metastatic lung cancers through inhibition of cancer stem cell-like properties. *Am J Transl Res.* 2017; 9:3676-3686.
 18. Li F. Anticancer drug FL118 is more than a survivin inhibitor: Where is the Achilles' heel of cancer? *Am J Cancer Res.* 2014; 4:304-311.
 19. Li F, Ling X, Harris DL, Liao J, Wang Y, Westover D, Jiang G, Xu B, Boland PM, Jin C. Topoisomerase I (Top1): A major target of FL118 for its antitumor efficacy or mainly involved in its side effects of hematopoietic toxicity? *Am J Cancer Res.* 2017; 7:370-382.
 20. Westover D, Ling X, Lam H, Welch J, Jin C, Gongora C, Del Rio M, Wani M, Li F. FL118, a novel camptothecin derivative, is insensitive to ABCG2 expression and shows improved efficacy in comparison with irinotecan in colon and lung cancer models with ABCG2-induced resistance. *Mol Cancer.* 2015; 14:92.
 21. Ling X, Cao S, Cheng Q, Keefe JT, Rustum YM, Li F. A novel small molecule FL118 that selectively inhibits survivin, Mcl-1, XIAP and cIAP2 in a p53-independent manner, shows superior antitumor activity. *PloS One.* 2012; 7:e45571.
 22. Ling X, Liu X, Zhong K, Smith N, Prey J, Li F. FL118, a novel camptothecin analogue, overcomes irinotecan and topotecan resistance in human tumor xenograft models. *Am J Transl Res.* 2015; 7:1765-1781.
 23. Inagaki Y, Matsumoto Y, Tang W, Sekimizu K. Dividing phase-dependent cytotoxicity profiling of human embryonic lung fibroblast identifies candidate anticancer reagents. *Drug Discov Ther.* 2016; 10:195-200.
 24. Li J, Wang X, Hou J, Huang Y, Zhang Y, Xu W. Enhanced anticancer activity of 5-FU in combination with Bestatin: Evidence in human tumor-derived cell lines and an H22 tumor-bearing mouse. *Drug Discov Ther.* 2015; 9:45-52.
 25. Wels J, Kaplan RN, Rafii S, Lyden D. Migratory neighbors and distant invaders: Tumor-associated niche cells. *Genes Dev.* 2008; 22:559-574.
 26. Cao H, Zhang Z, Zhao S, He X, Yu H, Yin Q, Zhang Z, Gu W, Chen L, Li Y. Hydrophobic interaction mediating self-assembled nanoparticles of succinobucol suppress lung metastasis of breast cancer by inhibition of VCAM-1 expression. *J Control Release.* 2015; 205:162-171.
 27. Wu GS, Song YL, Yin ZQ, Guo JJ, Wang SP, Zhao WW, Chen XP, Zhang QW, Lu JJ, Wang YT. Ganoderiol A-enriched extract suppresses migration and adhesion of MDA-MB-231 cells by inhibiting FAK-SRC-paxillin cascade pathway. *PloS One.* 2013; 8:e76620.
 28. Mitra A, Mishra L, Li S. EMT, CTCs and CSCs in tumor relapse and drug-resistance. *Oncotarget.* 2015; 6:10697-10711.
 29. Onder TT, Gupta PB, Mani SA, Yang J, Lander ES, Weinberg RA. Loss of E-cadherin promotes metastasis *via* multiple downstream transcriptional pathways. *Cancer Research.* 2008; 68:3645-3654.
 30. Paccione RJ, Miyazaki H, Patel V, Waseem A, Gutkind JS, Zehner ZE, Yeudall WA. Keratin down-regulation in vimentin-positive cancer cells is reversible by vimentin RNA interference, which inhibits growth and motility. *Mol Cancer Ther.* 2008; 7:2894-2903.
 31. Lee SC, Kim OH, Lee SK, Kim SJ. IWR-1 inhibits epithelial-mesenchymal transition of colorectal cancer cells through suppressing Wnt/beta-catenin signaling as well as survivin expression. *Oncotarget.* 2015; 6:27146-27159.
 32. Mehrotra S, Languino LR, Raskett CM, Mercurio AM, Dohi T, Altieri DC. IAP regulation of metastasis. *Cancer Cell.* 2010; 17:53-64.
 33. Sarkar FH, Li Y, Wang Z, Kong D. The role of nutraceuticals in the regulation of Wnt and Hedgehog signaling in cancer. *Cancer Metastasis Rev.* 2010; 29:383-394.
 34. Ahmad A, Sarkar SH, Bitar B, Ali S, Aboukameel A, Sethi S, Li Y, Bao B, Kong D, Banerjee S, Padhye SB, Sarkar FH. Garcinol regulates EMT and Wnt signaling pathways *in vitro* and *in vivo*, leading to anticancer activity against breast cancer cells. *Mol Cancer Ther.* 2012; 11:2193-2201.

(Received November 17, 2017; Revised February 13, 2018; Accepted February 23, 2018)

Pain perception after colorectal surgery: A propensity score matched prospective cohort study

Fabian Grass^{1,§}, Matthieu Cachemaille^{2,§}, David Martin¹, Nicolas Fournier³, Dieter Hahnloser¹, Catherine Blanc², Nicolas Demartines^{1,*}, Martin Hübner¹

¹Department of Visceral Surgery, University Hospital CHUV, Lausanne, Switzerland;

²Department of Anaesthesiology, University Hospital CHUV, Lausanne, Switzerland;

³Institute for Social and Preventive Medicine, University Hospital CHUV, Lausanne, Switzerland.

Summary

The purpose of this prospective cohort study was to compare multimodal pain management and pain perception after open vs. laparoscopic colorectal surgery within enhanced recovery care. Pain scores at rest and at mobilization were prospectively assessed in consecutive patients using Visual Analog Scales (VAS 0-10) and consumption of different analgesics was recorded daily until 96 hours postoperatively. Uni- and multivariate risk factors for pain peaks ($\geq 4/10$) were identified by logistic regression and compared between two propensity score matched groups (open vs. laparoscopic). 156 open and 176 laparoscopic procedures were included. Mean VAS scores were consistently < 3 until 96 hours at rest and at mobilization. Patients operated by laparoscopy experienced more pain peaks (≥ 4) within 24 hours ($p < 0.05$), while patients operated by open approach experienced more pain peaks (≥ 4) during mobilization at 72 hours ($p < 0.05$). Independent risk factors for insufficient pain control (≥ 4) within 24 hours from surgery were duration of the procedure (OR 3.37, 95%CI 2.03-5.59), emergency surgery (OR 3.01, 95%CI 1.72-5.31), wound infiltration (OR 3.23, 95%CI 0.97-10.70), age < 70 years (OR 2.03, 95% CI 1.18-3.48) and ASA I-II score (OR 2.06, 95% CI 1.19-3.56). The perioperative adding of lidocaine \pm ketamine to opioids did not improve postoperative pain perception nor decrease morphine equivalents. In conclusion, overall pain scores were low after colorectal surgery. However, pain peaks remained a concern early after minimally invasive surgery and after epidural removal for open surgery. Multimodal strategies were not superior to opioids alone.

Keywords: Enhanced recovery, pain management, laparoscopy

1. Introduction

Minimally invasive approach for colorectal surgery promotes functional recovery and reduces length of stay without compromising oncological outcome (1-3). Enhanced recovery after surgery (ERAS) pathways advocate minimally invasive surgery to decrease surgical stress, morbidity, length of stay and costs (4). ERAS

care protocols including multimodal pain management strategies aim to facilitate recovery by an opioid-sparing attitude to avoid opioid-related side effects (5). Epidurals have been shown to be efficient after open surgery (6), and modern pain management strategies including intravenous lidocaine, wound infiltration or transverse abdominis plane (TAP) block emerge as alternatives for minimally invasive surgery (7). Most studies comparing open and laparoscopic surgery stated less pain after minimally invasive surgery (8,9), but only scarce data reporting on pain scores and actual analgesics consumption is available.

The aims of the present study were to compare pain management strategies in patients undergoing open and minimally invasive colorectal surgical procedures, to analyse pain perception in both settings and to

[§]These authors contributed equally to this work.

*Address correspondence to:

Prof. Nicolas Demartines, Department of Visceral Surgery, Lausanne University Hospital CHUV, Bugnon 46, 1011 Lausanne, Switzerland.

E-mail: demartines@chuv.ch

identify risk factors for insufficient pain control in the postoperative period.

2. Materials and Methods

2.1. Study design

This is a prospective cohort study including all consecutive adult patients (≥ 18 years) who underwent elective or emergent colorectal surgery in the Department of Visceral Surgery at Lausanne University Hospital (CHUV), Switzerland, between January 2014 and April 2015. Perioperative confusion or language disorders represented exclusion criteria. For patients operated several times, only the first procedure was retained for the present analysis.

The prospective pain database was part of a quality improvement project and informed consent was waived by the Institutional Review Board. The study was carried out in line with the STROBE statement (10) and registered under www.researchregistry.com (UN researchregistry 2292).

2.2. Surgical details

Colorectal surgical procedures included open and minimally invasive surgeries. Converted procedures were accounted for in the minimally invasive group in an *intention-to-treat* analysis. Rectum resection, proctocolectomy and total colectomy were regrouped as extended surgery, in contrast to segmental colectomy, stoma procedures (*i.e.* ileostomy closure and Hartmann reversal) and small bowel surgery. Small bowel surgery regrouped segmental resections of the terminal ileum and different procedures related to Crohn's disease. Further were recorded the setting (elective *vs.* emergency) and the duration of the procedure. All patients were treated within a comprehensive Institutional enhanced recovery (ERAS) protocol (11) with standardized care maps.

2.3. Pain management

Type and amount of administered analgesics was recorded in a prospectively maintained database. Intraoperatively, fentanyl or sufentanyl were administered in most patients followed by paracetamol, metamizole and ibuprofen (according to ERAS caremap) at the end of the procedure unless contraindicated. Perioperative pain was managed as follows: Epidural analgesia (EDA) was applied for open procedures unless contraindicated (anticoagulant therapy, sepsis or patient refusal) and maintained for 48 or 72 hours according to ERAS protocol and type of surgery with a relay medication comprising oxycodone (oxycontin[®] and oxynorm[®]). EDA was inserted at thoracic level (Th 8-10) before induction, and iterative boluses of bupivacaine 0.25% or 0.5% were administered during the intervention, followed by a solution containing bupivacaine 0.0625%,

fentanyl 2 $\mu\text{g}/\text{mL}$ and adrenaline 2 $\mu\text{g}/\text{mL}$ for the postoperative period. For minimally invasive procedures and open procedures with EDA contraindication, iv lidocaine (1.5 mg/kg for induction, then 2 mg/kg/h until recovery room) (12) and iv ketamine (0.25 mg/kg bolus followed by 0.25 mg/kg/h, maximum 1mg/kg) (13) were applied unless contraindicated (lidocaine: hepatic failure or lidocaine intolerance, ketamine: age > 70 years, ischemic heart disease or psychotic pathology). As an alternative, ultrasound-guided transversus abdominis plane (TAP) blocks and surgical wound infiltration using bupivacaine 0.25% or naropin 0.25% were applied upon anaesthesiologists' discretion.

Postoperative use of opioids (morphine, oxycodone, buprenorphine, tramadol) were recorded from recovery room (RR) until 96 hours postoperatively.

Standardized conversion factors were used to calculate morphine equivalents (14): *iv* or *sc* morphine (3 \times), oral oxycodone (2 \times), oral buprenorphine (75 \times), oral tramadol (0.1 \times). Total morphine equivalents were recorded for the following time periods: 24 h (including RR until the end of the first postoperative day), 48 h, 72 h and 96 h.

2.4. Data collection

Data regarding different demographic (age, gender, body mass index (BMI) and American Society of Anaesthesiologists (ASA) score), surgery- and pain management-related items as specified above was entered in a computerized database, which was prospectively maintained by the anaesthesiology care team (MC and CB) and a dedicated study nurse. Visual analogue scales (VAS) were used by two clinical nurses to assess pain at rest and at mobilization (0: no pain-10: maximal pain) at the following time points: RR, arrival patient's room, 2 h, 6 h, 12 h, 24 h, 36 h, 48 h, 72 h and 96 h. Clinical nurses were blinded to pain management protocols and/or actual pain medication consumption of the patient. Insufficient pain control was defined as VAS score of ≥ 4 (15).

2.5. Outcomes/study endpoints

The primary endpoint was postoperative pain perception as measured by VAS. After propensity score matching, patients experiencing insufficient pain control (VAS ≥ 4) were compared with patients with sufficient pain control (VAS < 4), and independent risk factors for insufficient pain control within 24 hours from surgery were identified by multivariate logistic regression.

2.6. Statistical analysis

Anonymized data analysis was performed using the Stata Software v. 14.2 (StataCorp, College Station, TX, USA). Categorical data was summarized as raw

Table 1. Demographic, surgical and anaesthesia-related items

Items	All patients (n = 332)	Open (n = 156)	Minimal invasive (n = 176)	P
Age (years) (median, IQR)	64, 53-75	68, 56-78	62, 51-72	0.004
Gender				0.3
Female (%)	159 (48)	70 (45)	89 (51)	
Male (%)	173 (52)	86 (55)	87 (49)	
BMI (kg/m ²) (median, IQR)	25, 21-28	24, 21-29	25, 21-28	0.581
ASA group				< 0.001
I-II (%)	214 (65)	86 (55)	128 (73)	
III-IV (%)	118 (36)	70 (45)	48 (27)	
Type of surgery (%)				< 0.001
Left colectomy	73 (22)	14 (9)	59 (34)	
Right colectomy	60 (18)	22 (14)	38 (22)	
Rectum resection	44 (13)	14 (9)	30 (17)	
Stoma procedure	74 (22)	69 (44)	5 (3)	
Small bowel	81 (25)	37 (24)	44 (25)	
Extended (%)	51 (15)	15 (10)	36 (21)	0.006
Emergency (%)	100 (30)	48 (31)	52 (30)	0.808
Duration of surgery (min) (median, IQR)	175, 113-243	163, 98-224	181, 124-261	0.016
Duration of procedure (min) (median, IQR)	220, 152-298	205, 140-276	235, 163-306	0.014
Epidural (%)	72 (22)	57 (37)	15 (9)	< 0.001
Lidocaine (%)	114 (34)	17 (11)	97 (55)	< 0.001
TAP Block (%)	27 (8)	20 (13)	7 (4)	0.003
Infiltration (%)	38 (11)	25 (16)	13 (7)	0.014

MI – Body Mass Index, ASA – American Society of Anesthesiologists, TAP – Transversus Abdominis Plane. Bold characters indicate significant values ($p < 0.05$).

frequencies and group percentages. Differences in categorical data distributions between groups were assessed using the chi-squared test, or the Fisher's exact test in case of insufficient sample size. Continuous data distribution was analyzed using Normal QQ-Plots. Gaussian data were summarized as mean and standard deviation (SD), while non-Gaussian data were summarized as median, interquartile range (IQR) and range. Differences in means between two groups for Gaussian data were assessed using the Student's *t*-test. Differences in distribution between two groups for non-Gaussian data were assessed using the Wilcoxon-Mann-Whitney ranksum test.

As the two study groups (open vs. laparoscopic) differed on several major characteristics, propensity score matching was performed. The propensity score was derived using a probit regression model with the following cofactors: age, gender, ASA score, surgery type (right colectomy, left colectomy, stoma procedure, rectum resection, small bowel) and setting (elective vs. emergency). Matching of the laparoscopic group to the open group was performed to the nearest neighbour with replacement. Figure 1 shows the Kernel plot of the propensity score. Univariate and multivariate logistic regression was used to assess the association between several factors and binary outcomes. A *p*-value < 0.05 was considered statistically significant.

3. Results

3.1. Patients

Three hundred and thirty-two consecutive patients

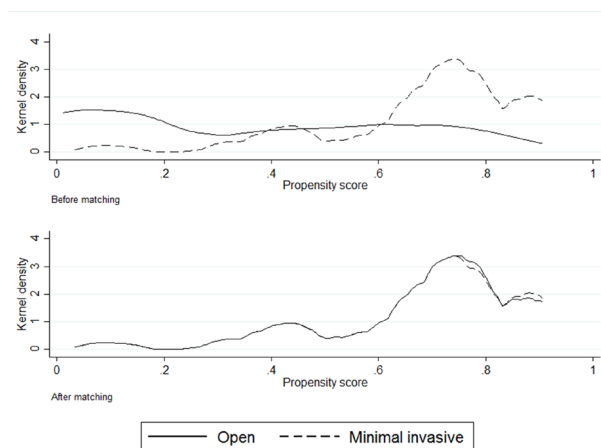


Figure 1. Propensity score matching. Kernel density plot with comparison of the two groups (open vs. minimally invasive) before (above) and after (below) propensity score matching.

underwent colorectal procedures during the study period. One hundred and fifty-six (47%) were performed by an open approach, while 176 (53%) were performed by laparoscopy. Nineteen (6%) laparoscopic procedures were converted to open approach and remained assigned to minimal invasive procedures according to the *intention-to-treat* principle. Demographic, surgery-related and pain management-related items before propensity score matching are displayed in Table 1.

3.2. Pain scores

Propensity score matching of the two groups (open vs. laparoscopic) led to a dropout of 125 patients

(38%) (Figure 1). Mean VAS scores for pain were < 3 for both comparative groups throughout the entire postoperative observation period, at rest and at mobilization. Mean VAS scores for minimal-invasively operated patients were significantly higher than for open procedures until 48 hours, at rest and mobilization ($p < 0.05$), while patients undergoing open procedures had significantly higher mean VAS scores at 72 and 96 hours at mobilization ($p < 0.05$) (Figure 2). More patients operated by minimally invasive surgery had insufficient pain control ($VAS \geq 4$) at 24 hours (19% vs. 5%, $p < 0.05$), while more patients in the open group experienced pain peaks (≥ 4) during mobilization at 72-96 hours (45% vs. 22%, $p < 0.05$) (Figure 3). Among the minimally invasive procedures, mean scores were similar throughout the observed time span when comparing patients receiving opioids only, patients receiving opioids and lidocaine and patients receiving opioids, lidocaine and ketamine, at rest and at mobilization (Figure 4). Morphine equivalent consumption was similar when comparing these 3 groups (Figure 4c).

3.3. Risk factors for insufficient pain control ($VAS \geq 4$) within 24 hours

Independent risk factors for insufficient pain control (≥ 4) were duration of procedure (Odds Ratio (OR) 3.37, 95% Confidence Interval (CI) 2.03-5.59), emergency surgery (OR 3.01, 95%CI 1.72-5.31), wound infiltration (OR 3.23, 95%CI 0.97-10.70), age < 70 years (OR 2.03, 95% CI 1.18-3.48) and ASA I-II score (OR 2.06, 95% CI 1.19-3.56) (Figure 5).

4. Discussion

Despite overall low pain scores throughout the observed time span, insufficient pain control ($VAS \geq 4$) represented a problem in the early postoperative phase in patients operated by minimal invasive approach, while open procedures were associated with pain peaks (≥ 4) at 72-96 hours. This coincides with retrieval of epidurals within ERAS care and hence insufficient management of pain relay. Further, multimodal pain management concepts did not appear to be beneficial in

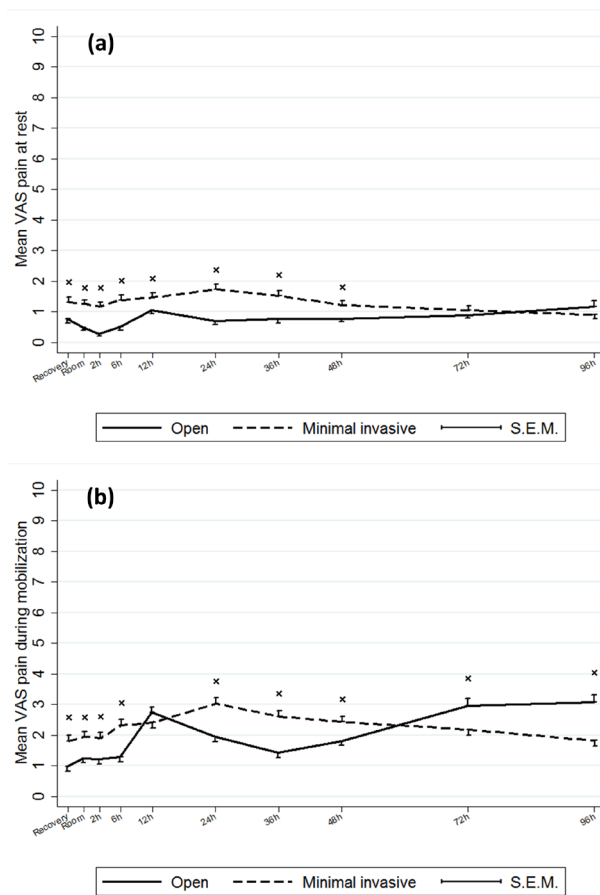


Figure 2. Evolution of pain scores over time (a) at rest, (b) at mobilization. Evolution of mean pain scores over time by comparing open and minimally invasive procedures at rest and at mobilization. x indicates statistical significance ($p < 0.05$). VAS – Visual Analog Scale, S.E.M. – Standard Error of the Mean, Recovery – Recovery room, Room – Arrival patient's room, h – hours.

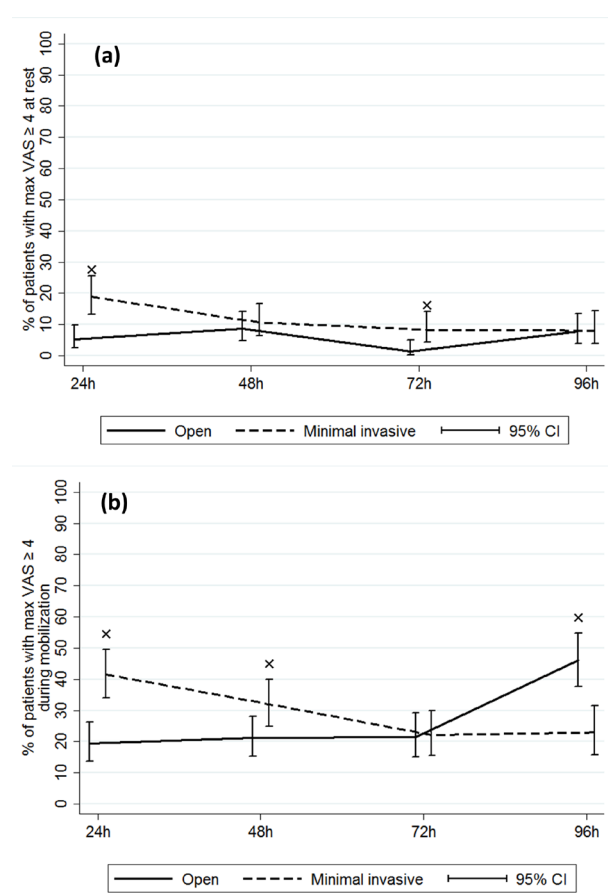


Figure 3. Patients with insufficient pain control ($VAS \geq 4$) (a) at rest, (b) at mobilization. Percentage of patients experiencing pain peaks ($VAS \geq 4$) over time by comparing open and minimal invasive procedures at rest and at mobilization. x indicates statistical significance ($p < 0.05$). VAS – Visual Analog Scale, 95% CI – 95% Confidence Interval

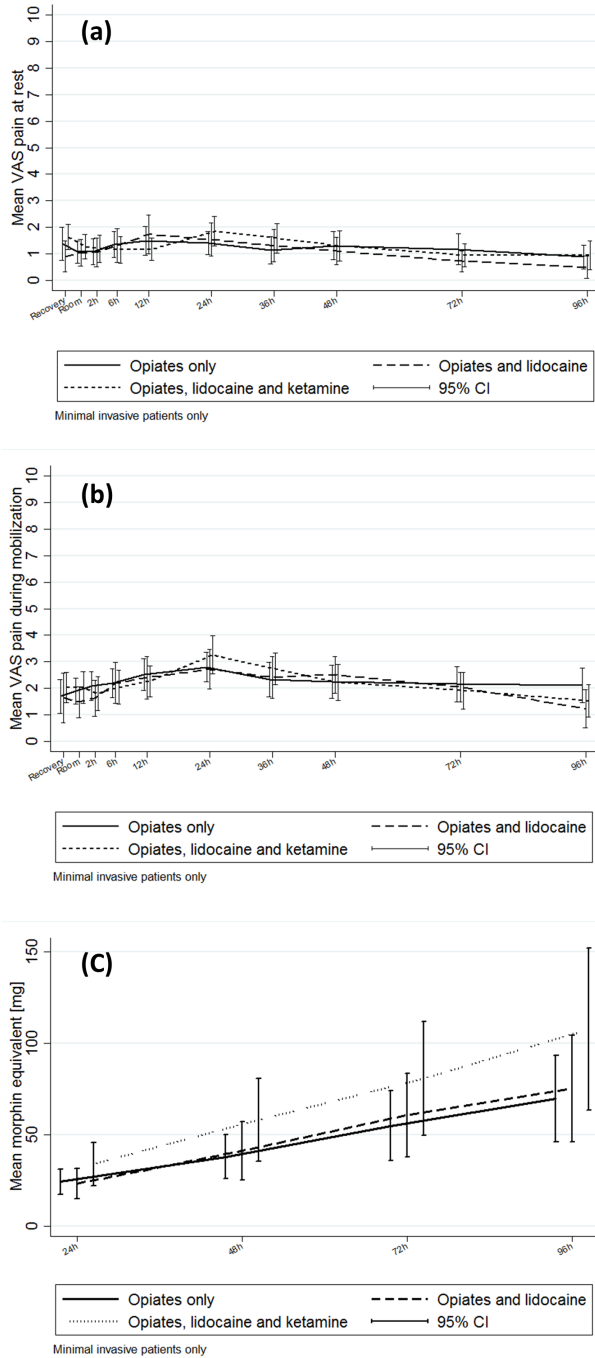


Figure 4. Pain scores and morphine requirements after laparoscopy (a) at rest, (b) at mobilization. Evolution of mean pain scores over time by comparing minimally invasively operated patients receiving perioperative opiates, opiates and lidocaine or opiates, lidocaine and ketamine. **(c) Morphine requirements.** Mean morphine equivalent consumption over time by comparing minimally invasively operated patients receiving perioperative opiates, opiates and lidocaine or opiates, lidocaine and ketamine. VAS – Visual Analog Scale, 95% CI – 95% Confidence Interval, Recovery – Recovery room, Room – Arrival patient's room, h - hours

the present cohort.

Adequate pain control after major abdominal surgery is the major concern of patients before surgery and directly related to their opinion on caregivers (16,17). Pain management is one important item of

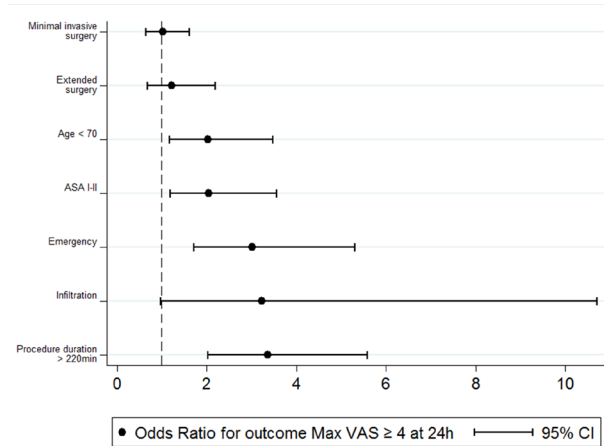


Figure 5. Independent risk factors for pain peaks (VAS ≥ 4) at 24 hours. Multivariable analysis of univariate risk factors for pain peaks (VAS ≥ 4) at 24 hours postoperatively. ASA – American Society of Anaesthesiologists, min – minutes, VAS – Visual Analog Scale, 95% CI – 95% Confidence Interval, Infiltration – perioperative wound infiltration

ERAS in colorectal surgery (18). Mid-thoracic epidural anaesthesia (EDA) is advocated for open procedures (6), while the evidence is less clear for minimal invasive surgery. EDA was associated with controversial results regarding postoperative morbidity (19,20) and slowed down recovery after laparoscopic surgery without evident benefits in recent randomized trials (21,22). Instead, numerous alternatives for peri- and postoperative pain management have been suggested for minimal invasive surgery, and the combination of different strategies in a multimodal concept has been advocated (7,23). However, despite this diversity, pain remains undermanaged even within enhanced recovery protocols (24), and a recent meta-analysis did not show any superiority of pain management within ERAS care regarding pain scores, length of stay and functional recovery (25).

Multimodal pain management strategies including non-opioid analgesia (*i.e.* acetaminophen and non-steroidal anti-inflammatory drugs), local infiltration or TAP blocks and intravenous lidocaine aim to decrease opioid consumption. This is important within enhanced recovery protocols, since opioids have been shown to impede prompt functional recovery by favoring postoperative nausea and vomiting, ileus and respiratory depression (24). However, despite a consensus for opioid-sparing management, multimodal treatment is not standardized, as shown by a recent large quality improvement survey (26), and opioids in different forms and combinations including patient controlled analgesia remain a mainstay of postoperative pain management (27).

In the present analysis, all patients were treated within an enhanced recovery protocol, and thus opioid-sparing therapy was part of perioperative care. EDA, intravenous lidocaine, TAP block and wound infiltration were used in different combinations according to

anaesthesiologist's discretion. Overall pain scores were low in the present cohort and compare well to previous reports on pain perception (26,27). However, pain scores were higher after minimally invasive surgery compared to open surgery, with up to 45% of patients experiencing pain peaks at mobilization during the first postoperative day. This contrasts with the repeatedly proven efficiency of minimal invasive surgery in decreasing postoperative pain (8,28,29). Two explanations might account for this discrepancy. First, EDA was efficient after open surgery in the present cohort, as pictured by a low number of patients with significant pain during the first 2, respectively 3 postoperative days with EDA in place. However, a significant increase of insufficient pain control (VAS \geq 4) at 72 hours indicates suboptimal management of pain relay. Since pain relay medication was standardized according to guidelines within ERAS care maps, reasons for this insufficient backup strategy might be the lack of proper surveillance of pain at EDA retrieval (30). Second, pain management after minimally invasive surgery was suboptimal and wound infiltration was even retained as independent risk factor for insufficient pain control within 24 hours in the present analysis (Figure 5). Park found in a recent randomized controlled trial that wound infiltration was less effective than TAP block in decreasing postoperative opioid consumption (31). A recent meta-analysis showed that novel infiltration techniques such as wound catheter, TAP block, and intraperitoneal instillation led to a decrease in pain scores (32). TAP block was rarely applied in the present cohort, but might represent an alternative to conventional wound infiltration (5,33). Another reason for insufficient pain relief by wound infiltration might be a lack of proper follow-up with consequent insufficient administration of backup pain medication. Taken together, the main reasons for higher pain levels in laparoscopic patients in the first 24 hours are an underestimation of actual pain after minimally invasive surgery and an overrating of multimodal pain strategies. The latter aspect was clarified by a subgroup analysis of 3 different pain strategies in laparoscopic patients as shown in the following paragraph.

In the present study, patients consumed the same amount of morphine equivalents postoperatively, regardless of adding on lidocaine and ketamine (Figure 4c). Intravenous lidocaine has been shown to reduce pain scores, intra- and postoperative analgesic requirements and to promote functional recovery (34). However, a recent Cochrane review questioned the efficiency of intravenous lidocaine and particularly its impact on pain scores, especially in the early postoperative phase, similar to the findings of the present cohort (12). Ketamine as a powerful blocker of nociceptive and inflammatory pain transmission proved efficiency in decreasing postoperative pain in recent trials (35,36). However, the optimal dose needs to be

determined by further clinical trials (37).

The present study showed thus inconclusive results using the applied multimodal pathway, and opioids remained a mainstay treatment even within an enhanced recovery pathway.

Several limitations need to be addressed. The study cohort was heterogeneous and modest in size, and no data on chronic pain issues was available for this analysis. Further, intraoperative pain management strategies were not standardized. However, perioperative care pathway was standardized (ERAS care) and applied with high compliance and in line with current recommendations. Furthermore, consecutive non-selected patients ("all-comers") were reported limiting selection bias and reflecting a "real-world" situation.

In conclusion, overall, pain was well controlled in a non-selected cohort of colorectal surgical patients, but pain peaks remained a major concern despite close adherence to ERAS guidelines including modern pain strategies. Multimodal pain concepts could not decrease morphine consumption in the present cohort. Efforts should focus on providing evidence-based standardized care protocols regarding pain management in minimally invasive surgery and for patients after open surgeries without or after removal of epidural catheter.

Acknowledgements

The authors have no conflict of interest or funding source to declare.

References

1. Bonjer HJ, Hop WC, Nelson H, Sargent DJ, Lacy AM, Castells A, Guillou PJ, Thorpe H, Brown J, Delgado S, Kuhrij E, Haglind E, Pahlman L; Transatlantic Laparoscopically Assisted vs Open Colectomy Trials Study Group. Laparoscopically assisted vs open colectomy for colon cancer: A meta-analysis. *Arch Surg.* 2007; 142:298-303.
2. Law WL, Lee YM, Choi HK, Seto CL, Ho JW. Impact of laparoscopic resection for colorectal cancer on operative outcomes and survival. *Ann Surg.* 2007; 245:1-7.
3. Jackson TD, Kaplan GG, Arena G, Page JH, Rogers SO, Jr. Laparoscopic versus open resection for colorectal cancer: a metaanalysis of oncologic outcomes. *J Am Coll Surg.* 2007; 204:439-446.
4. Greco M, Capretti G, Beretta L, Gemma M, Pecorelli N, Braga M. Enhanced recovery program in colorectal surgery: a meta-analysis of randomized controlled trials. *World J Surg.* 2014; 38:1531-1541.
5. Keller DS, Tahilramani RN, Flores-Gonzalez JR, Ibarra S, Haas EM. Pilot study of a novel pain management strategy: evaluating the impact on patient outcomes. *Surg Endosc.* 2016; 30:2192-2198.
6. Guay J, Nishimori M, Kopp S. Epidural local anaesthetics versus opioid-based analgesic regimens for postoperative gastrointestinal paralysis, vomiting and pain after abdominal surgery. *Cochrane Database Syst Rev.* 2016; 7:CD001893.

7. Levy BF, Tilney HS, Dowson HM, Rockall TA. A systematic review of postoperative analgesia following laparoscopic colorectal surgery. *Colorectal Dis.* 2010; 12:5-15.
8. Reza MM, Blasco JA, Andradas E, Cantero R, Mayol J. Systematic review of laparoscopic versus open surgery for colorectal cancer. *Br J Surg.* 2006; 93:921-928.
9. Abraham NS, Young JM, Solomon MJ. Meta-analysis of short-term outcomes after laparoscopic resection for colorectal cancer. *Br J Surg.* 2004; 91:1111-1124.
10. Vandembroucke JP, von Elm E, Altman DG, Gøtzsche PC, Mulrow CD, Pocock SJ, Poole C, Schlesselman JJ, Egger M; STROBE Initiative. Strengthening the reporting of observational studies in epidemiology (STROBE): explanation and elaboration. *Epidemiology.* 2007; 18:805-835.
11. Roulin D, Donadini A, Gander S, Griesser AC, Blanc C, Hubner M, Schafer M, Demartines N. Cost-effectiveness of the implementation of an enhanced recovery protocol for colorectal surgery. *Br J Surg.* 2013; 100:1108-1114.
12. Kranke P, Jokinen J, Pace NL, Schnabel A, Hollmann MW, Hahnenkamp K, Eberhart LH, Poepping DM, Weibel S. Continuous intravenous perioperative lidocaine infusion for postoperative pain and recovery. *Cochrane Database Syst Rev.* 2015;CD009642.
13. Berti M, Baciarello M, Troglio R, Fanelli G. Clinical uses of low-dose ketamine in patients undergoing surgery. *Curr Drug Targets.* 2009; 10:707-715.
14. Gerbershagen HJ, Aduckathil S, van Wijck AJ, Peelen LM, Kalkman CJ, Meissner W. Pain intensity on the first day after surgery: A prospective cohort study comparing 179 surgical procedures. *Anesthesiology.* 2013; 118:934-944.
15. Alschuler KN, Jensen MP, Ehde DM. Defining mild, moderate, and severe pain in persons with multiple sclerosis. *Pain Med.* 2012; 13:1358-1365.
16. Hughes M, Coolson MM, Aahlin EK, Harrison EM, McNally SJ, Dejong CH, Lassen K, Wigmore SJ. Attitudes of patients and care providers to enhanced recovery after surgery programs after major abdominal surgery. *J Surg Res.* 2015; 193:102-110.
17. Gan TJ, Habib AS, Miller TE, White W, Apfelbaum JL. Incidence, patient satisfaction, and perceptions of post-surgical pain: results from a US national survey. *Curr Med Res Opin.* 2014; 30:149-160.
18. Gustafsson UO, Scott MJ, Schwenk W, *et al.* Guidelines for perioperative care in elective colonic surgery: Enhanced Recovery After Surgery (ERAS[®]) Society recommendations. *World J Surg.* 2013; 37:259-284.
19. Hughes MJ, Ventham NT, McNally S, Harrison E, Wigmore S. Analgesia after open abdominal surgery in the setting of enhanced recovery surgery: A systematic review and meta-analysis. *JAMA Surg.* 2014; 149:1224-1230.
20. Chilvers CR, Nguyen MH, Robertson IK. Changing from epidural to multimodal analgesia for colorectal laparotomy: An audit. *Anaesth Intensive Care.* 2007; 35:230-238.
21. Hubner M, Blanc C, Roulin D, Winiker M, Gander S, Demartines N. Randomized clinical trial on epidural versus patient-controlled analgesia for laparoscopic colorectal surgery within an enhanced recovery pathway. *Ann Surg.* 2015; 261:648-653.
22. Levy BF, Scott MJ, Fawcett W, Fry C, Rockall TA. Randomized clinical trial of epidural, spinal or patient-controlled analgesia for patients undergoing laparoscopic colorectal surgery. *Br J Surg.* 2011; 98:1068-1078.
23. Garimella V, Cellini C. Postoperative pain control. *Clin Colon Rectal Surg.* 2013; 26:191-196.
24. Tan M, Law LS, Gan TJ. Optimizing pain management to facilitate Enhanced Recovery After Surgery pathways. *Can J Anaesth.* 2015; 62:203-218.
25. Chemali ME, Eslick GD. A Meta-Analysis: Postoperative Pain Management in Colorectal Surgical Patients and the Effects on Length of Stay in an Enhanced Recovery After Surgery (ERAS) Setting. *Clin J Pain.* 2017; 33:87-92.
26. Regenbogen SE, Mullard AJ, Peters N, Brooks S, Englesbe MJ, Campbell DA Jr, Hendren S. Hospital Analgesia Practices and Patient-reported Pain After Colorectal Resection. *Ann Surg.* 2016; 264:1044-1050.
27. Maheshwari K, Cummings KC, 3rd, Farag E, Makarova N, Turan A, Kurz A. A temporal analysis of opioid use, patient satisfaction, and pain scores in colorectal surgery patients. *J Clin Anesth.* 2016; 34:661-667.
28. Lourenco T, Murray A, Grant A, McKinley A, Krukowski Z, Vale L. Laparoscopic surgery for colorectal cancer: safe and effective? - A systematic review. *Surg Endosc.* 2008; 22:1146-1160.
29. Schwenk W, Haase O, Neudecker J, Muller JM. Short term benefits for laparoscopic colorectal resection. *Cochrane Database Syst Rev.* 2005;CD003145.
30. Genord C, Frost T, Eid D. Opioid exit plan: A pharmacist's role in managing acute postoperative pain. *J Am Pharm Assoc (2003).* 2017; 57:S92-S98.
31. Park JS, Choi GS, Kwak KH, Jung H, Jeon Y, Park S, Yeo J. Effect of local wound infiltration and transversus abdominis plane block on morphine use after laparoscopic colectomy: a nonrandomized, single-blind prospective study. *J Surg Res.* 2015; 195:61-66.
32. Ventham NT, O'Neill S, Johns N, Brady RR, Fearon KC. Evaluation of novel local anesthetic wound infiltration techniques for postoperative pain following colorectal resection surgery: A meta-analysis. *Dis Colon Rectum.* 2014; 57:237-250.
33. Walter CJ, Maxwell-Armstrong C, Pinkney TD, Conaghan PJ, Bedforth N, Gornall CB, Acheson AG. A randomised controlled trial of the efficacy of ultrasound-guided transversus abdominis plane (TAP) block in laparoscopic colorectal surgery. *Surg Endosc.* 2013; 27:2366-2372.
34. McCarthy GC, Megalla SA, Habib AS. Impact of intravenous lidocaine infusion on postoperative analgesia and recovery from surgery: A systematic review of randomized controlled trials. *Drugs.* 2010; 70:1149-1163.
35. Laskowski K, Stirling A, McKay WP, Lim HJ. A systematic review of intravenous ketamine for postoperative analgesia. *Can J Anaesth.* 2011; 58:911-923.
36. Jouguelet-Lacoste J, La Colla L, Schilling D, Chelly JE. The use of intravenous infusion or single dose of low-dose ketamine for postoperative analgesia: A review of the current literature. *Pain Med.* 2015; 16:383-403.
37. Vadivelu N, Schermer E, Kodumudi V, Belani K, Urman RD, Kaye AD. Role of ketamine for analgesia in adults and children. *J Anaesthesiol Clin Pharmacol.* 2016; 32:298-306.

(Received December 15, 2017; Revised January 19, 2018; Accepted February 12, 2018)

Outcome of elderly patients after acute biliary pancreatitis

Didier Roulin^{1,§}, Raphaël Girardet^{1,§}, Rafael Duran², Steven Hajdu², Alban Denys², Nermin Halkic¹, Nicolas Demartines^{1,*}, Emmanuel Melloul¹

¹Department of Visceral Surgery, University Hospital of Lausanne (CHUV), Switzerland;

²Department of Radiology, University Hospital of Lausanne (CHUV), Switzerland.

Summary

The specific management and outcome of acute biliary pancreatitis in elderly patients is not well established. The aim of this study was to assess the outcome of elderly compared to younger patients after acute biliary pancreatitis. Retrospective analysis of consecutive patients admitted with acute biliary pancreatitis between January 2006 and December 2012. Elderly patients (≥ 70 years) were compared to younger patients (< 70 years) in a case-control study. Comorbidities were assessed according to the Charlson score. Clinical (Atlanta score) and radiological (Balthazar and computed tomography severity index scores) severity were analyzed, as well as clinical outcome. Among 212 patients admitted with acute biliary pancreatitis, 76 were > 70 years (35.8%). Elderly patients had a higher Charlson comorbidity index score at admission ($p < 0.001$). No difference was observed in terms of clinical and radiological severity of acute pancreatitis. The median hospital stay was longer in elderly (11 days, interquartile range 7-15) than in younger patients (7 days, interquartile range 5-11) ($p < 0.001$). No difference was observed regarding in-hospital 90-day mortality (3 vs. 1 patients, $p = 0.133$). Elderly patients had similar clinical and radiological severity of acute biliary pancreatitis compared to younger patients.

Keywords: Pancreatitis, aged, gallstones

1. Introduction

Acute pancreatitis is a common cause of surgical admission with an annual incidence that varies between 4.0-45.3 /100,000 and an overall mortality risk of 3-20% (1). Gallstone is the most frequent cause of acute pancreatitis (24 to 71%) and its incidence increase with age (1-4).

Different studies addressing the relation between age and prognosis of acute pancreatitis displayed conflicting results (4-6). A study published in 1988 found higher mortality in patients over 75 years, but complication rate and the proportion of patients with severe disease was not different (4). On the other hand, more recent studies observed that acute pancreatitis was more severe in elderly patients without increased mortality (5,6).

However, none of these studies focused exclusively on biliary pancreatitis.

This present study aimed to evaluate the clinical severity, radiological presentation, and outcome of acute biliary pancreatitis in elderly patients over 70 years compared to younger patients.

2. Materials and Methods

2.1. Study design

Case-control study comparing patients over 70 years (study group) to younger patients (control group).

A retrospective analysis was performed of all consecutive patients admitted or secondarily referred with acute biliary pancreatitis to our institution, a tertiary referral center, between January 2006 and December 2012. The Institutional Review Board approved the study (119/13). The study was registered on www.researchregistry.com (UIN 2363). The study was conducted in accordance with the STrengthening the Reporting of OBServational studies in Epidemiology (STROBE) criteria (<http://strobe-statement.org/>). Data

[§]These authors contributed equally to this work.

*Address correspondence to:

Prof. Nicolas Demartines, Department of Visceral Surgery, University Hospital Lausanne (CHUV), Bugnon 46, 1011 Lausanne, Switzerland.

E-mail: demartines@chuv.ch

was collected in 2014. All consecutive patients (> 18 years) with a diagnosis of acute biliary pancreatitis were included. The diagnosis of acute pancreatitis required 2 of the following 3 features: abdominal pain consistent with acute pancreatitis, serum lipase (or amylase) higher than at least 3 times the upper limit of normal, and characteristic findings of acute pancreatitis on contrast-enhanced computed tomography or magnetic resonance imaging or transabdominal ultrasonography (7). A biliary etiology of acute pancreatitis was determined by the presence of gallstone or sludge in the gallbladder or in the common bile duct, with neither evidence for alcohol abuse nor for another cause. Patients with pancreatitis secondary to endoscopic retrograde cholangiopancreatography, were not included.

2.2. Outcome measures

Demographics data included age at the time of admission, gender, previous episode of acute biliary pancreatitis before the study period, and previous cholecystectomy. Patients' comorbidities were assessed including arterial hypertension, obesity (defined as a Body Mass Index (BMI) > 30 kg/m²), diabetes, hypercholesterolemia, hypertriglyceridemia, ischemic heart disease, congestive heart failure, chronic obstructive pulmonary disease and chronic renal failure. The Charlson comorbidity index was calculated for every patient (8).

Clinical severity of acute pancreatitis was defined according to the revised Atlanta criteria (7). Radiological severity of acute pancreatitis was assessed using the Balthazar grade (9), the Computed Tomography Severity Index (CTSI) (10) and the modified CTSI (11). Local complications such as pseudocyst formation, portal venous thrombosis, pleural effusion, and intra-abdominal pseudoaneurysmal bleeding were assessed.

Patients underwent abdominal MultiDetector Computed Tomography (MDCT) scans which were performed 48 hours following the appearance of symptoms. MDCT scans were performed on a 64-detector row scanner (Lightspeed VCT; 64 Pro, GE Healthcare; Milwaukee, WI, USA). The imaging protocol included the whole abdomen and pelvis (120 kV, 300-400 mA, pitch 1.375). After an unenhanced phase (2.5/2 mm reconstructed axial slices), iodinated contrast medium was injected (Accupaque[®], 300 mgI/mL; GE Healthcare; volume in mL = body weight+30 mL) at a flow rate of 4 mL/s, followed by an arterial phase (25 s, 1.25/1mm reconstructed axial slices) and a venous phase (80 s, 2.5/2mm reconstructed axial slices) scans. Image analysis was performed by 2 board-certified radiologists (R.D. and S.H, with 9 and 6 years of experience in abdominal imaging, respectively) during a consensus reading. The Balthazar grading and CTSI score were assessed. Radiologists were blinded to clinical outcomes.

The different treatments performed were assessed, including: antibiotics, Endoscopic Retrograde

Cholangiopancreatography (ERCP), percutaneous or transgastric drainage of intra-abdominal fluid collections and surgical necrosectomy. Hospital and intensive care unit length of stay, as well as in-hospital 90-day mortality was noted. Patient's discharge destination (home or nursing home) was collected. The rate of cholecystectomy (excluding patients with previous cholecystectomy) as well as the interval between admission for acute pancreatitis and cholecystectomy was measured. The recurrence of acute biliary pancreatitis during the study period was also recorded.

2.3. Statistical analysis

Descriptive statistics for categorical variables were reported as numbers and percentages, while continuous variables were reported as medians and interquartile ranges for non-normally distributed data or means and standard deviations for normally distributed data. The Student *t* test or the Mann-Whitney *U* test were used to compare continuous variables. Fisher's exact test or Chi-Square test were used for the comparison of categorical variables. A *p* value < 0.05 was considered statistically significant. All statistical analyses were performed using SPSS 22.0 software (SPSS Inc., Chicago, IL, USA).

3. Results

During the study period, 481 patients were hospitalized for acute pancreatitis (Figure 1). Among them, a total of 212 patients (aged 18 - 99 years) with acute biliary pancreatitis were included in the analysis. Seventy-six patients were 70 years or over (study group) and 136 were younger than 70 years (control group).

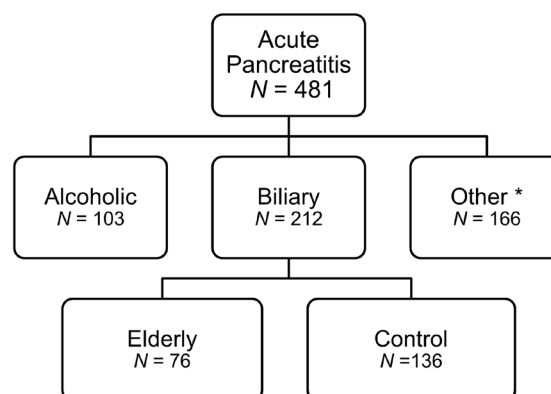


Figure 1. Flow diagram of patients admitted with acute pancreatitis. *Others: idiopathic (*N* = 110), traumatic or following endoscopic retrograde cholangiopancreatography (*N* = 26), drug-induced (*N* = 12), tumoral (*N* = 7), hypertriglyceridemia-induced (*N* = 3), mucoviscidosis (*N* = 2), pancreas divisum (*N* = 1), duodenal diverticula (*N* = 1), perforated ulcer (*N* = 1), hemobilia (*N* = 1), auto-immune (*N* = 1), hypercalcemia (*N* = 1). Elderly: ≥ 70 years; Control < 70 years.

3.1. Patients demographics and comorbidities

Patients demographics and comorbidities are listed in Table 1. The study group had a mean age of 81 years, and the control group a mean age of 45 years. There was no significant difference in the number of acute episodes of pancreatitis before admission ($p = 1.000$) and history of cholecystectomy between both groups ($p = 0.491$). Elderly patients had a significantly higher Charlson comorbidity score ($p < 0.001$), with a higher rate of hypertension ($p = 0.001$), diabetes ($p = 0.012$), ischemic heart disease ($p = 0.001$), chronic obstructive pulmonary disease ($p = 0.026$), and chronic renal disease ($p = 0.001$), than the control group.

3.2. Clinical and radiological severity

According to the Atlanta classification, the clinical severity of pancreatitis was similar in elderly and young patients with most mild acute pancreatitis in both groups (67% vs. 65%, respectively), as shown in Table 2. The radiological extent of pancreatitis assessed by the Balthazar grading was similar between elderly and young patients ($p = 0.172$). No significant differences were observed between the study and control groups in terms of median CTSI score (2 vs. 2, $p = 0.160$) or modified CTSI score (2 vs. 2, $p = 0.693$). The CTSI could not be established in 31 elderly patients (41%) and in 34 in the control group (25%). Among these patients with unknown CTSI, 11 vs 1 had a computed tomography without intravenous contrast, 12 vs 21 had an abdominal ultrasound or magnetic resonance imaging, and 8 vs. 12 had no imaging in the study vs.

Table 1. Patients demographics and comorbidities

N (%)	Elderly, N = 76	Control, N = 136	p value
Age, years, median (IQR)	79 (75-85)	47 (30-57)	< 0.001
Sex ratio, M:F	26 : 50	56 : 80	0.378
Previous pancreatitis (%)	4 (5.3)	8 (5.9)	1.000
Previous cholecystectomy (%)	10 (13.2)	13 (9.6)	0.491
Charlson score, median (IQR)	1 (0-3)	0 (0-0)	< 0.001
Hypertension (%)	49 (64.5)	33 (24.3)	< 0.001
Obesity (%)	8 (10.5)	11 (8.1)	0.619
Diabetes (%)	20 (26)	16 (12)	0.012
Hypercholesterolemia (%)	13 (17.1)	18 (13.2)	0.544
Hypertriglyceridemia (%)	4 (5.3)	5 (3.7)	0.725
Ischemic heart disease (%)	22 (28.9)	7 (5.1)	< 0.001
Chronic obstructive pulmonary disease (%)	6 (7.9)	2 (1.4)	0.026
Congestive heart failure	4 (5.3)	1 (0.7)	0.057
Chronic renal disease (%)	20 (26.3)	3 (2.2)	< 0.001
Dialysis (%)	0 (0)	0 (0)	1.000

IQR, interquartile range.

Table 2. Clinical and radiological severity of acute biliary pancreatitis

N (%)	Elderly, N = 76	Control, N = 136	p value
Atlanta classification			0.210
Mild	51 (67.1)	88 (64.7)	
Moderately severe	21 (27.6)	46 (33.8)	
Severe	4 (5.3)	2 (1.5)	
Balthazar grade			0.172
A (%)	16 (21.1)	25 (18.4)	
B (%)	8 (10.5)	10 (7.4)	
C (%)	21 (27.6)	26 (19.1)	
D (%)	5 (6.6)	23 (16.9)	
E (%)	10 (13.2)	27 (19.9)	
Unknown (%)	16 (21.1)	25 (18.4)	
CTSI, median (IQR)	2 (1-3)	2 (1-4)	0.160
Mild (0-3)	35 (46.1)	66 (48.5)	
Moderate (4-6)	6 (7.9)	33 (24.3)	
Severe (7-10)	4 (5.3)	3 (2.2)	
Unknown	31 (40.8)	34 (25.0)	
Modified CTSI, median (IQR)	2 (2-4)	2 (0-6)	0.693
Mild (0-2)	26 (34.2)	51 (37.5)	
Moderate (4-6)	15 (19.7)	39 (28.7)	
Severe (8-10)	4 (5.3)	12 (8.8)	
Unknown	31 (40.8)	34 (25.0)	

CTSI: Computed tomography severity index.

control group, respectively ($p = 0.089$).

3.3. Complications

As shown on Table 3, a higher rate of portal vein thrombosis was observed in the elderly patients compared to young patients (12% vs. 2%, respectively; $p=0.018$). There was no significant difference in terms of occurrence of pseudocysts (8 vs. 6, $p = 0.146$), pseudoaneurysmal bleeding (0 vs. 2, $p = 0.538$), and pleural effusion (19 vs. 30, $p = 0.616$).

3.4. Management

Elderly patients required more ERCP (38% vs. 21%, respectively; $p = 0.009$) and endoscopic drainage of infected intra-abdominal collections (4% vs. 0%, respectively; $p = 0.045$) compared to younger patients. No statistically significant differences were observed for antibiotherapy, percutaneous drainage, or the need for surgical necrosectomy or bowel resection (Table 4).

3.5. Outcome

In comparison to the control group, elderly patients had a longer hospital length of stay (median, 11 vs. 7 days,

in study and control groups, respectively; $p < 0.001$), with a higher proportion (26% vs. 2%, $p < 0.001$) of them being discharged to a nursing home or another hospital as they needed further nursing care due to their advanced age and comorbidities (Table 5). Three elderly and one younger patients were dead within 90 days. Three patients died from multiorgan failure and one patient died from septic shock. Seven elderly patients (9%) required admission to the intensive care unit (ICU) compared to 5 younger patients (4%) ($p = 0.103$) with a similar median ICU length of stay (8 vs. 6 days, $p = 0.870$). No difference was observed between the two groups regarding in-hospital 90-day mortality (3 vs. 1 patients, $p = 0.133$). Following recovery, the control group underwent significantly more elective laparoscopic cholecystectomy than the study group (109/123 patients (88.6%) and 35/66 patients (53.0%), respectively ($p = 0.041$)).

4. Discussion

The present study is, to our knowledge, the largest study focusing on elderly patients with acute biliary pancreatitis. The results suggest that despite higher pre-existing comorbidities in elderly patients, clinical and radiological severity of acute biliary pancreatitis

Table 3. Local complications during in-hospital stay

N (%)	Elderly, N = 76	Control, N = 136	p value
Pseudocyst (%)	8 (11.8)	6 (4.4)	0.146
Portal venous thrombosis (%)	8 (11.8)	3 (2.2)	0.018
Pseudoaneurysmal bleeding (%)	0 (0)	2 (0.7)	0.538
Pleural effusion (%)	19 (25.0)	30 (22.1)	0.616

Table 4. Management of acute biliary pancreatitis

N (%)	Elderly, N = 76	Control, N = 136	p value
Antibiotherapy (%)	19 (25.0)	30 (22.1)	0.616
ERCP (%)	29 (38.2)	28 (20.6)	0.009
Percutaneous drainage (%)	6 (7.9)	5 (3.7)	0.207
Endoscopic drainage (%)	3 (3.9)	0 (0)	0.045
Surgical necrosectomy (%)	2 (2.6)	3 (2.2)	1.000
Bowel resection	2 (2.6)	0 (0)	0.127

ERCP: Endoscopic retrograde cholangiopancreatography.

Table 5. Outcome following acute biliary pancreatitis

N (%)	Elderly, N = 76	Control, N = 136	p value
Hospital length of stay, median (IQR)	11 (7-15)	7 (5-11)	< 0.001
ICU length of stay, median (IQR)	8 (2-11)	6 (4-30)	0.870
In-hospital 90-day mortality (%)	3 (3.9)	1 (0.7)	0.133
Discharged home (%)	52 (68.4)	132 (97.1)	< 0.001
Recurrence of acute pancreatitis (%)	8 (10.5)	16 (11.8)	1.000

IQR, Interquartile range ; ICU : Intensive care unit.

is comparable to younger patients. However, a longer length of hospital stay was observed, with a higher proportion of elderly patients requiring secondary transfer to nursing home or another hospital.

Despite multiple comorbidities and higher Charlson index in the elderly group at admission, the present study suggests that age did affect neither mortality nor severity of acute biliary pancreatitis. These results are supported by data from previous studies showing that only 6% of patients older than 65 years developed severe acute pancreatitis (12), while others found no link between age and the risk of mortality from pancreatitis (2). There was no significant difference in the radiological severity between elderly and younger patients as assessed by both CTSI and modified CTSI. Both CTSI indexes were evaluated as being more accurate than the APACHE II score to diagnose clinically severe disease and did better correlate with pancreatic infection and the need for intervention (13). Furthermore, the modified CTSI seemed to correlate better with clinical outcome compared to the CTSI (14).

On the other hand, the complications and management of acute biliary pancreatitis seemed to be different between young and elderly patients. Elderly had a significantly higher rate of portal vein thrombosis. According to a recent systematic review, the prevalence of portal vein thrombosis in acute pancreatitis is 6% (15). The later study suggested that the risk of extrahepatic portal vein thrombosis was increased in patients with pseudocysts (16). Although the present study was not designed to address this issue, there was no difference between the young and elderly patients in the rate of pseudocyst formation. In addition, elderly patients needed more invasive procedures like percutaneous or endoscopic transgastric drainage of infected collections. This more invasive approach may result from a higher susceptibility of elderly to infection, and hence a lower threshold to initiate invasive treatment of intra-abdominal fluid collections in this group.

In case of mild biliary pancreatitis, early or same-admission cholecystectomy is recommended to avoid recurrent gallstone-related complications as confirmed by a recent randomized trial (17). The present study suggests that laparoscopic cholecystectomy is safe in elderly patients with a similar timing between acute pancreatitis and surgery when compared to young patients. Of note, more ERCP were performed in elderly during their hospital stay due to higher rate of obstructive cholangitis. According to a recent study including patients older than 65 years with acute biliary pancreatitis and acute cholangitis, 25% of elderly patients presented relapsed biliary complications after discharge (12). According to a previous study where ERCP in older patients with no cholecystectomy reduced the risk of developing further episode of biliary pancreatitis, ERCP with sphincterotomy should

be considered when cholecystectomy is postponed or contra-indicated following an episode of biliary pancreatitis in elderly patients (18).

Several limitations to this study need to be addressed. First, this is a retrospective study from a single center, but data were collected prospectively what could decrease selection bias. As a direct consequence of the retrospective study design, no systematic follow-up could be performed. Therefore, cholecystectomy rate needs to be cautiously interpreted, as this operation could have been performed in another hospital. The number of severe pancreatitis was low in both group and no specific conclusion could be drawn for severe pancreatitis. A significant proportion of patients (41% in the elderly patients and 25% in the control group) had no injected computed tomography to establish the radiological severity based on validated scores. This was mainly due to contraindications to the injection of soluble contrast medium (such as previous contrast medium allergic reaction or renal failure), and the use of another imaging modality such as magnetic resonance imaging. However, this reflects daily management of patients out of a specific clinical trial what would have led to a "study-effect". Nonetheless, all available imaging was systematically reviewed by two experienced radiologists.

In conclusion, the results of this study suggest that radiological and clinical severity of acute biliary pancreatitis is similar between young and elderly patients. However, elderly patients required more invasive procedures to treat intraabdominal infected collections and developed more extrahepatic portal vein thrombosis compared to young patients. This data should be considered to be proactive in the management of acute biliary pancreatitis among elderly patients.

References

1. Yadav D, Lowenfels AB. Trends in the epidemiology of the first attack of acute pancreatitis: A systematic review. *Pancreas*. 2006; 33:323-330.
2. Gullo L, Migliori M, Olah A, Farkas G, Levy P, Arvanitakis C, Lankisch P, Beger H. Acute pancreatitis in five European countries: Etiology and mortality. *Pancreas*. 2002; 24:223-227.
3. de Beaux AC, Palmer KR, Carter DC. Factors influencing morbidity and mortality in acute pancreatitis; an analysis of 279 cases. *Gut*. 1995; 37:121-126.
4. Fan ST, Choi TK, Lai CS, Wong J. Influence of age on the mortality from acute pancreatitis. *Br J Surg*. 1988; 75:463-466.
5. Kim JE, Hwang JH, Lee SH, Cha BH, Park YS, Kim JW, Jeong SH, Kim N, Lee DH. The clinical outcome of elderly patients with acute pancreatitis is not different in spite of the different etiologies and severity. *Arch Gerontol Geriatr*. 2012; 54:256-260.
6. Losurdo G, Iannone A, Principi M, Barone M, Rinaldo N, Ierardi E, Di Leo A. Acute pancreatitis in elderly patients: A retrospective evaluation at hospital admission. *Eur J Intern Med*. 2016; 30:88-93.

7. Banks PA, Bollen TL, Dervenis C, Gooszen HG, Johnson CD, Sarr MG, Tsiotos GG, Vege SS; Acute Pancreatitis Classification Working Group. Classification of acute pancreatitis – 2012: Revision of the Atlanta classification and definitions by international consensus. *Gut*. 2013; 62:102-111.
8. Charlson ME, Pompei P, Ales KL, MacKenzie CR. A new method of classifying prognostic comorbidity in longitudinal studies: Development and validation. *J Chronic Dis*. 1987; 40:373-383.
9. Balthazar EJ, Ranson JH, Naidich DP, Megibow AJ, Caccavale R, Cooper MM. Acute pancreatitis: prognostic value of CT. *Radiology*. 1985; 156:767-772.
10. Balthazar EJ, Robinson DL, Megibow AJ, Ranson JH. Acute pancreatitis: Value of CT in establishing prognosis. *Radiology*. 1990; 174:331-336.
11. Morteale KJ, Wiesner W, Intriére L, Shankar S, Zou KH, Kalantari BN, Perez A, vanSonnenberg E, Ros PR, Banks PA, Silverman SG. A modified CT severity index for evaluating acute pancreatitis: improved correlation with patient outcome. *AJR Am J Roentgenol*. 2004; 183:1261-1265.
12. Garcia-Alonso FJ, de Lucas Gallego M, Bonillo Cambrodon D, Algaba A, de la Poza G, Martin-Mateos RM, Bermejo F. Gallstone-related disease in the elderly: is there room for improvement? *Dig Dis Sci*. 2015; 60:1770-1777.
13. Bollen TL, Singh VK, Maurer R, Repas K, van Es HW, Banks PA, Morteale KJ. Comparative evaluation of the modified CT severity index and CT severity index in assessing severity of acute pancreatitis. *AJR Am J Roentgenol*. 2011; 197:386-392.
14. Raghuwanshi S, Gupta R, Vyas MM, Sharma R. CT evaluation of acute pancreatitis and its prognostic correlation with CT severity index. *J Clin Diagn Res*. 2016; 10:TC06-11.
15. Xu W, Qi X, Chen J, Su C, Guo X. Prevalence of splanchnic vein thrombosis in pancreatitis: A systematic review and meta-analysis of observational studies. *Gastroenterol Res Pract*. 2015; 2015:245460.
16. Rebours V, Boudaoud L, Vullierme MP, Vidaud D, Condat B, Hentic O, Maire F, Hammel P, Ruszniewski P, Levy P. Extrahepatic portal venous system thrombosis in recurrent acute and chronic alcoholic pancreatitis is caused by local inflammation and not thrombophilia. *Am J Gastroenterol*. 2012; 107:1579-1585.
17. da Costa DW, Bouwense SA, Schepers NJ, *et al*. Same-admission versus interval cholecystectomy for mild gallstone pancreatitis (PONCHO): A multicentre randomised controlled trial. *Lancet*. 2015; 386:1261-1268.
18. Trust MD, Sheffield KM, Boyd CA, Benarroch-Gampel J, Zhang D, Townsend CM, Jr., Riall TS. Gallstone pancreatitis in older patients: Are we operating enough? *Surgery*. 2011; 150:515-525.

(Received November 30, 2017; Revised January 15, 2018; Accepted February 12, 2018)

Safety and feasibility of a novel non-thermal device for tissue dissection: A preliminary study of the DD1 differential dissector

Nao Yoshida¹, Shintaro Yamazaki^{1,*}, Masahiko Sugitani², Tadatoshi Takayama¹

¹Department of Digestive Surgery, Nihon University School of Medicine, Tokyo, Japan;

²Department of Pathology, Nihon University School of Medicine, Matsumoto, Tokyo, Japan;

Summary

Energy devices can cause significant thermal damage to surrounding tissues causing unanticipated organ trauma. To evaluate the safety and feasibility of a novel electric device (DD1) for soft tissue dissection. Three series of measurements were performed in a pig model. First, macro- and microscopic tissue damage was compared between the DD1 and an electric scalpel (ES). Second, the time course of tissue temperature was measured for the DD1 and three other energy devices (ES, Harmonic and LigaSure). Third, the time required for mobilization of a peripheral artery of the intestine was compared between the DD1 and manual, non-energized forceps. First, the tissue damage area caused by ES was significantly larger compared to that in the DD1 at all time points ($p < 0.0001$). The number of damaged cells due to thermal damage was significantly larger for ES than for DD1, even when the DD1 was applied to a single point at maximum power for 60 sec ($p < 0.0001$). Second, the maximum temperature of Harmonic was 160°C 3 sec after use and dropped to 68°C after 10 sec. At the same time points after use, we observed: ES (84°C, 45°C), LigaSure (61°C, 49°C), and DD1 (30.5°C, 29°C). Third, the median dissection time for the artery using DD1 was significantly shorter than that for dissecting forceps (DD1: 100 sec, range 70-205 sec vs. forceps: 130 sec, range 90-210 sec, $p = 0.0325$). DD1 was a safe non-thermal device which causes less tissue damage while also providing shorter dissection times than manual dissection.

Keywords: Tissue dissection, thermal damage, animal model

1. Introduction

Surgical dissection is a broad term that encompasses the general activities of separating and dividing tissues (1). It is usually divided into sharp and blunt dissection, distinguished as slicing tissues (sharp) and teasing tissues apart (blunt). Some surgeons would add a third type, energy or coagulating dissection, in which electric current or another source of heat is used to simultaneously coagulate and divide tissues (2-11).

Energy dissectors have undergone a tremendous transformation over the past 20 years, yielding instruments that are multi-functional (sharp, blunt, vessel sealing, e.g. bipolar and ultrasonic instruments) and that are now broadly used for almost all dissection

during a surgical procedure. Energy dissectors, however, have significant limitations due to the large amounts of heat they produce. These limitations lead to several intraoperative complications, such as accidental thermal trauma to blood vessels, nerves, ureters, and bowels (12-18). Furthermore, thermal instruments can unintentionally fuse adjacent layers, leading to misinterpretation of tissue layers and, subsequently, dissection into the wrong plane. Some studies indicate that by using powerful hemostatic device did not affect operative time (2-3). Therefore, surgeons need new instruments that improve blunt dissection, providing them with the ability to dissect quickly but without the safety compromises created by current energy dissectors.

The Model DD1 Differential Dissector is a newly developed non-thermal surgical instrument designed for blunt dissection (PhyScient, USA) which preserves vessels and nerves in connective tissues with minimal damage to the target organ. The DD1 is designed to selectively dissect loose connective tissue while having little effect on dense connective tissue. It thus selectively

*Address correspondence to:

Dr. Shintaro Yamazaki, Department of Digestive Surgery, Nihon University School of Medicine, 30-1 Ohayaguchi kamimachi, Itabashi-ku, Tokyo 173-8610, Japan.
E-mail: yamazaki-nmed@umin.ac.jp

dissects along tissue planes.

In this study, we assess the safety and feasibility of DD1, comparing other energy devices in an abdominal surgical model in pigs.

2. Materials and Methods

2.1. Overview of experiments

The DD1 has a plastic tip made of polyetheretherketone (PEEK) that rapidly vibrates to mechanically tease tissues apart. (Figure 1) Vibration is driven by a motor and batteries that are in the handle, making the device cordless. A control knob in the handle adjusts the vibration speed. The surgeon controls dissection by determining the point of application of the vibrating tip, the speed of vibration, the force with which the tip is pushed into the tissue plane, and the force of counter-traction.

Three different types of experiments were conducted on live, anesthetized pigs: First, tissue trauma arising from transient contact with a variety of different tissues was evaluated for two devices: DD1 and electric scalpel (ES); Second, thermal measurements were made for four devices (DD1, ES, Harmonic (Ethicon, USA), and LigaSure (Covidien, Ireland)) *via* thermal videography. Third, the speed of dissection was compared between the DD1 and manual forceps for mobilizing the mesentery arteries of the small intestine. In our experience, 50% power setting (middle vibration speed) is suitable for most tissues. Additionally, the DD1 works best when the tissues are moist, so moistening the surface with saline permits more delicate dissection while also reducing the risk of desiccation.

2.2. Animals

Five pigs aged two to three months and weighing 35 to 45 kg were used. For anesthesia, a mixture of intramuscular ketamine (10 mg/kg), xylazine hydrochloride (2 mg/kg), and atropine sulfate (0.5 mg/head) were used. To keep anesthesia (PRO-45 Va, Acoma Inc. Tokyo, Japan), a mixture of 1 to 3% isoflurane and oxygen was given *via* a tracheal tube (NS-5000A, Acoma Inc., Japan). After the operation, the animals were put under deep anesthesia and blood was drained from the inferior vena cava. Each test site on the tissues was excised, fixed with 10% formalin, and embedded in paraffin. The paraffin block was sliced in 5 μ m slices at the marking site, then histopathological evaluation was performed after hematoxylin eosin (HE) staining. All procedures were performed by a single surgeon with 20 years of experience.

The handling of experimental animals was in accordance with *the National Academy of Sciences' Guide for the Care and Use of Laboratory Animals* as well as the Act on Welfare and Management of

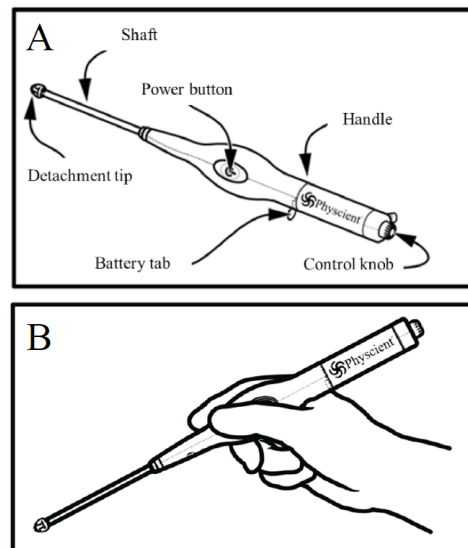


Figure 1. Schema of DD1. A plastic tip made of polyether/ether/ketone on the shaft of the DD1 vibrates to mechanically tease tissues apart (A). A control knob at the handle adjusts the vibration speed. The weight of DD1 is 150g, including the built-in batteries which allow cordless operation (B).

Animals (Act No. 105 of October 1, 1973). The study protocol of this study and the handling of animals were approved by the institutional review board (Animal Care and Usage Committee) of Narita Experimental Laboratory, NAS Laboratory Co., Ltd. (Approval number: 15L-S079, 16L-S002).

2.3. Tissue trauma arising from transient contact

DD1 is applied to tissues with force applied by the surgeon. To standardize treatments with the DD1 such that a force of approximately 100 ± 50 g was consistently applied, the surgeon practiced at the beginning of each surgery by pressing the DD1 against an electronic balance 20 times for 2 sets. Multiple sites on a variety of tissues were tested for trauma from dissection. (Table 1), including parenchymal organs (liver, kidneys, and pancreas), luminal organs (ureter, bladder, thick and middle arteries, and thick and middle veins), and nerves (femoral nerve). Treatments for these tissues were:

- Non-parenchymal tissues (ureter, abdominal aorta, inferior vena cava, common iliac artery and vein, renal artery and vein, and femoral nerves): only the DD1 was used – one speed (medium) for two durations of contact (5 and 30 seconds). Each tissue: 4 test sites per organ in each animal, 16 per tissue total. Bladder: 2 test sites per animal, 8 total.

- Liver: ES – 2 seconds contact at 30W; DD1– two speeds (medium and high) for four durations of contact each (5, 15, 30, 60 seconds). 36 test sites per animal, 144 total.

- Pancreas and kidney: ES – 2 seconds contact at 30W; DD1 – one speed (medium) for two durations

Table 1. Sites and number for test in DD1 and Electric scalpel

Items	DD1		Electric scalpel		Number of test sites per animal	Total
	Power	"Time (seconds)"	Power (W)	Time (seconds)		
Liver	maximum and middle	5, 15, 30 and 60	30	2	36**	144
Kidney	middle	5 and 30	30	2	6	24
Pancreas	middle	5 and 30	30	2	4	16
Thick and Medium artery	middle	5 and 30	.*	-	4	16
Thick and Medium vein	middle	5 and 30	.*	-	4	16
Nerve	middle	5 and 30	.*	-	4	16
Ureter	middle	5 and 30	.*	-	4	16
Bladder	middle	5 and 30	.*	-	2	8

* Not tested because damage is obvious and ES is never used clinically for these tissue. ** For 4 lobes per animal.

of contact (5 and 30 seconds). Kidney: 6 test sites per kidney, 24 total. Pancreas: 4 test sites per animal, 16 total.

Note that in parenchymal organs (liver, kidney, and pancreas), tissue damage caused by the DD1 was compared to ES because ES is widely used for dissection of these tissues. However, trauma from ES was not measured for the non-parenchymal organs (vessels, ureter and nerves) because such damage is obvious, and ES is never used clinically for the dissection of tissue planes around these tissues.

Each site was tested as follows: A randomized schedule for instrument use was prepared for each animal. Prior to treatment, the site was marked with indigo-carmin to permit later localization and excision. Then the respective instrument was applied to that site for a predetermined time and speed, according to the randomized schedule.

In the liver, kidney, and pancreas, the extent of tissue damage area (length × depth measured on the histological slide) was evaluated macroscopically on a computer monitor after scanning the test site with a NanoZoomer (Hamamatsu Photonics Inc., Hamamatsu, Japan). Microscopic examination was used to measure cell degeneration, destruction of liver serosa, and intra-parenchymal bleeding. Microscopic analysis of trauma to the liver was determined by two metrics: the number of degenerate nuclei and the number of nuclei with an aspect ratio (ratio of height: width) > 1.25. All cells were counted within a field of view for 400× magnification.

2.4. The time course of device temperature

The time course of temperature changes in the mesentery of the small intestine was measured for 4 devices: Harmonic, ES, LigaSure, and DD1. Prior to use, warm water was used to maintain all devices at 29°C. Each device was applied to the tissue for 3 seconds and then removed. The temperature of devices at the point of application was measured before activation of the devices (0 sec), immediately after energy was turned off and the instrument removed from

the tissue (3 sec), and again at 10, 20 and 30 seconds. Temperatures were measured by infrared thermography: Testo 875-2i (Testo Inc., Lenzkirch, Germany). The temperature was analyzed using software (Testo IRSoft, Testo Inc., NJ, USA), and the maximum temperature of the tissue for each device and the change of temperature after use was measured. Each device was measured ten times under the same conditions and compared with DD1.

2.5. Time for removal of the peripheral artery in the small intestine

The straight arteries in the mesentery of the small intestine were used to provide an array of similar vessels for comparison of dissection speed between the DD1 and another technique for cold dissection – non-energized forceps. The time required to mobilize a length of 3 cm of a single straight artery was compared between the forceps and the DD1. The success of dissection was evaluated as follows: if bleeding occurred during dissection, failure to achieve hemostasis by simply applying pressure for five seconds or failure to detect blood flow due to occlusion were deemed as failures. Dissection was performed at 15 sites for each technique in each animal (150 arteries mobilized total, 75 for each technique). The time and success of dissection were evaluated by a surgeon who was not involved in the study by video examination. As a second test, the mobilization of renal vessels also was performed and assessed from video examination by another surgeon.

2.6. Statistical analysis

All continuous variables are described as medians and ranges. For the comparison between the two groups, we used a Student's t-test for the parametric variables and Wilcoxon rank sum test for the non-parametric variables. *P* values of less than 0.05 indicated a significant difference. All statistical analyses were performed using JMP 10.0.2 (SAS Institute Inc., Cary, NC, USA).

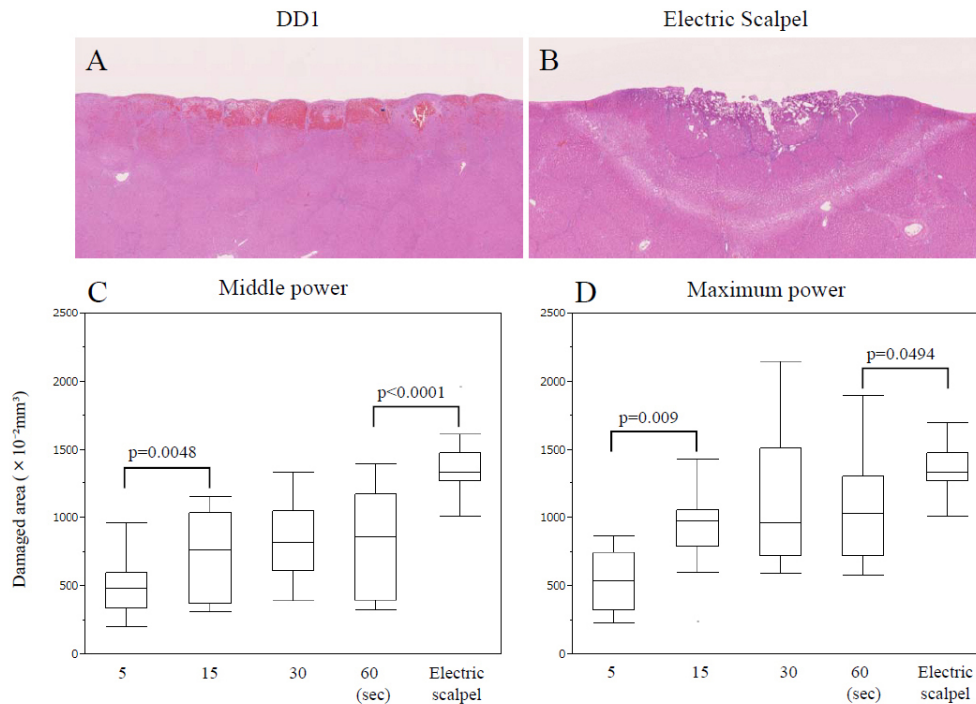


Figure 2. Macroscopic tissue damage and damaged area. DD1 resulted in a subserosal dish-shaped damage and minor subserosal bleeding without rupture of the serosa on the contact surface (A). Electric scalpel resulted in a wide semicircular damaged area with serosal rupture (B). The damaged area reached a plateau in 15 seconds. The damage area of DD1 in any time points were significantly smaller than that of electric scalpel at middle (C) and maximum power (D).

Table 2. Damaged area of the parenchymal and non-parenchymal organs

Organs	Damaged area ($\times 10^{-2}$ mm ²)			p value*
	Middle5	Middle30	Electric scalpel	
Liver	480 (0-1530)	821 (188-2100)	1330 (812-1960)	0.002
Kidney	0 (0-420)	172 (70-700)	1112 (825-2000)	0.0001
Pancreas	0 (0-21)	20 (0-108)	1046 (85-1675)	0.0037
Thick and Medium artery	Not damaged		N.T.	N.T.
Thick and Medium vein	Not damaged		N.T.	N.T.
Nerve	Not damaged		N.T.	N.T.
Ureter	Not damaged		N.T.	N.T.
Bladder	Not damaged		N.T.	N.T.

Data express, median with range, * middle 30 vs Electric scalpel, N.T.: Not tested.

3. Results

3.1. Macroscopic damage

In the liver, the DD1 for all durations of contact and both speeds resulted in mild subserosal dish-shaped damage but without serosal rupture on the contact surface (Figure 2A). The region of subserosal damage was characterized by minor bleeding within the parenchyma but with no evidence of liver tissue degeneration (Figure 2A). On the other hand, ES resulted in a larger semicircular damaged area at the contact surface with serosal rupture and wide liver tissue degeneration (Figure 2B). For the DD1, the range of damage of liver parenchyma reached a plateau in 15 seconds for both powers (Figure 2C, D). The damage area of DD1 at middle power was significantly

smaller than that of ES (30W, 2 seconds) for all time points (Figure 2C). Also at Maximum power (5, 15, 30, 60 sec), the damage area of liver parenchyma using DD1 was significantly smaller than that of ES (30 W, 2 sec) ($p = 0.0494$) (Figure 2D).

Similar results were observed for the other parenchymal organs (kidney/pancreas) (Table 2). The damage area of DD1 (middle power, 5, 30 seconds) was significantly smaller than that of ES (30 W, 2 seconds), (kidney: $p = 0.0001$, pancreas: $p = 0.0037$ for DD1, middle power, 30 seconds which was the harshest condition). At first, the microscopic study of the liver showed that DD1 was obviously less harmful rather than other energy device. Therefore, the similar results as the liver was expected, the experimental for other parenchymal organs were omitted. No macroscopic

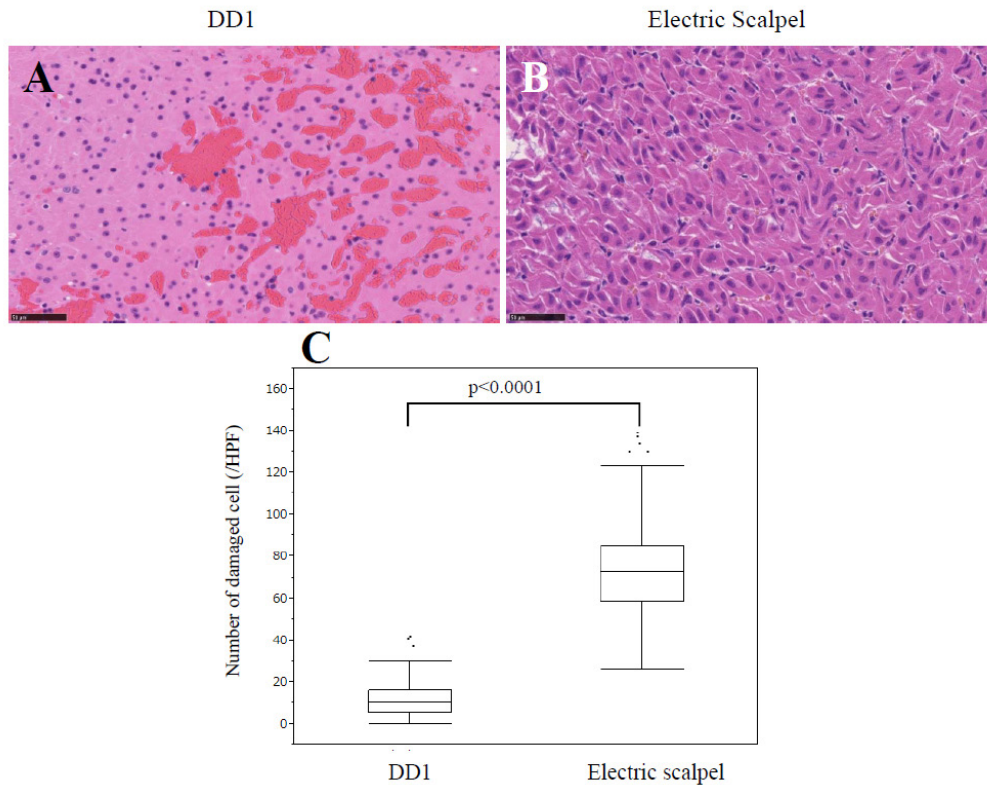


Figure 3. Microscopic findings and number of damaged cell. The damage caused by DD1 (maximum power, 60 sec) was slight intra-parenchymal bleeding without cell degeneration (A). In contrast, the electric scalpel caused massive cell degeneration (B). The damaged cell number recorded within the field of a 400× microscopic objective was significantly lower in DD1 than the electric scalpel (C).

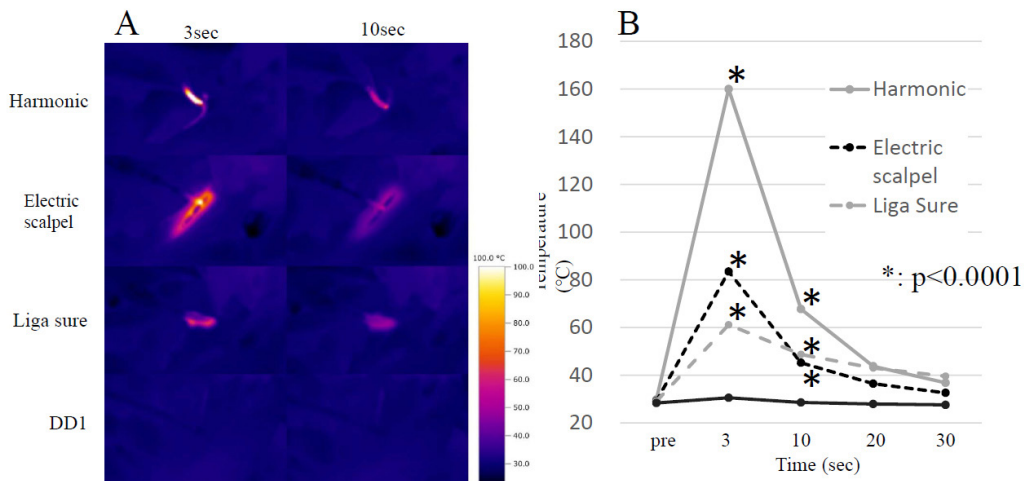


Figure 4. Time course of temperature in each energy device. The temperature rapidly increased after 3 seconds use of each energy devices. The temperature gradually decreased after 10 seconds. The temperature of DD1 was unchanged at any time points. (A) The temperature of the DD1 was always significantly lower than the temperature for the other devices for any time after use.

damage was seen from the DD1 in the non-parenchymal organs (vessels, ureters, and nerves).

3.2. Microscopic damage

The difference in the quality of tissue damage in liver caused by each device was significant. Most of the cells present in the range of damage of ES possessed H/W ≥ 1.25 (Figure 3B). As for DD1, there was no change other

than slight bleeding in the parenchyma, with the H/W of the nucleus preserved in most of the cells (Figure 3A). The number of damaged nuclei in DD1 was significantly less than ES ($p < 0.0001$) (Figure 3C).

3.3. Time course of temperature in each energy device

Significant increases in tissue temperatures were observed for Harmonic, ES, and LigaSure after three

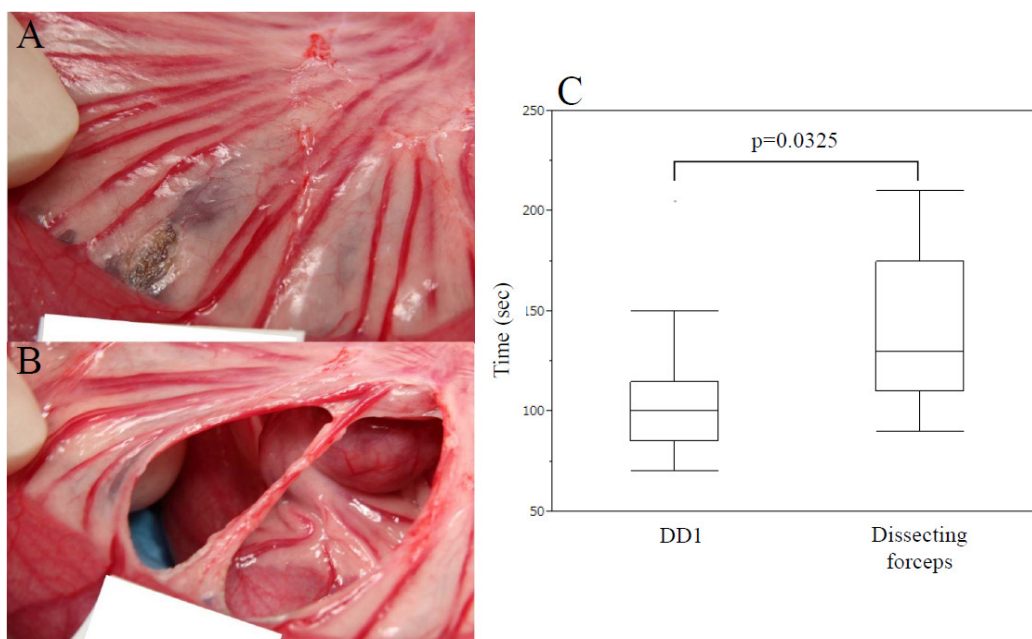


Figure 5. Removal of the peripheral artery in small intestine. The removal time of 3 cm or more in the longitudinal axis of the single straight artery in the mesentery of the small intestine was compared between dissecting forceps and DD1. (before (A) and after (B) dissection) The median time for dissection was significantly shorter in DD1 than that in the forceps (C).

seconds of energy application. The maximum measured temperature in the dissection field rapidly increased to 160°C for Harmonic, 84°C for ES, and 61°C for LigaSure at 3 seconds when activation ceased. After 10 seconds, the temperature gradually decreased to 68°C for Harmonic, 45°C for ES and 49°C for Liga Sure. On the other hand, the temperature of DD1 was unchanged at any time point (from 31°C to 29°C) (Figure 4A). The temperature of DD1 was significantly lower than that in any other energy device during activation ($p < 0.0001$) and after activation ($p < 0.0001$) (Figure 4B)

3.4. Time for removal of the peripheral artery and renal veins

In the dissection of the peripheral straight artery in the mesentery of the small intestine, there was no occurrence of dissection failures using either the DD1 (Figure 5A, B) or the non-energized forceps. The median removal time of DD1 was significantly shorter than that of the forceps (100 seconds vs. 130 seconds, $p = 0.0325$) (Figure 5C). In addition, for dissection and mobilization of the renal veins (a more complicated structure), DD1 was able to safely expose the target vessels as determined by visual inspection in surgery and confirmed by independent review of videotape (Figure 6A, B).

4. Discussion

DD1 is a novel category of electric device designed for tissue dissection with minimum damage. The intellectual property of DD1 is hold by Physcient in

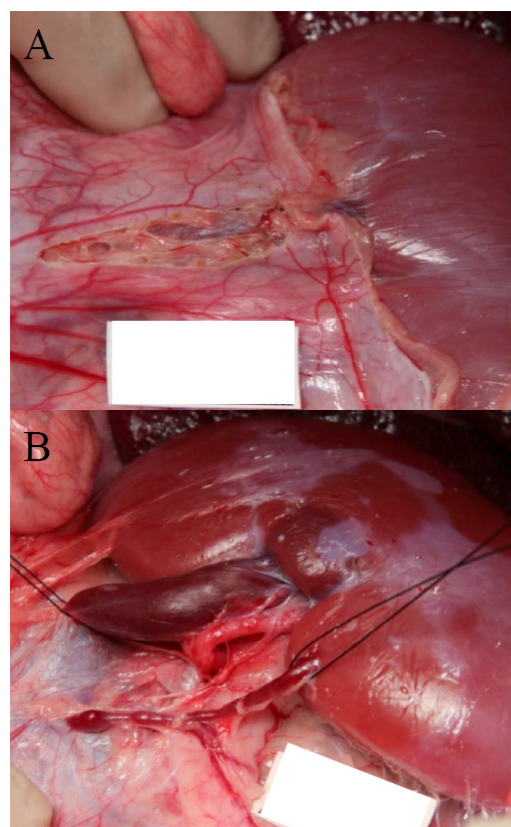


Figure 6 Removal of the renal vein. The incision was made in the serosa lining the renal hilus prior to the dissection (A). Dissection and mobilization of the renal structures (artery, vein and ureter) was performed without visible trauma to any of the structures (B).

U.S. DD1 is a commercial stage not only in U.S. but also in Japan. Several conventional surgical procedures

were performed safely with the DD1 without significant bleeding and without thermal trauma. During normal use, only a few seconds of contact time in a single point is required for dissection, so the durations of exposure tested here (as long as 60 seconds) demonstrate that DD1 has a sufficient safety margin for a variety of surgical procedures.

DD1 offers several advantages over other energy devices. Vessel sealing systems (*e.g.* Harmonic and LigaSure) perform coagulation hemostasis by generating heat at the tip of the device. However, unexpected secondary organ damage can occur by thermal injury (12-18). Therefore, it is necessary to maintain a safety margin such that heat does not directly spread into surrounding tissues during coagulation. This problem is sufficiently large that vessel sealers should not be used near vessels and nerves which need to be preserved (19-20). Conversely, DD1 quickly dissected tissues with only slight bleeding, generating a small damage area, and creating no rise in tissue temperature. No thermal trauma was observed. Even with the use of maximum power for 60 seconds, the damage area of the parenchymal organs was significantly smaller than ES. Additionally, DD1 did not induce unexpected reflexes by stimulation of nerves, unlike ES. Therefore, DD1 can be used safely without irreversible damage to tissues, even near important organs.

It is important to recognize the tissue planes separating blood vessels and nerves from connective tissues during dissection. DD1 is an electric device which dissects by using high-speed vibration. DD1 dissects the loose connective tissue alone. The tight connective tissue, blood vessel wall, nerve fiber and serosa do not have serious damage. When it uses suitable touch to the tissues, it can dissect with small amount of blood loss. Furthermore, the DD1 is faster than conventional blunt dissection with forceps, as demonstrated from measurements of dissection times for the peripheral thin artery in the small intestine. Thus, DD1 is a convenient device capable of consistent and safe dissection.

DD1 also has an advantage in cost because it is battery powered and does not require an energy generator. Furthermore, the battery is built into the main body, so there is no cord, and handling during surgery is better. Further improvements are planned for DD1 to enable use in laparoscopic operations.

We validated the safety and efficacy of the DD1 by demonstrating a reduction in tissue damage and absence of heat generation during dissection in surgical procedures simulating clinical use. The DD1 was effective for a variety of dissections in several different tissues. DD1 allows a safe and quick dissection in procedures including the preservation of nerve function, the complex dissection of vessels, and tunneling into tissues. We believe that DD1 can contribute to the safety and convenience of surgery and surgeons will find broad application in a variety of surgical

procedures. Now, we proceed to the clinical test phase and the safety of the DD1 will validate in near future.

Acknowledgement

Author thanks to Hugh Crenshaw for his assistants of editing this manuscript.

References

1. Shinohara H, Haruta S, Ohkura Y, Udagawa H, Sakai Y. Tracing dissectable layers of mesenteries overcomes embryologic restrictions when performing infrapyloric lymphadenectomy in laparoscopic gastric cancer surgery. *J Am Coll Surg.* 2015; 220:e81-e87.
2. Campagnacci R, de Sanctis A, Baldarelli M, Rimini M, Lezoche G, Guerrieri M. Electrothermal bipolar vessel sealing device. ultrasonic coagulating shears in laparoscopic colectomies: A comparative study. *Surg Endosc.* 2007; 21:1526-1531.
3. Rimonda R, Arezzo A, Garrone C, Allaix ME, Giraud G, Morino M. Electrothermal bipolar vessel sealing system vs. harmonic scalpel in colorectal laparoscopic surgery: A prospective, randomized study. *Dis Colon Rectum.* 2009; 52:657-661.
4. Silva-Filho AL, Rodrigues AM, Vale de Castro Monteiro M, da Rosa DG, Pereira e Silva YM, Werneck RA, Bavoso N, Triginelli SA. Randomized study of bipolar vessel sealing system versus conventional suture ligation for vaginal hysterectomy. *Eur J Obstet Gynecol Reprod Biol.* 2009; 146:200-203.
5. Siperstein AE, Berber E, Morkoyun E. The use of the harmonic scalpel vs conventional knot tying for vessel ligation in thyroid surgery. *Arch Surg.* 2002; 137:137-142.
6. Petrakis IE, Kogerakis NE, Lasithiotakis KG, Vrachassotakis N, Chalkiadakis GE. LigaSure versus clamp-and-tie thyroidectomy for benign nodular disease. *Head Neck.* 2004; 26:903-909.
7. Saint Marc O, Cogliandolo A, Piquard A, Famà F, Pidoto RR. LigaSure vs clamp-and-tie technique to achieve hemostasis in total thyroidectomy for benign multinodular goiter: A prospective randomized study. *Arch Surg.* 2007; 142:150-156.
8. Youssef T, Mahdy T, Farid M, Latif AA. Thyroid surgery: Use of the LigaSure Vessel Sealing System versus conventional knot tying. *Int J Surg.* 2008; 6:323-327.
9. Miccoli P, Materazzi G, Miccoli M, Frustaci G, Fosso A, Berti P. Evaluation of a new ultrasonic device in thyroid surgery: Comparative randomized study. *Am J Surg.* 2010; 199:736-740.
10. Markogiannakis H, Kekis PB, Memos N, Alevizos L, Tsamis D, Michalopoulos NV, Lagoudianakis EE, Toutouzas KG, Manouras A. Thyroid surgery with the new harmonic scalpel: A prospective randomized study. *Surgery.* 2011; 149:411-415.
11. Mourad M, Rulli F, Robert A, Scholtes JL, De Meyer M, De Pauw L. Randomized clinical trial on Harmonic Focus shears versus clamp-and-tie technique for total thyroidectomy. *Am J Surg.* 2011; 202:168-174.
12. Kadesky KM, Schopf B, Magee JF, Blair GK. Proximity injury by the ultrasonically activated scalpel during

- dissection. *J Pediatr Surg.* 1997; 32:878-9.
13. Emam TA, Cuschieri A. How safe is high-power ultrasonic dissection? *Ann Surg.* 2003; 237:186-191.
 14. Perko Z, Pogorelić Z, Bilan K, Tomić S, Vilović K, Krnić D, Družijanić N, Kraljević D, Jurčić J. Lateral thermal damage to rat abdominal wall after harmonic scalpel application. *Surg Endosc.* 2006; 20:322-324.
 15. Pogorelić Z, Perko Z, Družijanić N, Tomić S, Mrklič I. How to prevent lateral thermal damage to tissue using the harmonic scalpel: Experimental study on pig small intestine and abdominal wall. *Eur Surg Res.* 2009; 43:235-240.
 16. Humes DJ, Ahmed I, Lobo DN. The pedicle effect and direct coupling: Delayed thermal injuries to the bile duct after laparoscopic cholecystectomy. *Arch Surg.* 2010; 145:96-98.
 17. Družijanić N, Pogorelić Z, Perko Z, Mrklič I, Tomić S. Comparison of lateral thermal damage of the human peritoneum using monopolar diathermy, Harmonic scalpel and LigaSure. *Can J Surg.* 2012; 55:317-321.
 18. Applewhite MK, White MG, James BC, Abdulrasool L, Kaplan EL, Angelos P, Grogan RH. Ultrasonic, bipolar, and integrated energy devices: Comparing heat spread in collateral tissues. *J Surg Res.* 2017; 207:249-254.
 19. Wu CW, Chai YJ, Dionigi G, Chiang FY, Liu X, Sun H, Randolph GW, Tufano RP, Kim HY. Recurrent laryngeal nerve safety parameters of the Harmonic Focus during thyroid surgery: Porcine model using continuous monitoring. *Laryngoscope.* 2015; 125:2838-2845.
 20. Kwak HY, Dionigi G, Kim D, Lee HY, Son GS, Lee JB, Bae JW, Kim HY. Thermal injury of the recurrent laryngeal nerve by THUNDERBEAT during thyroid surgery: Findings from continuous intraoperative neuromonitoring in a porcine model. *J Surg Res.* 2016; 200:177-182.

(Received December 11, 2017; Revised January 7, 2018; Accepted January 23, 2018)

Neither ischemic parenchymal volume nor severe grade complication correlate transient high transaminase elevation after liver resection

Tokio Higaki, Shintaro Yamazaki*, Yusuke Mitsuka, Masaru Aoki, Nao Yoshida, Yutaka Midorikawa, Hisashi Nakayama, Tadatoshi Takayama

Department of Digestive Surgery, Nihon University School of Medicine, Tokyo, Japan.

Summary

To clarify whether high transient elevation of serum transaminase predicts severe complications and is related to the ischemic area on CT. Postoperative laboratory data and ischemia area on CT were analyzed on the basis of the presence of high transaminase elevation (aspartate aminotransferase (AST) > 1,000 IU/L within postoperative day (POD) 2 after liver resection. In the high elevation group, volume of ischemic areas was assessed by CT on POD2. The 538 patients were divided into a high transaminase group ($n = 51$) and a control group ($n = 487$). Median operation time (527 min vs. 360 min, $p < 0.01$) and liver ischemia time (121 min vs. 70 min, $p < 0.01$) were significantly longer, and intraoperative blood loss (478 mL [85-1572 mL] vs. 269 mL [5-4491 mL], $p < 0.01$) was significantly greater in the high transaminase group. No significant differences observed in frequency of severe complications (Clavien-Dindo classification Grade III or more) or postoperative hospitalization. Operation time (> 500 min; odds ratio (OR), 4.86; 95% confidence interval (CI), 2.40-9.89; $p < 0.01$) and liver ischemia time (> 120 min; OR, 3.47; 95%CI, 1.67-7.17; $p < 0.01$) were independent predictors of high transaminase elevation. No relationship was observed between degree of transaminase elevation and ischemic area (correlation coefficients: AST, $R^2 < 0.001$; alanine aminotransferase, $R^2 = 0.005$) CT volumetry on POD2. In conclusions, high transaminase elevations do not predict severe complications or reflect remnant ischemic area.

Keywords: CT volumetry, serum transaminase level, clavien-dindo classification

1. Introduction

Recent liver resection for cancer has been performed with satisfactory operative morbidity and mortality (1-5). Serum transaminase levels are a most convenient and reliable indicator of liver ischemia following surgery (6-7). Serum transaminase levels easily increase following liver transection, hepatic pedicle clamping during liver resection and other operation-related factors (6,8,9). However, the increase in serum transaminases was commonly transient and recovered to within normal ranges for the first 7 days postoperatively.

High elevations in aspartate aminotransferase (AST) or alanine aminotransferase (ALT) in the early postoperative period are considered one of the phenomena reflecting severe complications. Because, the lack of remnant liver parenchyma or wide ischemic area in the remnant liver after resection may be the principal issues leading to severe complications (5). Therefore, surgeons pay attention to high postoperative transaminase levels as a marker of crisis.

In clinical situation, we sometimes encountered high elevation of transaminase ($\geq 1,000$ IU/L) after liver resection however, the importance of this issue remains unsettled. (6) No studies to date have analyzed the area of ischemia at the time of high transaminase elevation. Thus, we routinely checked the postoperative liver ischemic area on POD2 to clarify whether a high transaminase elevation predicts severe complications and reflects the ischemic area on CT.

*Address correspondence to:

Dr. Shintaro Yamazaki, Department of Digestive Surgery, Nihon University School of Medicine, 30-1 Oyaguchikamimachi, Itabashi-ku, Tokyo 173-8610, Japan.
E-mail: yamazaki-nmed@umin.ac.jp

2. Patients and Methods

2.1. Patients

We retrospectively analyzed the data of consecutive patients who underwent liver resection for cancers. Perioperative laboratory data were collected before the operation, just after the operation, and on postoperative day (POD) 1, 2, 3, 5, 7, 30, 90 and 180. Then, the patients were divided into two groups according to the presence of high transaminase elevation (AST > 1,000 IU/L) on POD2. Operation-related variables (tumor factors, operation time, liver ischemia time, intraoperative blood loss and procedure) and outcomes in the early period (all complications, severe grade complications according to Clavien-Dindo classification > grade3 and duration of postoperative hospital stay) were analyzed (10).

2.2. Volumetry

On POD2 all patients were routinely performed to check ischemic area and portal vein thrombus. Volumetric analysis was performed when the serum AST level reached $\geq 1,000$ IU/L within POD2. Three-phase contrast-enhanced dynamic CT scans (unenhanced and hepatic arterial, portal venous, and liver parenchymal phases) were performed using a 64-detector row scanner (Aquilion 64; Toshiba Medical Systems, Tokyo, Japan). The total dose of nonionic iodinated contrast medium was 600 mgI/kg body weight of iomeprol (350 mgI/mL), administered over the course of 30 s using an automatic injector. Scanning was performed in the arterial phase (37 s), in the portal venous phase (60 s), and in the delayed phase (150 s). Portal-phase images were used for volumetry. When ischemic regions were confirmed on CT, CT-based volumetry was performed using portal venous phase images. The calculation of ischemic liver area has been described elsewhere (11-13). Follow-up CT was performed at 1 week and at 1, 3, and 6 months after operation.

2.3. Surgical procedures

Anatomical resection of Couinaud's segment was the first-line operative procedure for hepatocellular carcinoma (HCC) when the patient had sufficient functional reserve. In cases of metastatic liver tumor, partial resection with adequate surgical margins was the first-line procedure. Details of the indications and procedures have been described previously (14-16). Minor hepatectomy was defined as limited resection or resection of up to two Couinaud's segments. Hepatic parenchymal transection was guided ultrasonographically and performed by the clamp-crushing method with the inflow-blood-occlusion technique, and Glisson's pedicle was tied and divided

with silk thread. Standard systemic antibiotic therapy with cefazolin was routinely administered immediately before surgery, then twice daily on POD1-3.

2.4. Statistical analysis

Data are expressed as median and range or as absolute value and percentage. Student's *t* test, the χ^2 test, and Fisher's exact test were used for univariate analysis, as required. Multivariate analysis was performed using logistic regression. Odds ratios with 95% confidence intervals derived from logistic regression analysis were calculated. The period until the onset of infection was analyzed using the Kaplan-Meier method, with comparison by the log-rank test. Values of $P < 0.05$ were considered indicative of statistical significance. All analyses were performed using a statistical software package (JMP version 9.0; SAS Institute, USA).

3. Results

3.1. Patients

Between January 2008 and December 2010, a total of 538 patients underwent liver resection for malignancy. These patients were divided into a high transaminase group ($n = 51$) and a control group ($n = 487$) according to laboratory data on POD1 (Table 1). Age (median, 64 years [range, 41-84 years] vs. 69 years [range, 20-84 years], $p = 0.006$), proportion of patients with cancer (HCC, 26 patients [51.0%] vs. 342 [70.0%]; $p = 0.005$ or liver metastasis, 21 [41.1%] vs. 112 [22.9%], $p = 0.007$) differed significantly between groups. Preoperative platelet count was significantly higher (21.2 $\text{mm}^3/\mu\text{L}$ [range, 6.2-39.5 $\text{mm}^3/\mu\text{L}$] vs. 16.6 $\text{mm}^3/\mu\text{L}$ [range, 4.2-54.9 $\text{mm}^3/\mu\text{L}$], $p = 0.006$), total bilirubin level was lower (0.57 mg/dL [range, 0.31-1.39 mg/dL] vs. 0.59 mg/dL [range, 0.19-1.83], $p = 0.006$) and indocyanine green retention rate at 15 min was better (7.8% [range, 2.3-22.8%] vs. 11.45% [range, 1.1-82.3%], $p < 0.001$) in the high transaminase group. Preoperative serum AST level ($p = 0.743$), preoperative serum ALT level ($p = 0.484$) and proportion of Child-Pugh class B cases ($p = 0.746$) did not differ significantly between groups (Table 1).

3.2. Surgical outcomes and transaminase levels

Operation time (527 min [range, 310-752 min] vs. 360 min [range, 112-831 min], $p < 0.001$) and liver ischemia time (121 min [range, 45-243 min] vs. 70 min [range, 0-222 min], $p < 0.001$) were significantly longer in the high transaminase elevation group. Intraoperative blood loss (478 mL [range, 85-1572 mL] vs. 269 mL [range, 5-4491 mL], $p < 0.001$) was significantly greater and number of liver resections (2 [range, 1-20] vs. 1 [range, 1-4], $p = 0.013$) was higher in the high transaminase

Table 1. Characteristics of patients

Items	High transaminase >1,000 IU/L (n = 51)	Control < 1,000 IU/L (n = 487)	p value
Age (years)	64 (41-84)	69 (20-84)	0.006
Sex (male/female)	39/12	340/147	0.323
Presenting illness			
Hepatocellular carcinoma	26 (51.0%)	342 (70.2%)	0.005
Metastatic liver cancer	21 (41.1%)	112 (23.0%)	0.007
Intrahepatic cholangiocarcinoma	2 (3.9%)	14 (2.9%)	0.636
Gallbladder cancer	0 (0%)	7 (1.4%)	0.314
Others	2 (3.9%)	12 (2.5%)	0.571
Platelet account (mm ³ /uL)	21.2 (6.2-39.5)	16.6 (4.2-54.9)	0.006
Aspartate aminotransferase (IU/L)	28 (12-213)	36 (9-265)	0.742
Alanine aminotransferase (IU/L)	28 (8-217)	28 (5-296)	0.484
Total bilirubin (mg/dL)	0.57 (0.31-1.39)	0.59 (0.19-1.83)	0.006
Albumin (g/dL)	4.1 (2.7-5.3)	4.0 (2.0-5.3)	0.112
Prothrombin time (%)	100 (78-100)	100 (52-100)	0.347
ICGR15 (%)	7.8 (2.3-22.8)	11.45 (1.1-82.3)	< 0.001
Child-Pugh class B	1 (2.0%)	7 (1.4%)	0.746

[†]Values represent median with range. ICGR15, indocyanine green retention test at 15 min.

Table 2. Surgical outcomes

Items	High transaminase >1,000 IU/L (n = 51)	Control < 1,000 IU/L (n = 487)	p value
Operation time (min)	527 (310-752)	360 (112-831)	< 0.001
Ischemic time (min)	121 (45-243)	70 (0-222)	< 0.001
Intraoperative blood loss (g)	478 (85-1572)	269 (5-4491)	< 0.001
Multiple liver resection	21 (41.2%)	117 (24.0%)	0.013
Anatomical resection	23 (45.1%)	163 (33.5%)	0.097
Major hepatectomy	6 (11.7%)	34 (7.0%)	0.218
Complications (Total)	21 (41.2%)	136 (27.9%)	0.047
Complications (Severe)*	9 (17.6%)	68 (14.0%)	0.474
Postoperative hospital stay (days)	14 (8-38)	12 (8-62)	0.072

[†]Values represent median with range. *Clavien classification grade III or more.

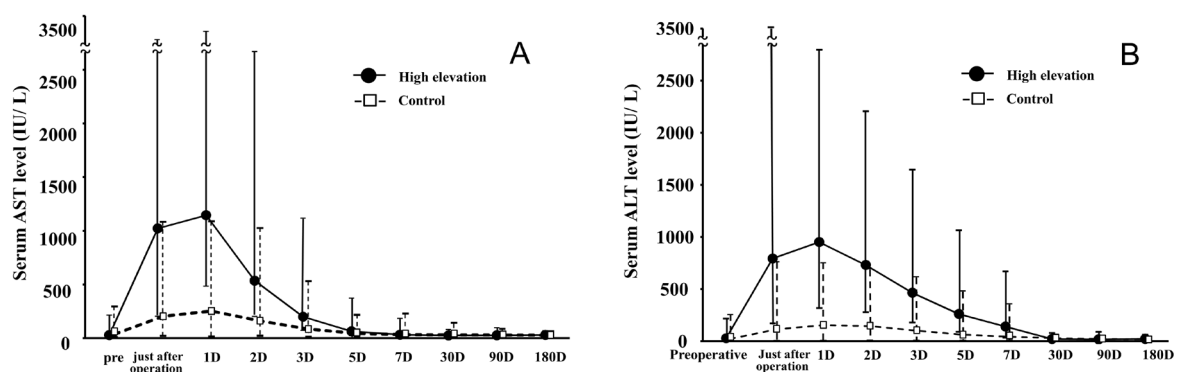


Figure 1. Trends in perioperative serum aspartate aminotransferase (AST) and alanine aminotransferase (ALT) levels. Transaminase levels increased rapidly just after operation and peaked by POD2 in AST (A) and ALT (B). Concentrations then gradually decreased and returned to within normal range by POD7.

elevation group (Table 2). Total number of postoperative complications was significantly higher in the high transaminase elevation group (9 [17.6%] vs. 68 [14.0%], $p = 0.04$), whereas the number of severe complications according to the Clavien-Dindo classification (> Grade III) ($p = 0.474$) and duration of postoperative hospital stay ($p = 0.07$) did not differ significantly.

Transaminase levels increased rapidly just after

operation and peaked by POD2 (Figure 1A,B). Concentrations then gradually decreased and returned to within normal range by POD7.

3.3. Multivariate analysis for high transaminase elevation

Operation-related variables were further analyzed by

Table 3. Multivariate analysis for high transaminase elevation

Items	Odds ratio	95%CI (Hi-Low)	p value
Operation time (> 500 min)	4.86	2.40-9.89	< 0.001
Liver ischemia time (> 120 min)	3.47	1.67-7.17	< 0.001
Number of liver resections (single)	1.33	0.67-2.60	0.401
Intraoperative blood loss (> 1,000 mL)	1.24	0.50-3.31	0.642

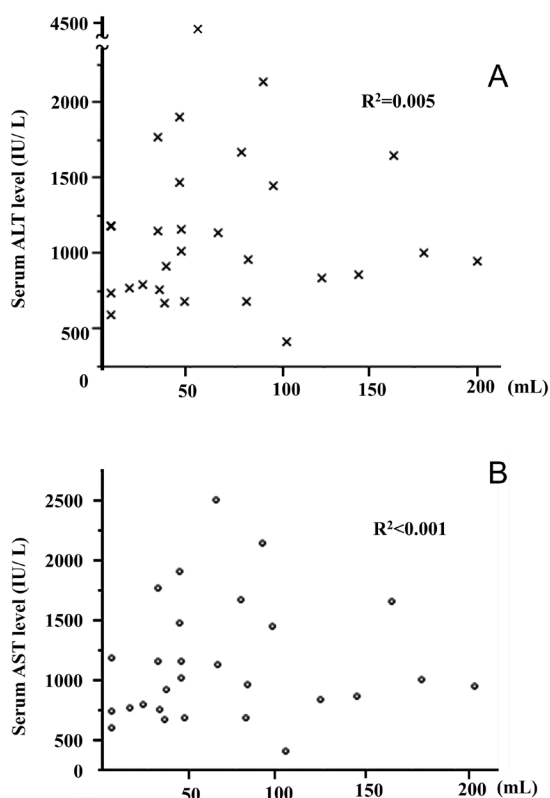


Figure 2. Relationship between serum transaminase level and ischemia area after high transaminase elevation by volumetry. Correlation coefficients are $R^2 = 0.0049$ for serum AST (A) and $R^2 = 0.0049$ for ALT (B). No relationship is apparent between transaminase level and liver ischemia area by volumetry.

multivariate analysis regarding influences on high transaminase elevation (Table 3). Operation time > 500 min (odds ratio, 4.86; 95% confidence interval, 2.40-9.89; $p < 0.001$) and liver ischemia time >120 min (odds ratio, 3.47; 95% confidence interval, 1.97-7.17; $p < 0.001$) were independent predictors of high transaminase elevation.

3.4. Volumetry

The median volume of ischemia was 63 mL (ranged, 4-210 mL) when the high transaminase elevation was confirmed on POD2. The correlation coefficient of AST was $R^2 < 0.001$ and ALT was $R^2 = 0.005$. No causal relationships were observed between each transaminase level and volume of ischemic area on POD2 (Figure 2A,B).

4. Discussion

We identified operation time (> 500 min) and liver ischemia time (> 120 min) as significant predictors for high transaminase elevation, although this elevation was only transient and did not predict severe complications. Moreover, the ischemic area just after operation did not correlate with the concentration of transaminase.

High serum transaminase levels after liver resection strongly suggest severe damage to the liver parenchyma. Severe liver injury in which transaminase levels exceeded 1,000 IU/L just after the operation has been considered to predict secondary liver failure. The mechanism of injury mainly depends on ischemic reperfusion injury during liver resection or the presence of an ischemic area in the remnant liver at a result of liver resection and other reasons related to the operative procedure. However, whether a significant correlation exists between high transaminase elevation and severe complications remains unclear (17-19). Moreover, which factor is the main cause of high transaminase elevation is unclear. The present study revealed that the main cause of high elevation did not reflect the ischemic area in the remnant liver, but rather ischemia time during the operation.

Multivariate analysis revealed operation time (> 500 min) and liver ischemia time (> 120 min) as the significant prognostic factor for high transaminase elevation. However, the occurrence of severe complications and postoperative hospital stay did not differ significantly between groups, because this population had significant better liver functional reserve. Therefore, complex or large-scale liver resections were performed for patients with sufficient liver function. As a result, a large release of liver enzymes is seen from livers with good functional reserve.

Elevation of transaminases is well known to be transient and to subside within one week. In contrast, the recovery of liver parenchyma after liver resection is not fully understood. In the present study, three-phase enhanced CT enabled visualization of the ischemic area in liver parenchyma. This enabled to confirm blood flow in the liver parenchyma phase by phase. Ischemic areas may recover with hypertrophy of the remnant parenchyma or apoptosis of the ischemic liver parenchyma. However, no previous study has shown the relationship between high elevation of transaminases and ischemic area on CT. We found that the median

ischemic area on CT volumetry was only 63 mL, even if transaminase level exceeded 1,000 IU/L.

In conclusion, postoperative routine CT on POD2 is useful to check the ischemic area and portal vein thrombus due to the operation procedure. High elevation of transaminases reflects mainly the length of liver resection and does not predict severe complications, even for > 1,000 IU/L. Because it is not correlate to the liver ischemic area after operation.

References

1. Reissfelder C, Rahbari NN, Koch M, Kofler B, Sutedja N, Elbers H, Büchler MW, Weitz J. Postoperative course and clinical significance of biochemical blood tests following hepatic resection. *Br J Surg.* 2011; 98:836-844.
2. Capussotti L, Muratore A, Amisano M, Polastri R, Bouzari H, Massucco P. Liver resection for hepatocellular carcinoma on cirrhosis: Analysis of mortality, morbidity and survival – A European single center experience. *Eur J Surg Oncol.* 2005; 31:986-993.
3. Poon RT, Fan ST, Lo CM, Liu CL, Lam CM, Yuen WK, Yeung C, Wong J. Improving perioperative outcome expands the role of hepatectomy in management of benign and malignant hepatobiliary diseases: Analysis of 1222 consecutive patients from a prospective database. *Ann Surg.* 2004; 240:698-710.
4. Imamura H, Seyama Y, Kokudo N, Maema A, Sugawara Y, Sano K, Takayama T, Makuuchi M. One thousand fifty-six hepatectomies without mortality in 8 years. *Arch Surg.* 2003; 138:1198-1206.
5. Rahbari NN, Garden OJ, Padbury R, *et al.* Posthepatectomy liver failure: A definition and grading by the International Study Group of Liver Surgery (ISGLS). *Surgery.* 2011; 149:713-724.
6. Teramoto K, Nakamura N, Ito K, Kudo A, Noguchi N, Takamatsu S, Kawamura T, Tanaka S, Aii S. Strong association between frequency of intermittent inflow occlusion and transient increase in serum liver enzymes after hepatic resection. *Hepatogastroenterology.* 2008; 55:636-640.
7. Pelton J, Hoffman J, Eisenberg. Comparison of liver function tests hepatic lobectomy and hepatic wedge resection. *Am Surg.* 1998; 64:408-414.
8. Noun R, Jagot P, Farges O, Sauvanet A, Belghiti J. High preoperative serum alanine transferase levels: Effect on the risk of liver resection in Child grade a cirrhotic patients. *World J Surg.* 1997; 21:390-395.
9. Giovannini II, Chiarla C, Giuliante F, Vellone M, Ardito F, Sarno G, Nuzzo G. Analysis of the components of hypertransaminasemia after liver resection. *Clin Chem Lab Med.* 2007; 45:357-60.
10. Dindo D, Demartines N, Clavien PA. Classification of Surgical complications. *Ann Surg.* 2004;240:205-213.
11. Costello P, Duszlak EJ, Lokich J, Matelski H, Clouse ME. Assessment of tumor response by computed tomography liver volumetry. *J Comput Tomogr.* 1983; 7:323-326.
12. Kawasaki S, Makuuchi M, Matsunami H, Hashikura Y, Ikegami T, Chisuwa H, Ikeno T, Noike T, Takayama T, Kawarazaki H. Preoperative measurement of segmental liver volume of donors for living related liver transplantation. *Hepatology.* 1993; 18:1115-1120.
13. Honda H, Onitsuka H, Masuda K, Nishitani H, Nakata H, Watanabe K. Chronic liver disease: Value of volumetry of liver and spleen with computed tomography. *Radiat Med.* 1990; 8:222-226.
14. Yamazaki S, Takayama T, Moriguchi M, Okada S, Hayashi Y, Nakayama H, Higaki T, Sugitani M. Validation of biological and clinical outcome between with and without thoracotomy in liver resection: A matched cohort study. *World J Surg.* 2012; 36:144-150.
15. Hayashi Y, Takayama T, Yamazaki S, Moriguchi M, Ohkubo T, Nakayama H, Higaki T. Validation of perioperative steroids administration in liver resection: A randomized controlled trial. *Ann Surg.* 2011; 253:50-53.
16. Yamazaki S, Takayama T, Kimura Y, Moriguchi M, Higaki T, Nakayama H, Fujii M, Makuuchi M. Transfusion criteria for fresh frozen plasma in liver resection. *Arch Surg.* 2011; 146:1293-1299.
17. Gerald Y Minuk. Canadian Association of Gastroenterology Practice Guidelines: Evaluation of abnormal liver enzyme tests. *Can J Gastroenterol.* 1998; 12:417-421.
18. Man K, Fan ST, Ng IO, Lo CM, Liu CL, Yu WC, Wong J. Tolerance of the liver to intermittent pringle maneuver in hepatectomy for liver tumors. *Arch Surg.* 1999; 134:533-539.
19. Wu CC, Hwang CR, Liu TJ, P'eng FK. Effects and limitations of prolonged intermittent ischaemia for hepatic resection of the cirrhotic liver. *Br J Surg.* 1996; 83:121-124.

(Received January 23, 2018; Revised February 13, 2018; Accepted February 16, 2018)

Arterial infusion of cisplatin plus S-1 against unresectable intrahepatic cholangiocarcinoma

Tokio Higaki, Osamu Aramaki*, Masamichi Moriguchi, Hisashi Nakayama, Yutaka Midorikawa, Tadatoshi Takayama

Department of Digestive Surgery, Nihon University School of Medicine, Itabashi-ku, Tokyo, Japan.

Summary

Conventional regimens for unresectable intrahepatic cholangiocarcinoma are considered of limited effectiveness. To evaluate the efficacy and toxicity of combination chemotherapy with hepatic arterial infusion of IA-call (a fine-powder formulation of cisplatin) plus oral S-1 in patients with unresectable intrahepatic cholangiocarcinoma. The clinicopathological data and long-term outcome of 12 patients who were received with IA-call plus S-1 were compared with those of 16 patients who were received other treatments, such as radiation therapy, trans-arterial chemoembolization, and systemic chemotherapy. The IA-call plus S-1 regimen consisted of IA-call (65 mg/m², administered into the hepatic artery) on day 1 and oral S-1 (60 mg/m²/day) on days 1-28, every 42 days, repeated cycle. Prognostic factors of these patients were evaluated by uni- and multivariate analysis. There was no significant difference between the two groups in the disease status, such as the number of tumor and the tumor size. The overall survival was significantly longer in the patients receiving the arterial IA-call and S-1 regimen (median survival time = 10.1; range, 3.6-24.2 months) than in the receiving other treatments (median survival time = 4.0; range; 0.3-24.2 months, $p = 0.01$). The multivariate analysis revealed that chemotherapy regimen was significantly related to survival, with a hazard ratio of 3.97 ($p = 0.02$). In the IA-call plus S-1 group, the overall response rate was 33.3%. The major toxic effect was grade 3 anemia, occurring in 1 patient (4.5%). Combination chemotherapy with arterial IA-call plus oral S-1 is an effective regimen that may improve survival in patients with unresectable intrahepatic cholangiocarcinoma.

Keywords: Arterial infusion chemotherapy, IA-call

1. Introduction

Although surgical resection is the only potentially curative treatment for intrahepatic cholangiocarcinoma (ICC), the resectability rate is about 30% (1,2). Moreover, the 5-year survival rate is 20% to 40% after potentially curative resection, accompanying by the high recurrence rate about 50% (1,2). Systemic chemotherapy is indicated for patients with unresectable disease, however, a standard regimen has yet to be established (3). Various studies of chemotherapy for ICC have suggested that fluoropyrimidine-

based regimens are promising (4). S-1 (TS-1, Taiho Pharmaceutical Co., Ltd., Tokyo, Japan) is a novel oral fluoropyrimidine preparation combining tegafur, gimeracil, and oteracil potassium. In phase II studies of S-1 monotherapy in patients with biliary tract cancer, the response rate ranged from 21% to 35%, with median overall survival of 8.3 to 9.4 months (5,6). Fluoropyrimidines are known to act synergistically with cisplatin (7). A phase II study of S-1 and intravenous cisplatin reported a response rate of 30% and median overall survival of 8.7 months in patients with biliary tract cancer (8). Chemotherapy delivered by transcatheter hepatic arterial infusion (TAI) is a particularly promising, minimally invasive treatment for unresectable liver tumors (9).

We conducted a pilot study to examine the safety and effectiveness of TAI using cisplatin plus oral S-1 in patients with inoperable unresectable ICC.

*Address correspondence to:

Dr. Osamu Aramaki, Department of Digestive Surgery, Nihon University School of Medicine, 30-1 Ohya-guchikami-machi, Itabashi-ku, Tokyo 173-8610, Japan.
E-mail: takayama.tadatoshi@nihon-u.ac.jp

2. Patients and Methods

2.1. Patients

Between 2007 and 2011, we studied 28 patients with unresectable ICC. From April 2010 through December 2011, 12 of these patients received TAI using a fine-powder formulation of cisplatin (IA-call) plus oral S-1 (IA-call plus S-1 group). From April 2007 through March 2010, the other 16 patients (other treatment group) received various conventional treatments. Two patients were given radiation therapy, 1 received trans-arterial chemoembolization (TACE) with epirubicin, and 13 were treated with various regimens of chemotherapy. Six patients received intravenous gemcitabine (GEM, 1000mg/m² weekly), 1 received a combination of intravenous cisplatin, epirubicin, and 5-fluorouracil (5-FU), and 6 received TAI of IA-call (4 in combination with a daily 24-hour continuous intravenous infusion of 5-FU 1,000 mg/m²/day, and 2 without 5-FU). Since April 2010, we have changed our strategy in the treatment of unresectable ICC, and the IA-call plus oral S-1 therapy has been applied from this time. In this study, all the patients with unresectable ICC were divided into two groups at the time of changing the treatment strategy.

A diagnosis of ICC was based on either histopathological or radiologic findings. All patients were deemed unresectable upon exploration due to the locally advanced, intrahepatic and bilateral dissemination, or distant metastases. All patients had good performance status (Eastern Cooperative Oncology Group (ECOG) performance status, 0-2), adequate liver function (bilirubin level < 2.0 mg/dL), adequate hematologic and bone marrow function (leukocyte count > 4,000/uL, platelet count > 100,000/ μ L), adequate renal function (creatinine level < 2.0 mg/dL), and measurable disease on computed tomography or magnetic resonance imaging. In addition, all patients could undergo angiography and selective visceral catheterization. Patients with biliary obstruction underwent endoscopic retrograde cholangiopancreatography-based or percutaneous transhepatic biliary drainage before administration of TAI and were required to have serum bilirubin levels of < 2.0 mg/dL. All the treatments were started soon after the definite diagnosis.

2.2. Treatment schedule

IA-call[®] (cisplatin 100 mg/vial, 1.43 mg/mL; Nippon Kayaku Co., Ltd., Tokyo, Japan;) was dissolved in 70 mL of saline, heated to 50°C. A dose of 65 mg/m² cisplatin was then infused into the hepatic artery at a rate of 2 mL/min. on day 1 of each cycle. A catheter was placed in the femoral artery and introduced into the hepatic artery under angiographic guidance. After the procedure patients were observed overnight to manage pain and nausea, patients were routinely discharged

home the following morning after evaluation of the results of laboratory studies.

S-1 was administered orally at a dose of 60 mg/m² per day according to body-surface area (< 1.25 m², 80mg daily; \geq 1.25 m² to < 1.5 m², 100 mg daily; and \geq 1.50 m², 120 mg daily), divided into two doses. S-1 was given on days 1-28, every 42 days. This cycle was repeated if patients had recovered sufficiently from any drug-related toxicity. If patients had hematologic toxicity of grade 3 or higher or non-hematologic toxicity of grade 2 or higher, treatment was postponed until the toxicity subsided to grade 1 or lower.

2.3. Follow-up and toxicity assessment

After discharge, laboratory values were checked weekly on an outpatient basis. All patients underwent follow-up imaging studies 6 to 8 weeks after each TAI procedure. Tumor response was assessed according to the Response Evaluation Criteria in Solid Tumors (10). In addition, serum carcinoembryonic antigen and CA19-9 levels were measured and included in the evaluation of therapeutic efficacy. Toxicity was evaluated using the National Cancer Institute Common Toxicity Criteria version 4.0.

2.4. Statistical analysis

Overall survival was calculated from the date of the first day of treatment to the date of death from any cause. Survival data were analysed using the Kaplan-Meier method. The statistical significance of differences between survival curves was determined with the log-rank test. Univariate analysis was performed using chi-square tests. Multivariate analysis was performed with a Cox proportion-hazards model. Differences with *p*-values of < 0.05 were considered statistically significant. All analyses were performed using IBM SPSS Statistics 19 software (IBM SPSS, Tokyo, Japan).

3. Results

Twelve patients (median age 76 years [range: 61-83]) received a combination of hepatic arterial infusion of IA call plus oral S-1, and 16 (median age 67 years [57-79]) received conventional treatments (Table 1). There was no significant difference between the two groups in the disease status, such as the number of tumor and the tumor size (Table 1).

The median follow-up period for IA call plus S-1 and other treatment group were 10.1 (range 3.6-24.2 months) and 5.8 (range 1.5-24.2 months), respectively. A median of 4 cycles of IA-call plus S-1 (range, 2-9) were administered (Table 2). All of the 12 patients in the IA-call plus S-1 group completed 2 or more courses of chemotherapy. Three patients underwent surgery and had recurrent disease. Intrahepatic recurrence occurred in all the patients, and 1 patient also had

multiple lung metastases. Eight patients are still alive, and 4 died of tumor progression 4.3 to 11.1 months after initial treatment. No patient had a complete response (CR), 4 (33.3%) had partial responses (PR), 2 (16.6%) had stable disease (SD), and the other 6 (50%) had progressive disease (PD). All of the patients had decreased levels of the tumor marker CA-19-9.

About toxicity in these patients (Table 3), only

one patient (4.5%) had grade 3 anemia, and non-hematologic toxicity was generally mild, including nausea and vomiting. There was no treatment-related death. One patient was refused further chemotherapy because of toxicity (patient No. 1). All patients in the other treatment group died of tumor progression.

The overall survival was significantly longer in patients receiving TAI of IA-call plus S-1 (median

Table 1. Characteristics of patients with unresectable intrahepatic cholangiocarcinoma

Items	Total	IA call+S-1	Other	p value
No. of patients	28	12 (42.8%)	16 (57.1%)	
Age (year)				
Median [Range]	73 [57-83]	76 [61-83]	67 [57-79]	0.13
> 65	19 (67.9%)	10 (88.3%)	9 (56.3%)	
Gender				
Male	19 (67.9%)	8 (66.7%)	11 (68.8%)	0.9
Female	9 (32.1%)	4 (33.3%)	5 (31.3%)	
ECOG ^a performance status				
0	23 (82.1%)	10 (83.3%)	13 (81.3%)	0.89
1	5 (17.9%)	2 (16.7%)	3 (18.8%)	
Disease status				
Solitary	18 (64.3%)	7 (58.3%)	11 (68.8%)	0.57
Multiple	10 (35.7%)	5 (41.7%)	5 (31.3%)	
Tumor size > 5 cm	21 (75.0%)	8 (66.7%)	13 (81.3%)	0.38
Vascular invasion	14 (50.0%)	4 (33.3%)	10 (62.5%)	0.13
Distant metastasis	10 (35.7%)	5 (41.7%)	5 (31.3%)	0.57
Lymph node metastasis	7 (25.0%)	4 (33.3%)	3 (18.8%)	0.38
CEA ^b > ULN ^c	10 (35.7%)	2 (16.7%)	8 (50.0%)	0.07
CA19-9 > ULN ^c	24 (85.7%)	9 (75.0%)	15 (93.8%)	0.16

^a Eastern Cooperative Oncology Group. ^b Carcinoembryonic antigen. ^c Upper limit of normal.

Table 2. Characteristics of the patients treated with IA call and S-1

Patient No.	Age	Maximum response	Liver resection	Cycles of IA-call+S-1	Highest CA 19-9 before therapy (U/mL)	Lowest CA 19-9 after therapy (U/mL)
1	83	PD	Absent	2	381	76.3
2	77	PD	Absent	3	102.8	79.3
3	75	PR	Absent	5	398.2	51.1
4	76	SD	Absent	5	140.7	33.9
5	64	PD	Absent	4	> 1,000,000	198,900
6	81	PR	Absent	5	59.2	5.9
7	74	SD	Absent	9	42.5	12.9
8	67	PD	Absent	4	4.5	2.9
9	81	PD	Present	5	26.4	6.4
10	74	PR	Present	3	277.5	88.2
11	61	PR	Absent	3	131,800	42,230
12	77	SD	Present	3	47.7	20.9

PD: Progressive disease, PR: Partial response, SD: Stable disease

Table 3. Toxicity in patients receiving the arterial infusion of IA-call and S-1

Toxicity profile (n = 22)	Grade 1	Grade 2	Grade 3	Grade 4	Grade 3-4 (%)
Hematologic					
Leukopenia	1	5	0	0	0
Neutropenia	1	5	0	0	0
Anemia	4	5	1	0	1 (4.54%)
Thrombocytopenia	3	2	0	0	0
Non-hematologic					
Nausea	2	3	0	0	0
Vomiting	1	1	0	0	0

National Cancer Institute Common Toxicity Criteria Version 4.0

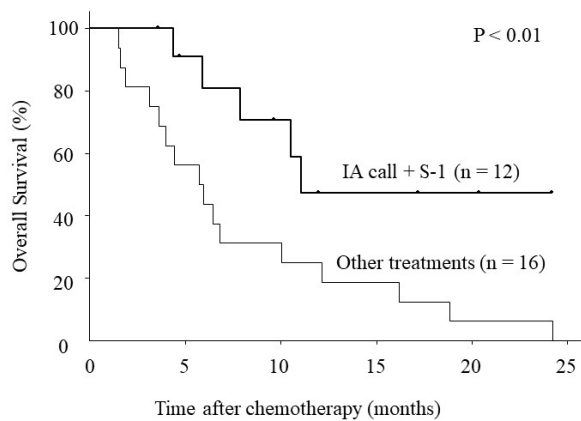


Figure 1. Overall survival of patients receiving the transarterial infusion of IA-call and S-1 regimen vs. those receiving other treatments. The overall survival was significantly longer in patients receiving transarterial infusion of IA-call plus S-1 (median survival time = 10.1; range, 3.6-23.2 months) than in those receiving other treatments (median survival time = 4.0; range; 0.3-24.2 months) ($P < 0.01$).

survival time = 10.1; range, 3.6-23.2) than in those receiving other treatments (median survival time = 4.0; range; 0.3-24.2; Figure 1; $p < 0.01$).

To determine the prognostic factors on survival in patients with unresectable ICC, univariate analyses were conducted (Table 4). The results of univariate analysis indicated that two variables, age and type of treatment, significantly affected the patients' overall survival (Table 4). Cox's proportional-hazard analysis including 3 variables (age, tumor size, and type of treatment) showed that only the type of treatment (IA call + S-1 vs. Other treatment, hazard ratio 3.97; 95% CI 1.28-12.3, $p = 0.02$) was an independent risk factor for overall survival.

4. Discussion

In this study, we evaluated the efficacy and toxicity of TAI using cisplatin plus oral S-1 in patients with unresectable ICC. Our results showed that overall survival was significantly longer in patients receiving TAI of IA-call plus S-1 (median survival time = 10.1; range, 3.6-23.2) than in those receiving other treatments (median survival time = 4.0; range; 0.3-24.2; $p < 0.01$). Moreover, IA-call plus S-1 was associated with moderate toxicity, with grade 3 anemia occurring in only 1 patient (4.5%).

Although systemic chemotherapy is indicated for unresectable ICC, conventional regimens are considered of limited effectiveness. There is an acute need for new treatment approaches. We used TAI of IA-call and S-1 to treat unresectable ICC for several reasons. ICC can extend in a multimodal and locoregional manner by means of infiltration of the parenchyma, the formation of intrahepatic satellite nodules, and vascular invasion (11). The remnant liver is the most common site of recurrence (12,13). To prevent ICC from extending to

Table 4. Univariate analysis of prognostic factors of overall survival

Items	Hazard ratio	95% Confidence interval	p value
Gender			
Male			
Female	0.56	0.20-1.59	0.28
Age			
≤ 64			
> 65	2.82	1.09-7.27	0.03
Tumor size			
≤ 5			
> 5	2.79	0.81-9.66	0.11
Vascular invasion			
Absent			
Present	2.08	0.83-5.23	0.12
Lymph node metastasis			
Absent			
Present	1.45	0.55-4.04	0.48
Number of tumors			
Solitary			
Multiple	2.18	0.79-5.99	0.13
CA19-9			
$< \text{ULNa}$			
$> \text{ULNa}$	2.04	0.47-8.92	0.34
Treatment			
IA call + S-1			
Other treatment	4.21	1.40-12.63	0.01

^aUpper limit of normal.

the lymph nodes or other organs *via* vascular invasion, systemic chemotherapy might be useful. To date, the most promising approaches have used single-agent GEM. Median survival times of 14 months and 11 months have been obtained with combinations of GEM plus capecitabine (14) and GEM plus docetaxel (15), respectively. However, the therapeutic usefulness of these GEM-based combined regimens in patients with unresectable ICC has been limited by toxicity (16). In contrast, recent phase 2 trials of S-1 monotherapy in patients with biliary tract cancer have obtained high response rates with mild toxicity (5,6). Therefore, we selected S-1 for systemic chemotherapy to prevent the spread of ICC to lymph nodes or other organs.

TAI allows the delivery of high doses of chemotherapeutic drugs directly to tumors, with minimal systemic drug exposure. Consequently, techniques for TAI-based chemotherapy have been developed to achieve higher therapeutic efficacy than that possible with intravenous administration of anticancer agents. With TAI, an anticancer agent is infused into an artery supplying the target tumor, thereby producing high drug concentrations at the target site in the liver. Because the blood supply of the biliary tree is derived from the hepatic artery, and ICC is usually confined to the liver, TAI might be a rational approach. To prevent the spread of ICC in the liver, TAI-based chemotherapy is considered promising (17). Moreover, to obtain higher drug concentrations than those produced by conventional formations of cisplatin

(0.5 mg/mL), we used IA-call (1.43 mg/mL), a fine-powder formulation of cisplatin (9). To our knowledge, only a few studies have evaluated the effectiveness of hepatic arterial chemotherapy in patients with biliary tract carcinomas such as ICC. Melichar *et al.* treated 17 patients with ICC and 15 with gallbladder carcinoma with a combination of 5-FU, cisplatin, and folinic acid, administered through the hepatic artery. This regimen was effective and improved survival (18). Cantore *et al.* gave 25 patients with ICC and 5 with gallbladder carcinoma a combination of epirubicin and cisplatin administered through the hepatic artery plus a systemic infusion of 5-FU. The overall response rate was 40%, with median overall survival of 13.2 months (19). Kelsen *et al.* reported that the administration of cisplatin through the hepatic artery provides a high drug concentration in the perfused blood, whereas the systemic concentration is much lower (20). The few side effects with IA-call plus S-1 may thus be attributed by the lower systemic exposure to cisplatin.

Combination chemotherapy with arterial IA-call plus oral S-1 might have a higher risk of some complications than conventional systemic chemotherapy. Angiography is generally a very safe procedure, and of the 12 patients, no complications related to the angiographic technique were observed. However, there is a small chance of minor or serious complications occurring, such as hemorrhage, arterial obstruction, and pseudoaneurysms (21). To prevent these complications, we try to do the examination as patriotically as possible.

In conclusion, this pilot study suggests that TAI of IA-call plus S-1 is a safe and effective regimen. Our promising initial results warrant further phase II and III trials to confirm the feasibility and efficacy of IA-call plus S-1 in patients with unresectable ICC.

Acknowledgements

This work was mainly supported by a Grant-in-Aid for Scientific Research (A) 24249068 from the Ministry of Education, Culture, Sports, Science and Technology (MEXT), Japan.

References

1. Ohtsuka M, Ito H, Kimura F, Shimizu H, Togawa A, Yoshidome H, Miyazaki M. Results of surgical treatment for intrahepatic cholangiocarcinoma and clinicopathological factors influencing survival. *Br J Surg.* 2002; 89:1525-1531.
2. Khan SA, Davidson BR, Goldin R, Pereira SP, Rosenberg WM, Taylor-Robinson SD, Thillainayagam AV, Thomas HC, Thursz MR, Wasan H; British Society of Gastroenterology. Guidelines for the diagnosis and treatment of cholangiocarcinoma: Consensus document. *Gut.* 2002; 51 Suppl 6:VII-9.
3. Glimelius B, Hoffman K, Sjöden PO, Jacobsson G, Sellström H, Enander LK, Linné T, Svensson C.

Chemotherapy improves survival and quality of life in advanced pancreatic and biliary cancer. *Ann Oncol.* 1996; 7:593-600.

4. Mazhar D, Stebbing J, Bower M. Chemotherapy for advanced cholangiocarcinoma: What is standard treatment? *Future Oncol.* 2006; 2:509-514.
5. Ueno H, Okusaka T, Ikeda M, Takezako Y, Morizane C. Phase II study of S-1 in patients with advanced biliary tract cancer. *Br J Cancer.* 2004; 91:1769-1774.
6. Furuse J, Okusaka T, Boku N, Ohkawa S, Sawaki A, Masumoto T, Funakoshi A. S-1 monotherapy as first-line treatment in patients with advanced biliary tract cancer: A multicenter phase II study. *Cancer Chemother Pharmacol.* 2008; 62:849-855.
7. Shirasaka T, Shimamoto Y, Ohshimo H, Saito H, Fukushima M. Metabolic basis of the synergistic antitumor activities of 5-fluorouracil and cisplatin in rodent tumor models *in vivo*. *Cancer Chemother Pharmacol.* 1993; 32:167-172.
8. Kim YJ, Im SA, Kim HG, *et al.* A phase II trial of S-1 and cisplatin in patients with metastatic or relapsed biliary tract cancer. *Ann Oncol.* 2008; 19:99-103.
9. Yoshikawa M, Ono N, Yodono H, Ichida T, Nakamura H. Phase II study of hepatic arterial infusion of a fine-powder formulation of cisplatin for advanced hepatocellular carcinoma. *Hepatol Res.* 2008; 38:474-483.
10. Therasse P, Arbuck SG, Eisenhauer EA, Wanders J, Kaplan RS, Rubinstein L, Verweij J, Van Glabbeke M, van Oosterom AT, Christian MC, Gwyther SG. New guidelines to evaluate the response to treatment in solid tumors. European Organization for Research and Treatment of Cancer, National Cancer Institute of the United States, National Cancer Institute of Canada. *J Natl Cancer Inst.* 2000; 92:205-216.
11. Inoue K, Makuuchi M, Takayama T, Torzilli G, Yamamoto J, Shimada K, Kosuge T, Yamasaki S, Konishi M, Kinoshita T, Miyagawa S, Kawasaki S. Long-term survival and prognostic factors in the surgical treatment of mass-forming type cholangiocarcinoma. *Surgery.* 2000; 127:498-505.
12. Yamamoto M, Takasaki K, Otsubo T, Katsuragawa H, Katagiri S. Recurrence after surgical resection of intrahepatic cholangiocarcinoma. *J Hepatobiliary Pancreat Surg* 2001; 8:154-157.
13. Weber SM, Jarnagin WR, Klimstra D, DeMatteo RP, Fong Y, Blumgart LH. Intrahepatic cholangiocarcinoma: Resectability, recurrence pattern, and outcomes. *Am Coll Surg* 2001; 193:384-391.
14. Knox JJ, Hedley D, Oza A, Feld R, Siu LL, Chen E, Nematollahi M, Pond GR, Zhang J, Moore MJ. Combining gemcitabine and capecitabine in patients with advanced biliary cancer: A phase II trial. *J Clin Oncol* 2005; 23:2332-2338.
15. Kuhn R, Hribaschek A, Eichelmann K, Rudolph S, Fahlke J, Ridwelski K. Outpatient therapy with gemcitabine and docetaxel for gallbladder, biliary, and cholangio-carcinomas. *Invest New Drugs.* 2002; 20:351-356.
16. Dingle BH, Rumble RB, Brouwers MC; Cancer Care Ontario's Program in Evidence-Based Care's Gastrointestinal Cancer Disease Site Group. The role of gemcitabine in the treatment of cholangiocarcinoma and gallbladder cancer: A systematic review. *Can J Gastroenterol.* 2005; 19:711-716.

17. Melichar B, Cerman J Jr, Dvorák J, Jandík P, Mergancová J, Melicharová K, Tousková M, Krajina A, Voboril Z. Regional chemotherapy in biliary tract cancers – A single institution experience. *Hepatogastroenterology*. 2002; 49:900-906.
18. Vexler AM, Mou X, Gabizon AA, Gorodetsky R. Reduction of the systemic toxicity of cisplatin by intra-arterial hepatic route administration for liver malignancies. *Int J Cancer*. 1995; 60:611-615.
19. Cantore M, Mambrini A, Fiorentini G, Rabbi C, Zamagni D, Caudana R, Pennucci C, Sanguinetti F, Lombardi M, Nicoli N. Phase II study of hepatic intraarterial epirubicin and cisplatin, with systemic 5-fluorouracil in patients with unresectable biliary tract tumors. *Cancer*. 2005; 103:1402-1407.
20. Kelsen DP, Hoffman J, Alcock N, Cheng E, Bailey E, Young C, Golbey R, Fortner J. Pharmacokinetics of cisplatin regional hepatic infusions. *Am J Clin Oncol*. 1982; 5:173-178.
21. Hessel SJ, Adams DF, Abrams HL. Complications of angiography. *Radiology*. 1981; 138:273-281.

(Received December 26, 2017; Revised February 2, 2018; Accepted February 6, 2018)

Tracking hospital costs in the last year of life — The Shanghai experience

Bifan Zhu^{1,§}, Fen Li^{1,§}, Changying Wang¹, Linan Wang¹, Zhimin He², Xiaoxi Zhang¹, Peipei Song³, Lingling Ding², Chunlin Jin^{1,*}

¹Shanghai Health Development Research Center, Shanghai, China;

²Xiangya School of Public Health, Central South University, Hunan Province, China;

³Graduate School of Frontier Sciences, The University of Tokyo, Tokyo, Japan.

Summary

One aim of the current study was to track end-of-life care using individual data in Shanghai, China to profile hospital costs for decedents and those for the entire population. A second aim of this study was to clarify the effect of proximity to death. Data from the Information Center of the Shanghai Municipal Commission of Health and Family Planning (SMCHFP) were examined. For decedents who died in medical facilities in 2015, inpatient care was tracked for 1 year before death. A total of 43,765 decedents were included in the study, accounting for 35% of total deaths in 2015 in Shanghai. Hospital costs were higher for people who died before the age of 45 (14,228.62 USD) than for those aged 90 or older (8,696.34 USD). The ratio of costs for decedents to the entire population declined significantly with age. Women received less care than men in the last year of life ($t = -15.1244$, $p < 0.05$). Average tertiary hospital costs per decedent declined significantly with age, whereas average secondary hospital costs increased slightly with age. Among the top 14 causes of death classified using the ICD-10, rectal cancer incurred the greatest costs (13,973 USD per decedent). Over 43% of hospital costs were incurred during the month before death. Declining costs in the last year of life with age as well as with distance to death demonstrate the existence of a proximity to death phenomenon in health care expenses. Disease-specific studies should be conducted and attention should be paid to gender equity when examining end-of-life medical costs in the future.

Keywords: Aging, proximity to death, health care expenditures

1. Introduction

China is aging rapidly; the proportion of people aged 60 or older has increased from 7.0% in 2000 to 16.1% in 2015 (1). According to a population survey in Shanghai, people aged 60 or older accounted for 19.5% of the entire resident population in 2015 while people aged 65 or older accounted for 12.3%. These demographic changes have resulted in increasing demands for health care at the end of life, but to date there is little information about the healthcare expenditures at the end of life, and this is

particularly true in developing countries.

Results of international studies have indicated that healthcare expenditures are affected by a proximity to death (PTD) phenomenon. Patients often receive excessive care at the end of life, resulting in mounting medical expenses (2-5). PTD can skew the effects of population aging on medical expenses due to the high mortality rate and greater end-of-life medical demands of the elderly (6). The PTD phenomenon varies among different age groups, costs, and categories of disease. Polder *et al.* (4) and Shugarman *et al.* (7) concluded that in the Netherlands and the United States, the average medical expenses in the last year of life were greater for people dying at younger ages (< 70) than older decedents. Gozalo *et al.* (8) found that hospice care can substitute for acute medical care at the end of life. An increase in hospice care was related to a 2.4 percentage-

[§]These authors contributed equally to this work.

*Address correspondence to:

Dr. Chunlin Jin, Shanghai Health Development Research Center, No. 1477 West Beijing Road, Shanghai 200040, China.
E-mail: jin Chunlin@shdrc.org

point reduction in the rate of hospital transfers and a 7.1 percentage-point reduction in care in an intensive care unit (ICU). Older elderly receive more nursing care and palliative care at the end of life but account for fewer ambulatory and hospital costs (7), indicating a continuing shift from acute medical care to long-term care late in life. A comparable conclusion was reached by Spillman and Lubitz (9). Wong *et al.* (10) found that people dying from cancer incur the most costs in the last year of life, while people dying from myocardial infarction incur the least costs. Another study found that payments for care to dying patients accounted for 27.2% to 30.6% of all Medicare payments (11).

Better knowledge of the characteristics of healthcare expenditures at the end of life and the combined effect of population aging and proximity to death is crucial to better policymaking. Shanghai is one region of China that faces the early challenges of aging, and Shanghai has accumulated a wealth of experience in health care management and health system reform. Since previous studies were mostly conducted in developed countries, the aims of the current study were to track end-of-life medical care using individual level data in Shanghai, China to profile hospital costs for decedents and those for the entire population; to describe age patterns and differences between causes of death for men and women; and to clarify the effect of PTD.

2. Subjects and Methods

An administrative database from the Information Center of the Shanghai Municipal Commission of Health and Family Planning was used to track the end-of-life inpatient care received by decedents in Shanghai. The database covers all outpatients and inpatients in every type of medical facility in Shanghai in 2015. For decedents who died in medical facilities between January 1 to December 31, 2015, inpatient care received in different medical facilities was tracked for 1 year before death. Hence, decedents with a single hospital stay longer than 1 year were excluded from this study. Medical records were linked at individual level using age, gender, and an identification number. The front page of each medical record was reviewed to obtain information regarding age, gender, type of basic medical insurance scheme, diagnosis, date of admission and discharge, and costs for each category of medical care. The latest record of admission was used to ascertain the cause of death, and the date of discharge served as the date of death. Individuals without basic medical insurance were excluded since most were patients from other provinces. Hence, subjects represent the resident population of Shanghai.

Hospital costs were calculated by gender, age, cause of death, and the level of medical facility. The hospital costs in the 12 months prior to death were calculated for decedents in 2015. Health care expenditures by the

entire population in 2015 were calculated as well. Some of those individuals also died in 2015 but in places other than medical facilities for whom we were not able to identify as decedents, which may narrow the gap between decedents and the entire population. Decedents and the entire population were compared only in terms of expenditures in 2015. All Chinese currency figures in this study were adjusted to comparable amounts in USD using the average exchange rate in 2015 (6.2284 RMB = 1 USD).

A *t*-test was used to compare continuous data while a chi-square test was used to compare categorical data. Pearson's correlation coefficient (*r*) was used to analyze the relationship between different variables. Prescriptive and statistical analysis were performed using STATA 13.0, and a significance level of 0.05 was set for hypothesis testing.

3. Results and Discussion

3.1. Basic characteristics

A total number of 43,812 decedents were identified through the database. Forty-seven decedents were hospitalized for longer than 1 year in a single stay and were excluded as subjects. As a result, 43,765 decedents who died in medical facilities were included in this study. These individuals accounted for approximately 35% of the total deaths in 2015 in Shanghai. Table 1 shows some basic characteristics of the patients who died in medical facilities in 2015, and 81.77% of those patients were elderly people age 65 or older. Males accounted

Table 1. Basic characteristics of subjects (n = 43,765)

Indicators	Values
Age (Mean ± SD)	76.95 ± 12.85
Gender (n (%))	
Male	24,312 (55.56)
Female	19,453 (44.44)
Insurance scheme (n (%))*	
UEBMI	35,800 (81.80)
URBMI	4,811 (10.99)
NCMS	1,145 (2.62)
Other type	2,009 (4.59)
Cause of death (n (%))	
Cancer	15,115 (34.54)
Circulatory disease	11,464 (26.19)
Respiratory disease	9,825 (22.45)
Other cause	7,361 (16.82)
Level of the medical facility (number of admissions (%))	
Tertiary hospital	46,120 (31.67)
Secondary hospital	89,037 (61.15)
Primary care facility	10,457 (7.18)

*The 3 basic medical insurance schemes in Shanghai include Urban Employee Basic Medical Insurance (UEBMI), Urban Resident Basic Medical Insurance (URBMI), and the New Rural Cooperative Medical Insurance System (NCMS), which cover over 95% of the residents of Shanghai.

Table 2. Average annual hospital costs per person, in USD

Age group (year)	In the last year of life			Regardless of proximity to death		
	Female	Male	Both	Female	Male	Both
< 1	3,150.63	3,848.27	3,499.45	1,011.09	1,336.91	1,179.47
1~4	14,429.82	30,427.14	25,094.70	128.84	170.83	151.16
5~9	3,322.60	30,384.53	16,853.56	89.50	120.63	106.11
10~14	9,632.01	23,167.09	16,399.54	78.80	116.23	98.64
15~19	11,714.65	17,546.21	14,769.27	77.64	88.61	83.60
20~24	21,214.21	7,480.24	14,347.23	84.37	55.70	68.98
25~29	18,380.35	23,404.55	20,740.21	147.49	72.54	108.77
30~34	11,533.36	15,106.30	13,221.36	153.01	83.88	117.48
35~39	16,060.05	16,310.53	16,184.57	133.82	99.95	116.04
40~44	11,625.88	10,803.46	11,109.14	154.28	140.39	146.89
45~49	11,154.63	11,520.36	11,383.00	232.53	227.36	229.79
50~54	10,900.00	11,289.01	11,161.00	281.53	297.57	290.04
55~59	12,649.24	11,299.42	11,727.94	322.34	403.06	363.48
60~64	11,079.94	11,010.75	11,032.37	397.82	533.91	465.72
65~69	10,494.43	10,842.19	10,730.47	529.61	700.95	616.98
70~74	9,822.30	9,997.73	9,935.38	676.15	925.11	800.79
75~79	8,628.57	9,127.05	8,916.77	889.10	1,142.69	1,008.11
80~84	7,834.50	8,812.16	8,352.74	1,131.81	1,442.54	1,264.63
85~89	7,417.46	10,360.24	8,818.95	1,468.18	2,255.46	1,771.05
≥ 90	6,356.31	11,819.05	8,696.34	1,509.07	3,022.85	2,007.90

Note: Costs have been converted into USD using the average exchange rate in 2015 (the same applies to the table below). Costs for both genders mean the average costs for both genders in each age group. Costs regardless of proximity death refer to the average costs for the entire population of Shanghai in 2015.

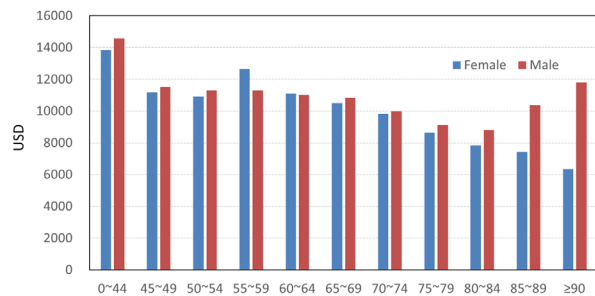


Figure 1. Average hospital costs (in USD) per decedent in the last year of life by age and sex in 2015.

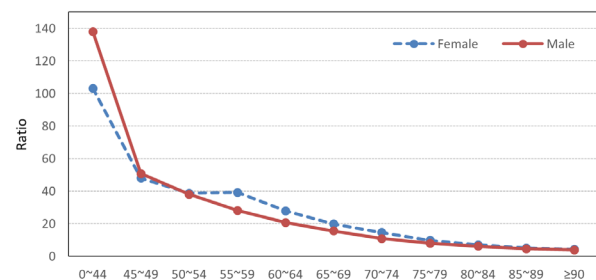


Figure 2. Ratio of average hospital costs for decedents in the last year of life to average costs for the entire population, by age and sex, in 2015.

for 55.56%. The most frequent cause of death was cancer, which accounted for 34.54% of deaths among decedents, followed by circulatory diseases (26.19%) and respiratory diseases (22.45%). Most inpatient care received during the last year of life was provided at secondary (61.15%) and tertiary hospitals (31.67%), and only 7.18% was provided at primary care facilities.

3.2. Age and gender

The per person-year hospital costs in 2015 by sex, age, and PTD are shown in Table 2. Costs for the entire population (regardless of PTD) varied more than 18-fold from 106.11 USD for individuals aged 5-9 to 2,007.90 USD for individuals over the age of 90.

Hospital costs in the last year of life were inversely related to age (Figure 1). Costs were 14,228.62 USD for individuals aged 0-44 compared to 8,696.34 USD for individuals aged 90 or older ($r = -0.0894, p < 0.05$). This

inverse relationship was more evident among women ($r = -0.1746, p < 0.05$), while for men the average hospital costs rebounded after the age of 85. This can be partly explained by the different age patterns for men and women to seek health care at different levels of facilities.

Hospital costs in the last year of life decline with increasing age at death (Figure 1). Our figures demonstrated that in Shanghai, people who died at age 95 or older accounted for about 80% of inpatient expenditures compared to decedents aged 65-70. This decrease is relatively smaller than that found in other studies and might be affected by filial piety in Chinese culture. Polder *et al.* (4) and Serup-Hansen *et al.* (12) estimated a larger decrease in the Netherlands and in Denmark, while the figure for Germany was about 43-47% (13). For the United States, the figure was about 40% (14) or 52% (15).

The ratio of costs for decedents and the entire population declines with increase in age. Figure 2

Table 3. Hospital costs in the last year of life by gender and cause of death*

Items	Average costs per decedent (USD)			Total costs	
	Female	Male	Both	USD 1mln	%
Rectal cancer	13,127	14,421	13,973	8.97	1.69
Colon cancer	12,876	14,577	13,795	16.50	3.11
Stomach cancer	12,585	13,930	13,418	22.58	4.26
Respiratory failure	11,787	13,826	12,934	13.63	2.57
COPD	10,821	13,757	12,785	31.83	6.01
Sequelae of cerebrovascular disease	12,091	13,372	12,692	13.45	2.54
Other respiratory disorders	10,437	14,355	12,500	40.72	7.68
Pancreatic cancer	11,711	12,949	12,384	13.77	2.60
Chronic ischemic heart disease	10,476	14,640	12,275	40.24	7.59
Lung cancer	11,010	12,511	12,092	44.26	8.35
Pneumonia	9,206	13,670	11,675	23.22	4.38
Liver cancer	9,348	10,841	10,435	14.39	2.71
Stroke	7,982	9,100	8,562	30.57	5.77
Myocardial infarction	7,566	8,741	8,230	5.51	1.04
Other cause	11,273	13,782	12,584	210.47	39.70
Total	10,777	13,181	12,113	530.11	100.00

*Average costs per decedent in USD. Total costs for all decedents in 2015 (million USD, share in %)

shows that the ratio of costs declines for both males and females, with a ratio of almost 120 for people under the age of 45 to a ratio of less than 5 for people aged 85 or older. Women aged 50-79 had a relatively high ratio of costs in comparison to men. This was caused by lower costs for the entire female population instead of higher costs for female decedents. An average cost ratio of 32.9 was found between decedents and the whole population with a broad range from 4.3 to 119.5. This ratio is higher than that reported by Polder *et al.* (4), who reported an overall ratio of 13.5 (from 30 to less than 5), and that reported by Serup-Hansen *et al.* (12), who estimated ratios of 9.4 and 13.3 for Danish men and women, respectively. The ratio for the elderly population (from 17.4 to 4.3 for those aged 65 or older) was comparable to that reported by McGrail *et al.* (2), who reported a ratio ranging from 16.6 to 2.5 for the Canadian population aged 65 or older.

Economists have long regarded health as one form of human capital (16-18). According to Theodore W. Schultz, investment in health enhances the quality of human resource, which is one of the main drivers of economic growth (19). In Michael Grossman's model of the demand for health, health can be viewed as a durable capital stock that produces an output of healthy time, and investment in health is assumed to increase productivity and to yield greater economic benefits (20). The inverse relationship between end-of-life hospital costs and age at death could partly be explained by the combination of these two theories. The younger population is believed to have a longer life expectancy and greater productivity, hence investment in the health of young people is expected to yield greater economic benefits, especially at the end of life.

3.3. Cause of death

The top 14 causes of death were classified based on the ICD-10 to determine the relationship between the type of disease and end-of-life hospital costs. Of all decedents, 61.77% died from one of those 14 diseases. The most prevalent cause of death was lung cancer, accounting for 8.35% of total hospital costs.

A stroke or heart attack incurred relatively low costs, with an average of 8,562 and 8,230 USD, respectively, per decedent. This was partly due to the high fatality of these diseases. The average costs of rectal cancer appeared to be the highest (13,973 USD per decedent), though the overall burden did not seem to be severe (costs for rectal cancer accounted for 1.69% of total costs). Costs of the top 14 causes of death varied significantly ($F = 19.47, p < 0.05$), indicating that costs vary more widely among people dying from different diseases than among people dying of a certain disease (Table 3). Hence, more disease-specific studies of end-of-life medical costs should be conducted to further understand the effects of population aging and epidemiological changes on health care expenditures.

For people dying from different disease groups, the declining age pattern of end-of-life hospital costs was less prominent for men than for women, especially after 69 years old. The average hospital costs for men who died from a certain cause slightly rebounded after the age of 84, which was consistent with the age patterns of total inpatient expenditures. Hospital costs for people dying from cancer declined sharply at younger ages (< 45), especially for men. Circulatory diseases incurred lower costs and costs varied less among different age groups (Figure 3). In each category of disease, men had higher average costs than women ($p < 0.05$). In general, the deceased cancer patients generated higher hospital costs than patients dying from other major disease ($F = 50.42, p < 0.05$).

3.4. Facilities

Average tertiary hospital costs per decedent declined significantly with age ($r = -0.0678, p < 0.05$), whereas average secondary hospital costs increased slightly with age ($r = 0.0128, p < 0.05$), exceeding the costs incurred at tertiary hospitals for individuals after age 79. Figure 4 shows some notable differences in the age patterns of decedents and the entire population seen at secondary and tertiary hospitals. The age pattern of tertiary hospitalization costs is contrary for decedents and the entire population, in spite of the particularly high

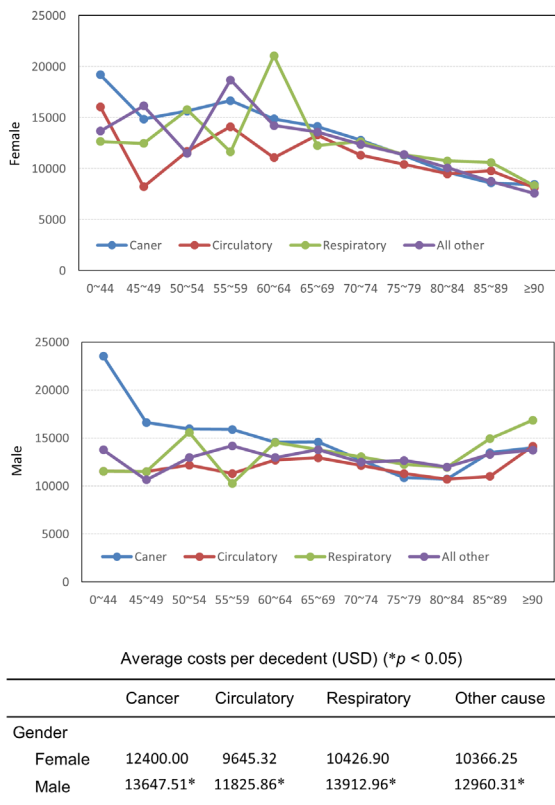


Figure 3. Average hospital costs (in USD) in the last year of life for people who died in 2015, by age and cause of death.

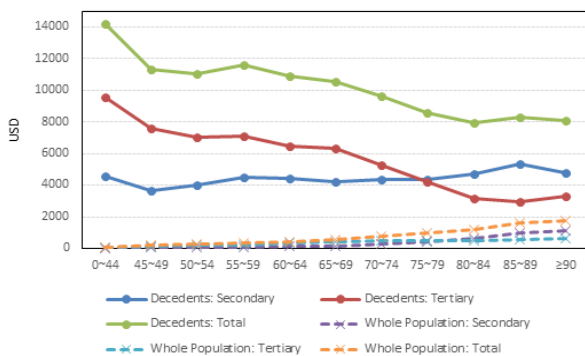
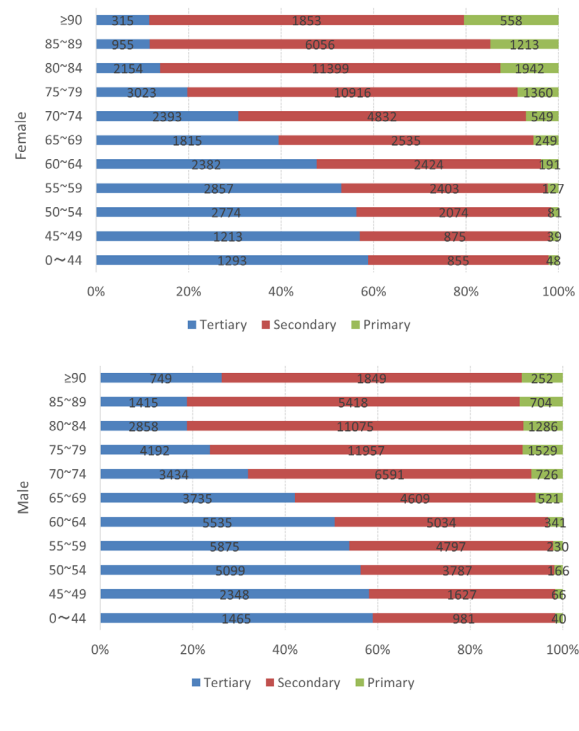


Figure 4. Average hospital costs (in USD) for decedents in their last year of life and the entire population in 2015, by age and level of hospital. Secondary hospitals: mainly provide rehabilitation, nursing, and other less-intensive care, versus Tertiary hospitals: mainly provide more intensive care.

costs for decedents, while for secondary hospitals the age pattern for decedents and the entire population is almost the same. Such a difference reflects, to a certain extent, the different characteristics of care provided at secondary and tertiary hospitals in Shanghai due to variations in the severity of disease. More advanced medical technologies and care are provided at tertiary hospitals while secondary hospitals mainly provide rehabilitation, nursing, and other less-intensive care.

Older terminal patients received a greater proportion of inpatient care at the primary care level, indicating that elderly patients are more likely to go to community health centers for care at the end of their lives. However, according to Shanghai Statistical Yearbook 2016, the limited number of beds at the community care level in Shanghai (17,099 beds, accounting for 14% of the total) may mean that the healthcare needs of terminal patients are not being met. According to Hartman *et al.* (21), an increase in nursing home care has resulted in a decrease in the ratio of costs for people aged 85 or older and the working-age population. In Shanghai, the average hospital costs per decedent in primary care facilities were 30% of the costs in tertiary hospitals (Figure 5). Allocating additional resources to primary care and encouraging patients to be seen



Level	Number of patients (%)	Average costs per patient (USD)
Tertiary	16,439 (28.49)	13754.55*
Secondary	35,192 (60.98)	10178.71*
Primary	6,080 (10.54)	4009.10

(* $p < 0.05$)

Figure 5. Admissions to different levels of medical facilities in the last year of life for people who died in 2015, by age and level of facility.

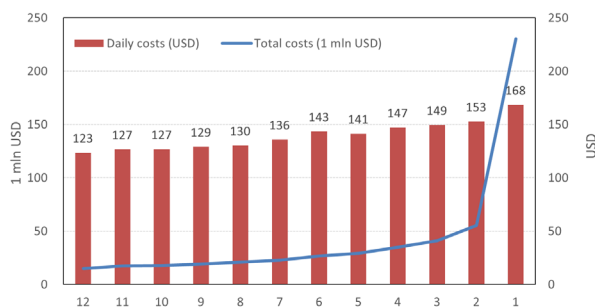


Figure 6. Hospital costs (in million USD) and daily costs (in USD) over the last 12 months of life.

at primary care facilities are key ways to use funds more efficiently, even though the end-of-life care is still predominantly provided by hospitals. Healthcare resources at the level of primary care, and particularly nursing and hospice resources, need to be enhanced in Shanghai so that healthcare needs at the end of life can be met and healthcare costs can be curtailed.

The current study indicated that there were significant sex differences ($t = -15.1244$, $p < 0.05$) in hospital costs in the last year of life (higher in men). This finding differs from results of other studies (5). This is partly due to the absence of sudden death, reflecting a higher incidence rate among males (e.g. death from road accidents or occupational injuries). Another possible explanation is the difference in medical facilities where individuals are seen, and especially the older elderly. Admissions to tertiary hospitals declined with age. Except that among men aged 85, the proportion of admissions to tertiary hospitals started to increase, from 18.77% for individuals aged 85-89 to 26.28% for individuals aged 90 or older (Figure 5). The average hospital costs per patient in tertiary hospitals are higher than those of lower level medical facilities ($p < 0.05$), so the difference in health-seeking behavior in later life might cause a difference in health care expenditures by men and women. The reasons for these differences in health-seeking behavior by men and women need to be further explored. The influence of social attitudes, in combination with the human capital theory, could explain gender differences in end-of-life medical costs. When men suffer from a severe disease, they are more likely to receive intensive and extensive medical care. Hence, more attention needs to be paid to gender equity in the provision of health care.

3.5. PTD

In the current study, over 43% of hospital costs for decedents in the last year of life were incurred during the month before death, and that proportion declined significantly with the distance to death, dropping to 2.78% in the 12th month before death. Lubitz and Rily (11) reported comparable results; in both 1976

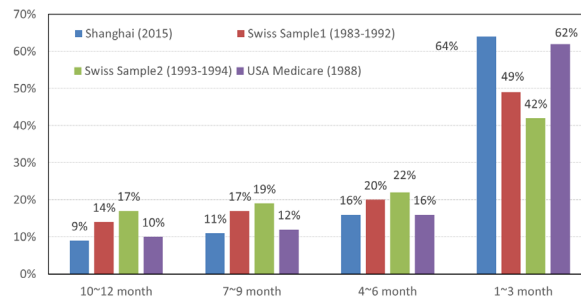


Figure 7. Hospital costs over the last four quarters of life for people aged 65 or older.

and 1988, about 40% of the Medicare costs in the last year of life were incurred in the last 30 days. Upon reflection, the current study indicated that the average daily hospital costs increased gradually with PTD by 36.59% from 123 USD 12 months before death to 168 USD 1 month prior to death (Figure 6). Felder *et al.* (22) found that in OECD countries, medical expenses were mainly spent on diseases at the end of life. Their finding that medical expenses increased abruptly in the last month of life indicated that PTD is a major factor influencing medical expenditures. Seshamani and Gray (23) found that the impact of aging on health care expenditures might be affected by PTD due to the concentration of morbidities and costs in the last year of life. Another study noted higher general practitioner costs closer to death, while finding that costs were not significantly impacted by age (24). Most studies have concluded that age has less of an impact than PTD (2,23,25,26), while one study that controlled for PTD found that population aging was an important factor influencing the increase in medical expenses (27).

Figure 7 shows health care expenditures for people aged 65 or older during the last year of life according to different studies. In the current study, hospital costs incurred in the last quarter of life accounted for 64% of the cumulative hospital costs in the last year of life. In the United States, about 60% of all Medicare payments were incurred in the last quarter of life, and this share has remained unchanged since 1976 (11). In two Swiss samples, the proportion of health care expenditures (based on payments to sick funds) in the last quarter of life amounted to 49% and 42% (6). Medical expenditures in the last 4 quarters of life in Shanghai have a distribution like that of the Medicare figures. The surge in costs near death in the Swiss samples is less marked than in the corresponding data from Shanghai and the US, which may be attributable to the high rate of government subsidization of institutional care in Switzerland. Health care received increases closer to death, so the increase in medical expenses could have been mitigated.

Theoretically, due to the co-existence of a PTD phenomenon and prolonged life expectancy, the decline in age-specific mortality rates over time postpones

death to later ages, pushing back death-related costs. The occurrence of a PTD phenomenon further reveals how aging causes an increase in healthcare spending. The rise in healthcare expenditures is not merely the result of age and health status but is also influenced by other key factors such as end-of-life care and changes in patterns of seeking healthcare. The combined effect of age and population size (caused by longer life expectancy) has resulted in a larger number of people with vast medical needs, challenging the sustainability of the healthcare and financing system.

One limitation of the current study is that subjects were only decedents who died in medical facilities while a large proportion of individuals (over 60%) died at home or somewhere else. This may decrease the generalizability of the current findings.

In conclusion, hospital costs for the entire population appear to increase with age. However, declining costs in the last year of life with increasing age as well as with distance to death demonstrate the existence of a PTD phenomenon in health care expenses. The combined effects of population aging and greater costs closer to death pose a substantial challenge to future projections of health care expenditures. Disease-specific studies should be conducted and attention should be paid to gender equity when examining end-of-life medical costs in the future.

Acknowledgements

This work was supported by the Prosperity Fund of the Foreign & Commonwealth Office of the United Kingdom and by the Fourth Round of Shanghai Three-year Action Plan on Public Health Discipline and Talent Program: Evidence-based Public Health and Health Economics (No. 15GWZK0901). The authors wish to thank the Shanghai Municipal Health and Family Planning Commission Information Center and the Shanghai Municipal Center for Disease Control & Prevention for providing access to data on medical care received and its cost to residents of Shanghai.

References

- National Health and Family Planning Commission. Chinese yearbook of health and family planning 2016. Peking Union Medical College Press, Beijing, China, 2016; 336.
- Mcgrail K, Green B, Barer ML, Evans RG, Hertzman C, Normand C. Age, costs of acute and long-term care and proximity to death: Evidence for 1987-88 and 1994-95 in British Columbia. *Age Ageing*. 2000; 29:249-253.
- Barnato AE, McClellan MB, Kagay CR, Garber AM. Trends in inpatient treatment intensity among Medicare beneficiaries at the end of life. *Health Serv Res*. 2004; 39:363-376.
- Polder JJ, Barendregt JJ, van Oers H. Health care costs in the last year of life – The Dutch experience. *Soc Sci Med*. 2006; 63:1720-1731.
- Blakely T, Atkinson J, Kvizhinadze G, Nghiem N, Mcleod H, Wilson N. Health system costs by sex, age and proximity to death, and implications for estimation of future expenditure. *N Z Med J*. 2014; 127:12-25.
- Zweifel P, Felder S, Meiers M. Ageing of population and health care expenditure: A red herring? *Health Econ*. 1999; 8:485-496.
- Shugarman LR, Campbell DE, Bird CE, Gabel J, A Louis T, Lynn J. Differences in Medicare expenditures during the last 3 years of life. *J Gen Intern Med*. 2004; 19:127-135.
- Gozaolo P, Plotzke M, Mor V, Miller SC, Teno JM. Changes in Medicare costs with the growth of hospice care in nursing homes. *N Engl J Med*. 2015; 372:1823-1831.
- Spillman BC, Lubitz J. The effect of longevity on spending for acute and long-term care. *N Engl J Med*. 2000; 342:1409-1415.
- Wong A, van Baal PH, Boshuizen HC, Polder JJ. Exploring the influence of proximity to death on disease-specific hospital expenditures: A carpaccio of red herrings. *Health Econ*. 2011; 20:379-400.
- Lubitz JD, Rily GF. Trends in Medicare payments in the last year of life. *N Engl J Med*. 1993; 328:1092-1096.
- Madsen J, Serup-Hansen N, Kristiansen IS. Future health care costs – Do health care costs during the last year of life matter? *Health Policy*. 2002; 62:161-172.
- Brockmann H. Why is less money spent on health care for the elderly than for the rest of the population? Health care rationing in German hospitals. *Soc Sci Med*. 2002; 55:593-608.
- Riley G, Lubitz J, Prihoda R, Rabey E. The use and costs of Medicare services by cause of death. *Inquiry*. 1987; 24:233-244.
- Perls TT. Acute care costs of the oldest old. *Hosp Pract (1995)*. 1997; 32:123-124,129-132, 137.
- Mushkin SJ. Health as an investment. *J Polit Econ*. 1962; 70:129-157.
- Becker GS. Human capital revisited. In: *Human Capital: A Theoretical and Empirical Analysis with Special Reference to Education* (3rd edition) (Becker GS, eds.). The University of Chicago Press, Chicago, US, 1993; 15-26.
- Fuchs VR. Some economic aspects of mortality in developed countries. In: *The Economics of Health and Medical Care* (Perlman M, eds.). Palgrave Macmillan, London, UK, 1974; 174-176.
- Schultz TW. Investment in human capital. *Am Econ Rev*. 1961; 51:1-17.
- Grossman M. On the concept of health capital and the demand for health. *J Polit Econ*. 1972; 80:223-255.
- Hartman M, Catlin A, Lassman D, Cylus J, Heffler S. U.S. health spending by age, selected years through 2004. *Health Aff (Millwood)*. 2008; 27:w1-w12.
- Felder S, Meier M, Schmitt H. Health care expenditure in the last months of life. *J Health Econ*. 2000; 19:679-695.
- Seshamani M, Gray A. Time to death and health expenditure: An improved model for the impact of demographic change on health care costs. *Age Ageing*. 2004; 33:556-561.
- O'Neill C, Groom L, Avery AJ, Boot D, Thornhill K. Age and proximity to death as predictors of GP care costs: Results from a study of nursing home patients. *Health Econ*. 2000; 9:733-738.

25. Seshamani M, Gray A. Ageing and health-care expenditure: The red herring argument revisited. *Health Econ.* 2004; 13:303-314.
26. Werblow A, Felder S, Zweifel P. Population ageing and health care expenditure: A school of 'red herrings'? *Health Econ.* 2007; 16:1109-1126.
27. Bjørner TB, Arnberg S. Terminal costs, improved life expectancy and future public health expenditure. *Int J Health Care Finance Econ.* 2012; 12:129-143.

(Received September 30, 2017; Revised January 31, 2018; Accepted February 6, 2018)

Exploring the determinants that influence end-of-life hospital costs of the elderly in Shanghai, China

Fen Li^{1,§}, Bifan Zhu^{1,§}, Zhimin He², Xiaoxi Zhang¹, Changying Wang¹, Linan Wang¹, Peipei Song³, Lingling Ding², Chunlin Jin^{1,*}

¹Shanghai Health Development Research Center, Shanghai, China;

²Xiangya School of Public Health, Central South University, Hunan, China;

³Graduate School of Frontier Sciences, The University of Tokyo, Tokyo, Japan.

Summary

The aim of this study was to use data from the Information Center of the Shanghai Municipal Commission of Health and Family Planning (SMCHFP) to determine the factors affecting end-of-life hospital costs of patients. A total number of 43,806 decedents who died in medical facilities in 2015 were examined. These individuals, accounted for 34.85% of all deaths in 2015 in Shanghai. Descriptive analysis and multiple linear regression analysis were performed using STATA 13.0. Results indicated that 88.94% of the decedents who died in medical facilities were over age 60. Males accounted for 55.57% of decedents, and the insured were mostly covered by Urban Employee Basic Medical Insurance (UEBMI) (81.93%). Cancer and circulatory disease were the main causes of death, causing 34.53% and 26.19% of deaths. Hospital costs were higher for males (male vs. female: 9,013 USD vs. 7,844 USD), individuals insured by UEBMI (8,784 USD), and individuals with cancer (10,156USD). Twenty-nine-point-zero-three percent of admissions occurred in the month before death and accounted for 37.82% of costs. Multiple linear regression analysis indicated that hospital costs were correlated with gender, cause of death (cancer, circulatory disease, or respiratory disease), time-to-death, insurance schemes, level of medical facilities, and length of stay (LOS) ($p < 0.05$ for all). After controlling for other factors, age was not a significant factor ($p > 0.05$). A proximity-to-death (PTD) phenomenon was evident in Shanghai. This study suggested that the PTD should be considered when predicting medical cost. Primary medical care should be enhanced and gaps in insurance coverage should be reduced to improve the efficiency and equity of medical funding. More attention should be paid to the population with a heavier disease burden.

Keywords: Proximity to death, hospital costs, multiple linear regression analysis

1. Introduction

According to population sample surveys conducted by the Bureau of Statistics of Shanghai, 12.32% of residents were over age 65 in 2015; this proportion is projected to rise to 14.81% in 2020 and to 32.97% in 2050 (1). A study has plotted health care costs with respect to age and used age-cost curves to quantify the relationship between age and health care cost (2). Average per capita health

care cost for Americans age 65 and older was more than triple that for a benchmark group (ages 34-44) in 1999 (3). Per capita spending for the elderly was about 5 times higher than spending for children (4). Thus, health policymakers are concerned about how smaller numbers of younger people and increased numbers of elderly will affect health care cost.

Recent studies have argued that approaching death, rather than age, is the demographic driver of health care costs because of a proximity-to-death (PTD) phenomenon. PTD refers to the fact that terminal patients are likely to use more healthcare resources, resulting in higher healthcare expenditures, than survivors use (5-10). The 'terminal' period varies from 1 to 5 years (10-12). According to Zweifel, Felder, and Meiers, the high

[§]These authors contributed equally to this work.

*Address correspondence to:

Dr. Chunlin Jin, Shanghai Health Development Research Center, No. 1477 West Beijing Road, Shanghai 200040, China. E-mail: jinchunlin@shdrc.org

mortality rate of the elderly and tremendous end-of-life medical costs leads to the "inconvenient fact" of PTD, which is that population aging has increased overall medical cost (10). Most studies have concluded that age was less influential than PTD (5,11-13), though a few studies that controlled for time-to-death found that prolonged life expectancy was still a factor influencing the increase in medical cost (14).

Other factors including gender, type of insurance, type of disease, and care received have been examined as predictors of medical cost. Some evidence has shown that males have greater total medical cost per inpatient and a longer length of stay (LOS) (15) since traditional Chinese culture values males over females, but other evidence has shown that women have higher health care cost in general and are closer to death (16). The PTD phenomenon has been noted in most diseases. The cost before death are highest for cancer and lowest for cardiovascular diseases (7,17). A previous study indicated that patients' LOS and inpatient costs varied depending on their health insurance and hospital stay. Uninsured patients had lower cost (18). Place of discharge was associated with hospital costs (12).

Health care cost as a result of population aging are mostly attributable to higher mortality rates in combination with high costs of dying. A better understanding of the costs of dying is crucial to curbing health care costs as a result of population aging (19). However, few studies have examined the determinants of end-of-life medical cost in China due to a lack of data. Thus, the aim of the current study was to investigate whether PTD exists in Shanghai and to identify the factors that influence hospital costs in Shanghai. The findings should help policymakers improve the provision of medical care to the elderly.

2. Subjects and Methods

2.1. Subjects

Data were collected from the Information Center of the Shanghai Municipal Commission of Health and Family Planning and cover all admissions to any medical facility and all age groups in the population of Shanghai. A total of 43,812 decedents died in medical facilities between January 1, 2015 and December 31, 2015. Six decedents were hospitalized for longer than 2 years in a single stay and were excluded as subjects. Hence, a total number of 43,806 decedents served as subjects. These individuals accounted for 34.85% of all deaths in 2015 in Shanghai. The inpatient care received and its cost were tracked for 2 years before death. All records were coded for an individual using an identification number. Other information from medical records included age, gender, type of basic medical insurance, diagnosis, date of admission and discharge, and cost of medical care.

2.2. Dependent variables

The dependent variable was hospital costs of decedents. Hospital costs 2 years prior to death were calculated.

2.3. Independent variables

Demographic indicators: Demographic factors including age and gender were examined as potential determinants of hospital costs.

Cause of death: The cause of death was identified based on the latest record of admission for each decedent. The International Classification of Diseases (ICD-10) was used to classify a decedent's disease.

Time-to-death: The time prior to death was calculated in months. The inpatient care received and its cost were tracked separately 24 months before death.

Related indicators of medical care received: Related indicators of medical care received included the type of insurance scheme, the level of the medical facility, and LOS. Insurance schemes were classified as Urban Employee Basic Medical Insurance (UEBMI), Urban Resident Basic Medical Insurance (URBMI) and New Rural Cooperative Medical Insurance System (NCMS), or other types. 'Other' types of insurance schemes mostly referred to a state medical scheme (covering senior officials) or a supplementary medical insurance scheme, which provides greater reimbursement for the insured. Medical facilities were divided into municipal hospitals (tertiary hospitals), district hospitals (most were secondary hospitals), or primary care facilities (most were community health service centers). LOS was included in the model as a continuous variable.

2.4. Statistical analysis

Multiple linear regression analysis was performed to simulate hospital costs with a set of explanatory variables including age, gender, cause of death, time-to-death, type of insurance scheme, the level of medical facility, and LOS. The least sum of squares method was used to estimate the quantitative relationship between the dependent variable *hospital cost* and explanatory variables. The model is shown below:

$$\ln Y_{\text{exp}} = \beta_0 + \beta_1 A + \beta_2 G + \beta_3 \text{Cau} + \beta_4 \text{TTD} + \beta_5 \text{Ins} + \beta_6 \text{Lev} + \beta_7 \text{Los} + \varepsilon$$

where *A* denotes calendar age in years and *Los* denotes the actual length of stay of inpatients. *G* was a dummy variable for gender (0 if female and 1 if male). *Cau* referred to cause of death (otherwise = 0 as the benchmark) and *Ins* referred to the type of insurance scheme (otherwise = 0 as the benchmark), and the two were included in the model as nominative variables. *Lev* indicated the level of medical facility, which was included as an ordinal variable; a primary care facility

served as the benchmark.

Since hospital costs had a skewed distribution, a logistic conversion was applied. All statistical analysis was performed using STATA 13.0. A significance level of 0.05 was used for hypothesis testing. All Chinese currency figures in this study were adjusted to comparable prices in USD using the average exchange rate in 2015 (6.2284 RMB = 1 USD).

3. Results and Discussion

In this study, 43,806 inpatients were examined, of whom 88.94% were over the age of 60. Males accounted

Table 1. The age, gender, cause of death, TTD, and related indicators of medical care received by decedents in Shanghai, China in 2015 (n = 43,806)

Indicators	Values
Age (Mean ± SD)	77.32 ± 12.81
Gender (n (%))	
Male	24,343 (55.57)
Female	19,463 (44.43)
Cause of death (n (%))	
Cancer	15,128 (34.53)
Circulatory disease	11,472 (26.19)
Respiratory disease	9,829 (22.44)
Gastrointestinal disease	2,162 (4.94)
Other cause	5,215 (11.90)
Insurance Scheme (n (%))	
UEBMI	35,891 (81.93)
URBMI	4,786 (10.93)
NCMS	1,136 (2.59)
Other type	1,993 (4.55)
LOS (Mean ± SD)	95.19 ± 145.73
Hospital costs (Mean ± SD)	13,893.46 ± 19,425.47

LOS, length of stay; NCMS, New Rural Cooperative Medical Insurance System; SD, standard deviation; TTD, time-to-death; UEBMI, Urban Employee Basic Medical Insurance; URBMI, Urban Resident Basic Medical Insurance. Other types of insurance schemes mostly referred to a state medical scheme or a supplementary medical insurance scheme.

for 55.57%, and the insured were mostly covered by UEBMI (81.93%). Cancer (34.53%), circulatory disease (26.19%), respiratory disease (22.44%), and gastrointestinal disease (4.94%) accounted for 88.10% of all causes of death. The average hospital cost per person in the last 2 years was 13,893 USD, and the average LOS was 95 days (Table 1).

As shown in Figure 1, more than half of the admissions (59.73%) during the last 2 years of life were to district hospitals and 33.26% were to municipal hospitals. Thirty-seven-point-two-four percent of hospital costs were incurred in municipal hospitals, 58.76% were incurred in district hospitals, and 4.00% were incurred in primary care facilities. Seven-point-zero-two percent of inpatient care provided at primary care facilities was for terminal elderly patients, compared to 2.60% of the total elderly population when survivors were included. The figures indicated that patients were more likely to visit primary care facilities at the end of their life.

3.1. Hospital costs by population groups

Per capita hospital costs did not increase with age. On the contrary, individuals ages 25-29 had the highest cost (up to 31,941 USD per capita). The interval hospital costs per capita of the elderly age 60 or older were 12,165 USD to 16,380 USD, and the average cost for the elderly were 13,487 USD in the last 2 years of life, as shown in Figure 2. The high average cost for the elderly was probably due to their high mortality rate, though end-of-life care is costly regardless of whether a patient is age 40 or age 70 (11-13). In fact, costs were greater for younger age groups than for older age groups.

One hundred and seventy-four thousand, thirty-one hospital records were examined for 2 years before decedents died. Twenty-nine-point-zero-three percent of admissions occurred in the month before death, and those

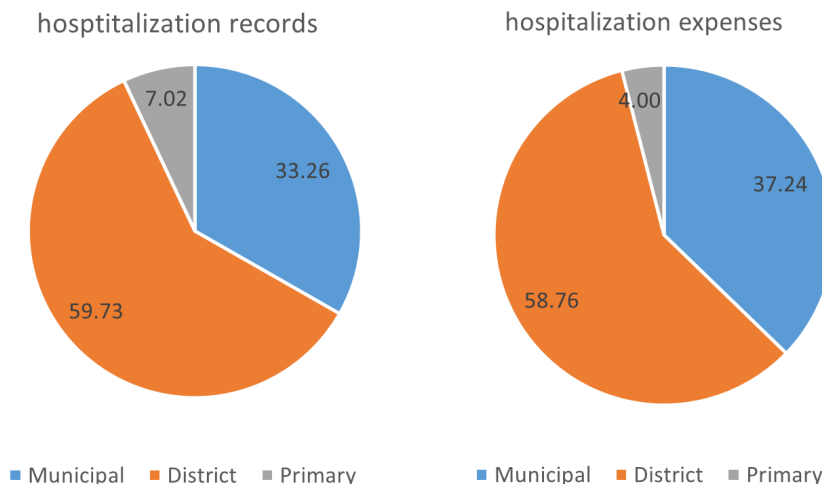


Figure 1. Hospital records and costs during the last 2 years of life in medical facilities in Shanghai, China in 2015.

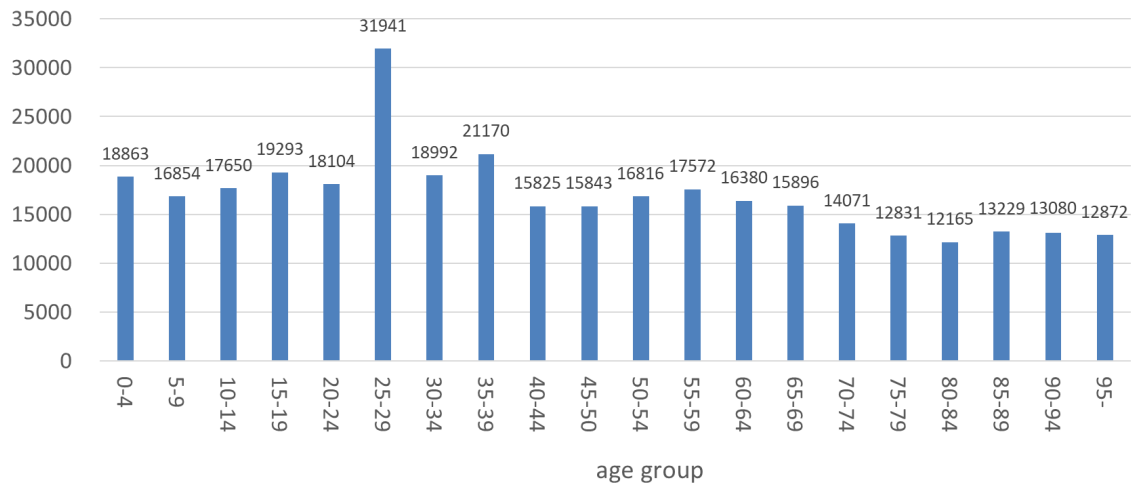


Figure 2. Hospital costs per decedent in the last 2 years of life by age in Shanghai, China in 2015 (USD).

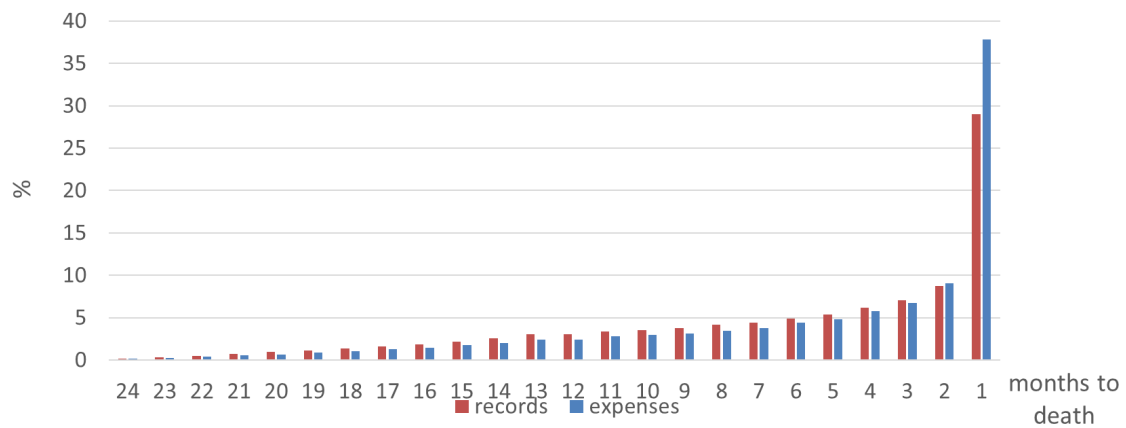


Figure 3. Hospital records and costs in the last 24 months in Shanghai, China in 2015.

Table 2. Hospital records and costs in the last 24 months of life in Shanghai, China in 2015

Months to death	Monthly cost (USD)	Cumulative proportion (%)	Hospital records	Cumulative proportion (%)
1	230,200,255	37.82	50,527	29.03
2	55,215,780	46.90	15,241	37.79
3	40,948,190	53.62	12,257	44.83
4	34,955,633	59.37	10,687	50.97
5	29,322,976	64.19	9,409	56.38
6	26,635,464	68.56	8,544	61.29
7	22,767,909	72.30	7,708	65.72
8	21,075,637	75.77	7,250	69.89
9	19,149,939	78.91	6,583	73.67
10	17,818,905	81.84	6,134	77.19
11	17,269,843	84.68	5,915	80.59
12	14,744,503	87.10	5,359	83.67
13	14,603,365	89.50	5,252	86.69
14	12,284,234	91.52	4,444	89.24
15	10,608,182	93.26	3,783	91.41
16	8,944,79	94.73	3,249	93.28
17	7,769,126	96.01	2,823	94.90
18	6,557,102	97.08	2,339	96.24
19	5,271,144	97.95	1,912	97.34
20	4,155,078	98.63	1,611	98.27
21	3,528,526	99.21	1,248	98.99
22	2,363,562	99.60	850	99.48
23	1,538,910	99.85	570	99.81
24	887,818	100.00	336	100.00

Table 3. Average hospital costs by population groups in Shanghai, China in 2015 (USD)*

Population groups	Mean	P25	P50	P75
Gender (per capita)				
Male	15,075	3,866	9,013	18,282
Female	12,415	3,284	7,844	16,050
Cause of death (per capita)				
Cancer	15,031	4,632	10,156	19,707
Circulatory disease	12,390	3,052	7,478	15,162
Respiratory disease	14,424	3,160	7,592	16,305
Gastrointestinal disease	12,150	3,344	7,642	14,630
Other cause	13,625	3,106	7,925	16,508
Insurance Scheme (per capita)				
UEBMI	13,336	3,836	8,784	17,489
URBMI	9,592	2,572	6,071	12,671
NCMS	5,280	1,241	3,411	6,833
Other type	39,165	6,238	18,053	51,748
Level of the medical facility (per day)				
Municipal hospital	420	169	260	446
District hospital	221	109	168	256
Primary care facility	41	21	32	49

NCMS, New Rural Cooperative Medical Insurance System; UEBMI, Urban Employee Basic Medical Insurance; URBMI, Urban Resident Basic Medical Insurance. Other types of insurance schemes mostly referred to a state medical scheme or a supplementary medical insurance scheme. P25 refers to the first quartile, P50 refers to the median and P75 refers to the third quartile.

*Because of the abnormal distribution of hospital costs, P50 was used to reflect average hospital costs.

Table 4. Results of multiple regression analysis of the determinants of hospital costs in Shanghai, China in 2015

Indicators	β	95% Wald CI	<i>p</i> value
Age	0.0007	(-0.0000-0.0014)	0.055
Gender (Female vs. Male)	0.0320	(0.0176-0.0470)	0.000
Cause of death			
Cancer (Cancer vs. other causes)	-0.9010	(-0.1167--0.634)	0.000
Circulatory disease (Circulatory vs. other causes)	0.0326	(0.0046-0.0606)	0.023
Respiratory disease (Respiratory vs. other causes)	0.0730	(0.0445-0.1014)	0.000
Gastrointestinal disease (Gastrointestinal vs. other causes)	0.0066	(-0.0346-0.0478)	0.753
Time-to-Death	-0.0183	(-0.194--0.0172)	0.000
Insurance schemes			
UEBMI (UEBMI vs. NCMS)	0.3116	(0.2604-0.3630)	0.000
URBMI (URBMI vs. NCMS)	0.2612	(0.2075-0.3149)	0.000
Other (Other vs. NCMS)	0.7536	(0.6922-0.8152)	0.000
Level of the medical facility			
Municipal (Municipal hospital vs. Primary care facility)	1.2956	(1.2641-1.3272)	0.000
District (District hospital vs. Primary care facility)	1.1707	(1.1409-1.2004)	0.000
LOS	0.0100	(0.0097-0.1025)	0.000

LOS, length of stay; NCMS, New Rural Cooperative Medical Insurance System; UEBMI, Urban Employee Basic Medical Insurance; URBMI, Urban Resident Basic Medical Insurance.

stays accounted for 37.82% of cost. In cumulative terms, 44.83% of records and 53.62% of cost were from the last 3 months before death, as shown in Figure 3 and Table 2. Inpatient care and hospital costs abruptly increase closer to death.

Average hospital costs by population groups are shown in Table 3. Total hospital costs for males were 9,013 USD, which were higher than those for females (7,844 USD) in the last 2 years of life. This finding is consistent with the results of related domestic studies (15,20,21). More attention needs to be paid to gender equity in health. Patients with cancer incurred the most costs (10,156 USD) while patients with respiratory diseases incurred the least (7,592 USD). Compared to other types of insurance schemes, NCMS provided the least reimbursement. The mean hospital costs were 3,411

USD for patients insured by NCMS, and those costs were lower than costs incurred by patients insured by some other type of insurance (18,053 USD), UEBMI (8,784 USD), or URBMI (6,071 USD). In Shanghai, the 4 types of insurance schemes varied widely in terms of their financing and reimbursement. Patients insured by supplementary insurance had the highest medical coverage, followed by those insured by UEBMI and NCMS (22). Municipal hospitals were 0.55 times more costly than district hospitals and 7.13 times more costly than primary care facilities, which means that a stay in a primary care facility costs much less than a stay in a hospital.

3.2. Regression models

The regression model was statistically significant ($F = 865.35$, $p < 0.05$), and the estimated coefficients (*i.e.*, the variance explained by those variables) of the explanatory variables indicated that 22.82% of the variance in hospital costs could be explained by gender ($\beta = 0.0320$, $p < 0.05$), cause of death (Cancer *vs.* other cause, $\beta = -0.9010$; Circulatory *vs.* other cause, $\beta = 0.0326$; Respiratory *vs.* other cause, $\beta = 0.0730$, $p < 0.05$ for all), time-to-death ($\beta = -0.0183$, $p < 0.05$), type of insurance scheme (UEBMI *vs.* NCMS, $\beta = 0.3116$; URBMI *vs.* NCMS, $\beta = 0.2612$; Other type *vs.* NCMS, $\beta = 0.7536$, $p < 0.05$ for all), the level of medical facility (Municipal hospital *vs.* Primary care facility, $\beta = 1.2956$; District hospital *vs.* Primary care facility, $\beta = 1.1707$, $p < 0.05$ for both), and LOS ($\beta = 0.0100$, $p < 0.05$), as shown in Table 4.

After controlling for other factors, regression analysis indicated that age was not significantly associated with hospital costs. The current study noted a PTD phenomenon since time-to-death was a significant factor influencing end-of-life hospital costs. For each individual, per capita hospitalization is not necessarily affected by the aging of the population due to an increase in life expectancy. Rather, the increased proportion of the elderly population resulted in more admissions of older individuals, leaving per capita cost unchanged (10). Rolden, van Bodegom, and Westendorp created an economic model of hospital cost based on patients' age and time-to-death to predict hospital expenditures from 2002 to 2026 in England, and their results indicated that the predicted annual increase was half of the rate predicted with a traditional method (19), indicating that a more accurate projection model should consider the concentration of cost towards the end of life (23). At the population level, the increase in life expectancy suggests a larger elderly population, which poses a great challenge to healthcare financing. In order to ensure the sustainability of healthcare financing, excessive medical cost at the end of life should be rationally curtailed.

The type of medical insurance is an important factor that affects the medical care received and its cost (24-28). Patients who had supplementary hospital insurance incurred significantly higher healthcare expenditures in Switzerland (10,13,18). The current results indicated that insurance schemes significantly influence the end-of-life hospital costs. Individuals insured by NCMS had a significantly lower median rate of admission compared to individuals insured by other types of insurance. The difference in end-of-life hospitalization among types of insurance suggests that individuals with better coverage might receive far more care than individuals with poorer coverage.

Regression analysis indicated that higher levels of medical facilities were most costly. Improving the resources of primary care facilities is one way to meet the needs of terminal patients and to curtail total medical cost. However, the limited number of beds at primary

care facilities (17, 099 beds, accounting for 13.92% of total beds) (29) and prolonged LOS mean that admission to a primary care facility is unlikely.

Patients with cancer incurred the greatest costs and patients with gastrointestinal diseases incurred the least. The increased cost of cancer treatment has placed a heavy burden on patients and families (30). Cancer was the leading cause of death in Shanghai, so the government needs to pay special attention to avoiding financial risks and clinicians need to perform a cost-effectiveness analysis.

The current study had several limitations. It only included decedents who died in medical facilities while a large proportion of individuals who died (over 60%) at home or somewhere else. This may have limited the generalizability of the current findings.

In conclusion, this study found that PTD exists in Shanghai since time-to-death was a significant factor for end-of-life hospital costs. In addition, hospital costs were correlated with gender, cause of death (cancer, circulatory disease, or respiratory disease), time-to-death, insurance scheme, the level of medical facility, and LOS ($p < 0.05$, for all). When the aforementioned factors were controlled for, age was not related to end-of-life cost. This study has suggested that PTD should be considered when predicting medical cost to make the model more accurate. Primary medical care should be enhanced and gaps in insurance coverage should be reduced to improve the efficiency and equity of medical funding. More attention should be paid to the population with a heavier disease burden.

Acknowledgements

This work was supported by a grant from the *Foreign and Commonwealth Office (UK) Prosperity Fund* and the Fourth Round of Shanghai Three-year Action Plan on Public Health Discipline and Talent Program: *Evidence-based Public Health and Health Economics (No. 15GWZK0901)*. The authors wish to thank the Shanghai Municipal Health and Family Planning Commission Information Center and the Shanghai Center for Disease Control and Prevention Center for providing data on the receiving of medical care and the costs of that care for residents of Shanghai.

References

1. Wang Z, Zhou HW, Chen GZ, Gao H. A study on stances and steps to control the size and composition of Shanghai's population. *Journal of Social Sciences*. 2014; 2:56-65.
2. Seshamani M, Gray A. The impact of ageing on expenditures in the National Health Service. *Age Ageing*. 2002; 31:287-294.
3. Reinhardt UE. Does the aging of the population really drive the demand for health care? *Health Aff (Millwood)*. 2003; 22:27-39.
4. Lassman D, Hartman M, Washington B, Andrews K,

- Catlin A. US health spending trends by age and gender: Selected years 2002-10. *Health Aff (Millwood)*. 2014; 33:815-822.
5. Mcgrail K, Green B, Barer ML, Evans RG, Hertzman C, Normand C. Age, costs of acute and long-term care and proximity to death: Evidence for 1987-88 and 1994-95 in British Columbia. *Age Ageing*. 2000; 29:249-253.
 6. Barnato AE, McClellan MB, Kagay CR, Garber AM. Trends in inpatient treatment intensity among Medicare beneficiaries at the end of life. *Health Serv Res*. 2004; 39:363-375.
 7. Polder JJ, Barendregt JJ, van Oers H. Health care costs in the last year of life--the Dutch experience. *Soc Sci Med*. 2006; 63:1720-1731.
 8. Blakely T, Atkinson J, Kvizhinadze G, Nghiem N, McLeod H, Wilson N. Health system costs by sex, age and proximity to death, and implications for estimation of future expenditure. *N Z Med J*. 2014; 127:12-25.
 9. Seshamani M, Gray AM. A longitudinal study of the effects of age and time to death on hospital costs. *J Health Econ*. 2004; 23:217-235.
 10. Zweifel P, Felder S, Meiers M. Ageing of population and health care expenditure: A red herring? *Health Econ*. 1999; 8:485-496.
 11. Wong A, van Baal PH, Boshuizen HC, Polder JJ. Exploring the influence of proximity to death on disease-specific hospital expenditures: A carpaccio of red herrings. *Health Econ*. 2011; 20:379-400.
 12. Seshamani M, Gray A. Ageing and healthcare expenditure: The red herring argument revisited. *Health Econ*. 2004; 13:303-314.
 13. Werblow A, Felder S, Zweifel P. Population ageing and health care expenditure: A school of 'red herrings'? *Health Econ*. 2007; 16:1109-1126.
 14. Bjørner TB, Arnberg S. Terminal costs, improved life expectancy and future public health expenditure. *Int J Health Care Finance Econ*. 2012; 12:129-143.
 15. Yan S, Ying B. Gender differences in the use of health care in China: Cross-sectional analysis. *Int J Equity Health*. 2014; 13:8.
 16. Forma L, Rissanen P, Aaltonen M, Raitanen J, Jylhä M. Age and closeness of death as determinants of health and social care utilization: A case-control study. *Eur J Public Health*. 2009; 19:313-318.
 17. Lubitz J, Cai L, Kramarow E, Lentzner H. Health, life expectancy, and health care spending among the elderly. *N Engl J Med*. 2003; 349:1048-1055.
 18. Bradley CJ, Dahman B, Bear HD. Insurance and inpatient care: Differences in length of stay and costs between surgically treated cancer patients. *Cancer*. 2012; 118:5084-5091.
 19. Rolden HJ, van Bodegom D, Westendorp RG. Variation in the costs of dying and the role of different health services, socio-demographic characteristics, and preceding health care expenses. *Soc Sci Med*. 2014; 120:110-117.
 20. Hu SY, Nan SX. An analysis of health disparities between urban and rural elderly residents--Based on an analysis of 2011 baseline data from CHARLS. *Scientific Research on Aging*. 2016; 1:74-80. (in Chinese)
 21. Xu J. Gender differences of the elderly health in China and its decomposition. *Journal of Northwest Normal University (Social Sciences)*, 2015; 1:139-144. (in Chinese)
 22. Zhang XX, Li F, Wang CY, Lin J, Cai DQ, Wang X. A study on the Medical Assistance System in Shanghai in 2015. *Chinese Health Economics*. 2017; 36:24-28. (in Chinese)
 23. Wei N, Zhou LL. Aging and medical expenditures: Based on an analysis of the effects of 'dying'. *Chinese Health Economics*. 2016; 35:51-53. (in Chinese)
 24. Li YY, Yang F, Chen MS, Qian DF. A study of factors influencing rural residents' desire to receive medical care and other changes in Jiangsu before and after the new healthcare reform. *Chinese Health Service Management*. 2016; 338:605-608. (in Chinese)
 25. Wang CP, Zhang T, Li JJ, Xu LZ. Current state of and factors influencing the use of health services by the elderly in Shandong Province. *Chinese J Gerontology*. 2016; 4: 949-951. (in Chinese)
 26. Gao H, Sun H, Wu QH, Hao YH, Li Y, He JW, Zhu HH, Li X. Analysis of factors influencing the use of medical services by the elderly population in Heilongjiang Province in 2013. *Chinese Health Resources*, 2016; 6:503-506. (in Chinese)
 27. Lu RY, Gao JM, Xu YJ, Li YP, Zheng ZJ. Status and decomposition of health equity among the elderly in Fujian Province. *Chinese J Public Health*. 2016; 9:1159-1163. (in Chinese)
 28. Chen PR, Wu L, Zhu LS. Analysis of the utilization of health care and their influencing factors among the elderly: Based on CHARLS Data. *Chinese J Social Med*, 2015; 2:153-155. (in Chinese)
 29. Shanghai Municipal Statistics Bureau. *Shanghai Statistical Yearbook 2016*. China Statistics Press, Beijing, China, 2016. (in Chinese)
 30. Haga K, Matsumoto K, Kitazawa T, Seto K, Fujita S, Hasegawa T. Cost of illness of the stomach cancer in Japan - A time trend and future projections. *BMC Health Serv Res*. 2013; 13:283.

(Received September 30, 2017; Revised January 30, 2018; Accepted February 5, 2018)

The response of common marmoset immunity against cedar pollen extract

Yoshie Kametani^{1,*}, Yuko Yamada^{1,2}, Shuji Takabayashi³, Hideki Kato³, Kenji Ishiwata⁴, Naohiro Watanabe⁴, Erika Sasaki², Sonoko Habu⁵

¹Department of Molecular Life Science, Tokai University School of Medicine, Kanagawa, Japan;

²Central Institute for Experimental Animals, Kanagawa, Japan;

³Hamamatsu University School of Medicine, Shizuoka, Japan;

⁴Department of Tropical Medicine, Jikei University School of Medicine, Tokyo, Japan;

⁵Department of Immunology, Juntendo University School of Medicine, Tokyo, Japan.

Summary

The *in vivo* model of pollinosis has been established using rodents, but the model cannot completely mimic human pollinosis. We used *Callithrix jacchus*, the common marmoset (CM), to establish a pollinosis animal model using intranasal weekly administration of cedar pollen extract with cholera toxin adjuvant. Some of the treated CMs exhibited the symptoms of snitching, excess nasal mucus and/or sneezing, but the period was very short, and the symptoms disappeared after several weeks. The CD4+CD25+ cell ratio in the peripheral blood increased in CMs quickly after the nasal administration of cedar pollen extract, but the timing was not parallel with the symptoms. IL-10 mRNA was enhanced in the peripheral blood mononuclear cells (PBMCs), suggesting CM-induced tolerance for cedar pollen administration. Similarly, Foxp3 mRNA was also detected in the PBMC. Additive sensitization of these CMs with *Ascaris* egg administration did not enhance chronic inflammation of type 1 allergy to induce the symptoms. These results suggest that the environmental immune cells develop transient allergic symptoms and subsequent immune-tolerance in the intranasally sensitized CMs.

Keywords: Pollinosis model, tolerance, cytokine, Treg

1. Introduction

The cause of immune-related diseases such as allergy and autoimmune disease is widely accepted as the rupture of the valance among the effector T cells and suppressive T cells, including regulatory T cells (Treg) at an individual level (1). However, the trigger has not been clarified yet. To investigate the relationship of the cytokine valance and the onset of such allergy/autoimmune disease, good *in vivo* models mimicking human symptoms are needed. The model animal needs

to possess a very similar immune system to that of humans, including the ratio of T cell subsets in the body, the T cell differentiation pathway, the capacity for cytokine production and other effector functions.

Rodents and primates are evolutionarily distant and the difference of immune-related genes between these groups have already been reported (2). There are some allergy models that use rodents, but they do not completely mimic human allergy symptoms (3). On the other hand, non-human primates (NHPs) occasionally develop spontaneous allergies such as pollinosis, but most NHPs do not develop such allergic symptoms (4).

The reason is not clear, but Jeong *et al.* analyzed the expression of interferon (IFN)- γ , a Th1 cytokine, and interleukin (IL)-4, a Th2 cytokine and both receptors in old world monkeys and human peripheral blood mononuclear cells (PBMCs) (5). They found the expression of IFN- γ was lower in the human compared to the apes while the expression of IL-4 was significantly higher than in the apes. The cytokine

Released online in J-STAGE as advance publication January 15, 2018.

*Address correspondence to:

Dr. Yoshie Kametani, Department of Molecular Life Science, Tokai University School of Medicine, 143 Shimokasuya, Isehara, Kanagawa 259-1193, Japan.

E-mail: y-kametn@is.icc.u-tokai.ac.jp

receptors were expressed similarly. The results clarified that human beings possess a more Th2-dominant cytokine environment compared to NHPs (5). The reason why human immunity is Th2 dominant is not clear, but if the Th2-dominant immunity creates a tendency for allergy-development in humans, NHPs might not be a good model animal to induce a type-1 allergy similar to that in humans. However, Iwashita *et al.* used some parasitic worms to infect the old world monkeys and succeeded in developing allergy model animals (6). The result suggests it may be possible to use NHPs as human allergy model animals. On the other hand, the tolerance is frequently induced and the onset of allergy is suppressed. How the onset of allergy is induced or suppressed is not clarified.

Callithrix jacchus (common marmoset; CM) is a new world monkey (7), for which genome sequence analysis and transgenic animals have been established (8,9). We reported that CM possesses CD4T cells, CD8T cells and B cells in the similar ratio in PBMC and the T cells express CD25 and various cytokines after the activation, similarly to the cells of mouse and human (8). This evidence indicates that the CM is useful as a model to analyze human immune disease. In fact, the CM has been used to establish an experimental autoimmune encephalomyelitis (EAE) model animal and multiple sclerosis (MS) model animal, and recently an animal model of neuronal diseases (10-12). For the allergy, no detailed research has been reported, but we developed a CM-specific anti-CD117 monoclonal antibody and identified CD117+ mast cells of CM that play key roles in allergy and anaphylaxis (13). Moreover, by transplanting CM hematopoietic stem cells into severely immunodeficient NOG mice (14), we succeeded in developing mast cells *in vitro* and *in vivo*. These results suggested that the induction of type I allergy in CMs was possible, although the CM cytokine profile showed that they also possessed a Th1-shifted cytokine environment similar to other NHPs (15).

In this study, we tried to develop pollinosis with chronic inflammation in CMs by intranasally sensitizing them to cedar pollen extract and infecting them with parasitic worms.

2. Materials and Methods

2.1. Animals

Common marmosets (CMs) were obtained from CLEA Japan, Inc. (Tokyo, Japan) and maintained in specific pathogen-free conditions at the Central Institute for Experimental Animals (CIEA, Kawasaki, Japan) or Hamamatsu Medical University during the experiments. CMs were housed in single cages 39 cm (W) × 55 (D) × 70 (H) in size on 12:12 h light/dark cycles. Room temperature and humidity were maintained at 26-27°C and 40-50%, respectively. Experiments using

CMs were approved by the Institutional Committee for Animal Care and Use and performed at CIEA and Hamamatsu Medical University according to the institutional guidelines. CM age was 1 year, and sexes were arbitrary.

2.2. Sensitization of the CM

In total, 35 healthy CMs (1 year old) were enrolled for the whole experiment (Table 1). Four groups (Group 1 to Group 4) were used for the intranasal administration of cedar pollen extract (100 µg/head) (Cosmo Bio, Tokyo, Japan) with cholera toxin (5 µg/head) (List Biological Labs. Inc., CA, USA) every 7 days. Details are shown in Figure 1A. Before the first intranasal administration, in Group 3 CMs, cedar pollen extract (100 µg/head) was immunized intraperitoneally with alum adjuvant (5 mg/head Thermo Fisher Scientific, Inc., MA, USA) and human recombinant interleukin 4 (1 mg/head, Chemicon International, Inc., CA, USA). The administration was continued for 70 weeks. After an interval of 6 months, Group 1 and Group 3 CMs were submitted for an additional treatment of oral *Ascaris* infection (3,000 or 6,000 embryonated eggs/head). After 3 weeks, oral administration of Combantrin (100 mg/10 mL water, 3 mL/head, serially for 2 days) (Teika Pharmaceutical Inc., Toyama, Japan) was performed and the *Ascaris* were aborted. After the treatment, the same intranasal administration protocol was conducted in Group 1 (Group 1-2) and Group 3 (Group 3-2). The same protocol was used for the Group 5 CMs, which were all non-treated individuals. Blood was collected from the femoral vein of the CMs using fixator.

2.3. Flow cytometry

CM PBMCs (500 µL/head) were collected into a heparinized tube and centrifuged on Lymphocept (IBL Co. Takasaki, Japan) at 670 × g for 30 min. Mononuclear cells were collected, and the remaining erythrocytes were lysed with low osmotic buffer (20 mM Tris-HCl, pH 7.4, 0.15 M NH₄Cl). After the lysis of remaining erythrocytes, they were suspended in RPMI1640 medium (Nissui, Tokyo, Japan) containing 10% (v/v) heat-inactivated fetal calf serum (FCS; SAFC Biosciences, Tokyo, Japan). These cells were incubated with appropriately diluted, fluorescence-labeled primary mAb for 15 min at 4°C and washed with 1% (w/v) bovine serum albumin (BSA)-containing phosphate-buffered saline (PBS). In some cases, cells were re-incubated with labeled secondary antibody. The mAbs used were as follows: anti-human CD3-Peridinin chlorophyll protein-cyanine5.5 (PerCPCy5.5) (SP34-2), streptavidin-PE and allophycocyanin (APC)-labeled streptavidin were purchased from BD Biosciences (NJ, USA). Anti-CM CD4 and anti-CM CD25 monoclonal antibodies were prepared previously (8). Cells were

incubated with appropriately diluted, fluorescence-labeled primary mAb for 15 min at 4°C and washed with 1% (w/v) BSA-containing PBS. In some cases, the cells were re-incubated with a labeled secondary antibody for 15 min at 4°C and washed in the same buffer mentioned above. Stained cells were analyzed on FACSCalibur (BD Biosciences) and CellQuest software (CellQuest, FL, USA)

2.4. Semi-quantitative RT-PCR

RNA was extracted from cells by using RNeasy Mini Kit (Qiagen, Germantown, MD, USA). RNA (50 ng) was reverse-transcribed, and generated cDNA was amplified using primers and OneStep RT-PCR kit (Qiagen). Reverse transcription was at 50°C for 30 min, polymerase activation at 95°C for 15 min with 33 cycles of PCR, each cycle consisted of denaturation at 94°C for 1 min, annealing at 60°C for 1 min, and extension at 72°C for 1 min. PCR products were

subjected to agarose gel electrophoresis. The primers used are summarized in Table 2.

3. Results and Discussion

At first, we made a CM group, to which we administered cedar pollen extract mixed with cholera toxin as an adjuvant every week in a long period. Cholera toxin was used because it has been considered a strong T helper type 2-skewing adjuvant (16) and reported to promotes a balanced Th1/Th2/Th17 response previously (17). The protocol is shown in Figure 1A in detail. The blood was collected sequentially and checked to see if the treatment induced an immune reaction. PBMCs were prepared in order to analyze the kinetics of activated helper T (Th) cells. We monitored an activation marker of the IL-2 receptor, CD25, whose expression is known to increase early after T cell activation. As a result, shortly after the nasal administration, the CD4+CD25+ activated/regulatory

Table 1. List of common marmosets used for sensitization with cedar pollen extract

Groups	CM No.	Treatment	First symptom (wk)	Sneeze	Other symptoms	Total symptoms	Ascaris No.	Institute
Group 1	635M	Cedar pollen / Cholera toxin i.n.	(-)	×	×	0		CIEA
	2932M		(-)	×	×	0		CIEA
	2933M		(-)	×	×	0		CIEA
Group 2	I2923	Cedar pollen / Cholera toxin i.n.	28th	×	○	6		CIEA
	I2925		28th	×	○	6		CIEA
	I2908		26th	×	○	15		CIEA
Group 3	I2912	Cedar pollen i.p./Cedar pollen-Cholera toxin i.n.	(-)	×	×	0		CIEA
	I2934		(-)	×	×	0	3000 (CIEA)	CIEA
	I2904		(-)	×	×	0	3000 (CIEA)	CIEA
Group1-2	635M	Ascaris/Cedar pollen / Cholera toxin i.n.	14th	×	○	5	6000 (CIEA)	Hamamatsu
	2932M		15th	×	○	4	6000 (CIEA)	Hamamatsu
	2933M		16th	×	○	7	6000 (CIEA)	Hamamatsu
Group3-2	I2912	Ascaris/Cedar pollen i.p./Cedar pollen-Cholera toxin i.n.	(-)	×	×	0	6000 (CIEA)	Hamamatsu
	I2934		(-)	×	×	0		Hamamatsu
	I2904		(-)	×	×	0		Hamamatsu
Group 4	I3286	Cedar pollen / Cholera toxin i.n.	4th	×	○	5		Hamamatsu
	I3288		3rd	○	○	16		Hamamatsu
	I3299		2nd	○	○	15		Hamamatsu
	I3300		2nd	○	○	13		Hamamatsu
	I3295		1st	×	○	4		Hamamatsu
	I3103		6th	○	○	7		Hamamatsu
	I3102		2th	○	○	30		Hamamatsu
	I3220a		(-)	×	×	2		Hamamatsu
	S158		6th	○	○	12		Hamamatsu
	I3105		1st	○	○	13		Hamamatsu
	I3101		13th	○	○	12	6000 (Hamamatsu)	Hamamatsu
Group 5	I3106	Ascaris/Cedar pollen i.p./Cedar pollen-Cholera toxin i,n	(-)	×	×	0	6000 (Hamamatsu)	Hamamatsu
	I3268		4th	○	○	11	6000 (Hamamatsu)	Hamamatsu
	I3271		1st	○	○	34	6000 (Hamamatsu)	Hamamatsu
	I3274		31th	○	○	5	6000 (Hamamatsu)	Hamamatsu
	I3284		0	×	×	0	6000 (Hamamatsu)	Hamamatsu
	X012		15th	×	○	1		Hamamatsu
Control	X013	No treatment	1st	○	○	20		Hamamatsu
	I3276		(-)	×	×	0		Hamamatsu
	S152		(-)	×	×	0		Hamamatsu

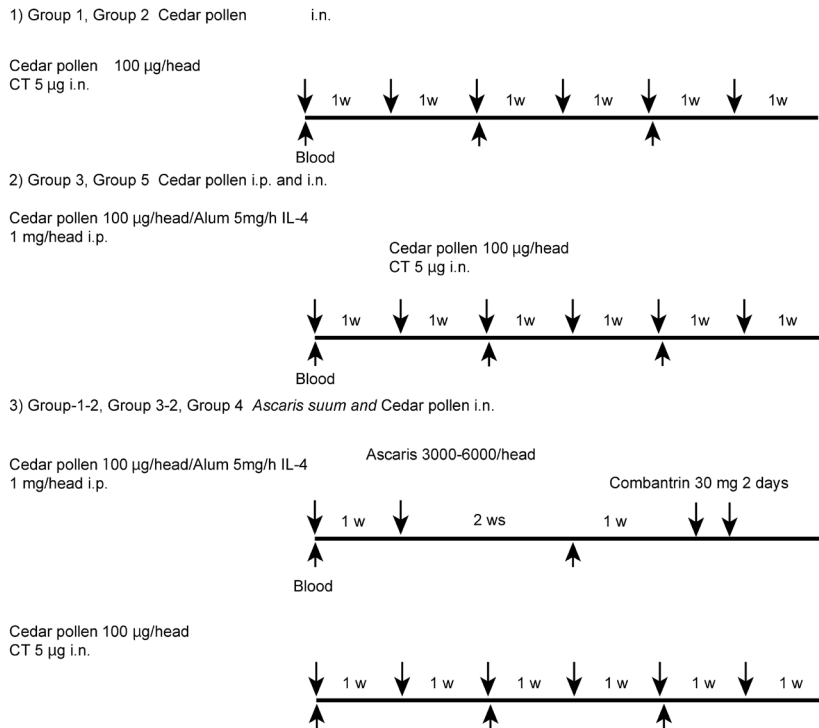
The first symptom (wk): the week that the symptom appeared for the first time; Other symptoms: other symptoms include nasal mucus and sneezing; Total symptoms: the total number of days that the symptoms were observed following treatment; Ascaris No.: the number of Ascaris inoculated in the CM; Institute: the institute in which the CMs were housed; Filled cell: the high-responder < 20 total symptoms.

Table 2. Primers for RT-PCR

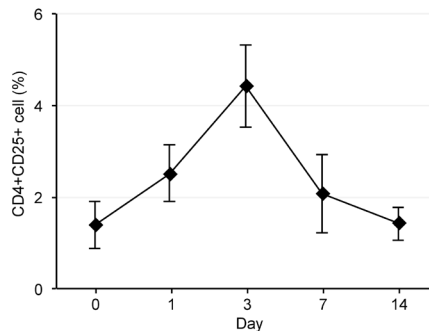
Genes	Forward strand primer	Reverse strand primer
IL-2	5'-ATGTACAGCATGCAGCTCGC-3'	5'-GCTTTGACAGAAGGCTATCC-3'
IL-4	5'-TGCCACGGACACAAGTGCGA-3'	5'-CATGATCGTCTTTAGCCTTTCC-3'
IL-5	5'-GCCAAAGGCAAACGCAGAACGTTTCAGAGC-3'	5'-AATCTTTGGCTGCAACAAACCAGTTTAGTC-3'
IL-6	5'-ATGAACTCCTTCTCCACAAGCGC-3'	5'-GAAGAGCCCTCAGGCTGGACTG-3'
IL-10	5'-GGTTACTGGGTTGCCAAGCCT-3'	5'-CTTCTATGTAGTTGATGAAGATGTC-3'
IL-17A	5'-CTCCTGGGAAGACCTCATTG-3'	5'-CAGACGGATATCTCTCAGGG-3'
IL-17F	5'-CAAAGCAAGCATCCAGCGCA-3'	5'-CATTGGGCTGTACAACCTCTG-3'
IFN- γ	5'-CTGTTACTGCCAGGACCCAT-3'	5'-CGTCTGACTCCTTCTCGCTT-3'
TNF- α	5'-GAGTGACAAGCCTGTAGCCCATGTTGTAGCA-3'	5'-GCAATGATCCCAAAGTAGACCTGCCAGACT-3'
Foxp3	5'-GAAAATGGCAGTGCCCAAGGG-3'	5'-GTCCATGTTGTGGAGGAACT-3'
HPRT	5'-CCACTTAGAACGTTCTCCAG-3'	5'-GCTCTACTAAGCAGATGGC-3'
β -actin	5'-TCTCCCAAGTTAGGTTTTGTC-3'	5'-ATCATGTTTGAGACCTTCAACAC-3'

Genes: the CM genes according to which the primer was designed. Abbreviations: IL-2, interleukin-2; IL-4, interleukin-4; IL-5, interleukin-5; IL-6, interleukin-6; IL-10, interleukin-10; IL-17A, interleukin-17A; IL-17F, interleukin-17F; IFN- γ , interferon- γ ; TNF- α , tumor necrosis factor- α ; HPRT, hypoxanthine-guanine phosphoribosyltransferase.

a



b



c



Figure 1. Immune reaction of CMs with the sensitization with cedar pollen extract. (a). Protocol for Group 1 to Group 5 CM sensitization. Serial blood collection was optional. **(b).** Kinetics of CD4+CD25+ T cell subset in the PBMC after cedar pollen administration (representative data of Group 1 and 2 CMs). **(c).** Group 2 I2908 after the 26th treatment. Immediately after administration, the CMs began to sneeze and nasal mucus was observed.

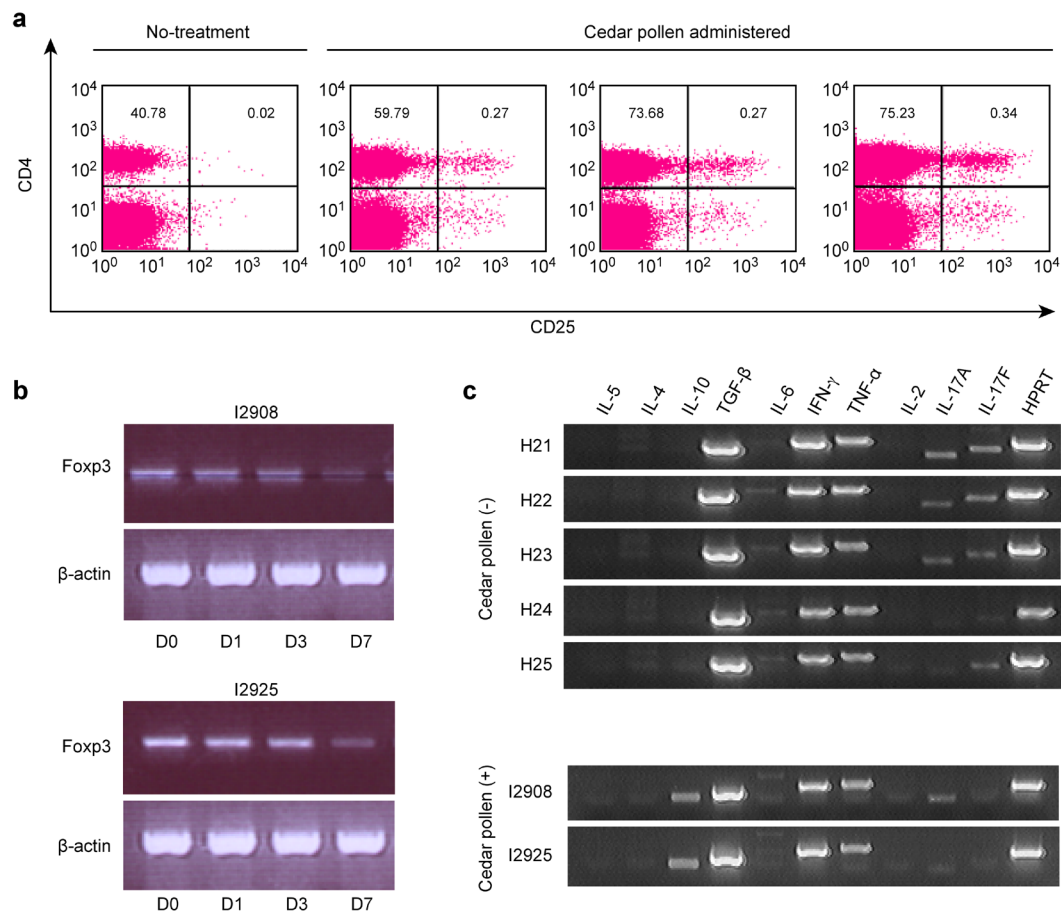


Figure 2. Immune suppression of CM after repeated sensitization with cedar pollen extract. (a). CD4+CD25+ T cell analysis of CM PBMC. Upper panels: CM without the treatment (S152); lower panels: CMs sensitized with cedar pollen extract for 6 weeks (with symptoms). The percentages of CD4+CD25- single positive Th cells (upper left) and CD4+CD25+ double positive Th cell/Treg cells (upper right) in the CD3+ T cell gate (data not shown) was shown in each panel. **(b).** RT-PCR for CM Foxp3 in the sera of the PBMC of two CMs (I2908 and I2925 after the 6th treatment). β -Actin was used for the positive control. D0-D7 means day 0 to day 7 after the treatment. **C.** RT-PCR for CM cytokines of non-treated CM PBMCs (upper panels; H21-H25, not enrolled CMs) and treated (lower panels; I2908 and I2925 with symptoms) PBMC mRNAs. HPRT was used for the positive control.

T cell ratio was increased. The ratio was highest at day 3 and gradually decreased (Figure 1B) suggesting the CD4+ cells were activated and expressed IL-2 receptor by the treatment. As the immune reaction could be induced in these CMs, we continued the administration and checked if pollinosis-like symptoms were observed. For Group 3 CMs, intraperitoneal administration of cedar pollen extract was performed before the nasal administration in order to activate systemic immune response against cedar pollen antigens. As shown in Table 1, among these three groups, only the three CMs in Group 2 developed symptoms similar to pollinosis after 26-28 weeks, including sneezing and nasal mucus immediately after the nasal administration of cedar pollen extract (Figure 1C). However, the symptoms disappeared in 3 months and no CMs developed chronic inflammation. The Group 4 CMs developed the pollinosis-like symptoms earlier than Groups 1 to 3. There was a high responder in Group 4, which showed more than 20 instances of symptom observation. However, the symptoms also disappeared similarly to

the other groups.

Next, we analyzed if the ratio of CD4+CD25+ cells were stably high after the 6th administration, the period in which all three CMs expressed some symptoms. As a result, the ratios of the CD4+CD25+ cells in the treated CMs (0.27% for I3300, 0.27% for I3288 and 0.34% for I3286) was stably higher than control CMs (0.02%) as shown in Figure 2A. However, the CD4+CD25+ cells, which transiently increased early after the nasal administration of cedar pollen extract, are known to contain not only activated effector T cells but also tolerant Treg cells (1). The master transcription factor of Treg cells is known to be Foxp3 in mouse and human cells, although human T cells can express Foxp3 without regulatory activity (18). Therefore, in order to detect the existence of Treg cells, in which Foxp3 transcription factor was expressed, we extracted mRNA from the PBMCs and the expression of Foxp3 mRNA was analyzed by semi-quantitative RT-PCR. As a result, we observed the expression of Foxp3 in these cells, which indicate the fractions contain Treg

cells, although the level did not largely increase shortly after the treatment (Figure 2B). The expression was decreased after 7 days, indicating the enhancement of the expression was transient in this time point

On the other hand, we simultaneously analyzed the cytokine profiles of these CM PBMCs by semi-quantitative RT-PCR. The cytokines include IL-2, TNF- α and IFN- γ as Th1 cytokines, IL-4, IL5 and IL-10 as Th2 cytokines, IL-17 as a Th17 cytokine and IL-10 as a Treg cytokine. Transforming growth factor (TGF)- β and IL-6 are inflammatory cytokines, which can induce Treg and/or Th17 cells as well (19). In non-treated CM, TGF- β , TNF- α and IFN- γ tended to have high expressions, similarly to the report of Fujii *et al.* (15). On the other hand, while non-treated CM PBMCs expressed very low levels of IL-10 mRNA and higher sensitivity was needed to detect the band in RT-PCR (data not shown), the expression of IL-10 mRNA was clearly detected in the treated CM PBMCs (Figure 2C). Other cytokines showed very similar levels between treated and non-treated CM PBMCs. These results showed that nasal administration of cedar pollen with cholera toxin did not induce pollinosis in CMs effectively.

As Iwashita *et al.* succeeded in the induction of pollinosis in NHPs using swine *Ascaris* as adjuvant, we tried to induce pollinosis in these CMs by employing the same protocol. Swine *Ascaris* was used to infect CMs of Group 1 and Group 3 after the 6-month interval and resulting symptoms were observed. The detail of the infection and the administration of cedar pollen extract are shown in Figure 1A. Similar to the first administration of cedar pollen, it took more than 14 weeks to observe the symptoms of pollinosis in Group 1-2, while Group 3-2 showed no symptoms by this treatment (Table 1). Group 5 CMs showed the symptoms earlier and in a higher ratio compared to Group 1-2 and Group 3-2. There are two high responders in Group 5. Again, although the CM individuals developed transient symptoms of sneeze and nasal mucosa immediately after the nasal administration of cedar pollen extract, the symptoms were not maintained and shortly after the development of the symptoms, they disappeared. Overall, the appearance of the symptoms in the groups only given cedar pollen extract and CT was not largely different from the Groups with *Ascaris*.

Th2 cells tend to develop under the IL-4 abundant environment, while Treg cells are induced under a TGF- β dominant environment, similarly to Th17 development (20). Differentiation of T cells into each cell lineage is reported to be largely affected by the TGF- β level and other cytokine environment (21,22). According to our results shown in Figure 2C and as Fujii *et al.* reported, TGF- β mRNA level was high and those of IL-6 and IL-4 were low in CMs without treatment. IL-17 was expressed at a detectable level (8,

15). The cytokine environment observed in CM PBMCs was predicted not to be adequate to Th2 development, but adequate to Treg and IL-27 enhanced IL-10 secreting cell differentiation. Moreover, as we observed, only IL-10 mRNA expression was increased after the intranasal cedar pollen extract administration. These results suggest that immune-tolerance was induced in these CMs. Although the induction of IL-10-producing CD4+ T cells in the Th2 environment is possible, it is more probable that Treg cells were developed in these CMs. The higher response of Group 5 compared to Group 3-2 might be attributed to the tolerance induction of Group 3 after the intranasal administration of cedar pollen extract. On the other hand, CM PBMCs expressed high levels of IFN- γ mRNA even after the treatment, suggesting the cytokine environment still maintains the Th1 immune cell environment. The result is in line with the previous report (8), and it is not surprising that the CM cytokine environment is Th1-dominant even after cholera toxin and *Ascaris* administration because most NHP species maintains Th1 environment (5). We also tried to detect CM IgE, by using ELISA method and mass spectrometry in CM plasma, but no detectable IgE was observed, while CM IgE gene has not been identified yet (23).

Although the same treatment in Groups 1, 2 and 4 induced different outputs, the unevenness of the symptom expression in the same treatment might be attributed to the fact that the MHC background of CM is not homologous. Because the immune reaction needs the specific peptide of cedar pollen extract and the MHC, which can present the peptide, the difference of MHC type might affect the response. The difficulty in using such experimental animals with heterogeneous backgrounds should be overcome by examining the MHC type and establishing MHC homozygous CMs.

CM also has a unique character for antigen recognition. CM expresses Caja-G proteins, which are orthologous to human leukocyte antigen (HLA)-G, an immune-suppressive, non-classical HLA class I molecule found throughout the body (24). Shiina *et al.* determined the gene structure of Caja-G. The Caja-G gene cluster contains 14 loci, at least 5 of which express functional gene products (25); plural alleles have been found in these loci (26-29). The variation and the binding of peptide suggested that it is more similar to classical HLA in humans, but the real function of Caja-G is yet to be clarified. If CM possesses the suppressive class I MHC, it might easily induce immune suppression after the sensitization even with *Ascaris* or cholera toxins. While allergy is a non-preferable condition, more wildlife-derived animals such as CMs are rarely affected by the allergy while pet animals are occasionally affected by the disease. The main reason might be the frequency of infection, which may induce strong Th1 immunity. However, it is curious that the experimental animals without such infection also have

Th1-preferred immunity. Although CM is housed in the environment for experimental animals, which avoids the infectious diseases, the immunological character is maintained in these experimental animals. If the environment is not shifted to some allergy-inducing ones, the immunity might be basically Th1 type in this species. The reason why the Hamamatsu CM is more prone to induce the symptoms might be some difference between the two institutes independent from the required uncontaminating condition. We might need to clarify the factors or another tool to induce strong allergy-inducible factors such as pollution-related factors to establish CM models for the allergy research.

Acknowledgements

We thank CIEA and Hamamatsu Medical College members for their excellent animal care skills. We thank the members of the Teaching and Research Support Center in the Tokai University School of Medicine for their technical skills. This work was supported by a research grant from Japan Science Promotion (Tokyo, Japan) to S.H.

References

1. Sakaguchi S, Yamaguchi T, Nomura T, Ono M. Regulatory T cells and immune tolerance. *Cell*. 2008; 133:775-787.
2. Mestas J, Hughes C. Of mice and not men: Differences between mouse and human immunology. *J Immunol*. 2004; 172:2731-2738.
3. Krishnamoorthy N, Timothy B, Oriss T, Paglia M, Fei M, Yarlagadda M, Vanhaesebroeck B, Ray A, Ray P. Activation of c-Kit in dendritic cells regulates T helper cell differentiation and allergic asthma. *Nat Med*. 2008; 14:565-573.
4. Gershwin L. Comparative immunology of allergic responses. *Annu Rev Anim Biosci*. 2015; 3:327-346.
5. Jeong A, Nakamura S, Mitsunaga F. Gene expression profile of Th1 and Th2 cytokines and their receptors in human and nonhuman primates. *J Med Primatol*. 2008; 37:290-296.
6. Iwashita K, Kawasaki H, Sawada M, In M, Mataka Y, Kuwabara T. Shortening of the induction period of allergic asthma in cynomolgus monkeys by *Ascaris suum* and house dust mite. *J Pharmacol Sci* 2008; 106:92-99.
7. Mansfield K, Tardif S, Eichler E. White paper for complete sequencing of the common marmoset. White Paper. 2004.
8. Kametani Y, Suzuki D, Kohu K, *et al*. Development of monoclonal antibodies for analyzing immune and hematopoietic systems of common marmoset. *Exp Hematol* 2009 37:1318-1329.
9. Sato K, Oiwa R, Kumita W, *et al*. Generation of a nonhuman primate model of severe combined immunodeficiency using highly efficient genome editing. *Cell Stem Cell*. 2016; 19:127-138.
10. Boon L, Brok H, Bauer J, Ortiz-Buijsse A, Schellekens M, Ramdien-Murli S, Blezer E, van Meurs M, Ceuppens J, de Boer M, 't Hart B, Laman J. Prevention of experimental autoimmune encephalomyelitis in the common marmoset (*Callithrix jacchus*) using a chimeric antagonist monoclonal antibody against human CD40 is associated with altered B cell responses. *J Immunol*. 2001; 167:2942-2949.
11. 't Hart B, Brok H, Remarque E, Benson J, Treacy G, Amor S, Hintzen R, Laman J, Bauer J, Blezer E. Suppression of ongoing disease in a nonhuman primate model of multiple sclerosis by a human-anti-human IL-12p40 antibody. *J Immunol*. 2005; 175:4761-4768.
12. Yun J, Ahn J, Kang B. Modeling Parkinson's disease in the common marmoset (*Callithrix jacchus*): overview of models, methods, and animal care. *Lab Anim Res*. 2015; 31:155-165.
13. Nunomura S, Shimada S, Kametani Y, *et al*. Double expression of CD34 and CD117 on bone marrow progenitors is a hallmark of the development of functional mast cell of *Callithrix jacchus* (common marmoset). *Int Immunol*. 2012; 24:593-603.
14. Shimada S, Nunomura S, Mori S, *et al*. Common marmoset CD117-positive hematopoietic cells possess multipotency. *Int Immunol*. 2015; 27:567-577.
15. Fujii Y, Kitaura K, Matsutani T, Shirai K, Suzuki S, Takasaki T, Kumagai K, Kametani Y, Shiina T, Takabayashi S, Katoh H, Hamada Y, Kurane I, Suzuki R. Immune-related gene expression profile in laboratory common marmosets assessed by an accurate quantitative real-time PCR using selected reference genes. *PLoS One*. 2013; 8:e56296.
16. Marinaro M, Staats H, Hiroi T, Jackson R, Coste M, Boyaka P, Okahashi N, Yamamoto M, Kiyono H, Bluethmann H, Fujihashi K, McGhee J. Mucosal adjuvant effect of cholera toxin in mice results from induction of T helper 2 (Th2) cells and IL-4. *J Immunol*. 1995; 155:4621-4629.
17. Mattsson J, Schön K, Ekman L, Fahlén-Yrliid L, Yrliid U, Lycke N. Cholera toxin adjuvant promotes a balanced Th1/Th2/Th17 response independently of IL-12 and IL-17 by acting on G α in CD11b⁺ DCs. *Mucosal Immunol*. 2015; 8:815-827.
18. Harbuz R, Lespinasse J, Boulet S, Francannet C, Creveaux I, Benkhelifa M, Jouk P, Lunardi J, Ray P. Identification of new FOXP3 mutations and prenatal diagnosis of IPEX syndrome. *Prenat Diagn*. 2010; 30:1072-1078.
19. Raphael I, Nalawade S, Eagar T, Forsthuber T. T cell subsets and their signature cytokines in autoimmune and inflammatory diseases. *Cytokine*. 2015; 74:5-17.
20. Dons E, Raimondi G, Cooper D, Thomson A. Induced regulatory T cells: mechanisms of conversion and suppressive potential. *Hum Immunol*. 2012; 73:328-334.
21. Roncarolo M, Gregori S, Battaglia M, Bacchetta R, Fleischhauer K, Levings M. Interleukin-10-secreting type 1 regulatory T cells in rodents and humans. *Immunol Rev*. 2006; 212:28-50.
22. Kimura A, Kishimoto T. IL-6: Regulator of Treg/Th17 balance. *Eur J Immunol*. 2010; 40:1830-1835.
23. Schmidt S, Neubert R, Schmitt M, Neubert D. Studies on the immunoglobulin-E system of the common marmoset in comparison with human data. *Life Sci*. 1996; 59:719-730.
24. Carosella E, Rouas-Freiss N, Tronik-Le Roux D, Moreau P, LeMaoult J. HLA-G: An immune checkpoint molecule. *Adv Immunol*. 2015; 127:33-144.
25. Kono A, Brameier M, Roos C, Suzuki S, Shigenari A,

- Kametani Y, Kitaura K, Suzuki R, Inoko H, Walter L, Shiina T. Genomic sequence analysis of the major histocompatibility complex (MHC) class I G/F segment in common marmoset (*Callithrix jacchus*). *J Immunol*. 2014; 192:3239-3246.
26. van der Wiel M, Otting N, de Groot N, Doxiadis G, Bontrop R. The repertoire of MHC class I genes in the common marmoset: evidence for functional plasticity. *Immunogenetics*. 2013; 65:841-849.
27. Cao Y, Fan J, Li A, Liu H, Li L, Zhang C, Zeng L, Sun Z. Identification of MHC I class genes in two Platyrrhini species. *Am J Primatol*. 2015; 77:527-534.
28. Antunes S, de Groot N, Brok H, Doxiadis G, Menezes A, Otting N, Bontrop R. The common marmoset: a new world primate species with limited Mhc class II variability. *Proc Natl Acad Sci U S A*. 1998; 95:11745-11750.
29. Neehus A, Wistuba J, Ladas N, Eiz-Vesper B, Schlatt S, Müller T. Gene conversion of the major histocompatibility complex class I Caja-G in common marmosets (*Callithrix jacchus*). *Immunology*. 2016; 149:343-352.

(Received September 6, 2017; Revised January 5, 2018; Accepted January 7, 2018)

Guide for Authors

1. Scope of Articles

BioScience Trends is an international peer-reviewed journal. BioScience Trends devotes to publishing the latest and most exciting advances in scientific research. Articles cover fields of life science such as biochemistry, molecular biology, clinical research, public health, medical care system, and social science in order to encourage cooperation and exchange among scientists and clinical researchers.

2. Submission Types

Original Articles should be well-documented, novel, and significant to the field as a whole. An Original Article should be arranged into the following sections: Title page, Abstract, Introduction, Materials and Methods, Results, Discussion, Acknowledgments, and References. Original articles should not exceed 5,000 words in length (excluding references) and should be limited to a maximum of 50 references. Articles may contain a maximum of 10 figures and/or tables.

Brief Reports definitively documenting either experimental results or informative clinical observations will be considered for publication in this category. Brief Reports are not intended for publication of incomplete or preliminary findings. Brief Reports should not exceed 3,000 words in length (excluding references) and should be limited to a maximum of 4 figures and/or tables and 30 references. A Brief Report contains the same sections as an Original Article, but the Results and Discussion sections should be combined.

Reviews should present a full and up-to-date account of recent developments within an area of research. Normally, reviews should not exceed 8,000 words in length (excluding references) and should be limited to a maximum of 100 references. Mini reviews are also accepted.

Policy Forum articles discuss research and policy issues in areas related to life science such as public health, the medical care system, and social science and may address governmental issues at district, national, and international levels of discourse. Policy Forum articles should not exceed 2,000 words in length (excluding references).

Case Reports should be detailed reports of the symptoms, signs, diagnosis, treatment, and follow-up of an individual patient. Case reports may contain a demographic profile of the patient but usually describe an unusual or novel occurrence. Unreported or unusual

side effects or adverse interactions involving medications will also be considered. Case Reports should not exceed 3,000 words in length (excluding references).

News articles should report the latest events in health sciences and medical research from around the world. News should not exceed 500 words in length.

Letters should present considered opinions in response to articles published in BioScience Trends in the last 6 months or issues of general interest. Letters should not exceed 800 words in length and may contain a maximum of 10 references.

3. Editorial Policies

Ethics: BioScience Trends requires that authors of reports of investigations in humans or animals indicate that those studies were formally approved by a relevant ethics committee or review board.

Conflict of Interest: All authors are required to disclose any actual or potential conflict of interest including financial interests or relationships with other people or organizations that might raise questions of bias in the work reported. If no conflict of interest exists for each author, please state "There is no conflict of interest to disclose".

Submission Declaration: When a manuscript is considered for submission to BioScience Trends, the authors should confirm that 1) no part of this manuscript is currently under consideration for publication elsewhere; 2) this manuscript does not contain the same information in whole or in part as manuscripts that have been published, accepted, or are under review elsewhere, except in the form of an abstract, a letter to the editor, or part of a published lecture or academic thesis; 3) authorization for publication has been obtained from the authors' employer or institution; and 4) all contributing authors have agreed to submit this manuscript.

Cover Letter: The manuscript must be accompanied by a cover letter signed by the corresponding author on behalf of all authors. The letter should indicate the basic findings of the work and their significance. The letter should also include a statement affirming that all authors concur with the submission and that the material submitted for publication has not been published previously or is not under consideration for publication elsewhere. The cover letter should be submitted in PDF format. For example of Cover Letter, please visit <http://www.biosciencetrends.com/downcentre.php> (Download Centre).

Copyright: A signed JOURNAL PUBLISHING AGREEMENT (JPA) form must be provided by post, fax, or as a scanned file before acceptance of the article. Only forms with a hand-written signature are accepted. This copyright will ensure the widest possible dissemination of information. A form facilitating transfer of copyright can be downloaded by clicking the

appropriate link and can be returned to the e-mail address or fax number noted on the form (Please visit [Download Centre](#)). Please note that your manuscript will not proceed to the next step in publication until the JPA Form is received. In addition, if excerpts from other copyrighted works are included, the author(s) must obtain written permission from the copyright owners and credit the source(s) in the article.

Suggested Reviewers: A list of up to 3 reviewers who are qualified to assess the scientific merit of the study is welcomed. Reviewer information including names, affiliations, addresses, and e-mail should be provided at the same time the manuscript is submitted online. Please do not suggest reviewers with known conflicts of interest, including participants or anyone with a stake in the proposed research; anyone from the same institution; former students, advisors, or research collaborators (within the last three years); or close personal contacts. Please note that the Editor-in-Chief may accept one or more of the proposed reviewers or may request a review by other qualified persons.

Language Editing: Manuscripts prepared by authors whose native language is not English should have their work proofread by a native English speaker before submission. If not, this might delay the publication of your manuscript in BioScience Trends.

The Editing Support Organization can provide English proofreading, Japanese-English translation, and Chinese-English translation services to authors who want to publish in BioScience Trends and need assistance before submitting a manuscript. Authors can visit this organization directly at <http://www.iacmhr.com/iac-eso/support.php?lang=en>. IAC-ESO was established to facilitate manuscript preparation by researchers whose native language is not English and to help edit works intended for international academic journals.

4. Manuscript Preparation

Manuscripts should be written in clear, grammatically correct English and submitted as a Microsoft Word file in a single-column format. Manuscripts must be paginated and typed in 12-point Times New Roman font with 24-point line spacing. Please do not embed figures in the text. Abbreviations should be used as little as possible and should be explained at first mention unless the term is a well-known abbreviation (e.g. DNA). Single words should not be abbreviated.

Title Page: The title page must include 1) the title of the paper (Please note the title should be short, informative, and contain the major key words); 2) full name(s) and affiliation(s) of the author(s), 3) abbreviated names of the author(s), 4) full name, mailing address, telephone/fax numbers, and e-mail address of the corresponding author; and 5) conflicts of interest (if you have an actual or potential conflict of interest to disclose, it must be included as a footnote on the title page of the manuscript; if no conflict of

interest exists for each author, please state "There is no conflict of interest to disclose"). Please visit [Download Centre](#) and refer to the title page of the manuscript sample.

Abstract: The abstract should briefly state the purpose of the study, methods, main findings, and conclusions. For article types including Original Article, Brief Report, Review, Policy Forum, and Case Report, a one-paragraph abstract consisting of no more than 250 words must be included in the manuscript. For News and Letters, a brief summary of main content in 150 words or fewer should be included in the manuscript. Abbreviations must be kept to a minimum and non-standard abbreviations explained in brackets at first mention. References should be avoided in the abstract. Key words or phrases that do not occur in the title should be included in the Abstract page.

Introduction: The introduction should be a concise statement of the basis for the study and its scientific context.

Materials and Methods: The description should be brief but with sufficient detail to enable others to reproduce the experiments. Procedures that have been published previously should not be described in detail but appropriate references should simply be cited. Only new and significant modifications of previously published procedures require complete description. Names of products and manufacturers with their locations (city and state/country) should be given and sources of animals and cell lines should always be indicated. All clinical investigations must have been conducted in accordance with Declaration of Helsinki principles. All human and animal studies must have been approved by the appropriate institutional review board(s) and a specific declaration of approval must be made within this section.

Results: The description of the experimental results should be succinct but in sufficient detail to allow the experiments to be analyzed and interpreted by an independent reader. If necessary, subheadings may be used for an orderly presentation. All figures and tables must be referred to in the text.

Discussion: The data should be interpreted concisely without repeating material already presented in the Results section. Speculation is permissible, but it must be well-founded, and discussion of the wider implications of the findings is encouraged. Conclusions derived from the study should be included in this section.

Acknowledgments: All funding sources should be credited in the Acknowledgments section. In addition, people who contributed to the work but who do not meet the criteria for authors should be listed along with their contributions.

References: References should be numbered in the order in which they appear in the text. Citing of unpublished results, personal communications, conference abstracts, and theses in the reference list is not recommended but these sources may be mentioned in the text. In the reference list,

cite the names of all authors when there are fifteen or fewer authors; if there are sixteen or more authors, list the first three followed by *et al.* Names of journals should be abbreviated in the style used in PubMed. Authors are responsible for the accuracy of the references. Examples are given below:

Example 1 (Sample journal reference): Inagaki Y, Tang W, Zhang L, Du GH, Xu WF, Kokudo N. Novel aminopeptidase N (APN/CD13) inhibitor 24F can suppress invasion of hepatocellular carcinoma cells as well as angiogenesis. *Biosci Trends*. 2010; 4:56-60.

Example 2 (Sample journal reference with more than 15 authors): Darby S, Hill D, Auvinen A, *et al.* Radon in homes and risk of lung cancer: Collaborative analysis of individual data from 13 European case-control studies. *BMJ*. 2005; 330:223.

Example 3 (Sample book reference): Shalev AY. Post-traumatic stress disorder: diagnosis, history and life course. In: Post-traumatic Stress Disorder, Diagnosis, Management and Treatment (Nutt DJ, Davidson JR, Zohar J, eds.). Martin Dunitz, London, UK, 2000; pp. 1-15.

Example 4 (Sample web page reference): Ministry of Health, Labour and Welfare of Japan. Dietary reference intakes for Japanese. <http://www.mhlw.go.jp/houdou/2004/11/h1122-2a.html> (accessed June 14, 2010).

Tables: All tables should be prepared in Microsoft Word or Excel and should be arranged at the end of the manuscript after the References section. Please note that tables should not be image format. All tables should have a concise title and should be numbered consecutively with Arabic numerals. If necessary, additional information should be given below the table.

Figure Legend: The figure legend should be typed on a separate page of the main manuscript and should include a short title and explanation. The legend should be concise but comprehensive and should be understood without referring to the text. Symbols used in figures must be explained.

Figure Preparation: All figures should be clear and cited in numerical order in the text. Figures must fit a one- or two-column format on the journal page: 8.3 cm (3.3 in.) wide for a single column, 17.3 cm (6.8 in.) wide for a double column; maximum height: 24.0 cm (9.5 in.). Please make sure that the symbols and numbers appeared in the figures should be clear. Please make sure that artwork files are in an acceptable format (TIFF or JPEG) at minimum resolution (600 dpi for illustrations, graphs, and annotated artwork, and 300 dpi for micrographs and photographs). Please provide all figures as separate files. Please note that low-resolution images are one of the leading causes of article resubmission and schedule delays. All color figures will be reproduced in full color in the online edition of the journal at no cost to authors.

Units and Symbols: Units and symbols

conforming to the International System of Units (SI) should be used for physicochemical quantities. Solidus notation (*e.g.* mg/kg, mg/mL, mol/mm²/min) should be used. Please refer to the SI Guide www.bipm.org/en/si/ for standard units.

Supplemental data: Supplemental data might be useful for supporting and enhancing your scientific research and BioScience Trends accepts the submission of these materials which will be only published online alongside the electronic version of your article. Supplemental files (figures, tables, and other text materials) should be prepared according to the above guidelines, numbered in Arabic numerals (*e.g.*, Figure S1, Figure S2, and Table S1, Table S2) and referred to in the text. All figures and tables should have titles and legends. All figure legends, tables and supplemental text materials should be placed at the end of the paper. Please note all of these supplemental data should be provided at the time of initial submission and note that the editors reserve the right to limit the size and length of Supplemental Data.

5. Submission Checklist

The Submission Checklist will be useful during the final checking of a manuscript prior to sending it to BioScience Trends for review. Please visit [Download Centre](#) and download the Submission Checklist file.

6. Online Submission

Manuscripts should be submitted to BioScience Trends online at <http://www.biosciencetrends.com>. The manuscript file should be smaller than 5 MB in size. If for any reason you are unable to submit a file online, please contact the Editorial Office by e-mail at office@biosciencetrends.com.

7. Accepted Manuscripts

Proofs: Galley proofs in PDF format will be sent to the corresponding author via e-mail. Corrections must be returned to the editor (proof-editing@biosciencetrends.com) within 3 working days.

Offprints: Authors will be provided with electronic offprints of their article. Paper offprints can be ordered at prices quoted on the order form that accompanies the proofs.

Page Charge: Page charges will be levied on all manuscripts accepted for publication in BioScience Trends (\$140 per page for black white pages; \$340 per page for color pages). Under exceptional circumstances, the author(s) may apply to the editorial office for a waiver of the publication charges at the time of submission.

(Revised February 2013)

Editorial and Head Office:

Pearl City Koishikawa 603
2-4-5 Kasuga, Bunkyo-ku
Tokyo 112-0003 Japan
Tel: +81-3-5840-8764
Fax: +81-3-5840-8765
E-mail: office@biosciencetrends.com

JOURNAL PUBLISHING AGREEMENT (JPA)

Manuscript No.:

Title:

Corresponding Author:

The International Advancement Center for Medicine & Health Research Co., Ltd. (IACMHR Co., Ltd.) is pleased to accept the above article for publication in BioScience Trends. The International Research and Cooperation Association for Bio & Socio-Sciences Advancement (IRCA-BSSA) reserves all rights to the published article. Your written acceptance of this JOURNAL PUBLISHING AGREEMENT is required before the article can be published. Please read this form carefully and sign it if you agree to its terms. The signed JOURNAL PUBLISHING AGREEMENT should be sent to the BioScience Trends office (Pearl City Koishikawa 603, 2-4-5 Kasuga, Bunkyo-ku, Tokyo 112-0003, Japan; E-mail: office@biosciencetrends.com; Tel: +81-3-5840-8764; Fax: +81-3-5840-8765).

1. Authorship Criteria

As the corresponding author, I certify on behalf of all of the authors that:

- 1) The article is an original work and does not involve fraud, fabrication, or plagiarism.
- 2) The article has not been published previously and is not currently under consideration for publication elsewhere. If accepted by BioScience Trends, the article will not be submitted for publication to any other journal.
- 3) The article contains no libelous or other unlawful statements and does not contain any materials that infringes upon individual privacy or proprietary rights or any statutory copyright.
- 4) I have obtained written permission from copyright owners for any excerpts from copyrighted works that are included and have credited the sources in my article.
- 5) All authors have made significant contributions to the study including the conception and design of this work, the analysis of the data, and the writing of the manuscript.
- 6) All authors have reviewed this manuscript and take responsibility for its content and approve its publication.
- 7) I have informed all of the authors of the terms of this publishing agreement and I am signing on their behalf as their agent.

2. Copyright Transfer Agreement

I hereby assign and transfer to IACMHR Co., Ltd. all exclusive rights of copyright ownership to the above work in the journal BioScience Trends, including but not limited to the right 1) to publish, republish, derivate, distribute, transmit, sell, and otherwise use the work and other related material worldwide, in whole or in part, in all languages, in electronic, printed, or any other forms of media now known or hereafter developed and the right 2) to authorize or license third parties to do any of the above.

I understand that these exclusive rights will become the property of IACMHR Co., Ltd., from the date the article is accepted for publication in the journal BioScience Trends. I also understand that IACMHR Co., Ltd. as a copyright owner has sole authority to license and permit reproductions of the article.

I understand that except for copyright, other proprietary rights related to the Work (e.g. patent or other rights to any process or procedure) shall be retained by the authors. To reproduce any text, figures, tables, or illustrations from this Work in future works of their own, the authors must obtain written permission from IACMHR Co., Ltd.; such permission cannot be unreasonably withheld by IACMHR Co., Ltd.

3. Conflict of Interest Disclosure

I confirm that all funding sources supporting the work and all institutions or people who contributed to the work but who do not meet the criteria for authors are acknowledged. I also confirm that all commercial affiliations, stock ownership, equity interests, or patent-licensing arrangements that could be considered to pose a financial conflict of interest in connection with the article have been disclosed.

Corresponding Author's Name (Signature):

Date:

